Distribution Agreement

In presenting this thesis or dissertation as a partial fulfillment of the requirements for an advanced degree from Emory University, I hereby grant to Emory University and its agents the non-exclusive license to archive, make accessible, and display my thesis or dissertation in whole or in part in all forms of media, now or hereafter known, including display on the world wide web. I understand that I may select some access restrictions as part of the online submission of this thesis or dissertation. I retain all ownership rights to the copyright of the thesis or dissertation. I also retain the right to use in future works (such as articles or books) all or part of this thesis or dissertation.

Signature:

_____   _____
Rong Ni   Date

Regulation and Characterization of Amyloid Architectures:

Insight into Amyloid Cytotoxicity and Molecular

Self-Assembly

By

Rong Ni

Doctor of Philosophy

Chemistry

_____

Dr. David G. Lynn

Adviser

_____

Dr. Vincent P. Conticello

Committee Member

_____

Dr. Dale E. Edmondson

Committee Member

Accepted:

_____

Lisa A. Tedesco, Ph. D.

Dean of the James T. Laney School of Graduate Studies

_____

Date

Regulation and Characterization of Amyloid Architectures:

Insight into Amyloid Cytotoxicity and Molecular

Self-Assembly

By

Rong Ni

B. S., Hunan University, 2000

M. S., Hunan University, 2003

Adviser: David G. Lynn, Ph. D.

An Abstract of

A dissertation submitted to the Faculty of the

James T. Laney School of Graduate Studies of Emory University

in partial fulfillment of the requirements for the degree of

Doctor of Philosophy

in Chemistry

2010

Abstract

Regulation and Characterization of Amyloid Architectures:

Insight into Amyloid Cytotoxicity and Molecular

Self-Assembly

by Rong Ni

Amyloid assemblies have been widely studied, leading to identification of the amyloid-lipid interaction as one the most important factors on regulating amyloid cytotoxicity. Particularly, the amyloid β-peptides, as the source of naturally occurring building blocks, have been exploited in the nano-technology field. Unfortunately, the proposed 3-D structure models of amyloid fibrils and tubes did not provide enough information on the interactions at the bilayer interface. To unveil some new aspects of amyloid cytotoxicity and identify the role of bilayer interaction on molecular self-assembly, the extensive structural characterizations have been performed on the covalently coupled lipid-Aβ(16-22) hybrid assemblies.

This study led to a discovery of novel Aβ-peptide-amphiphile architectures, which arise from direct interaction between Aβ-peptide and the lipid alkanes through bending the terminal alkanes to fit in laminates without disrupting β-sheet structure. The formation of these architectures is independent on the sample incubation pH, the linking position of alkane (at either N or C-termini) and peptide orientation/registry, which suggests that amyloid peptide may have an inherent interaction with membrane lipid

carbon alkyl chains.

During the course of this study, the clear morphology and structure transitions have been observed when tuning the length or degree of bulkiness of terminal alkanes. Most strikingly, cross-sheet electrostatic interaction, not the hydrophobic clustering as claimed in literatures, has been identified as an important driving force to direct and stabilize the parallel β-sheet fibril formation.

In addition, we also evaluated the role of glutamine side chain H-bonding cross-strand pairing on amyloid assembled morphology and peptide organization, shedding light on the mechanism of glutamine-contained amyloid diseases. In another project, the peptide strand conformation within the longer amyloid peptide fragment (Aβ(10-35)) has been roughly defined using fluorescence resonance energy transfer (FRET) technology with a small FRET pair on four different positions. This conformation provides extra constraints for study of Aβ(10-35) fibrils structure.

Many discoveries in this study are complementary to our current knowledge, deepening our understanding of amyloid cytotoxicity mechanism and expanding our regulation factors (pairwise interactions) in the design of novel nanomaterials with desired morphology and structure.

Regulation and Characterization of Amyloid Architectures:

Insight into Amyloid Cytotoxicity and Molecular

Self-Assembly

By

Rong Ni

B. S., Hunan University, 2000

M. S., Hunan University, 2003

Adviser: David G. Lynn, Ph.D.

A dissertation submitted to the Faculty of the

James T. Laney School of Graduate Studies of Emory University

in partial fulfillment of the requirements for the degree of

Doctor of Philosophy

in Chemistry

2010

Acknowledgements

I would like to thank my advisor Dr. David G. Lynn for his excellent guidance during my graduate studies at Emory University. Dave's creative ideas, constructive suggestions, and the intellectual freedom in Lynn's lab were deeply appreciated. Besides his incredible intelligence, his endless patience and enthusiasm toward education create the ideal working environment for development of myself and other young scientists. I also like to express my gratitude to my committee members, Dr. Vincent Conticello and Dr. Dale E. Edmondson for the insightful critiques that were critical for my project accomplishments.

The Lynn's group members have created a very stimulating research environment as well as a friendly atmosphere. I deeply appreciate Dr. Anil Mehta, who is a very nice guy and expert in solid state-NMR, for running my solid state-NMR samples and providing critical discussion of my project. Many thanks go to Seth Childers for his invaluable discussion and insights on my project, as well as willing to proofread my papers and thesis. I also would like to convey my gratitude to Dr. Jijun Dong and Tiao Xie, who are really outstanding mentors and helped myself and my husband during transition to graduate school and thereafter. Special thanks to the former lab members Dr. Lizhi Liang, Dr. Xiaohua Li, Dr. Yingzhen Kong, Dr. Fang Fang, Dr. Kun Lu, Dr. Rong Gao, Dr. Teresa Hill, Dr. Justin Maresh, Dr. Peng Liu, Dr. Andrew Palmer, Dr. Melissa Bobeck, Dr. Trey Maddox, Dr. Ken Walsh, Dr. Yan Liang, Hsiao-Pei Liu, and all the current members Yue Liu, Yi-Han Lin, Chenrui Chen, Savannah Adams and Erin Schuler.

In addition, I also deeply appreciate Dr. Hong Yi at Electron Microscopy (EM) center for her wonderful and patient guidance in TEM and the training of the basic techniques for biological sample preparation. I also want to thank Jeannette Taylor at EM center for her patience and generous guidance in SEM, Cryo-SEM and other EM related techniques. I also acknowledge Dr. Ken Hardcastle for the help in the X-ray diffraction experiment and Dr. Fred Strobel in mass spectrometry facilities, Dr. Shaoxiong Wu and Dr. Bing Wang in NMR center. In addition, I also want to thank David, Ed, Patti, Sarah and Steve in the stock room for their nice and outstanding work.

I have really enjoyed my life at Emory partly because I have made many friends here and I will miss the wonderful days I had at Emory. I would thank all of you, particularly Lingfeng Liu, Yunyun Pei, Zhen Qian, Zhongbo Fei, Weiqiang Zhan, Hao Yang, Hao Li, Bo Chen and Songbai Liu.

Lastly and most importantly, I would like to thank my family members for their love, consistent support and encouragement, especially my husband Rongbiao Tong, my son Terry Tong and my parents. Thank you!

Table of Contents

List of Figures

List of Tables

Abbreviations

Aβ	amyloid-β
AD	Alzheimer's disease
AFM	atomic force microscopy
AI	Antiparallel In-registry
AO	Antiparallel Out-of registry
APP	amyloid precursor protein
BS-REDOR	Boltzmann statistics rotational echo double-resonance
CD	circular dichroism
CHCA	Cyano-4-hydroxycinnamic acid
CR	Congo red
Cr	chromium
Cryo-SEM	Cryo-scanning electron microscope
Dab	2, 4-diaminobutyric acid
DCC	N,N'-dicyclohexylcarbodiimide
DCM	dichloromethane
DIPEA	N,N-diisopropylethylamine
DMF	dimethylformamide
DMSO	dimethyl sulfoxide
Dpr	2, 3-diaminopropionic acid
DQF-DRAWS	double quantum filtered dipolar recoupling with a windowless sequence

EDT	1,2-ethanedithiol
FSPS	Fmoc solid phase synthesis
FMOC	9-fluorenylmethoxycarbonyl
FRET	fluorescence resonance energy transfer
FT-IR	Fourier Transform Infrared Raman Spectroscopy
GdnHCl	guanidine hydrochloride
HBTU	2-(1H-Benzotriazol-1-yl)-1,1,3,3-TetramethylUronium hexafluorophosphate
HFIP	hexafluoroisopropanol
HPLC	high-performance liquid chromatograph
Hr	hour
IAPP	islet amyloid polypeptide
IE-IR	isotope-editing IR
LRD	lamination repeating distance
Lys	lysine
MALDI-TOF	matrix assisted laser desorption ionization - time of flight mass spectrometry
MD	molecular dynamics
MES	2-(N-morpholino)ethanesulfonic acid
Min	minute

mM	milli molar
mL	milliliter
NADH	nicotinamide adenine dinucleotide
NMM	4-methylmorpholine
Orn	ornithine,
PA	peptide-amphiphile
PEG	Poly(ethylene glycol)
PI	Parallel In-registry.
PNA	peptide nucleic acid
PrP	Prion Protein
pS	phosphoserine
RGD	arginine-glycine-aspartic acid
RP-HPLC	reversed-phase high-performance liquid chromatograph
SAXS	small angle X-ray scattering
SEM	scanning electron microscopy
STEM	scanning and transmission electron microscopy
ss-NMR	solid state Nuclear Magnetic Resonance
TEM	transmission electron microscopy
TFA	trifluoroacetic acid
TFE	trifluoroethanol
TLC	thin layer chromatograph

UV	ultra-violet
WESA	water exposed surface area
μL	microliter
μM	micromolar

CHAPTER 1

Amyloid Cytotoxicity and Molecular Self-Assembly Based Nanomaterials: General Introduction

Alzheimer's disease and the amyloid β-peptide assembly

Neurodegenerative disorders and systemic amyloidoses, such as Alzheimer's disease (Figure 1-1), Parkinson's disease, type 2 diabetes and Prion disease (Kakio and Matsuzaki, 2003), are all accompanied with extracellular plaques or intracellular tangles through the misfolding and aggregation of disease-related proteins (i.e. Aβ, tau, α-synuclein, IAPP, and PrP, respectively) (National Institute on Aging; Sekijima et al., 2005; Soto, 2001). Structure characterization of these deposits reveals surprising common features shared by these amyloid diseases, irrespective of peptide sources, peptide length and sequence, including long, unbranched fibrils with diameters ranging between 7 to 10 nm (Terry, 1964) and cross-β structure with orthogonal peptide repeating distances of 4.7 Å and 10.6 Å (Serpell, 2000). These assemblies typically give green birefringence when bound to the histopathologic dye Congo red (Kammerer et al., 2004; Mihara et al., 2005).

Alzheimer's disease (AD) is the most common neurodegenerative disorder, characterized by memory loss, cognitive deficits, and behavioral changes. This dementing illness of the people over 65 years old occurs in about 18 million people

1

worldwide (AHAF, 2006); (Mega, 1996; Selkoe, 1991a). Unfortunately, no effective therapy has been developed for AD, even though the self-assembly of the amyloid β-peptide and its cytotoxicity have been investigated extensively (Selkoe, 1991b).
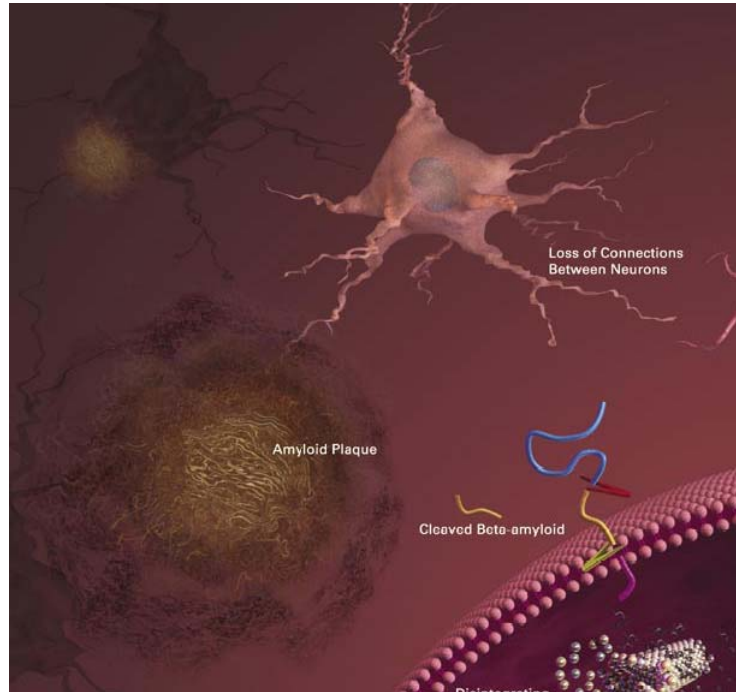
Figure 1-1. Cartoon of the amyloid plaques found in Alzheimer's Disease.
The Aβ aggregates of amyloid plaque contribute to the loss of connections between neurons (National Institute on Aging).

Production of amyloid β-peptide

The accumulation of extra-cellular neuritic plaques and intra-cellular neurofibrillary tangles in the brain is the hallmark of Alzheimer's disease (Bossy-Wetzel et al., 2004). The core structure of these deposits is composed of amyloid β-peptide containing 39 to 43 amino acids, which is generated in a two-step process from the enzyme-mediated cleavage of a transmembrane glycoprotein (100–130 kDa), the amyloid precursor protein (APP) (Weiming Xia, 2004). In order to understand the degradation mechanism of APP, two possible pathways: nonamyloidogenic and amyloidogenic, have been proposed

(Figure 1-2) (Vestergaard M, 2006; Weiming Xia, 2004). In the nonamyloidogenic pathway, the major route of APP processing is that APP is proteolyticaly cleaved by α-secretase and γ-secretase to produce P$_3$ protein (Koudinova NV, 2003); while in the amyloidogenic pathway, β-secretase, instead of α-secretase, cleaves APP, followed by γ-secretase to yield amyloid peptide with 28 amino acids from extracellular portion of APP and 11-15 amino acids from the transmembrane domain (LaFerla et al., 2007). Once the amyloid peptide is produced, it is released into the aqueous environment as a soluble monomer. This monomer may follow three different pathways depending on its concentration and the local environment: 1) self-aggregation in aqueous solution
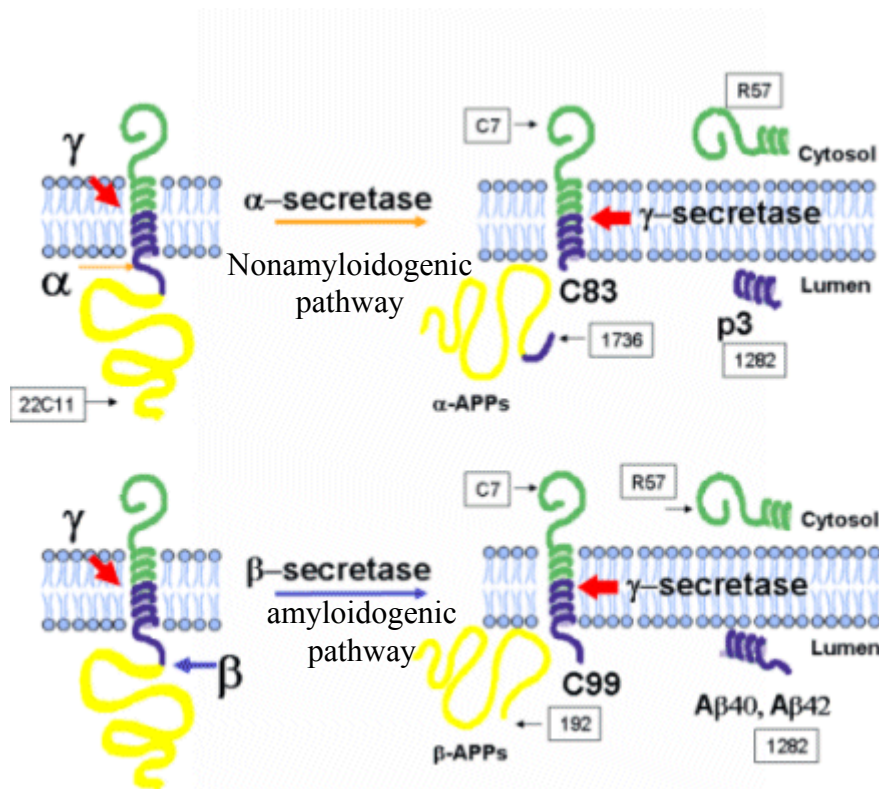
Figure 1-2. Two pathways of APP processing in cell membranes.
Non-amyloidogenic pathway produces P$_3$ protein by the cleavage of APP with α-secretase and γ-secretase; while amyloidogenic pathway results in the amyloid β-peptide production through cleavage of APP by β-secretase and γ-secretase (Weiming Xia, 2004).

(Bokvist et al., 2004); 2) association as β-sheets on the negatively charged membrane surface (McLaurin and Chakrabartty, 1997; Terzi et al., 1994); and 3) insertion into the membrane (Curtain et al., 2003). The Aβ-peptide begins exerting its damaging effects intra- and extra-cellularly once it is produced (Arispe et al., 2007; Stine et al., 2003).

Structure of Aβ fibrils

In 1959, Cohen and Calkins (Cohen, 1959) first observed fibrous amyloid fibrils with the assistance of transmission electron microscopy (TEM). Thereafter, characterization of amyloid fibrils with TEM become routine, and many other analytical technologies including atomic force microscopy (AFM), circular dichroism (CD), Fourier transform infrared spectroscopy (FTIR) and X-ray powder diffraction, have been employed to extensively characterize the amyloid fibril structure for better understanding amyloid assembly mechanism. Other high resolution techniques such as solution NMR and X-ray crystallography, however, are not applicable due to the low solubility and noncrystalline feature of amyloid fibrils. Up to date, the atomic-level structural information inside fibrils remains unknown.

Solid-state nuclear magnetic resonance (ssNMR), pioneered by Griffin and coworkers (Costa et al., 1997; Spencer et al., 1991), offers an ideal alternative approach to study amyloid fibrils. Due to the easy and homogeneous sample preparation and similar amyloid fibril formation, amyloid-β peptide fragments have frequently been chosen as model peptides to study amyloid fibrils structure. This first real structural information came from systematical isotope labeling to define the inter-peptide strand distance with ssNMR dipolar recoupling with a windowless sequence (DRAWS) experiments

(Benzinger et al., 1998; Benzinger et al., 2000; Bower et al., 1999; Gregory et al., 1997). This approach identified the parallel in-registry β-sheet within Aβ(10-35) fibrils. Taken together with small angle X-ray scattering and TEM results, the initial structural model of Aβ(10-35) fibrils was proposed where the extended peptide strands form parallel in-registry β-sheets with H-bonding distance of 4.7 Å. In this model, six sheets were stacked together with lamination distance of 9.8 Å to form mature fibrils (Figure 1-3a). Interestingly, these experimental data can also be fit to the β-helical model, in which

Extended β-sheet model   β-Helix Model
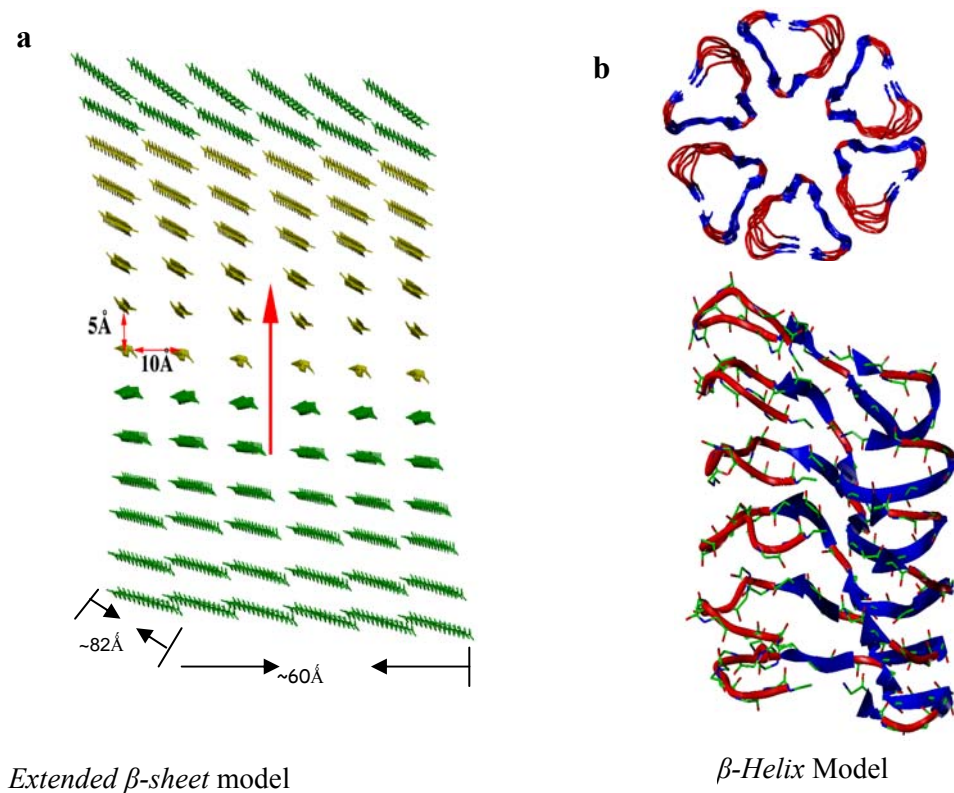
Figure 1-3. Two structure models of Aβ(10-35) fibrils.

(a) *Extended β-sheet* model with extended parallel in-registry monomer conformation. The hydrogen-bond distance of 5 Å and sheets stacking distance of 10 Å give the fibril dimension of 60Å ×80 Å (Benzinger et al., 1998; Benzinger et al., 2000; Burkoth et al., 2000).

(b) *β-helix* model with each monomer forming a triangle shape helical conformation (Lakdawala, 2003).

triangular-shaped peptide monomers stack to form a column in parallel fashion with the H-bonding distance of 4.7 Å (see Figure 1-3b), and six such columns packed together with the inter-column distance of 9.8 Å to form mature fibrils (Lakdawala, 2003). Since both models fit the structure data, further differentiation was required.

Recently, the ssNMR characterization of Aβ(1-40) fibrils, together with scanning transmission electron microscopy (STEM), led to a *turn* model (Petkova et al., 2002) (Figure 1-4). This model features: 1) the N-terminal first 10 residues adopt a random coil conformation and the rest of the peptide strand bends to form a non-β turn at G25, S26 and G29 with intra-strand distance of 10 Å; 2) these bent peptides stack in parallel fashion with H-bonding distance of 4.7 Å to form a sheet; and 3) four sheets pack together with an inter-sheet distance of 10 Å to form a matured fibril. The significant structural differences between Aβ(1-40) and Aβ(10-35) fibril raise several questions. If Aβ(10-35) is the central fragment of Aβ(1-40), why does Aβ(10-35) lose the C-terminal turn at G25, S26 and G29? Do the N-terminal 10 residues and C-terminal 5 residues impact the turn? In Aβ(10-35) fibril characterization, the mass per unit length is derived from the SAXS data, the average of the entire solution sample, this deviation maybe large since lateral association of the fibrils may generate larger aggregates. In contrast, the mass per unit length from STEM is from single specific fibrils, viewed on the EM image and the precision of the measurements may be an underestimate of the width. Therefore, further structure constraints are necessary to differentiate Aβ(10-35) and Aβ(1-40)fibril structures.

[1]DAEFRHDSG[10]YEVHHQKLVF[20]FAEDVGSNKG[30]AIIGLMVGGV[40]V

Side view   Top-view

Figure 1-4. Structure model of Aβ (1-40) fibrils.

The left panel is side view of a single sheet and the right panel is the top view of two stacked sheets. The color of each region in this model is corresponding to the same color coded peptide sequence (Petkova et al., 2006). Copyright permission has been requested.

Amyloid-lipid interaction

Mature amyloid fibrils have been recognized as toxic species (Selkoe, 2004), but the molecular processes that cause the formation of these nonnative architectures *in vivo* are not fully unveiled. Membrane lipids, especially negatively charged lipids, are known to significantly enhance the aggregation rate of Aβ-peptide relative to the lipid-free environments (Bokvist et al., 2004; Curtain et al., 2003; Kakio et al., 2002; Walsh et al., 2000; Wood et al., 2003). Recent related studies demonstrate that the mature fibrils and extracellular plaques are relatively inert and the intermediate species, such as oligomer and protofibrils, are correlated with amyloid cytotoxicity (Hardy and Selkoe, 2002). These soluble oligomers / protofibrils have been recognized to form ion channels (Figure

1-5a) (Quist et al., 2005) or to permeabilise cell membranes, allowing uncontrolled flow of ions and/or disrupting cell integrity/fluidity (Figure 1-5b) (Zhao et al., 2006a). It was found that lipid membranes, with proper composition and physical property, might trigger the formation of toxic intermediates (Hebda and Miranker, 2009; Kammerer et al., 2004; Zhao et al., 2004). Therefore, the mechanism of lipid-amyloid interaction may correlate with amyloid cytotoxicity. These undefined mechanisms raise the question about how Aβ interacts with membrane lipid and how amyloid causes cell and tissue damage.
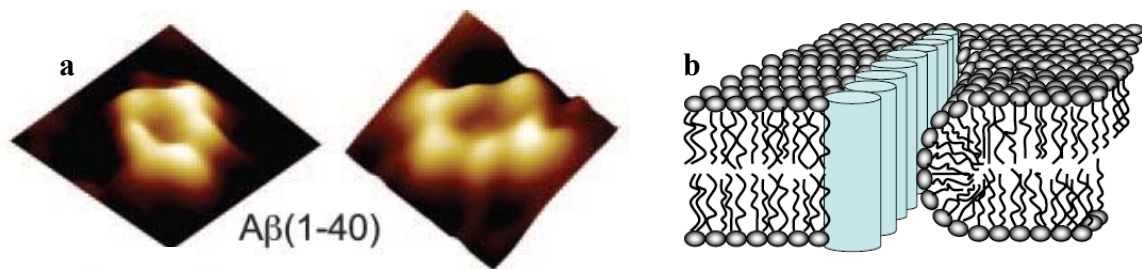
Figure 1-5. Insertion of amyloid oligomer in membrane lipid bilayers.
(a) AFM images of individual channel-like structure (Quist et al., 2005). (b) Cartoon of insertion of amyloid oligomers (light blue columns) across lipid bilayer (Zhao et al., 2006a). Copyright permission has been requested

Lipid accelerates Aβ formation

The aggregation process (Bokvist et al., 2004; Lau et al., 2006; Munishkina and Fink, 2007; Zhao et al., 2004) of Aβ peptides on membrane surfaces have been extensively explored with biophysical studies. With atomic force microscopy (AFM), direct impact of the nature of the lipid membranes and the property of the Aβ protein on Aβ aggregation rate and state have been observed (Lopes et al., 2007; Yip and McLaurin, 2001). Even though the exact mechanism of membrane lipids accelerating amyloid

formation remains unknown, a binding process involving three steps (Figure 1-6) has been proposed (Aisenbrey et al., 2008; Durell et al., 1994). These steps involve:

i) Amyloid β-peptide binds on the membrane surface through electrostatic interaction. Accumulating evidences suggest that electrostatic interaction is the main driving force for the Aβ–lipid interaction during the beginning process (Ikeda and Matsuzaki, 2008; Wong et al., 2009). For instance, neutral lipid or high salt concentration significantly inhibit Aβ binding on the model membranes (Simons et al., 1998); and electrostatic interactions have also been observed for membrane association with other toxins such as antimicrobial peptides and membrane-perturbing toxins (Seelig, 2004; Shai, 2002; Wieprecht et al., 2000).

ii) The dynamic nature of the lipid bilayer allows bound amyloid monomers to adjust their conformation and position on membrane surface.

iii) The increased local concentration of Aβ peptides on the membrane surface promotes
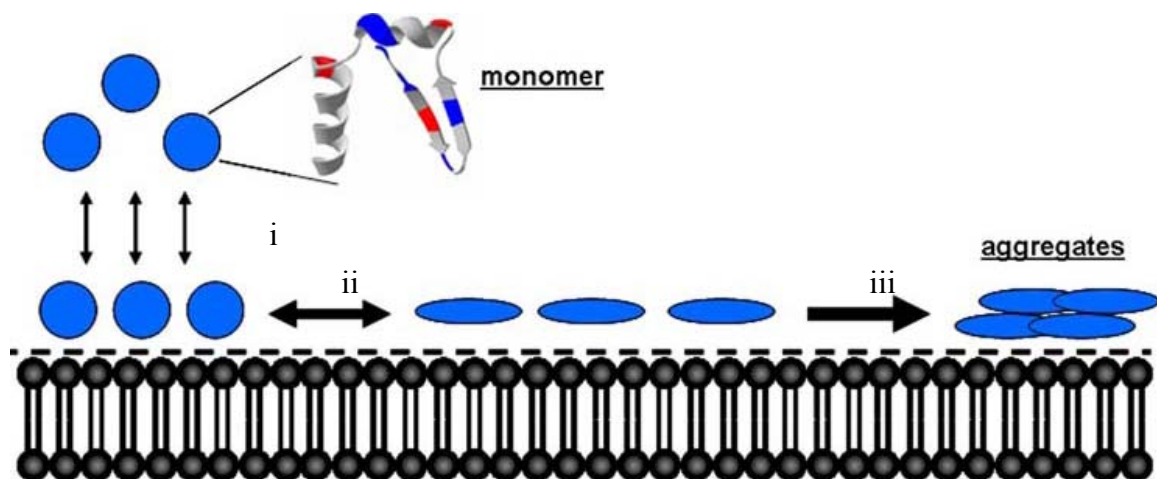
Figure 1-6. Illustration of Aβ binding and aggregation on lipid membranes.
i) Electrostatic interactions drive the association of Aβ on the membrane surface (Durell et al., 1994); ii) the dynamic nature of the membrane allows rearrangement and conformational adaptation of the Aβ monomer; and iii) the increased local concentration promotes Aβ aggregation by hydrophobic interaction between monomers (Aisenbrey et al., 2008).

aggregation. The proximity of the Aβ-peptide on the membrane surface induces hydrophobic interactions between protein monomers and accelerates the aggregation rate (Bokvist and Grobner, 2007; Giacomelli and Norde, 2005). Even though these processes have not been fully exploited, tremendous studies have already demonstrated that the Aβ-lipid interaction is highly correlated with amyloid cytotoxicity.

Mechanism of amyloid cytotoxicity

Amyloid toxicity has been found to be independent on sequence and protein amino acid chirality (Pastor et al., 2008), suggesting the generic feature of a certain aggregation state may be responsible for the toxicity (Kremer et al., 2000). Recently, the soluble intermediates such as oligomers and protofibrils have been identified to be toxic to cells through membrane permeabilisation (Zhao et al., 2006a). However, how these soluble species interact with the membrane to exert their pathological action is not clear. Several mechanisms regarding the interaction between amyloid and lipid membrane include: 1) Aβ peptides form ion channels, changing the conductance of membrane (Hirakura et al., 1999; Lin et al., 1999); 2) Aβ aggregates upon binding on or inserting into the membrane, disrupting membrane integrity or/and fluidity (Kremer et al., 2000; Mason et al., 1999); 3) aggregated peptides initiate free radical production and lipid peroxidation, which may cause calcium ion accumulation and cell death (Butterfield et al., 1999); and 4) Aβ, as a normal and functional apolipoprotein, may cause AD features by changing lipid metabolism (Koudinov et al., 1998).

Among these possible mechanisms of membrane-coupled toxicity, ion channel formation has been regarded as a major mechanism because of the accumulating evidence of pore structures and channel conductivity. Annular Aβ structures bound to the

membrane have been directly observed with AFM, consistent with Aβ forming channels or pores in the membrane (Lin et al., 2002). When Aβ–inserted vesicles were fused into planar bilayers, the β-sheet structured Aβ displayed single channel-like activity (de Planque et al., 2007). In addition, classical channel blockers could manipulate Aβ cytotoxicity (Simakova and Arispe, 2006). Moreover, when the membrane bilayer was treated with Aβ, membrane conductivity was significantly increased (Kourie et al., 2002; Quist et al., 2005), and the amount of calcium influx into cells dramatically increased (Demuro et al., 2005; Kawahara et al., 2000). The excess calcium in cells may stimulate apoptosis signaling to cause cell death, responsible for Aβ cytotoxicity.

Increasing evidence has also been accumulated in support of the disruption of membrane integrity/fluidity. In the presence of aggregated Aβ, encapsulated dyes are released from phospholipid vesicles (Lehtonen et al., 1996; Terzi et al., 1997). Interestingly, phospholipids in several cases have been found to incorporate amyloid fibrils and disrupt the membrane (Domanov and Kinnunen, 2008; Muller et al., 1998; Muller et al., 1995; Sood et al., 2008; Zhao et al., 2006a; Zhao et al., 2005; Zhao et al., 2004). In addition, the presence of Aβ is also accompanied with a change of membrane fluidity. The reduced membrane fluidity has been frequently observed upon addition of Aβ to mouse brain or human cortex membrane (Muller et al., 1998; Muller et al., 1995), or upon sonication of Aβ with phospholipid (Chauhan, 1993). Further, fluorescence studies demonstrated that an interaction between the hydrophobic patches of aggregated Aβ and hydrophobic alkanes of lipids reduced membrane fluidity (Kremer et al., 2001), and membrane fluidity was found to increase when Aβ was mixed with rat synaptic plasma membranes (Avdulov et al., 1997; Mason et al., 1999). These results all suggest

that Aβ-lipid interactions change membrane fluidity, directly or indirectly, impacting cell function.

For both channel-formation and membrane fluidity/integrity disruption, insertion of Aβ into lipid bilayer plays a critical role. Auto-insertion of Aβ into membranes has never been observed directly, but MD simulations indicate that Aβ(1-40) could insert into the lipid bilayer by adopting a transmembrane orientation (Ashley et al., 2006). However, *in vitro* studies showed that Aβ peptides could intercalate into rat synaptic plasma membranes (Tischer and Cordell, 1996).

So, what factors might regulate Aβ insertion and membrane permeability? Gafni et al. found that the Aβ-membrane binding and permeabilization were different processes (Figure 1-7) (Friedman et al., 2009; Mahalka and Kinnunen, 2009) and the binding was not sufficient for membrane permeabilization (Wong et al., 2009). Previous studies have established that membrane local environment strongly impact membrane permeabilization and amyloid toxicity since amyloid plaques are only observed in specific regions of the brain and they are toxic to only cerebral cortex and hippocampal cells (Selkoe, 2006). Lipids represent a most diverse class of biomaterials, and tens of thousands of different types of lipids have been found across mammalian cells and organelles (Kinnunen, 2009). Cholesterol, a common membrane component, has been found to be depleted in neuronal cell in AD patients and its impact on amyloid cytotoxicity has been debated. Cholesterol could promote neurodegenerative processes by promoting the activity of α-secretase to produce more amyloid peptide (Fassbender et al., 2001; Kojro et al., 2001). A modulation of plasma cholesterol on membrane fluidity and Aβ/membrane interaction has also been identified. Dencher et al. (Dante et al., 2006)

found that adding cholesterol into membrane, the penetration capability of Aβ(25-35) into membrane was reduced or completely inhibited. In addition, the inverse correlation between membrane cholesterol and Aβ-cell surface binding and cell death has also been established by McLaurin et al. through fluorescence anisotropy, fluorescence microscopy and in situ scanning probe studies (Yip et al., 2001). These results suggest that AD may be attenuated by modulation of membrane composition.
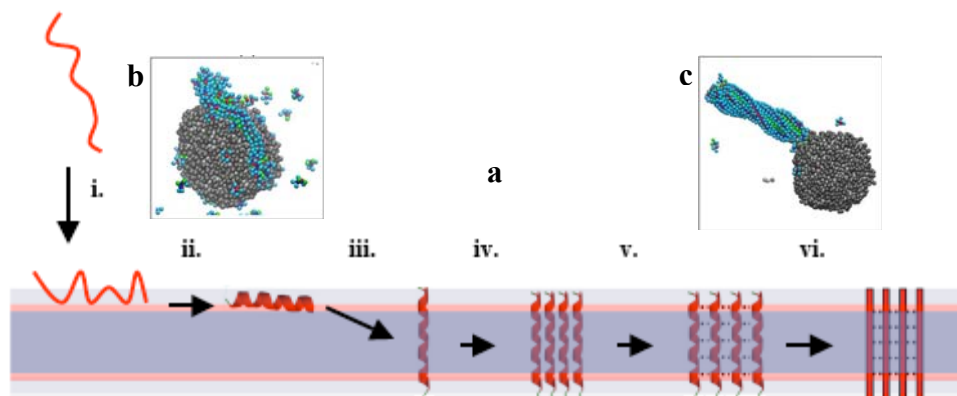
Figure 1-7. Proposed mechanisms of amyloid peptide binding, insertion and aggregation in the presence of lipid membranes (Friedman et al., 2009; Mahalka and Kinnunen, 2009).
 (a) The whole process: i) Aβ binding on membrane surface through electrostatic interaction; ii) rearrangement and conformation change of Aβ on membrane surface; iii) insertion of Aβ in membrane bilayers; iv) aggregation of Aβ (Klimov and Thirumalai, 2003; Knight et al., 2006); v) intermolecular H-bonding interaction within the oligomer; and vi) conformation switch from α-helix to β-sheet (Jahn and Radford, 2008).
Computational illustration: (b) Aβ binding and alignment on membrane surface; and (c) Aβ insertion and aggregation. The color codes: red line, ribbon and bar represents random coil, α-helix to β-sheet, respectively; grey ball is membrane and blue/red dot stands for Aβ monomer. Copyright permission has been requested.

Currently, a molecular understanding of Aβ-lipid membrane interaction remains poorly understood. Even though some computational studies shed some light on the atomic-level structure (Lemkul and Bevan, 2008), limited experimental evidence has been provided. Unfortunately, the heterogeneous species and interaction in lipid/Aβ

system in both *in vivo* and *in vitro* studies limits the application of NMR for structural characterization. Therefore, several questions remain to be answered:

1) How do amyloid peptides and lipids interact in lipid bilayer?

2) Do amyloid peptides and lipids form hybrid structures? How do amyloid fibrils accommodate lipid alkyl chains without structure disruption?

3) Is the amyloid-lipid interaction condition-dependent?

Molecular self-assembly based nanomaterials

Although amyloid fibrils are the misfolded state of amyloid β-peptides, the self-assembly offers a chance to develop novel nanomaterials with sub-nanometer precision through molecular recognition and assembly (Berl et al., 2000; Ramstrom et al., 2002). Certainly, many self-assembly systems have been developed with synthetically modified lipids, peptides and DNA (Hartgerink et al., 2001; Nowak et al., 2002; Petka et al., 1998; Schneider et al., 2002; Seeman, 2003; Seeman, 2004).

Biomolecule-based self-assembly

Phospholipids, the principle component of biological membranes, contain a hydrophilic head and a hydrophobic tail, and spontaneously self-assemble to membranes through hydrophobic interactions that bury the non-polar region in the bilayer center (Figure 1-8).
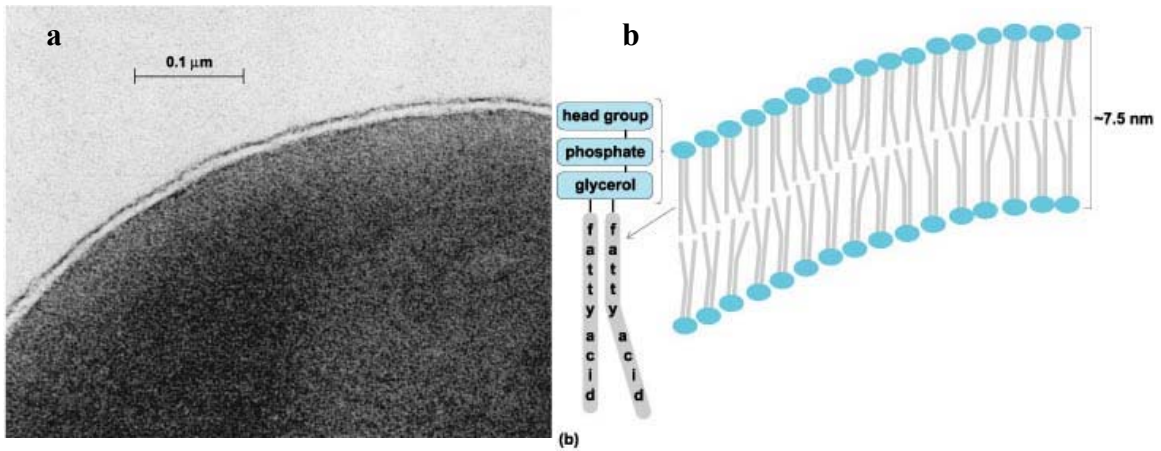
Figure 1-8. Bilayer structure of cell membrane (Robertson, 2002)**.**
(a) Micrograph of a thin section of human red blood cell. (b) The scheme of a lipid surfactant and the bilayer organization of phospholipids in the cell membrane.

By modification of the head groups or changing the length or saturation of the alkane tail, the artificial lipid surfactants are able to self-assemble to micellar-based aggregates or bilayer sheet-based aggregates with desired properties. The head group could be a nucleotide group (Yanagawa et al., 1989), or a short peptide (Ihara et al., 1986; Yamada et al., 1984); and the tail could include a single chain (Kunitake et al., 1980), or two chains (Jin et al., 2005) (Cho and Park, 1987). For example, the synthetic lipids with oligo(L-glutamic acid) as the hydrophilic head group can spontaneously form helical or tubular structures in water (Figure 1-9) (Yamada et al., 1984). Interestingly, the self-assembly of the oligo(L-aspartic acid) derivative involves a series of morphological transitions from globular aggregates, to fibril aggregates to ribbon-like aggregates (Ihara et al., 1986; Ihara et al., 2002). This discovery prompted the design and synthesis of new chiral lipids for nanofibril construction in water, which have been explored for new applications through coating with metals (Lvov et al., 2000).

15
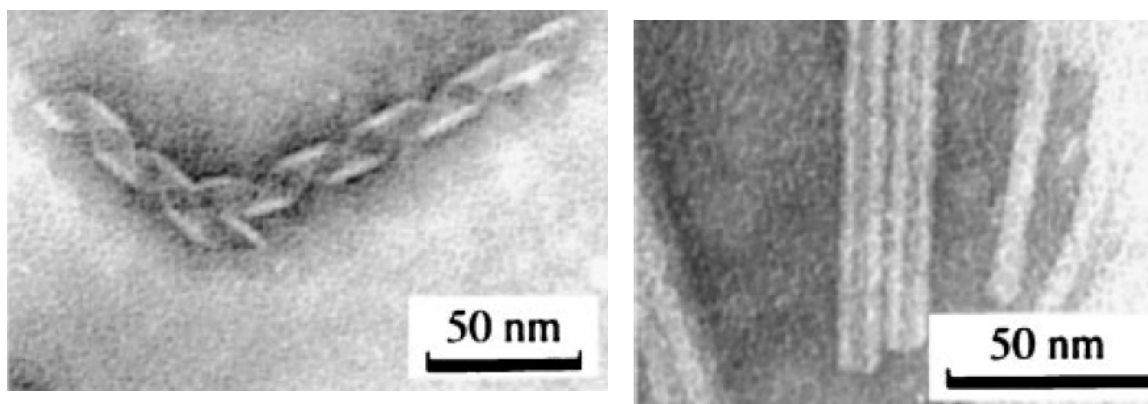
Figure 1-9. TEM images of self-assemblies from lipid surfactants.
(a) helix and (b) tubes (Yamada et al., 1984)**.** Copyright permission has been requested.

Peptides, due to their biocompatibility and structural diversity, extend the range of functions of self-assembled nanostructures (Shultz et al., 2000; Zutshi and Chmielewski, 2000). A new type of surfactants, **peptide-based surfactants**, have been produced by substitution of lipid hydrophobic tail with nonpolar amino acid such as glycine, alanine, valine, leucine or isoleucine (von Maltzahn et al., 2003) as well as replacement of hydrophilic head with charged amino acid such as glutamic acid, aspartic acid, lysine, histidine or arginine. These peptide-based surfactants containing 7 to 12 amino acids can then have similar length, hydrophobicity and electrostatic interactions as the lipid surfactants (Santoso et al., 2002; Vauthey et al., 2002; von Maltzahn et al., 2003; Yang and Zhang, 2006). However, structural modification of peptide surfactants could be achieved much more easily by simply changing the length of the tail (nonpolar amino acid), the peptide sequence or the charged amino acid headgroup.

A series of negatively charged peptide surfactants including V_6D, V_6D_2, G_nD_2 (n=4, 6, 8, 10) have been designed and synthesized (Santoso et al., 2002) for self-assembly to provide nanovesicles or nanotubes with average diameter of 30-50 nm and large inter-connected networks (Figure 1-10) (Santoso et al., 2002; Vauthey et al., 2002;

von Maltzahn et al., 2003). Considering the structural similarity between peptide surfactants and lipid surfactants, a bilayer structural model of these nanostructures was proposed (Santoso et al., 2002; Vauthey et al., 2002), in which the hydrophobic tail was buried in the bilayer interface and hydrophilic head was exposed to water. In addition to better mimicking the phospholipid, phosphoserine (pS) has been introduced as a hydrophilic head to provide pSA_6 or pSV_6, which could form ordered nanostructures as phospholipids (Lu et al., 2004). Changing the head group charge from negative to the positive, such as V_6K, V_6K_2 and A_6K, did not change the self-assembly properties (von Maltzahn et al., 2003; Zhao et al., 2006b). These findings suggest that self-assembly of these peptide surfactants involves a common mechanism.
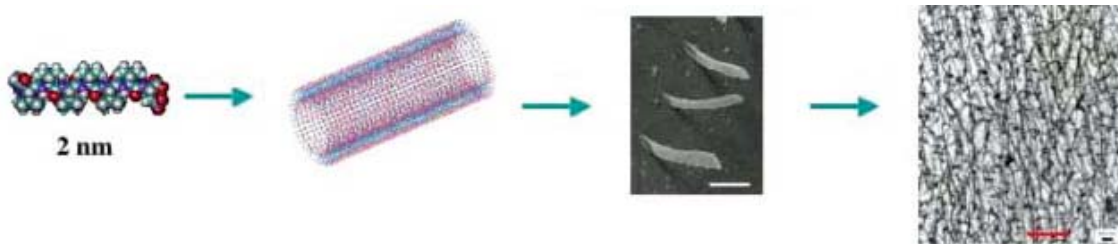
Figure 1-10. Peptide-based surfactants and the corresponding self-assemblies (Vauthey et al., 2002). (a) Structure of a short peptide surfactant, (b) Structure model proposed for this lipid surfactant, (c) TEM image of tubes formed from this peptide-surfactant, (d) the EM image at low magnification. Copyright permission has been requested.

Recently, Zhang's group extended the self-assembly of peptide-surfactants to form donut-shaped nanostructures by designing a cone-shaped monomer with the mixed amino acid sequence (Figure 1-11). This result indicates that the geometry and shape of self-assembled nanostructures can be finely tuned by different amino acid composition (Khoe et al., 2009).
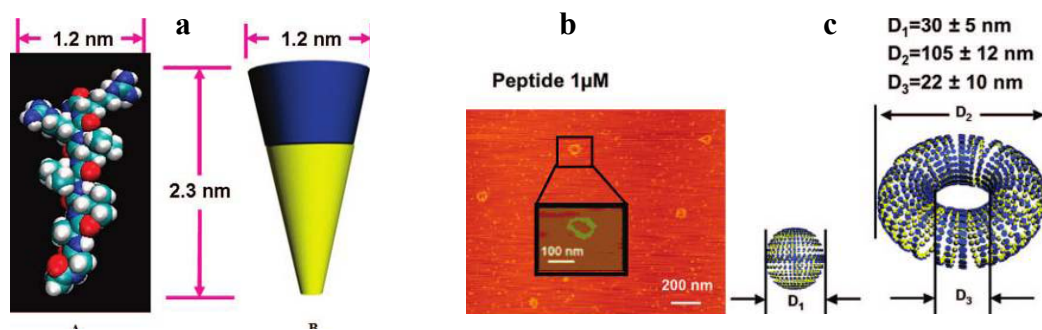
Figure 1-11. Nanodonut formatin from a cone-shaped peptide surfactant (Khoe et al., 2009). (a) Molecular model of the peptide Ac-GAVILRR-NH$_2$ with cone-shape. (b) AFM image of nanodonut formed from 1 μM peptide in water and (c) the proposed structural model. Copyright permission has been requested.

Peptide-surfactants have many advantages as compared to conventional surfactants. For example, the peptide-surfactants could better dissolve and stabilize some membrane proteins and serve as excellent agents to crystallize some membrane proteins for structure characterization (Kiley et al., 2005; Zhao et al., 2006b). In addition, due to biocompatibility and biodegradability, these peptide surfactants have also proven to be safer encapsulating and delivery systems for some proteins, bioactive peptides, small drug molecules and nucleic acids (Aramburu et al., 1999; Norman et al., 1999). These indicate that peptide-surfactants are a class of promising building blocks with easily tuned structure and function for future application in bionanotechnology.

By taking advantages of both lipids and peptide-surfactants, **peptide-amphiphiles**, as a new class of biomaterials, have been designed and constructed by substitution of the phosphate head group of lipids with peptide fragments (Beniash et al., 2005; Cui et al., 2009; Hartgerink et al., 2001; Hartgerink et al., 2002; Tysseling-Mattiace et al., 2008). These peptide-amphiphiles can self-assemble into well-defined and predictable

nanostructures and in the past decade, the numerous peptide-amphiphiles have been developed for application in nanotechnology and tissue engineering (Guler et al., 2005; Haines et al., 2005; Hartgerink et al., 2001; Petka et al., 1998; Tysseling-Mattiace et al., 2008).

Outstanding contributions in this area have been made by Stupp and coworkers, who extensively studied the self-assembly structure of peptide-amphiphiles with diverse sequences (Behanna et al., 2005; Beniash et al., 2005; Bull et al., 2005; Cui et al., 2009; Hartgerink et al., 2001; Hartgerink et al., 2002; Hsu et al., 2008; Palmer and Stupp, 2008; Tysseling-Mattiace et al., 2008). Their peptide-amphiphiles are usually composed of four segments: 1) a hydrophobic tail, 2) a β-sheet forming segment, 3) a flexible linker, and 4) a cell adhesion group (Figure 1-12a, b). In their cylindrical fibrils, their structural model places all alkyl tails buried in the fibril interior with the peptide region at fibril outer surface adopting parallel arrangement along both hydrogen-bonding and lamination directions (Hartgerink et al., 2001) (Figure 1-12c). An important discovery in their studies is that the self-assembled morphology and structure are peptide-sequence independent, which offers more opportunities to design biomimetic materials with the incorporation of functional peptide fragments. For instance, the incorporation of a RGD fragment or the cell adhesion region in the fibrils leads to potential applications in tissue regeneration (Hartgerink et al., 2002; Hosseinkhani et al., 2006). With the introduction of peptide nucleic acid (PNA) into their peptide-amphiphile, molecular devices were constructed to specifically bind RNA (Guler et al., 2005). In addition, a single phosphorylated serine residue in the peptide region served as template to mineralize hydroxyapatite crystals, mimicking the bone generation by collagen fibers in nature

19

(Hartgerink et al., 2001). Furthermore, their peptide-amphiphile nanofibrils also provide an efficient scaffold to nucleate cadmium sulfide and template the growth of semiconductor crystals (Sone and Stupp, 2004). Lastly, functionalization of peptide-amphiphile nanofibers with magnetic resonance activity broadens its application in medical science as diagnostics (Bull et al., 2005).
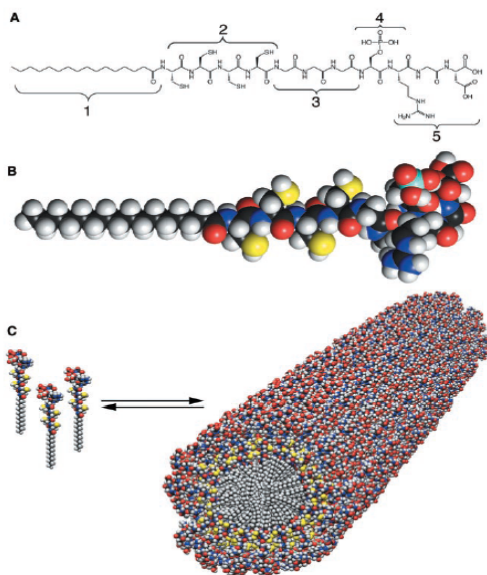
Figure 1-12. Structure model of cylindrical fibers formed from peptide-amphiphile (Hartgerink et al., 2001).

(a) Chemical structure proposed for the peptide amphiphile with 5 different segments: 1) alkyl tail, 2) β-sheet formation region and cross-linking segment, 3) flexible glycine linker, 4) phophorated serine as calcium ions binding site and 5) cell-adhesion region.

(b) Molecular model of the corresponding peptide-amphiphiles. Color scheme: C, black; H, white; O, red; N, blue; P, cyan; S, yellow.

(c) Cylindrical fibril model with all the alkyl chain buried in the fibril interior. Copyright permission has been requested.

In addition, Fuhrhop et. al developed another family of peptide-amphiphile, known as bolaamphiphiles, through conjugation of two amino acids at both ends of an alkyl chain (Schneider et al., 2000). The dominant role of alkyl chains for the self-assembly

offers more chances to modify and functionalize the self-assembled nanostructures, which is a great advantage for the rational design of novel nanomaterials.

In biological systems, **proteins and peptides** are major scaffold materials with a scale ranging from nano to macro levels. During the past decade, more and more research efforts have focused on the self-assembly of short peptides (Holmes, 2002). Many peptide-based self-assembly systems have been developed that display very interesting morphologies and properties. Some of these examples include hydrgels from artificial peptides (Petka et al., 1998; Schneider et al., 2002), nanotubes from Aβ peptide fragments (such as Aβ(16-22) (Lu et al., 2003; Mehta et al., 2008), phe-phe dipeptide (Ghosh et al., 2007; Reches and Gazit, 2003)) and D, L alternating cyclic peptides (Ghadiri et al., 1993), vesicles from Aβ(16-22) (Childers, unpublished), nanofibers from β-sheet peptide (Mehta et al., 2008; Morgan et al., 2002) and α-helical coiled-coil assemblies (Zimenkov et al., 2006). Their biocompatibility, immunogenicity and biodegradability secure the necessity of further exploration of peptide-based self-assemblies for potential applications in tissue regeneration where the assembled fibril networks are used as scaffold for the cell growth (Silva et al., 2004), gene/drug delivery where the assembled nanostructures serve as carriers (Yan et al., 2007a), electronic mineralization where the peptide nanostructures serve as template to nucleate and grow the nanowires, and as material in the food science and cosmetic industry (Hartgerink et al., 2001; Reches and Gazit, 2003; Sone and Stupp, 2004; Yuwono and Hartgerink, 2007). These self-assembly systems include both synthetic and naturally occurring peptides, both of which may contribute significantly to the development of molecular engineering in nanotechnology.

Synthetic peptides have attracted great attention due to the easy accessibility of versatile peptides. Ghadiri and coworkers designed the first peptide nanotubes from a cyclic peptide with D- and L- alternated amino acids (Ghadiri et al., 1993; Horne et al., 2005b). The planner rings of these cyclic peptides stack one by one to form a size controlled tubular structures (Figure 1-13). These tubes have already been used as transmembrane ionic channel (Ishida et al., 2001), antibacterial agents (Fernandez-Lopez et al., 2001) and in molecular electronics (Horne et al., 2005a). Another short synthetic peptide with alternating positive and negative L-amino acids readily assembled to fibrils, which had been applied to tissue engineering and regeneration, such as serving as scaffold to support neural cell growth (Ellis-Behnke et al., 2006).
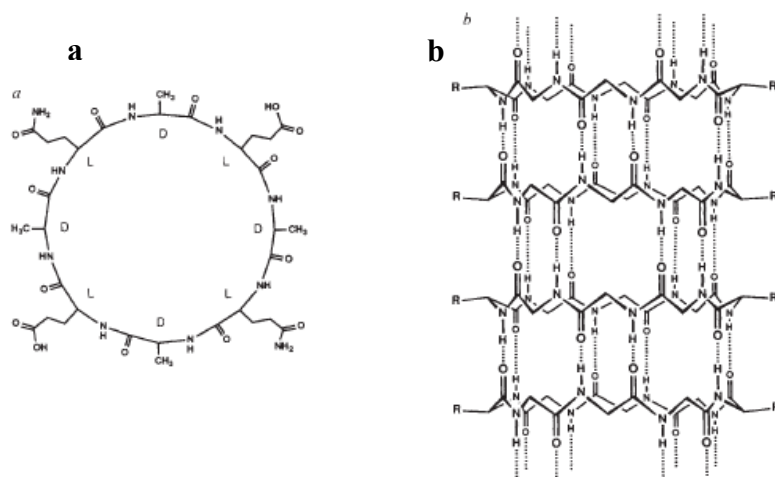
Figure 1-13. Structure model of peptide nanotubes formed from cyclic peptide (Ghadiri et al., 1993; Horne et al., 2005b).
(a) Chemical structure of the D-, L-alternating peptide; (b) the tubes formed by stacking these flat rings with intermolecular hydrogen-bonds. Copyright permission has been requested.

Naturally occurred peptides also offer the great opportunity for novel nanomaterial development. For example, amyloid peptides, even though their insoluble plaques are associated with degenerative diseases, offer diversified assembled morphologies ranging

from fibrils (Benzinger et al., 1998; Benzinger et al., 2000; Burkoth et al., 2000; Mehta et al., 2008), to nanotubes (Dong et al., 2006; Liu et al., 2008; Lu et al., 2003; Mehta et al., 2008), sheets, particles (Dong et al., 2005) and vesicles (Childers, unpublished). The assembly of the short peptide KLVFFAE Aβ(16-22) could be tuned by incubation pH (Lu et al., 2003; Mehta et al., 2008), amino acid mutation (Lu, 2005) and terminal modification (Gordon et al., 2004). Moreover, specific surface properties also serve as template for nanowires fabrication (Figure 1-14a) (Kun Lu, 2004), silver nanowires (Reches and Gazit, 2003) (Figure 1-14b) and platinum nanoparticles (Song et al., 2004).
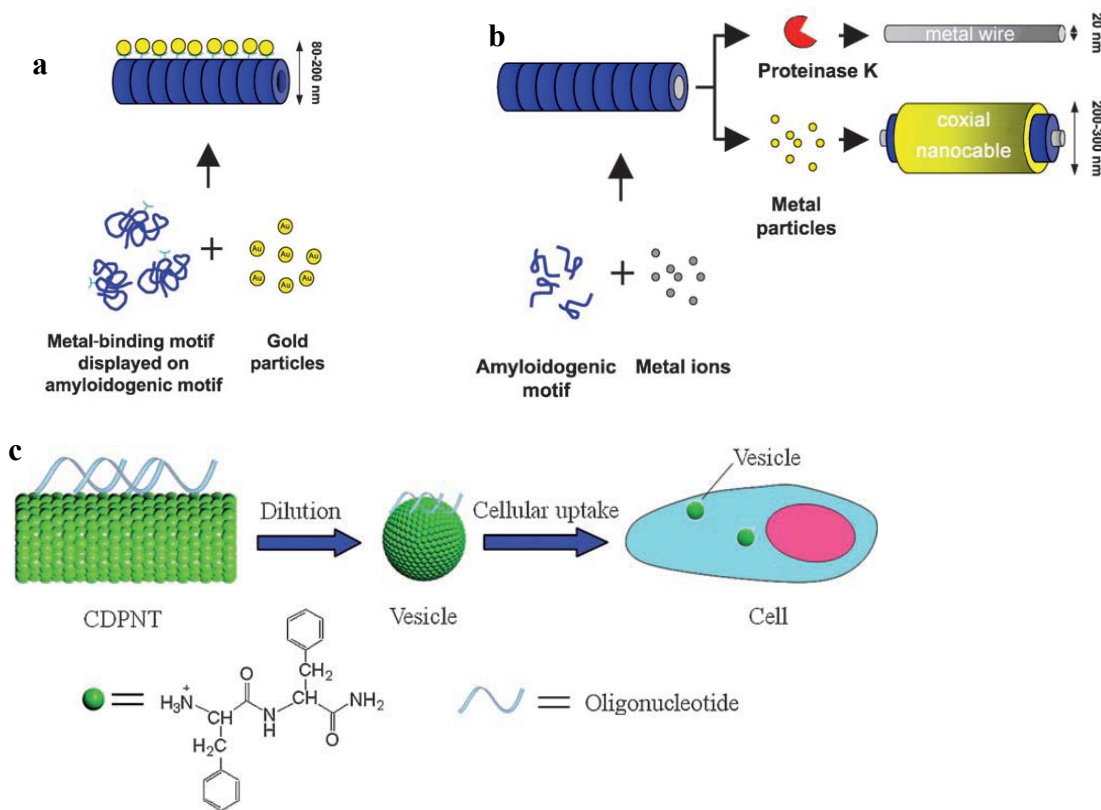
Figure 1-14. Illustration of amyloid as scaffold or template (Cherny and Gazit, 2008).
Formation of nanowires by (a) covalent or non-covalent binding of gold particles on the tube or fibril surface (Kun Lu, 2004), or (b) encapsulating the metal ion inside the tubes, which was reduced to form nanowires (upper panel) or addition of another metal particle to bind on the tube surface to make the coaxial metal wires (lower panel) (Scheibel et al., 2003); (c) The scheme showing how cationic dipeptide nanotube transports oligonucleotide into cells (Yan et al., 2007b). Copyright permission has been requested.

The N-terminal region of Sub35 also readily self-assembles to typical amyloid fibrils, and the incorporation of cystein residues successfully introduce reactive site to covalently couple with functional gold colloid. After silver enhancement, a conductive metal nanowire was prepared (Scheibel et al., 2003). Finally, the cationic peptide nanotubes formed from the N-terminal free phe-phe dipeptide has been shown to successfully transport DNA into cells (Figure 1-14c) (Yan et al., 2007b).

General forces that govern cross-β self-assembly

It is very important to uncover the driving forces which direct self-assembly not only for medical treatment of protein misfolding diseases, but also for fabrication of new materials. Several non-covalent interactions have already been identified to play certain roles for the peptide association, such as hydrogen-bonding (Bodles et al., 2004a; Doig et al., 2002; Hughes et al., 2000), hydrophobic effects (side chain or alkyl tail) (Gordon et al., 2004), electrostatic interactions (Mehta et al., 2008), Phe-Phe aromatic stacking (Reches and Gazit, 2003), cross-strand pairing (Liang et al., 2008b), van der Waals and metal coordination binding (Dong et al., 2006; Morgan et al., 2002). Although each of these interactions is weak and insignificant by itself, the combined forces may significantly drive the well-defined and stable 3D nanostructure formation (Zhao and Zhang, 2006).

Hydrogen-bonding is recognized as one of the main driving forces for peptide assembly. In amyloid assembly, methylation of the peptide backbone amide not only inhibits the fibril formation, but destabilizes preformed fibrils (Bodles et al., 2004a; Doig et al., 2002; Hughes et al., 2000), and restricts the degree of assembly (Clark et al., 1998).

24

Aβ(25-35) readily self-assembles to amyloid fibrils, but G^{33} N-methylation completely inhibits fibril formation and reduced the toxicity of preformed fibrils (Doig et al., 2002; Hughes et al., 2001). A peptide fragment α-synuclein (residue 68-78) with backbone N-methylation of G^{73} neither self-assembled into fibrils nor exhibited any toxicity to cells (Bodles et al., 2004b). Replacement of peptide backbone amide with an ester linkage also inhibits the amyloid fibril formation (Gordon and Meredith, 2003). Even within the peptide amphiphiles, methylation of the backbone amide close to the N-alkyl chain inhibits assembly (Paramonov et al., 2006).

In addition, the side chain hydrogen-bonding also plays an important role in amyloid assembly and morphology. Glutamine/Asparagine are both involved in several neurodegenerative diseases including Huntington's Disease (Chen et al., 2002) and spinal bulbar muscular atrophy (Skinner et al., 1998) as insoluble aggregates. Since glutamine and asparagine are the only two natural residues bearing amide group at the side chain, it has been hypothesized that they promote self-assembly via side chain hydrogen-bonding along a sheet (Marchut and Hall, 2006; Plumley and Dannenberg, 2010).

In the Aβ peptide, E22Q Dutch-mutation (HCHWA-D) (Massi and Straub, 2001) with the more severe cerebrovascular Aβ deposition is observed. *In vitro* experiment, mutant (Aβ(1-40)E22Q) shows markedly enhanced toxicity (Davis and VanNostrand, 1996) and Aβ fragments with this mutation (Aβ(13-26)E22Q) show higher aggregation rates (Clements et al., 1993). These results provided very strong evidence that hydrogen-bond formation of glutamine side chain plays very important role for amyloid fibril formation. However, so far no experimental data have been provided to explain how

glutamines direct self-assembly or how they dictate the molecular-level structure within the corresponding self-assemblies.

Hydrophobic effects are another important driving force for protein/peptide self-assembly. In nature, this interaction drives numerous assemblies including micells, phospholipid membranes and folded proteins (Beniash et al., 2005; Cejas et al., 2008; Edelhoch, 1978; Hartgerink et al., 2001). In nanomaterials, hydrophobic effects drive peptide/polymeric surfactants and peptide-amphiphiles assembly (Selinger et al., 1996; Spector et al., 1996). For example, the peptide-amphiphiles studied by Stupp and coworkers usually form cylindrical fibrils through alkyl chain hydrophobic clustering (Figure 1-12). When a medium length alkyl chain (octanoyl group) is covalently coupled on the N-terminus of Aβ(16-22), the peptide orientation is switched from antiparallel to parallel (Gordon et al., 2004). Clearly, hydrophobic interactions can modulate self-assembled morphology and structure.

Electrostatic interactions are another important driving force that contributes to the molecular self-assembly through charge complementary. This concept has been extensively utilized in the rational design of novel nanomaterials since Zhang and coworkers first discovered the formation of a biologically mimic membrane from an ionic complementary peptide in 1993 (Zhang et al., 1993). Since then, Zhang and coworkers constructed several charged self-complementary systems (Figure 1-15), which self-associate to form β-pleated sheet and further to larger supermolecular nanoarchitectures with great stability and functionality (Leon et al., 1998; Zhang et al., 1995). These novel nanomaterials have already been found in different applications such as tissue regeneration and drug delivery (Chen, 2005).

Another example for electrostatic interaction is the pH-dependence of Aβ(16-22) (KLVFFAE), which has two oppositely charged residues at peptide ends. At neutral pH, both lysine and glutamate are charged so that across-strand Lys16/Glu22 electrostatic interaction dictates antiparallel in-registry β-sheet fibril formation (Mehta et al., 2008). While at acidic pH, protonated glutamate weakens the electrostatic interaction and consequently allows Val18/Ala21 cross-strand pairing interaction to direct antiparallel
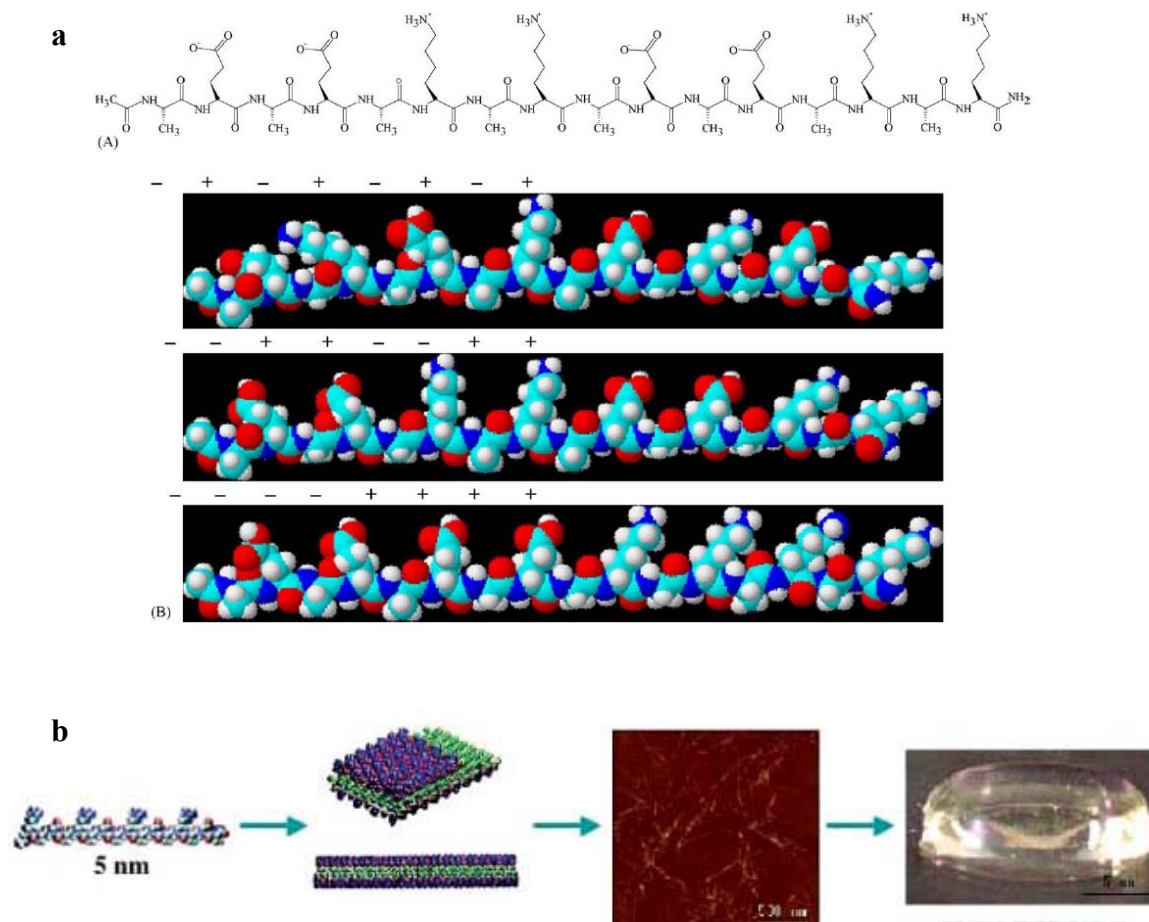
Figure 1-15. Self-assembly from ionic complimentary peptides.

(a) Chemical structure of EAK16-II. The three charge alternating patterns are listed with three models, such as − + − + − + − +, − − + + − − + +, and − − − − + + + +, respectively.

(b) From left to right is the chemical model structure of a ionic peptide and the structural model to show the β-sheet formation with charge complementary. The AFM image shows the fibrils and the bulk sample looks like a transparent gel (Zhang, 2003). Copyright permission has been requested.

out-of register β-sheet nanotube formation (Mehta et al., 2008). These examples demonstrate the important contribution of ionic complementary along β-sheets, but it remains unclear whether electrostatic interactions stabilize sheet-sheet association to modulate assembly architecture.

In addition, **phe-phe aromatic interactions, cross-strand pairing and metal coordination** have also been recognized in amyloid self-assembly. Many amyloidogenic peptide fragments contain one or more phenylalanines that promote amyloid self-assembly via aromatic π-π stacking (Gazit, 2002; Kim and Hecht, 2006). The self-assembly rate decreased following substitution of two phenylalanines in Aβ(1-42) with other hydrophobic residues (Kim and Hecht, 2006). Further studies showed that substitution of either phenylalanine in Aβ(16-22) disrupted the nanotube assembly (Lu, 2005). These results suggest that the two phenylalanines in Aβ(16-22) may promote the lamination growth by stabilizing sheet-sheet stacking through π-π interactions (Jack et al., 2006; Makin et al., 2005; Mehta et al., 2008). Either π-π stacking or facial complementarility seem important for amyloid assembly (Gorbitz, 2001; Gorbitz, 2006; Reches and Gazit, 2003).

Recently, cross-strand pairing with size complementary has been systematically studied through substitution of the branched residue Valine18 in Aβ(16-22) with other residues (Liang et al., 2008b). It has been found that the size complementary between the branched residue and the small sized residue directs β-sheets registry and final self-assembly morphology (Liang et al., 2008b). In addition, Dong et al. established that metal coordination within amyloid could significantly alter assembled morphology and peptide arrangement (Dong et al., 2006). Specifically, addition of Zn^{2+} to the peptide solution

(Aβ(13-21)K16A) changed the morphology from antiparallel β-sheet fibrils to parallel β-sheet tubes and ribbons by the coordination of Zn^{2+} with two N-terminal histidines revealed by solid-state NMR characterization.

Summary and the proposed strategies for pathological and nanotechnology studies

Although much is now known about the energetic contributors to β-sheet stability and lamination, the Aβ(16-22) peptide has introduced an entirely new dimension to cross-β assembly and the peptide bilayer (Figure 1-16a-d) (Mehta et al., 2008). With the extensive structure characterization by transmission electron microscopy (TEM), atomic force microscopy (AFM), circular dichroism (CD), isotope-edited infrared spectroscopy (IE-IR), small angle x-ray scattering (SAXS) and solid-state nuclear magnetic resonance (ssNMR), the 3-D structure models have been proposed for Aβ(16-22) nanotubes and fibrils (Figure1-16e, f). However, the peptide bilayer interaction may play an important role as interactions occurring in H-bonding and lamination directions, but less information has been resolved from the previous studies. Even though assembled morphology and peptide organization have been observed with peptide terminal modification (Gordon et al., 2004; Liang et al., 2008a; Lu, 2005), no systematical studies of this interaction currently exists. This prompts us to explore the structure and stability of the peptide bilayer interaction on amyloid assembly.
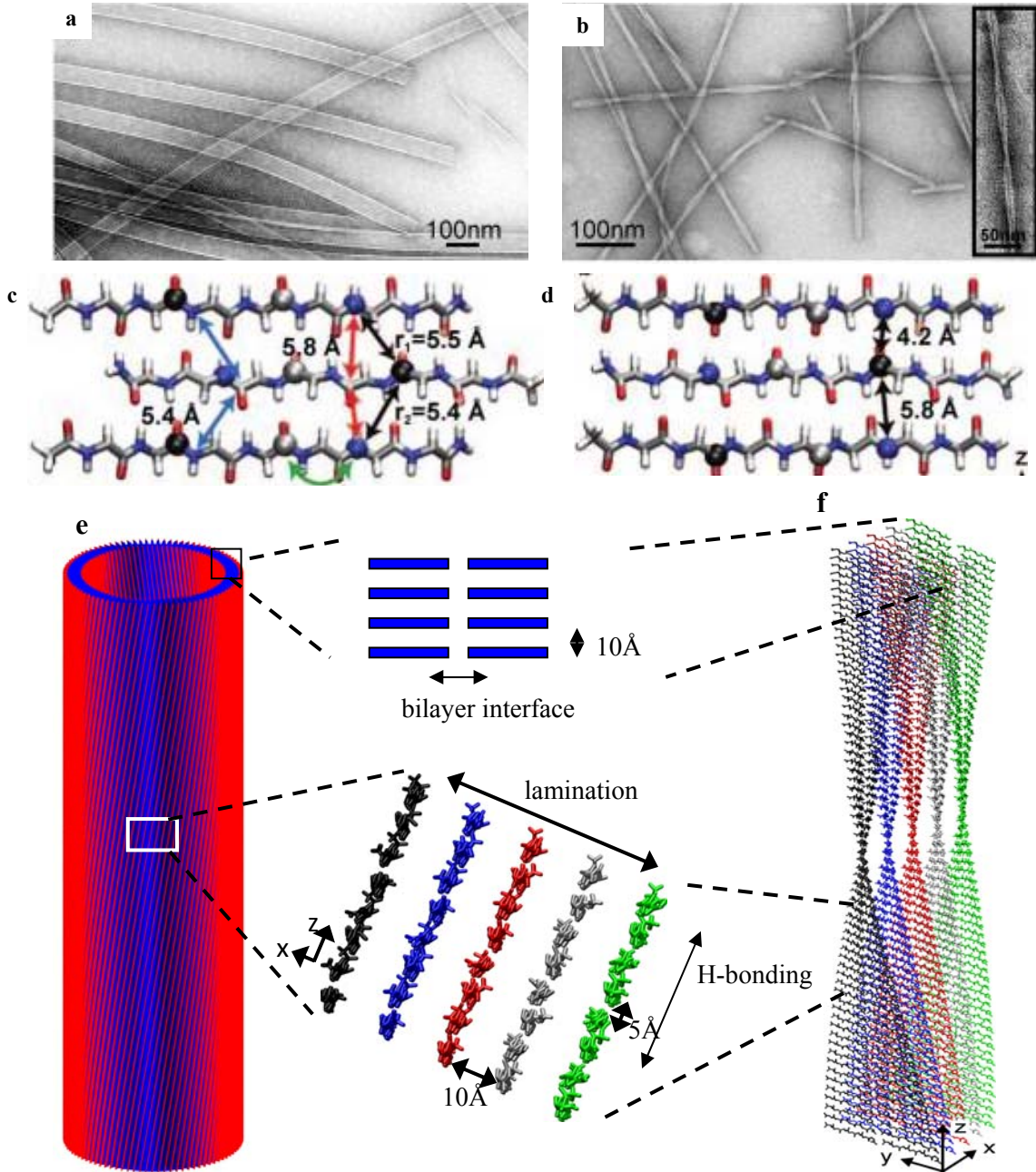
Figure 1-16. Electron micrographs of Aβ(16-22) nanotubes and fibrils, and their 3D structure models (Mehta et al., 2008).

TEM images of (a) Aβ(16-22) nanotubes assembled at acidic pH; (b) Aβ(16-22) fibrils formed at neutral pH.

Peptide β-sheet registry assigned based on ssNMR: (c) antiparallel one-residue out-of register β-sheet in nanotubes; (d) antiparallel in-register β-sheet in fibrils.

3D structure model of (e) nanotubes with H-bonding distance of 5 Å and lamination distance of 10 Å (central bottom figure), and the bilayer structure was proposed in tube wall (central upper figure); and (f)

fibrils with same H-bonding and lamination distances, as well as bilayer structure. In tubes, there are about 130 laminates, but in fibrils there are only limited (about 5 to 6) laminates. Copyright permission has been requested.

Inspired by the aforementioned peptide-amphiphiles, hybridization of peptide segments and lipid alkanes, we proposed to initiate the systematical study of peptide terminal interaction by covalently coupling Aβ(16-22) with a series of alkanes with different length and degree of branching. This approach should probe the impact of structure at the peptide bilayer on amyloid morphology and architecture, and also help to address following questions:

1) Will covalently coupled alkanes alter the assembly behavior of amyloid peptides? If amyloid peptide-lipid amphiphile forms hybrid assembly, where are the hydrophobic alkanes located?

2) With increasing the alkane length, what kind of structure transition will be produced? If there is structure switch, is it caused by the alkane steric, hydrophobic or other interactions?

3) Will tubes and fibrils share the same structural transition with same terminal modification?

4) Will alkanes play the same role when they are coupled to N or C-terminus?

5) Can the peptide layers within tube wall be tuned by peptide terminal modification?

At the same time, covalent coupling of Aβ with lipid alkanes also offer us strategy to generate a simple, intramolecular system to study the hydrophobic interaction between Aβ peptide and lipid alkanes, which may shed light on the mechanism of amyloid cytotoxicity. In addition, the mechanism of glutamine side chain H-bonding interaction on amyloid assembly has also been experimentally evaluated and Aβ(10-35) strand

31

conformation within fibrils has been identified. With this information in hand, it becomes more promising and feasible for rational design of amyloid inhibitors for the treatment of degenerative diseases, as well construction of novel nanomaterials for the development of nanotechnology.

References

AHAF, A. H. A. F. (2006). In, USA, ed. (Maryland: www.ahaf.org/alzdis/.).

Aisenbrey, C., Borowik, T., Bystrom, R., Bokvist, M., Lindstrom, F., Misiak, H., Sani, M. A., and Grobner, G. (2008). How is protein aggregation in amyloidogenic diseases modulated by biological membranes? Eur Biophys J Biophy *37*, 247-255.

Aramburu, J., Yaffe, M. B., Lopez-Rodriguez, C., Cantley, L. C., Hogan, P. G., and Rao, A. (1999). Affinity-driven peptide selection of an NFAT inhibitor more selective than cyclosporin A. Science (New York, NY *285*, 2129-2133.

Arispe, N., Diaz, J. C., and Simakova, O. (2007). Abeta ion channels. Prospects for treating Alzheimer's disease with Abeta channel blockers. Biochimica et biophysica acta *1768*, 1952-1965.

Ashley, R. H., Harroun, T. A., Hauss, T., Breen, K. C., and Bradshaw, J. P. (2006). Autoinsertion of soluble oligomers of Alzheimer's A beta(1-42) peptide into cholesterol-containing membranes is accompanied by relocation of the sterol towards the bilayer surface. Bmc Struct Biol *6*, (21) (http://www.biomedcentral.com/content/pdf/1472-6807-6-21.pdf)

Avdulov, N. A., Chochina, S. V., Igbavboa, U., O'Hare, E. O., Schroeder, F., Cleary, J. P., and Wood, W. G. (1997). Amyloid beta-peptides increase annular and bulk fluidity and induce lipid peroxidation in brain synaptic plasma membranes. J Neurochem *68*, 2086-2091.

Behanna, H. A., Donners, J. J., Gordon, A. C., and Stupp, S. I. (2005). Coassembly of amphiphiles with opposite peptide polarities into nanofibers. J Am Chem Soc *127*, 1193-1200.

Beniash, E., Hartgerink, J. D., Storrie, H., Stendahl, J. C., and Stupp, S. I. (2005). Self-assembling peptide amphiphile nanofiber matrices for cell entrapment. Acta Biomater *1*, 387-397.

Benzinger, T. L., Gregory, D. M., Burkoth, T. S., Miller-Auer, H., Lynn, D. G., Botto, R. E., and Meredith, S. C. (1998). Propagating structure of Alzheimer's beta-amyloid(10-35) is parallel beta-sheet with residues in exact register. Proc Natl Acad Sci U S A *95*, 13407-13412.

Benzinger, T. L., Gregory, D. M., Burkoth, T. S., Miller-Auer, H., Lynn, D. G., Botto, R. E., and Meredith, S. C. (2000). Two-dimensional structure of beta-amyloid(10-35) fibrils. Biochemistry *39*, 3491-3499.

Berl, V., Huc, I., Khoury, R. G., Krische, M. J., and Lehn, J. M. (2000). Interconversion of single and double helices formed from synthetic molecular strands. Nature *407*, 720-723.

Bodles, A. M., El-Agnaf, O. M., Greer, B., Guthrie, D. J., and Irvine, G. B. (2004a). Inhibition of fibril formation and toxicity of a fragment of alpha-synuclein by an N-methylated peptide analogue. Neurosci Lett *359*, 89-93.

Bodles, A. M., El-Agnaf, O. M. A., Greer, B., Guthrie, D. J. S., and Irvine, G. B. (2004b). Inhibition of fibril formation and toxicity of a fragment of alpha-synuclein by an N-methylated peptide analogue. Neurosci Lett *359*, 89-93.

Bokvist, M., and Grobner, G. (2007). Misfolding of amyloidogenic proteins at membrane surfaces: The impact of macromolecular crowding. J Am Chem Soc *129*, 14848

Bokvist, M., Lindstrom, F., Watts, A., and Grobner, G. (2004). Two types of Alzheimer's beta-amyloid (1-40) peptide membrane interactions: aggregation preventing transmembrane anchoring versus accelerated surface fibril formation. J Mol Biol *335*, 1039-1049.

Bossy-Wetzel, E., Schwarzenbacher, R., and Lipton, S. A. (2004). Molecular pathways to neurodegeneration. Nat Med, S2-S9.

Bower, P. V., Oyler, N., Mehta, M. A., Long, J. R., Stayton, P. S., and Drobny, G. P. (1999). Determination of torsion angles in proteins and peptides using solid state NMR. J Am Chem Soc *121*, 8373-8375.

Bull, S. R., Guler, M. O., Bras, R. E., Meade, T. J., and Stupp, S. I. (2005). Self-assembled peptide amphiphile nanofibers conjugated to MRI contrast agents. Nano Lett *5*, 1-4.

Burkoth, T. S., Benzinger, T. L. S., Urban, V., Morgan, D. M., Gregory, D. M., Thiyagarajan, P., Botto, R. E., Meredith, S. C., and Lynn, D. G. (2000). Structure of the beta-amyloid((10-35)) fibril. J Am Chem Soc *122*, 7883-7889.

Butterfield, D. A., Yatin, S. M., Varadarajan, S., and Koppal, T. (1999). Amyloid beta-peptide-associated free radical oxidative stress, neurotoxicity, and Alzheimer's disease. Methods in enzymology *309*, 746-768.

Cejas, M. A., Kinnney, W. A., Chen, C., Vinter, J. G., Almond, H. R., Balss, K. M., Maryanoff, C. A., Schmidt, U., Breslav, M., Mahan, A*., et al.* (2008). Thrombogenic collagen-mimetic peptides: Self-assembly of triple helix-based fibrils driven by hydrophobic interactions. Proc Natl Acad Sci USA *105*, 8513-8518.

Chauhan, A., Chauhan, V. P. S., Brockerhoff, H., and Wisniewski, H. M., ed. (1993). Alzheimer's Disease: AdVances in Clinical and Basic Research, (New York).

Chen, P. (2005). Self-assembly of ionic-complementary peptides: a physicochemical viewpoint. Colloid Surface A *261*, 3-24.

Chen, S. M., Ferrone, F. A., and Wetzel, R. (2002). Huntington's disease age-of-onset linked to polyglutamine aggregation nucleation. Proc Natl Acad Sci USA *99*, 11884-11889.

Cherny, I., and Gazit, E. (2008). Amyloids: Not only pathological agents but also ordered nanomaterials. Angew Chem Int Edit *47*, 4062-4069.

Childers, W. S. (unpublished), Emory University, 2010.

Cho, I., and Park, J. G. (1987). Giant Helical Superstructures Formed by Cationic Cholesterol-Containing Polymers. Chem Lett, 977-978.

Clark, T. D., Buriak, J. M., Kobayashi, K., Isler, M. P., McRee, D. E., and Ghadiri, M. R. (1998). Cylindrical beta-sheet peptide assemblies. J Am Chem Soc *120*, 8949-8962.

Clements, A., Walsh, D. M., Williams, C. H., and Allsop, D. (1993). Effects of the mutations Glu22 to Gln and Ala21 to Gly on the aggregation of a synthetic fragment of the Alzheimer's amyloid beta/A4 peptide. Neuroscience letters *161*, 17-20.

Cohen, A. S. C., E. (1959). Electron microscopic observation on a fibrous component in amyloid of diverse origins. Nature *183*, 1202-1203.

Costa, P. R., Kocisko, D. A., Sun, B. Q., Lansbury, P. T., and Griffin, R. G. (1997). Determination of peptide amide configuration in a model amyloid fibril by solid-state NMR. J Am Chem Soc *119*, 10487-10493.

Cui, H., Muraoka, T., Cheetham, A. G., and Stupp, S. I. (2009). Self-assembly of giant peptide nanobelts. Nano Lett *9*, 945-951.

Curtain, C. C., Ali, F. E., Smith, D. G., Bush, A. I., Masters, C. L., and Barnham, K. J. (2003). Metal ions, pH, and cholesterol regulate the interactions of Alzheimer's disease amyloid-beta peptide with membrane lipid. J Biol Chem *278*, 2977-2982.

Dante, S., Hauss, T., and Dencher, N. A. (2006). Cholesterol inhibits the insertion of the Alzheimer's peptide Abeta(25-35) in lipid bilayers. Eur Biophys J *35*, 523-531.

Davis, J., and VanNostrand, W. E. (1996). Enhanced pathologic properties of Dutch-type mutant amyloid beta-protein. Proc Natl Acad Sci USA *93*, 2996-3000.

de Planque, M. R. R., Raussens, V., Contera, S. A., Rijkers, D. T. S., Liskamp, R. M. J., Ruysschaert, J. M., Ryan, J. F., Separovic, F., and Watts, A. (2007). beta-sheet structured beta-amyloid(1-40) perturbs phosphatidylcholine model membranes. J Mol Biol *368*, 982-997.

Demuro, A., Mina, E., Kayed, R., Milton, S. C., Parker, I., and Glabe, C. G. (2005). Calcium dysregulation and membrane disruption as a ubiquitous neurotoxic mechanism of soluble amyloid oligomers. J Biol Chem *280*, 17294-17300.

Doig, A. J., Hughes, E., Burke, R. M., Su, T. J., Heenan, R. K., and Lu, J. (2002). Inhibition of toxicity and protofibril formation in the amyloid-beta peptide beta(25-35) using N-methylated derivatives. Biochemical Society transactions *30*, 537-542.

Domanov, Y. A., and Kinnunen, P. K. J. (2008). Islet amyloid polypeptide forms rigid lipid-protein amyloid fibrils on supported phospholipid bilayers. J Mol Biol *376*, 42-54.

Dong, J., Apkarian, R. P., and Lynn, D. G. (2005). Imaging amyloid beta peptide oligomeric particles in solution. Bioorg Med Chem *13*, 5213-5217.

Dong, J., Shokes, J. E., Scott, R. A., and Lynn, D. G. (2006). Modulating amyloid self-assembly and fibril morphology with Zn(II). J Am Chem Soc *128*, 3540-3542.

Durell, S. R., Guy, H. R., Arispe, N., Rojas, E., and Pollard, H. B. (1994). Theoretical-Models of the Ion-Channel Structure of Amyloid Beta-Protein. Biophys J *67*, 2137-2145.

Edelhoch, H. (1978). Protein-lipid interactions and the role of water. Horizons in biochemistry and biophysics *5*, 241-280.

Ellis-Behnke, R. G., Liang, Y. X., You, S. W., Tay, D. K., Zhang, S., So, K. F., and Schneider, G. E. (2006). Nano neuro knitting: peptide nanofiber scaffold for brain repair and axon regeneration with functional return of vision. Proc Natl Acad Sci USA *103*, 5054-5059.

Fassbender, K., Masters, C., and Beyreuther, K. (2001). Alzheimer's disease: molecular concepts and therapeutic targets. Naturwissenschaften *88*, 261-267.

Fernandez-Lopez, S., Kim, H. S., Choi, E. C., Delgado, M., Granja, J. R., Khasanov, A., Kraehenbuehl, K., Long, G., Weinberger, D. A., Wilcoxen, K. M., and Ghadiri, M. R. (2001). Antibacterial agents based on the cyclic D,L-alpha-peptide architecture (vol 412, pg 452, 2001). Nature *414*, 329-329.

Friedman, R., Pellarin, R., and Caflisch, A. (2009). Amyloid Aggregation on Lipid Bilayers and Its Impact on Membrane Permeability. J Mol Biol *387*, 407-415.

Gazit, E. (2002). A possible role for pi-stacking in the self-assembly of amyloid fibrils. Faseb J *16*, 77-83.

Ghadiri, M. R., Granja, J. R., Milligan, R. A., McRee, D. E., and Khazanovich, N. (1993). Self-assembling organic nanotubes based on a cyclic peptide architecture. Nature *366*, 324-327.

Ghosh, S., Reches, M., Gazit, E., and Verma, S. (2007). Bioinspired design of nanocages by self-assembling triskelion peptide elements. Angewandte Chemie (International ed *46*, 2002-2004.

Giacomelli, C. E., and Norde, W. (2005). Conformational changes of the amyloid beta-peptide (1-40) adsorbed on solid surfaces. Macromol Biosci *5*, 401-407.

Gorbitz, C. H. (2001). Nanotube formation by hydrophobic dipeptides. Chemistry (Weinheim an der Bergstrasse, Germany) *7*, 5153-5159.

Gorbitz, C. H. (2006). The structure of nanotubes formed by diphenylalanine, the core recognition motif of Alzheimer's beta-amyloid polypeptide. Chemical communications (Cambridge, England), 2332-2334.

Gordon, D. J., Balbach, J. J., Tycko, R., and Meredith, S. C. (2004). Increasing the amphiphilicity of an amyloidogenic peptide changes the beta-sheet structure in the fibrils from antiparallel to parallel. Biophys J *86*, 428-434.

Gordon, D. J., and Meredith, S. C. (2003). Probing the role of backbone hydrogen bonding in beta-amyloid fibrils with inhibitor peptides containing ester bonds at alternate positions. Biochemistry *42*, 475-485.

Gregory, D. M., Mehta, M. A., Shiels, J. C., and Drobny, G. P. (1997). Determination of local structure in solid nucleic acids using double quantum nuclear magnetic resonance spectroscopy. J Chem Phys *107*, 28-42.

Guler, M. O., Pokorski, J. K., Appella, D. H., and Stupp, S. I. (2005). Enhanced oligonucleotide binding to self-assembled nanofibers. Bioconjugate Chem *16*, 501-503.

Haines, L. A., Rajagopal, K., Ozbas, B., Salick, D. A., Pochan, D. J., and Schneider, J. P. (2005). Light-activated hydrogel formation via the triggered folding and self-assembly of a designed peptide. J Am Chem Soc *127*, 17025-17029.

Hardy, J., and Selkoe, D. J. (2002). Medicine - The amyloid hypothesis of Alzheimer's disease: Progress and problems on the road to therapeutics. Science *297*, 353-356.

Hartgerink, J. D., Beniash, E., and Stupp, S. I. (2001). Self-assembly and mineralization of peptide-amphiphile nanofibers. Science *294*, 1684-1688.

Hartgerink, J. D., Beniash, E., and Stupp, S. I. (2002). Peptide-amphiphile nanofibers: a versatile scaffold for the preparation of self-assembling materials. Proc Natl Acad Sci U S A *99*, 5133-5138.

Hebda, J. A., and Miranker, A. D. (2009). The Interplay of Catalysis and Toxicity by Amyloid Intermediates on Lipid Bilayers: Insights from Type II Diabetes. Ann Rev Biophys *38*, 125-152.

Hirakura, Y., Lin, M. C., and Kagan, B. L. (1999). Alzheimer amyloid abeta1-42 channels: effects of solvent, pH, and Congo Red. J Neurosci Res *57*, 458-466.

Holmes, T. C. (2002). Novel peptide-based biomaterial scaffolds for tissue engineering. Trends in biotechnology *20*, 16-21.

Horne, W. S., Ashkenasy, N., and Ghadiri, M. R. (2005a). Modulating charge transfer through cyclic D,L-alpha-peptide self-assembly. Chem-Eur J *11*, 1137-1144.

Horne, W. S., Ashkenasy, N., and Ghadiri, M. R. (2005b). Modulating charge transfer through cyclic D,L-alpha-peptide self-assembly. Chemistry (Weinheim an der Bergstrasse, Germany) *11*, 1137-1144.

Hosseinkhani, H., Hosseinkhani, M., and Kobayashi, H. (2006). Design of tissue-engineered nanoscaffold through self-assembly of peptide amphiphile. J Bioact Compat Pol *21*, 277-296.

Hsu, L., Cvetanovich, G. L., and Stupp, S. I. (2008). Peptide amphiphile nanofibers with conjugated polydiacetylene backbones in their core. J Am Chem Soc *130*, 3892-3899.

Hughes, E., Burke, R. M., and Doig, A. J. (2000). Inhibition of toxicity in the beta-amyloid peptide fragment beta -(25-35) using N-methylated derivatives: a general strategy to prevent amyloid formation. J Biol Chem *275*, 25109-25115.

Hughes, E., Burke, R. M., and Doig, A. J. (2001). Inhibition of toxicity in the beta-amyloid peptide fragment beta(25-35) using N-methylated derivatives - a general strategy to prevent amyloid formation. J Neurochem *77*, 10-10.

Ihara, H., Fukumoto, T., Hirayama, C., and Yamada, K. (1986). Exceptional Morphologies and Metamorphosis of Bilayer-Membranes Formed from Amphiphiles with Poly(L-Aspartic Acid)-Head Groups. Polym Commun *27*, 282-285.

Ihara, H., Sakurai, T., Yamada, T., Hashimoto, T., Takafuji, M., Sagawa, T., and Hachisako, H. (2002). Chirality control of self-assembling organogels from a lipophilic L-glutamide derivative with metal chlorides. Langmuir *18*, 7120-7123.

Ikeda, K., and Matsuzaki, K. (2008). Driving force of binding of amyloid beta-protein to lipid bilayers. Biochem Bioph Res Co *370*, 525-529.

Ishida, H., Qi, Z., Sokabe, M., Donowaki, K., and Inoue, Y. (2001). Molecular design and synthesis of artificial ion channels based on cyclic peptides containing unnatural amino acids. J Org Chem *66*, 2978-2989.

Jack, E., Newsome, M., Stockley, P. G., Radford, S. E., and Middleton, D. A. (2006). The organization of aromatic side groups in an amyloid fibril probed by solid-state H-2 and F-19 NMR spectroscopy. J Am Chem Soc *128*, 8098-8099.

Jahn, T. R., and Radford, S. E. (2008). Folding versus aggregation: polypeptide conformations on competing pathways. Arch Biochem Biophys *469*, 100-117.

Jin, Y. G., Qiao, Y. X., Li, M., Ai, P., and Hou, X. P. (2005). Langmuir monolayers of the long-chain alkyl derivatives of a nucleoside analogue and the formation of self-assembled nanoparticles. Colloid Surface B *42*, 45-51.

Kakio, A., and Matsuzaki, K. (2003). Formation of a membrane-active form of amyloid beta-protein (A beta) via lipid raft. Biophys J *84*, 155a-155a.

Kakio, A., Nishimoto, S., Yanagisawa, K., Kozutsumi, Y., and Matsuzaki, K. (2002). Interactions of amyloid beta-protein with various gangliosides in raft-like membranes: Importance of GM1 ganglioside-bound form as an endogenous seed for Alzheimer amyloid. Biochemistry *41*, 7385-7390.

Kammerer, R. A., Kostrewa, D., Zurdo, J., Detken, A., Garcia-Echeverria, C., Green, J. D., Muller, S. A., Meier, B. H., Winkler, F. K., Dobson, C. M., and Steinmetz, M. O. (2004). Exploring amyloid formation by a de novo design. Proc Natl Acad Sci USA *101*, 4435-4440.

Kawahara, M., Kuroda, Y., Arispe, N., and Rojas, E. (2000). Alzheimer's beta-amyloid, human islet amylin, and prion protein fragment evoke intracellular free calcium elevations by a common mechanism in a hypothalamic GnRH neuronal cell line. J Biol Chem *275*, 14077-14083.

Khoe, U., Yang, Y. L., and Zhang, S. G. (2009). Self-Assembly of Nanodonut Structure from a Cone-Shaped Designer Lipid-like Peptide Surfactant. Langmuir *25*, 4111-4114.

Kiley, P., Zhao, X., Vaughn, M., Baldo, M. A., Bruce, B. D., and Zhang, S. (2005). Self-assembling peptide detergents stabilize isolated photosystem I on a dry surface for an extended time. PLoS Biol *3*, e230.

Kim, W., and Hecht, M. H. (2006). Generic hydrophobic residues are sufficient to promote aggregation of the Alzheimer's Abeta42 peptide. Proc Natl Acad Sci USA *103*, 15824-15829.

Kinnunen, P. K. J. (2009). Amyloid Formation on Lipid Membrane Surfaces. The Open Biology Journal *2*, 163-175.

Klimov, D. K., and Thirumalai, D. (2003). Dissecting the assembly of Abeta16-22 amyloid peptides into antiparallel beta sheets. Structure *11*, 295-307.

Knight, J. D., Hebda, J. A., and Miranker, A. D. (2006). Conserved and cooperative assembly of membrane-bound alpha-helical states of islet amyloid polypeptide. Biochemistry *45*, 9496-9508.

Kojro, E., Gimpl, G., Lammich, S., Marz, W., and Fahrenholz, F. (2001). Low cholesterol stimulates the nonamyloidogenic pathway by its effect on the alpha - secretase ADAM 10. Proc Natl Acad Sci U S A *98*, 5815-5820.

Koudinov, A. R., Berezov, T. T., and Koudinova, N. V. (1998). Alzheimer's amyloid beta and lipid metabolism: a missing link? Faseb J *12*, 1097-1099.

Koudinova NV, K. A., Berezov TT, Koudinova AR (2003). Amyloid beta, neural lipids, cholesterol and Alzheimer's disease. Neurobiol Lipids *1*, 28-33.

Kourie, J. I., Culverson, A. L., Farrelly, P. V., Henry, C. L., and Laohachai, K. N. (2002). Heterogeneous amyloid-formed ion channels as a common cytotoxic mechanism - Implications for therapeutic strategies against amyloidosis. Cell Biochem Biophys *36*, 191-207.

Kremer, J. J., Pallitto, M. M., Sklansky, D. J., and Murphy, R. M. (2000). Correlation of beta-amyloid aggregate size and hydrophobicity with decreased bilayer fluidity of model membranes. Biochemistry *39*, 10309-10318.

Kremer, J. J., Sklansky, D. J., and Murphy, R. M. (2001). Profile of changes in lipid bilayer structure caused by beta-amyloid peptide. Biochemistry *40*, 8563-8571.

Kun Lu, V. P. C., and David G. Lynn (2004). Templating colloidal metal nanoparticle assemblies: use of the Abeta amyloid peptide nanotube. Mater Res Soc Synp Proc *1.6*.

Kunitake, T., Nakashima, N., Shimomura, M., Okahata, Y., Kano, K., and Ogawa, T. (1980). Unique Properties of Chromophore-Containing Bilayer Aggregates - Enhanced Chirality and Photochemically Induced Morphological Change. J Am Chem Soc *102*, 6642-6644.

LaFerla, F. M., Green, K. N., and Oddo, S. (2007). Intracellular amyloid-beta in Alzheimer's disease. Nature reviews *8*, 499-509.

Lakdawala, A. S. Ph.D. Thesis, Emory University, Atlanta, GA, USA (2003).

Lau, T. L., Ambroggio, E. E., Tew, D. J., Cappai, R., Masters, C. L., Fidelio, G. D., Barnham, K. J., and Separovic, F. (2006). Amyloid-beta peptide disruption of lipid membranes and the effect of metal ions. J Mol Biol *356*, 759-770.

Lehtonen, J. Y., Holopainen, J. M., and Kinnunen, P. K. (1996). Activation of phospholipase A2 by amyloid beta-peptides in vitro. Biochemistry *35*, 9407-9414.

Lemkul, J. A., and Bevan, D. R. (2008). A comparative molecular dynamics analysis of the amyloid beta-peptide in a lipid bilayer. Arch Biochem Biophys *470*, 54-63.

Leon, E. J., Verma, N., Zhang, S. G., Lauffenburger, D. A., and Kamm, R. D. (1998). Mechanical properties of a self-assembling oligopeptide matrix. J Biomat Sci-Polym E *9*, 297-312.

Liang, Y., Guo, P., Pingali, S. V., Pabit, S., Thiyagarajan, P., Berland, K. M., and Lynn, D. G. (2008a). Light harvesting antenna on an amyloid scaffold. Chem Commun (Camb), 6522-6524.

Liang, Y., Pingali, S. V., Jogalekar, A. S., Snyder, J. P., Thiyagarajan, P., and Lynn, D. G. (2008b). Cross-strand pairing and amyloid assembly. Biochemistry *47*, 10018-10026.

Lin, H., Bhatia, R., and Lal, R. (2002). Amyloid beta protein forms ion channels: implications for Alzheimer's disease pathophysiology (vol 15, pg 2433, 2001). Faseb Journal *16*

Lin, H., Zhu, Y. J., and Lal, R. (1999). Amyloid beta protein (1-40) forms calcium-permeable, Zn2+-sensitive channel in reconstituted lipid vesicles. Biochemistry *38*, 11189-11196.

Liu, P., Ni, R., Mehta, A. K., Childers, W. S., Lakdawala, A., Pingali, S. V., Thiyagarajan, P., and Lynn, D. G. (2008). Nucleobase-directed amyloid nanotube assembly. J Am Chem Soc *130*, 16867-16869.

Lopes, D. H. J., Meister, A., Gohlke, A., Hauser, A., Blume, A., and Winter, R. (2007). Mechanism of islet amyloid polypeptide fibrillation at lipid interfaces studied by infrared reflection absorption spectroscopy. Biophys J *93*, 3132-3141.

Lu, J. R., Swann, M. J., Peel, L. L., and Freeman, N. J. (2004). Lysozyme adsorption studies at the silica/water interface using dual polarization interferometry. Langmuir *20*, 1827-1832.

Lu, K. (2005) Discovery of Diverse Peptide Nanotube Architecture from the Self-assembly of Designed Amyloid Cassettes, Ph.D. Thesis, Emory University, Atlanta, GA, USA.

Lu, K., Jacob, J., Thiyagarajan, P., Conticello, V. P., and Lynn, D. G. (2003). Exploiting amyloid fibril lamination for nanotube self-assembly. J Am Chem Soc *125*, 6391-6393.

Lvov, Y. M., Price, R. R., Selinger, J. V., Singh, A., Spector, M. S., and Schnur, J. M. (2000). Imaging nanoscale patterns on biologically derived microstructures. Langmuir *16*, 5932-5935.

Mahalka, A. K., and Kinnunen, P. K. J. (2009). Binding of amphipathic alpha-helical antimicrobial peptides to lipid membranes: Lessons from temporins B and L. Bba-Biomembranes *1788*, 1600-1609.

Makin, O. S., Atkins, E., Sikorski, P., Johansson, J., and Serpell, L. C. (2005). Molecular basis for amyloid fibril formation and stability. Proc Natl Acad Sci USA *102*, 315-320.

Marchut, A. J., and Hall, C. K. (2006). Side-chain interactions determine amyloid formation by model polyglutamine peptides in molecular dynamics simulations. Biophys J *90*, 4574-4584.

Mason, R. P., Jacob, R. F., Walter, M. F., Mason, P. E., Avdulov, N. A., Chochina, S. V., Igbavboa, U., and Wood, W. G. (1999). Distribution and fluidizing action of soluble and aggregated amyloid beta-peptide in rat synaptic plasma membranes. J Biol Chem *274*, 18801-18807.

Massi, F., and Straub, J. E. (2001). Probing the origins of increased activity of the E22Q "Dutch" mutant Alzheimer's beta-amyloid peptide. Biophys J *81*, 697-709.

McLaurin, J., and Chakrabartty, A. (1997). Characterization of the interactions of Alzheimer beta-amyloid peptides with phospholipid membranes. European journal of biochemistry / FEBS *245*, 355-363.

Mega, M. S. C., J. L.; Fiorello, T.; Gornbein, J. (1996). The spectrum of behavioral changes in Alzheimer's disease. Neurology *46*, 130-135.

Mehta, A. K., Lu, K., Childers, W. S., Liang, Y., Dublin, S. N., Dong, J., Snyder, J. P., Pingali, S. V., Thiyagarajan, P., and Lynn, D. G. (2008). Facial symmetry in protein self-assembly. J Am Chem Soc *130*, 9829-9835.

Mihara, H., Matsumura, S., and Takahashi, T. (2005). Construction and control of self-assembly of amyloid and fibrous peptides. B Chem Soc Jpn *78*, 572-590.

Morgan, D. M., Dong, J., Jacob, J., Lu, K., Apkarian, R. P., Thiyagarajan, P., and Lynn, D. G. (2002). Metal switch for amyloid formation: insight into the structure of the nucleus. J Am Chem Soc *124*, 12644-12645.

Muller, W. E., Eckert, G. P., Scheuer, K., Cairns, N. J., Maras, A., and Gattaz, W. F. (1998). Effects of beta-amyloid peptides on the fluidity of membranes from frontal and parietal lobes of human brain. High potencies of A beta 1-42 and A beta 1-43. Amyloid *5*, 10-15.

Muller, W. E., Koch, S., Eckert, A., Hartmann, H., and Scheuer, K. (1995). beta-Amyloid peptide decreases membrane fluidity. Brain Res *674*, 133-136.

Munishkina, L. A., and Fink, A. L. (2007). Fluorescence as a method to reveal structures and membrane-interactions of amyloidogenic proteins. Bba-Biomembranes *1768*, 1862-1885.

National Institute on Aging, N. The Beta Amyloid. In, (USA: www.web-books.com/.../ Alzheimer_Amyloid.htm).

Norman, T. C., Smith, D. L., Sorger, P. K., Drees, B. L., O'Rourke, S. M., Hughes, T. R., Roberts, C. J., Friend, S. H., Fields, S., and Murray, A. W. (1999). Genetic selection of peptide inhibitors of biological pathways. Science (New York, NY *285*, 591-595.

Nowak, A. P., Breedveld, V., Pakstis, L., Ozbas, B., Pine, D. J., Pochan, D., and Deming, T. J. (2002). Rapidly recovering hydrogel scaffolds from self-assembling diblock copolypeptide amphiphiles. Nature *417*, 424-428.

Palmer, L. C., and Stupp, S. I. (2008). Molecular self-assembly into one-dimensional nanostructures. Acc Chem Res *41*, 1674-1684.

Paramonov, S. E., Jun, H. W., and Hartgerink, J. D. (2006). Self-assembly of peptide-amphiphile nanofibers: The roles of hydrogen bonding and amphiphilic packing. J Am Chem Soc *128*, 7291-7298.

Pastor, M. T., Kummerer, N., Schubert, V., Esteras-Chopo, A., Dotti, C. G., de la Paz, M. L., and Serrano, L. (2008). Amyloid toxicity is independent of polypeptide sequence, length and chirality. J Mol Biol *375*, 695-707.

Petka, W. A., Harden, J. L., McGrath, K. P., Wirtz, D., and Tirrell, D. A. (1998). Reversible hydrogels from self-assembling artificial proteins. Science *281*, 389-392.

Petkova, A. T., Ishii, Y., Balbach, J. J., Antzutkin, O. N., Leapman, R. D., Delaglio, F., and Tycko, R. (2002). A structural model for Alzheimer's beta -amyloid fibrils based on experimental constraints from solid state NMR. Proc Natl Acad Sci U S A *99*, 16742-16747.

Petkova, A. T., Yau, W. M., and Tycko, R. (2006). Experimental constraints on quaternary structure in Alzheimer's beta-amyloid fibrils. Biochemistry *45*, 498-512.

Plumley, J. A., and Dannenberg, J. J. (2010). The importance of hydrogen bonding between the glutamine side chains to the formation of amyloid VQIVYK parallel beta-sheets: an ONIOM DFT/AM1 study. J Am Chem Soc *132*, 1758-1759.

Quist, A., Doudevski, I., Lin, H., Azimova, R., Ng, D., Frangione, B., Kagan, B., Ghiso, J., and Lal, R. (2005a). Amyloid ion channels: a common structural link for protein-misfolding disease. Proc Natl Acad Sci U S A *102*, 10427-10432.

Quist, A., Doudevski, L., Lin, H., Azimova, R., Ng, D., Frangione, B., Kagan, B., Ghiso, J., and Lal, R. (2005b). Amyloid ion channels: A common structural link for protein-misfolding disease. Proc Natl Acad Sci USA *102*, 10427-10432.

Ramstrom, O., Bunyapaiboonsri, T., Lohmann, S., and Lehn, J. M. (2002). Chemical biology of dynamic combinatorial libraries. Biochim Biophys Acta *1572*, 178-186.

Reches, M., and Gazit, E. (2003). Casting metal nanowires within discrete self-assembled peptide nanotubes. Science (New York, NY *300*, 625-627.

Robertson, J. D., ed. (2002). Cell membranes, (McGraw-Hill Encyclopedia of Science & Technology, 9th ed.).

Santoso, S., Hwang, W., Hartman, H., and Zhang, S. G. (2002). Self-assembly of surfactant-like peptides with variable glycine tails to form nanotubes and nanovesicles. Nano Lett *2*, 687-691.

Scheibel, T., Parthasarathy, R., Sawicki, G., Lin, X. M., Jaeger, H., and Lindquist, S. L. (2003). Conducting nanowires built by controlled self-assembly of amyloid fibers and selective metal deposition. Proc Natl Acad Sci USA *100*, 4527-4532.

Schneider, J., Messerschmidt, C., Schulz, A., Gnade, M., Schade, B., Luger, P., Bombicz, P., Hubert, V., and Fuhrhop, J. H. (2000). Odd-even effects in supramolecular assemblies of diamide bolaamphiphiles. Langmuir *16*, 8575-8584.

Schneider, J. P., Pochan, D. J., Ozbas, B., Rajagopal, K., Pakstis, L., and Kretsinger, J. (2002). Responsive hydrogels from the intramolecular folding and self-assembly of a designed peptide. J Am Chem Soc *124*, 15030-15037.

Seelig, J. (2004). Thermodynamics of lipid-peptide interactions. Bba-Biomembranes *1666*, 40-50.

Seeman, N. C. (2003). DNA in a material world. Nature *421*, 427-431.

Seeman, N. C. (2004). Nanotechnology and the double helix. Sci Am *290*, 64-69, 72-65.

Sekijima, Y., Wiseman, R. L., Matteson, J., Hammarstrom, P., Miller, S. R., Sawkar, A. R., Balch, W. E., and Kelly, J. W. (2005). The biological and chemical basis for tissue-selective amyloid disease. Cell *121*, 73-85.

Selinger, J. V., MacKintosh, F. C., and Schnur, J. M. (1996). Theory of cylindrical tubules and helical ribbons of chiral lipid membranes. Physical review *53*, 3804-3818.

Selkoe, D. J. (1991a). Amyloid protein and Alzheimer's disease. Sci Am *265*, 68-71.

Selkoe, D. J. (1991b). The molecular pathology of Alzheimer's disease. Neuron *6*, 487-498.

Selkoe, D. J. (2004). Cell biology of protein misfolding: The examples of Alzheimer's and Parkinson's diseases. Nat Cell Biol *6*, 1054-1061.

Selkoe, D. J. (2006). The ups and downs of A beta. Nat Med *12*, 758-759.

Serpell, L. C. (2000). Alzheimer's amyloid fibrils: structure and assembly. Bba-Mol Basis Dis *1502*, 16-30.

Shai, Y. (2002). Mode of action of membrane active antimicrobial peptides. Biopolymers *66*, 236-248.

Shultz, M. D., Bowman, M. J., Ham, Y. W., Zhao, X. M., Tora, G., and Chmielewski, J. (2000). Small-molecule inhibitors of HIV-1 protease dimerization derived from cross-linked interfacial peptides. Angew Chem Int Edit *39*, 2710-2713.

Silva, G. A., Czeisler, C., Niece, K. L., Beniash, E., Harrington, D. A., Kessler, J. A., and Stupp, S. I. (2004). Selective differentiation of neural progenitor cells by high-epitope density nanofibers. Science (New York, NY *303*, 1352-1355.

Simakova, O., and Arispe, N. J. (2006). Early and late cytotoxic effects of external application of the Alzheimer's A beta result from the initial formation and function of A beta ion channels. Biochemistry *45*, 5907-5915.

Simons, M., Keller, P., De Strooper, B., Beyreuther, K., Dotti, C. G., and Simons, K. (1998). Cholesterol depletion inhibits the generation of beta-amyloid in hippocampal neurons. Proc Natl Acad Sci USA *95*, 6460-6464.

Skinner, P. J., Klement, I. A., Clark, H. B., Zoghbi, H. Y., and Orr, H. T. (1998). Molecular pathogenesis of a polyglutamine neurological disease: nuclear localization and aggregation in SCA1 transgenic mice. Brain Res *809*, A11-A11.

Sone, E. D., and Stupp, S. I. (2004). Semiconductor-encapsulated peptide-amphiphile nanofibers. J Am Chem Soc *126*, 12756-12757.

Song, Y., Challa, S. R., Medforth, C. J., Qiu, Y., Watt, R. K., Pena, D., Miller, J. E., van Swol, F., and Shelnutt, J. A. (2004). Synthesis of peptide-nanotube platinum-nanoparticle composites. Chemical communications (Cambridge, England), 1044-1045.

Sood, R., Domanov, Y., Pietiainen, M., Kontinen, V. P., and Kinnunen, P. K. J. (2008). Binding of LL-37 to model biomembranes: Insight into target vs host cell recognition. Bba-Biomembranes *1778*, 983-996.

Soto, C. (2001). Protein misfolding and disease; protein refolding and therapy. Febs Lett *498*, 204-207.

Spector, M. S., Easwaran, K. R., Jyothi, G., Selinger, J. V., Singh, A., and Schnur, J. M. (1996). Chiral molecular self-assembly of phospholipid tubules: a circular dichroism study. Proc Natl Acad Sci USA *93*, 12943-12946.

Spencer, R. G. S., Halverson, K. J., Auger, M., Mcdermott, A. E., Griffin, R. G., and Lansbury, P. T. (1991). An Unusual Peptide Conformation May Precipitate Amyloid Formation in Alzheimers-Disease - Application of Solid-State Nmr to the Determination of Protein Secondary Structure. Biochemistry *30*, 10382-10387.

Stine, W. B., Dahlgren, K. N., Krafft, G. A., and LaDu, M. J. (2003). In vitro characterization of conditions for amyloid-beta peptide oligomerization and fibrillogenesis. J Biol Chem *278*, 11612-11622.

Terzi, E., Holzemann, G., and Seelig, J. (1994). Reversible random coil-beta-sheet transition of the Alzheimer beta-amyloid fragment (25-35). Biochemistry *33*, 1345-1350.

Terzi, E., Holzemann, G., and Seelig, J. (1997). Interaction of Alzheimer beta-amyloid peptide(1-40) with lipid membranes. Biochemistry *36*, 14845-14852.

Tischer, E., and Cordell, B. (1996). Beta-amyloid precursor protein. Location of transmembrane domain and specificity of gamma-secretase cleavage. J Biol Chem *271*, 21914-21919.

Tysseling-Mattiace, V. M., Sahni, V., Niece, K. L., Birch, D., Czeisler, C., Fehlings, M. G., Stupp, S. I., and Kessler, J. A. (2008). Self-assembling nanofibers inhibit glial scar formation and promote axon elongation after spinal cord injury. J Neurosci *28*, 3814-3823.

Vauthey, S., Santoso, S., Gong, H., Watson, N., and Zhang, S. (2002). Molecular self-assembly of surfactant-like peptides to form nanotubes and nanovesicles. Proc Natl Acad Sci U S A *99*, 5355-5360.

Vestergaard M, K. K., Tamiya E. (2006). The study of Alzheimer's disease biomarkers: Current role and future prospects of nanosensor technology. NanoBiotechnology *2*, 5-16.

von Maltzahn, G., Vauthey, S., Santoso, S., and Zhang, S. U. (2003). Positively charged surfactant-like peptides self-assemble into nanostructures. Langmuir *19*, 4332-4337.

Walsh, D. M., Tseng, B. P., Rydel, R. E., Podlisny, M. B., and Selkoe, D. J. (2000). The oligomerization of amyloid beta-protein begins intracellularly in cells derived from human brain. Biochemistry *39*, 10831-10839.

Weiming Xia, H. X. (2004). Amyloid Precursor Protein: A Practical Approach. In, C. Press, ed.

Wieprecht, T., Apostolov, O., Beyermann, M., and Seelig, J. (2000). Membrane binding and pore formation of the antibacterial peptide PGLa: Thermodynamic and mechanistic aspects. Biochemistry *39*, 442-452.

Wong, P. T., Schauerte, J. A., Wisser, K. C., Ding, H., Lee, E. L., Steel, D. G., and Gafni, A. (2009). Amyloid-beta Membrane Binding and Permeabilization are Distinct Processes Influenced Separately by Membrane Charge and Fluidity. J Mol Biol *386*, 81-96.

Wood, W. G., Eckert, G. P., Igbavboa, U., and Muller, W. E. (2003). Amyloid beta-protein interactions with membranes and cholesterol: causes or casualties of Alzheimer's disease. Bba-Biomembranes *1610*, 281-290.

Yamada, K., Ihara, H., Ide, T., Fukumoto, T., and Hirayama, C. (1984). Formation of Helical Super Structure from Single-Walled Bilayers by Amphiphiles with Oligo-L-Glutamic Acid-Head Group. Chem Lett, 1713-1716.

Yan, X., He, Q., Wang, K., Duan, L., Cui, Y., and Li, J. (2007a). Transition of cationic dipeptide nanotubes into vesicles and oligonucleotide delivery. Angewandte Chemie (International ed *46*, 2431-2434.

Yan, X. H., He, Q., Wang, K. W., Duan, L., Cui, Y., and Li, J. B. (2007b). Transition of cationic dipeptide nanotubes into vesicles and oligonucleotide delivery. Angew Chem Int Edit *46*, 2431-2434.

Yanagawa, H., Ogawa, Y., Furuta, H., and Tsuno, K. (1989). Spontaneous Formation of Superhelical Strands. J J Am Chem Soc *111*, 4567-4570.

Yang, S. J., and Zhang, S. G. (2006). Self-assembling behavior of designer lipid-like peptides. Supramol Chem *18*, 389-396.

Yip, C. M., Elton, E. A., Darabie, A. A., Morrison, M. R., and McLaurin, J. (2001). Cholesterol, a modulator of membrane-associated Abeta-fibrillogenesis and neurotoxicity. J Mol Biol *311*, 723-734.

Yip, C. M., and McLaurin, J. (2001). Amyloid-beta peptide assembly: A critical step in fibrillogenesis and membrane disruption. Biophys J *80*, 1359-1371.

Yuwono, V. M., and Hartgerink, J. D. (2007). Peptide amphiphile nanofibers template and catalyze silica nanotube formation. Langmuir *23*, 5033-5038.

Zhang, S. G. (2003). Fabrication of novel biomaterials through molecular self-assembly. Nature Biotechnology *21*, 1171-1178.

Zhang, S. G., Holmes, T., Lockshin, C., and Rich, A. (1993). Spontaneous Assembly of a Self-Complementary Oligopeptide to Form a Stable Macroscopic Membrane. Proc Natl Acad Sci USA *90*, 3334-3338.

Zhang, S. G., Holmes, T. C., Dipersio, C. M., Hynes, R. O., Su, X., and Rich, A. (1995). Self-Complementary Oligopeptide Matrices Support Mammalian-Cell Attachment. Biomaterials *16*, 1385-1393.

Zhao, H., Sood, R., Jutila, A., Bose, S., Fimland, G., Nissen-Meyer, J., and Kinnunen, P. K. J. (2006a). Interaction of the antimicrobial peptide pheromone Plantaricin A with model membranes: Implications for a novel mechanism of action. Bba-Biomembranes *1758*, 1461-1474.

Zhao, H. X., Jutila, A., Nurminen, T., Wickstrom, S. A., Keski-Oja, J., and Kinnunen, P. K. J. (2005). Binding of endostatin to phosphatidylserine-containing membranes and formation of amyloid-like fibers. Biochemistry *44*, 2857-2863.

Zhao, H. X., Tuominen, E. K. J., and Kinnunen, P. K. J. (2004). Formation of amyloid fibers triggered by phosphatidylserine-containing membranes. Biochemistry *43*, 10302-10307.

Zhao, X., Nagai, Y., Reeves, P. J., Kiley, P., Khorana, H. G., and Zhang, S. (2006b). Designer short peptide surfactants stabilize G protein-coupled receptor bovine rhodopsin. Proc Natl Acad Sci U S A *103*, 17707-17712.

Zhao, X. J., and Zhang, S. G. (2006). Molecular designer self-assembling peptides. Chem Soc Rev *35*, 1105-1110.

Zimenkov, Y., Dublin, S. N., Ni, R., Tu, R. S., Breedveld, V., Apkarian, R. P., and Conticello, V. P. (2006). Rational design of a reversible pH-responsive switch for peptide self-assembly. J Am Chem Soc *128*, 6770-6771.

Zutshi, R., and Chmielewski, J. (2000). Targeting the dimerization interface for irreversible inhibition of HIV-1 protease. Bioorg Med Chem Lett *10*, 1901-1903.

CHAPTER 2

Amyloid Peptide / Lipid Chimeras Dictate Parallel β-Sheet Assembly: the Role of Electrostatics

Introduction

The peptide fragment Aβ of the APP protein associated with Alzheimer's disease is created within neurons and assembles at the membrane phospholipid aqueous interface. Disruption of plasma membrane function, through the interaction between lipid and amyloid peptide, may be the central to neurotoxicity of amyloid in amyloid-related diseases (Anguiano et al., 2002; Demuro et al., 2005; Janson et al., 1999). The structural characterization of any co-assemblies of Aβ with phospholipid *in vivo* is very limited. Fortunately, Aβ does assemble *in vitro*, which offers great opportunity to study the interaction of lipids with Aβ (Domanov and Kinnunen, 2008) during and following assembly. In that regard, Meredith et. al (Gordon et al., 2004) covalently attached simple linear alkane fatty acids to the central core of Aβ peptide and found that introduction of octanoyl group at the N-terminus of Aβ(16-22) (N-octanoyl-Aβ(16-22)) switched the peptide orientation from antiparallel to parallel at neutral pH. They proposed that hydrophobic interaction between alkyl chains overwhelmed the charge repulsions from N-Lysine and C-Glutamate residues to direct the peptide orientation (Beniash et al., 2005; Bull et al., 2005; Gordon et al., 2004; Hartgerink et al., 2001; Hartgerink et al., 2002).

The studies by Meredith et al did not consider the β-sheets stacking interactions that are essential to fibril assembly and stability, nor did they localize the alkyl chains within the assemblies. Several possible stacking arrangements might operate with specific alkyl chain positions and conformations, as precedented in the literature models such as cylindrical "worm-like" micelle fibril model (Hartgerink et al., 2001; Hartgerink et al., 2002) and β-sheet bilayer models (Lu et al., 2003; Mehta et al., 2008). In all of these
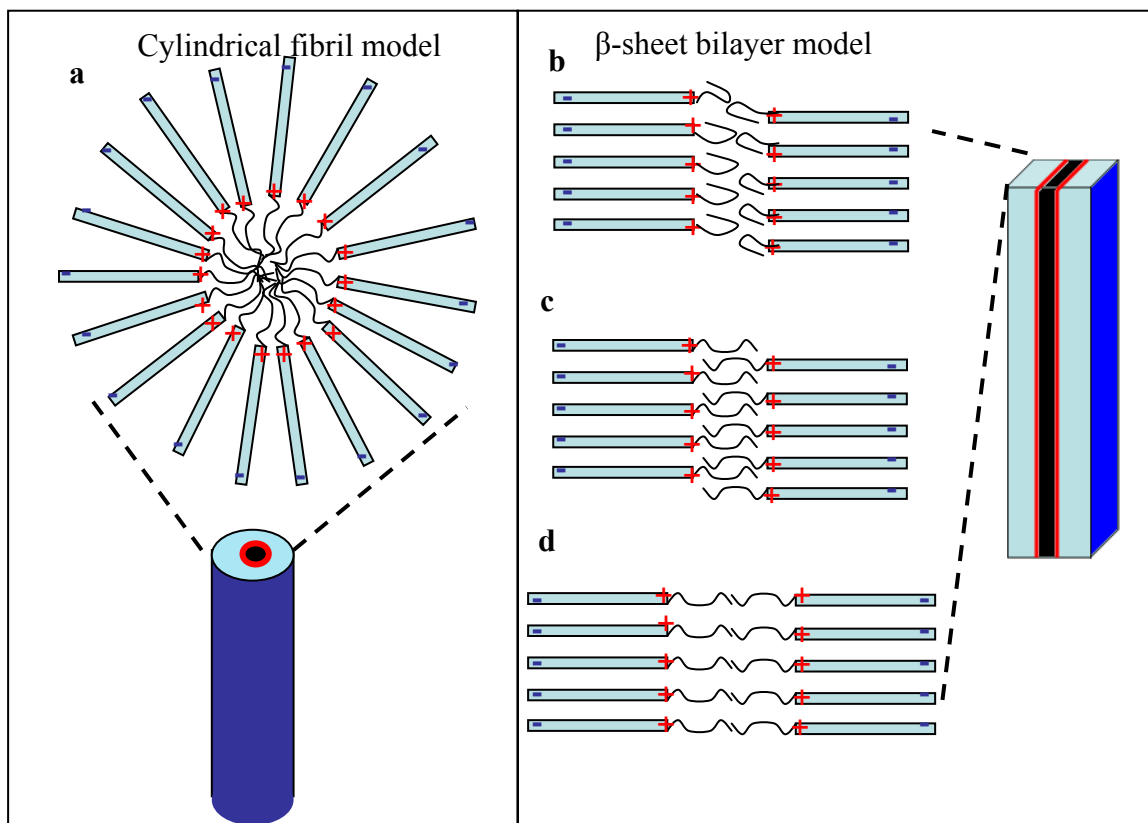
Figure 2-1. Structural models proposed for fibrils with N-terminal long alkyl chain.

In cylindrical fibril, (a) all the alkyl chains are buried in the center of fibrils with positive charges (red).

In the parallel β-sheet bilayer models, all the alkyl chains are buried in the bilayer with either (b) folded chains, (c) extended interdigitating chains or (d) extended alkyl chains that do not interdigitate, constrained by the H-bonding repeat distance of 4.7 Å.

In the fibril model, the negative charges (blue) are distributed at the outer edge surfaces and positive charges (red) are at the middle of fibrils. The positively-charged lysines and negatively charged glutamates are highlighted with red + and blue -, respectively. At neutral pH, both residues are charged and at acidic pH, only the lysine side chain is charged.

models, the self-assembly is entropically driven with hydrophobic segments buried in the bilayer/micelle interface to avoid water exposure (Hartgerink et al., 2001; Vauthey et al., 2002). Specifically, in the cylindrical "worm-like" model (Figure 2-1a), all the alkyl chains are buried within the fibril interior (Hartgerink et al., 2001; Hartgerink et al., 2002). In the β-sheet bilayer models (Figure 2-1b-d), packing of alkyl chains must be choreographed with the spacing of peptides in a cross-β configuration, either through interdigitation of the chains (Figure 2-1c) or some packing arrangement to fill the bilayer interface (Figure 2-1b, d) that would optimize alkyl chain packing. However, according to these models, the parallel sheets stacking places all lysines and all glutamates together at opposite ends, resulting in strong and energetically unfavorable charge repulsions that must be explained.

The presence of lysine and glutamate drives the pH-dependence of the self-assembled morphology and peptide arrangement of N-acetyl-Aβ(16-22). This peptide forms tubes with antiparallel one residue out-of register β-sheets at acidic pH and fibrils with antiparallel in-register β-sheets at neutral pH due to the electrostatic interactions (Lu et al., 2003; Mehta et al., 2008). Considering that the ionic complementary interaction appears to be a major force directing the β-sheet formation, it became necessary to consider other structural models. For example, if the charge interaction between lysine and glutamate plays a critical role in the structural transitions of amyloid assembly, and N-octanoyl-Aβ(16-22) parallel β-sheets in Meredith case could stack with antiparallel orientation with lysine and glutamate forming salt-bridge across-sheets (Figure 2-2), this arrangement exposes half of alkyl chains to water.

The fact that stable fibrils were formed from N-octanoyl-Aβ(16-22) suggests that
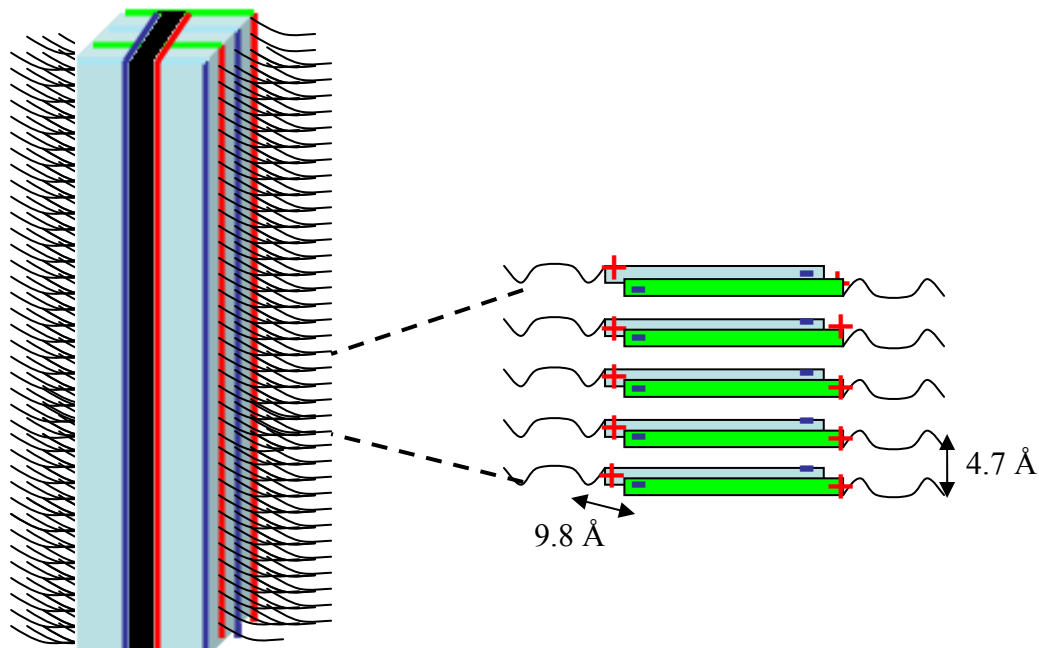
Figure 2-2. Proposed structural model for parallel β-sheet with antiparallel sheets stacking orientation.
The parallel β-sheets stack with antiparallel orientation to place the N-terminal lysine (positive charge, red +) close to C-terminal glutamate (negative charge, blue -) with half of alkyl chains (black line) exposed to the medium. In the right panel zoom in Figure, two sheets stack together with lamination distance of 9.8 Å and H-bonding distance of 4.7 Å.

hydrophobic interaction between alkyl chains in the parallel sheets orientation may overcome the charge repulsion or that charge attraction across the sheet in the antiparallel sheets orientation may overwhelm the repulsive interaction of alkyl chains with the aqueous medium. In order to determine the contributions of the hydrophobic interaction, charge repulsion, and charge attractive interactions, we have designed two sets of experiments. The first involves probing the hydrophobic interaction by capping with a systematic range of alkyl chains at the N-terminus of Aβ(16-22). This approach should identify systematic patterns as the hydrophobic interaction begins to overwhelm the electrostatic forces. Second, the cross-sheet charge interaction between the lysine and

glutamate has been systematically modulated through shortening the lysine side chains by one carbon atom in each of several analogs. These modifications should identify patterns that highlight the contributions played by each of these interactions.

Results

Is the self-assembled morphology altered by addition of alkyl chains at neutral pH?

A full series of alkyl chains were introduced at the N-terminus of Aβ(16-22) by amidation of the N-terminal amino acid with commercially available fatty acids in the last step of conventional solid phase peptide synthesis. These resulting chimerical peptides were more hydrophobic than the peptide alone, but could be easily purified by HPLC and characterized by MALDI-mass spectroscopy (see methods). At neutral pH (40% acetonitrile / water with 15 mM pH6 MES buffer), all the peptides N-X-Aβ(16-22) (X = acetyl to palmityl group) form fibrils (Figure 2-3). The similar fibril morphologies might suggest that no significant peptide registry changes occur with different N-alkane substitutions. However, the N-acetyl-Aβ(16-22) fibrils assemble as transparent gels, while N-propyl to N-palmityl fibrils precipitate from the aqueous solution. This precipitation may arise from exposure of a more hydrophobic surface that would mediate precipitation rather than gellation.
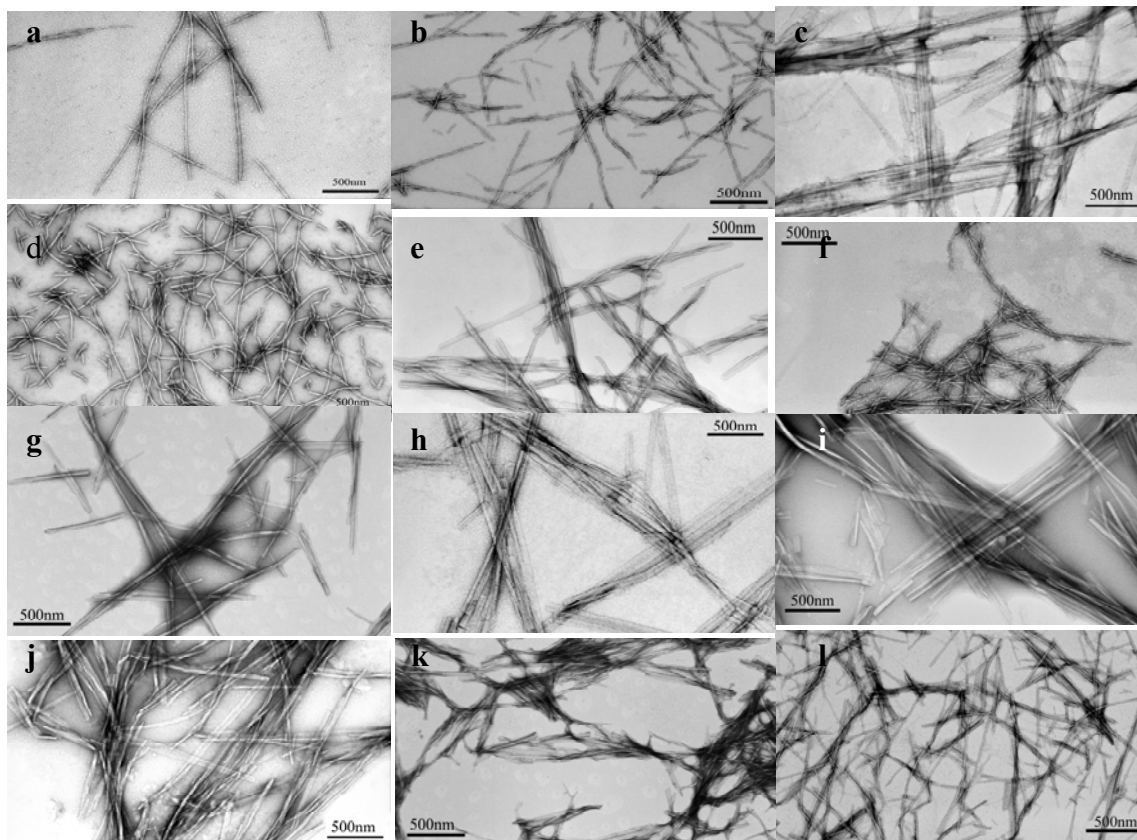
Figure 2-3. Electron micrographs of N-X-Aβ(16-22) (X=acetyl to palmityl) fibrils assembled at neutral pH.

(a) N-acetyl-Aβ(16-22), (b) N-propyl-Aβ(16-22), (c) N-butyl-Aβ(16-22), (d) N-isobutyl-Aβ(16-22), (e) N-valeryl-Aβ(16-22), (f) N-caproyl-Aβ(16-22), (g) N-octanoyl-Aβ(16-22), (h) N-pelargyl-Aβ(16-22), (i) N-decanoyl-Aβ(16-22), (j) N-lauryl-Aβ(16-22), (k) N-myristyl-Aβ(16-22), (l) N-palmityl-Aβ(16-22).

In each case, 1.0 mM peptide was incubated in the presence of 40% acetonitrile / water with 15 mM pH6 MES buffer at room temperature for 1 week. The EM samples were prepared by staining the fibrils with 2% uranyl acetate for 2 min, followed by drying in a desiccator overnight before imaging.

Does the N-terminal alkyl chain alter the peptide arrangement along the sheets?

To probe the impact of N-alkanes on peptide arrangements within β-sheets, [1-^{13}C]-labeled amino acids were incorporated into Aβ(16-22) to evaluate the off-resonance coupling across the entire ^{12}C coupling network (Halverson et al., 1991). The ^{13}C amide I

stretch red-shift is largest when ^{13}C-components are aligned along the β-sheet (Paul and Axelsen, 2005; Paul et al., 2004), and in this situation the ^{12}C component also shifts to higher wave numbers. The difference between ^{12}C and ^{13}C bands therefore reflects the extent of the packing along the entire β-sheets and the relative position of the ^{13}C isotope (Paul et al., 2004). The Isotope-Edited (IE)-IR spectra of N-acetyl-Aβ(16-22) fibrils (Lu et al., 2003; Mehta et al., 2008) is consistent with antiparallel in-registry β-sheets (Figure 2-4a), which has been verified by solid state NMR (ssNMR) (Mehta et al., 2008), and confirmed that the [1-^{13}C] F19 label provides characteristic backbone carbonyl coupling of the fibril assembly. The IR spectra of peptides containing this label show the characteristic antiparallel shoulder band at 1693 cm^{-1} (Figure 2-4) (Miyazawa, 1960) for N-acetyl-Aβ(16-22) fibrils only; while IR spectra of the rest of fibrils from N-propyl to N-palmityl display the lower wavenumber shoulder band at 1678 cm^{-1}, indicating of parallel β-sheets (Gordon et al., 2004). This finding suggests that a morphological transition from antiparallel to parallel occurs at N-propyl-Aβ(16-22) rather than N-octanoyl-Aβ(16-22). The band splitting magnitude, plotted as a function of the N-terminal capping group carbon number (Figure 2-4b), reveals another transition, which takes place between N-isobutyl and N-valeryl (Figure 2-4b), implying the longer alkyl chains alter the peptide stacking within β-sheet. N-acetyl-Aβ(16-22) fibrils and a lower parallel β-sheets wave number band at 1678 cm^{-1} (Gordon et al., 2004) for the rest of fibrils including N-propyl to N-palmityl Aβ(16-22).
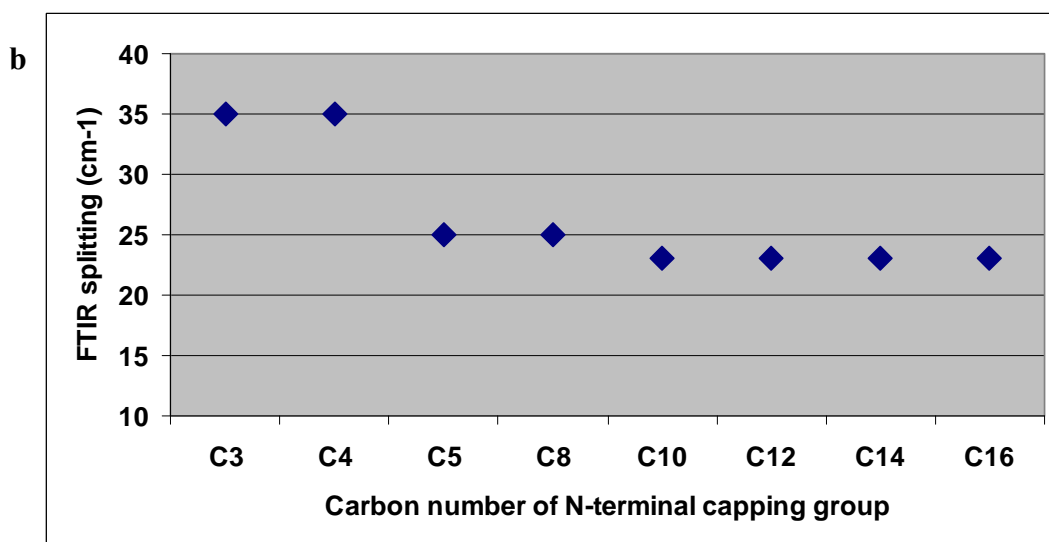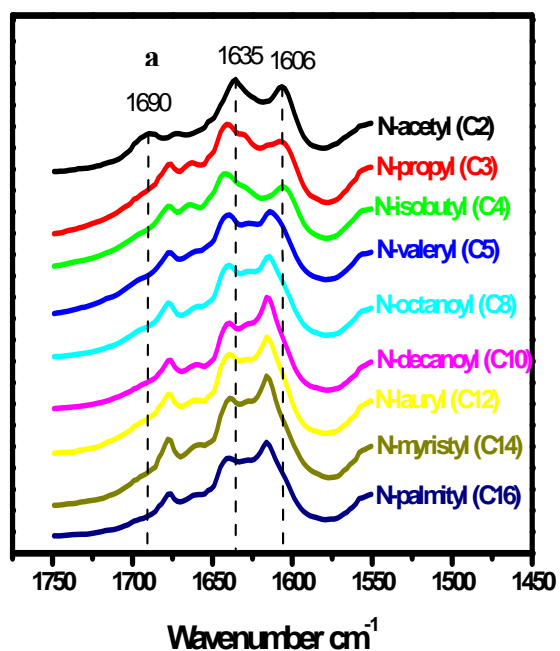
Figure 2-4. Isotope-edited IR spectra amide I region of fibrils at neutral pH.

(a) The stacked amide I region spectra with the bands at 1690 cm^{-1}, 1635 cm^{-1} and 1606 cm^{-1} highlighted with dashed lines. (b) The plot of ^{12}C / ^{13}C splitting amplitude as a function of N-alkyl chain carbon number.

Does the peptide orientation switch at N-propyl?

The FT-IR spectra shown in Figure 2-4 are of fibrils containing short N-terminal alkyl chains. The linear N-propyl-Aβ(16-22) and branched N-isobutyl-Aβ(16-22) are of similar chain length and share the same high wave number amide I band at 1678 cm^{-1} as the longer alkyl chain (N-octanoyl to N-palmityl) chimeras. To explore how this subtle substitution might change the peptide arrangement, [1-^{13}C] L17-labeled N-propyl and N-isobutyl-Aβ(16-22) were analyzed and compared with that of N-acetyl-Aβ(16-22) (antiparallel in-registry (Mehta et al., 2008)) and N-octanoyl-Aβ(16-22) (previously assigned as parallel in-registry (Gordon et al., 2004)) fibrils. Figure 2-5 depicts that FT-
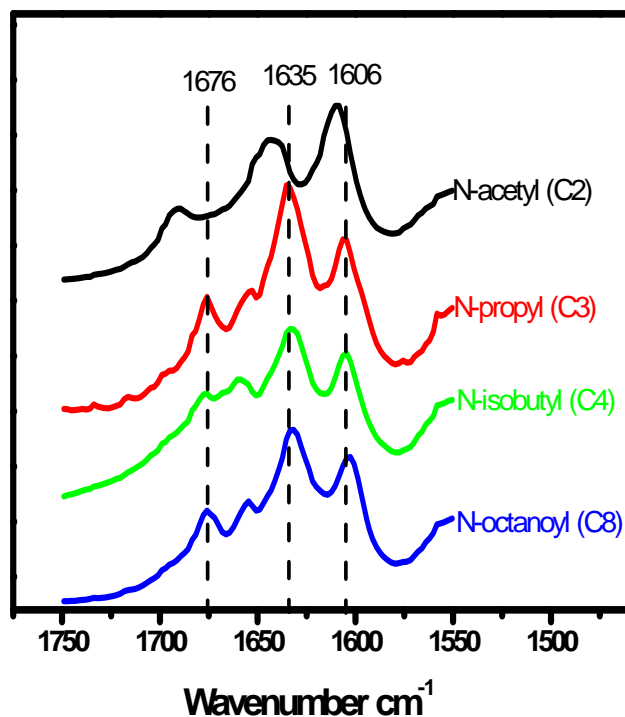
Figure 2-5. Stacked FT-IR amide I region spectra of [1-^{13}C] L17-labeled fibrils.
N-acetyl-, N-propyl-, N-isobutyl- and N-octanoyl-Aβ(16-22) fibrils were prepared by incubation 1.0 mM peptides at neutral pH in 40% acetonitrile / water with 15 mM pH6 MES buffer for 1 week. The bands at 1676 cm^{-1}, 1635 cm^{-1} and 1606 cm^{-1} are highlighted with dashed lines.

IR spectra of N-propyl, N-isobutyl and N-octanoyl-Aβ(16-22) fibrils have the same high absorbance wave number band at 1676 cm^{-1} and same amide I band splitting magnitude of 29 cm^{-1}, all of which are distinct from N-acetyl-Aβ(16-22) fibrils.

What is the peptide arrangement within β-sheets for the N-propyl- to N-palmityl-Aβ(16-22) fibrils at neutral pH?

To evaluate the peptide arrangement within fibrils, N-isobutyl-Aβ(16-22) was selected as representative and further characterized with solid-state NMR using dipolar recoupling with a windowless sequence (DRAWS) experiments, which works by measuring the distance between ^{13}C (Benzinger et al., 1998; Benzinger et al., 2000; Bower et al., 1999; Gregory et al., 1997). According to the model in Figure 2-6a, the
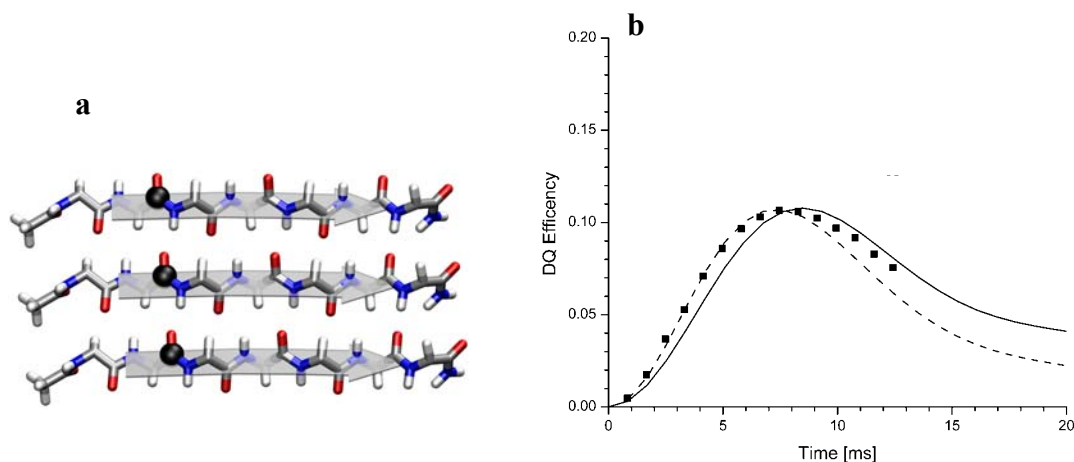
Figure 2-6. ssNMR DRAWS measurement profile of N-isobutyl-Aβ(16-22) [1-^{13}C]L17 parallel β-sheets.

(a) The parallel β-sheets model showing the predicted 4.7 Å between L17 carbonyls (black beads). Color codes: carbon (gray), oxygen (red), nitrogen (blue) and ^{13}C (black).

(b) DRAWS dipolar recoupling data (black square) collected on [1-^{13}C] L17-labeled N-isobutyl-Aβ(16-22) fibrils. The solid and dashed lines are the data fitting curves from which the distances were determined.

distance between L17 carbonyls is 4.7 Å for parallel in-registry, while the longer distance of 10 Å in antiparallel in-registry β-sheets could not be obtained by DRAWS due to the detection limit of 6-7 Å. As shown in Fig 2-6b, $[1-^{13}C]$ L17-labeled N-isobutyl-Aβ(16-22) fibrils dephasing best fit to a distance of 4.7 Å, confirming the isotope-edited IR data of a parallel in-registry β-sheets within the fibrils (Figure 2-5).

Does N-terminal alkyl chain interaction direct parallel β-sheet formation?

At neutral pH, N-X-Aβ(16-22) with alkane X longer than acetyl group (C2) apparently overwhelms the electrostatic constraint and switches the peptide orientation in the sheet from antiparallel to parallel. It is possible to eliminate the electrostatic contribution with N-octanoyl-Aβ(16-22)E22L substitution, and N-acetyl-Aβ(16-22)E22L was selected as a control based on previous work on this chimera (Lu, 2005). The N-octanoyl-Aβ(16-22)E22L forms small nanotubes with a radius of 19 nm at neutral pH (Figure 2-7c), slightly smaller than N-acetyl-Aβ(16-22) nanotubes at acidic pH (Lu, 2005; Mehta et al., 2008). FT-IR amide I spectra of $[1-^{13}C]$ L17-labeled N-octanoyl-Aβ(16-22) E22L, N-octanoyl-Aβ(16-22) and N-acetyl-Aβ(16-22) are shown in Figure 2-7. At neutral pH, a high wave number band at 1676 cm^{-1} for parallel β-sheets was observed for N-octanoyl-Aβ(16-22) fibrils (Figure 2-7d). However, the IR spectra of N-octanoyl-Aβ(16-22)E22L tubes at neutral pH show the antiparallel diagnostic high wave number shoulder band at 1691 cm^{-1}, along with identical ^{12}C and ^{13}C splitting as N-acetyl-Aβ(16-22) nanotubes at acidic pH, supporting the antiparallel β-sheets with one-residue out-of registry at neutral pH (Mehta et al., 2008).
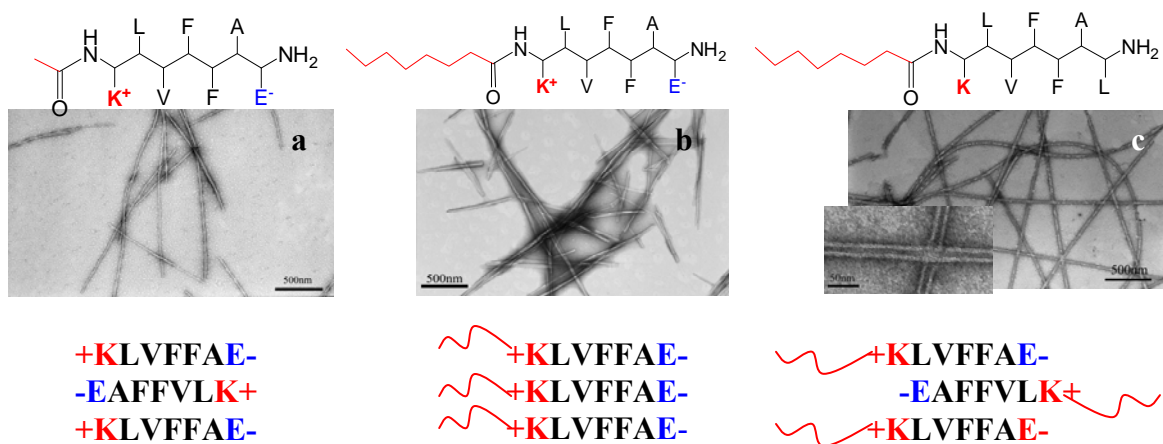
Figure 2-7. TEM images and IE-IR amide I spectra of leucine-substituted fibrils. Structures of N-acetyl-Aβ(16-22), N-octanoyl-Aβ(16-22) and N-octanoyl-Aβ(16-22)E22L at neutral pH. The terminal capping group is highlighted in red and the protonation state of lysine and glutamine at neutral pH are highlighted in red + and blue -, respectively.

The electron micrographs of fibrils and tubes formed from 1.5 mM (a) N-acetyl-Aβ(16-22), (b) N-octanoyl-Aβ(16-22) and (c) N-octanoyl-Aβ(16-22)E22L in 40% acetonitrile / water with 15 mM pH6 MES buffer at room temperature for 2 weeks.

The proposed peptide arrangement for each peptide based on the IR spectra is presented on the bottom of the EM images.

(d) IE-IR amide I band of [1-^{13}C] L17-labeled N-acetyl-Aβ(16-22), N-octanoyl-Aβ(16-22) and N-octanoyl-Aβ(16-22)E22L at acidic or neutral pH. The dashed lines are used as a reference for the 1691 cm^{-1}, 1629 cm^{-1} and 1610 cm^{-1} bands of the N-acetyl-Aβ(16-22) nanotubes.

Does the cross-sheet electrostatic interaction modulate the peptide arrangement?

To evaluate the role of cross-sheet charge attraction for the peptide orientation switch, the electrostatic interaction strength was modulated by shortening the lysine side chain. Four lysine analogs with different side chain length (Figure 2-8) were synthetically incorporated into N-isobutyl-Aβ(16-22).
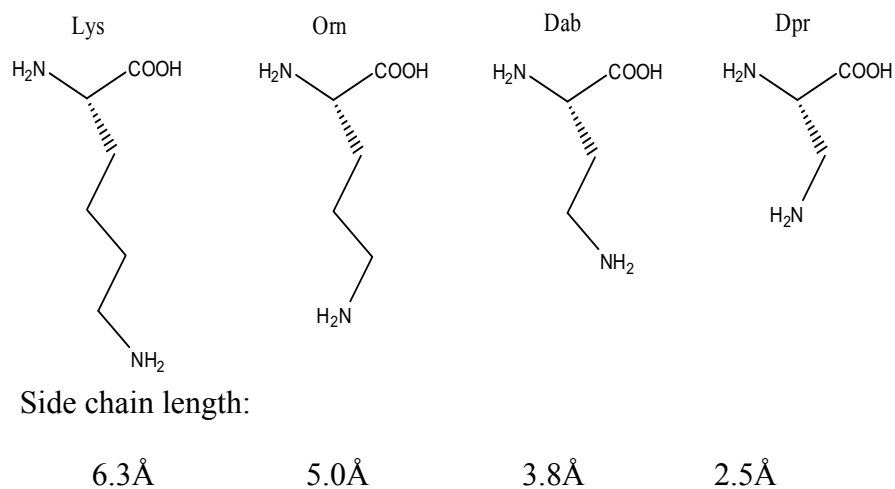
Figure 2-8. Chemical structure and side chain length of lysine analogs.

The abbreviations of each analog are placed on the top of each structure: Lys = lysine, Orn = ornithine, Dab = 2, 4-Diaminobutyric Acid and Dpr = 2, 3-Diaminopropionic acid. The predicted side chain length is estimated with ChemDraw and presented on the bottom of each analog.

At acidic pH, all four peptides form nanotubes (Figure 2-9a-d). And the FT-IR spectra of [1-^{13}C] F19-labeled nanotubes display the exact same high wave number band and amide I band stretches with ^{12}C at 1639 cm^{-1} and ^{13}C at 1599 cm^{-1} (Figure 2-9a), a diagnostic absorbance for antiparallel one-residue out-of registry. The same self-assembly morphology and peptide arrangement demonstrate that shortening lysine side chain has less impacts on the peptide self-assembly properties.

At neutral pH, the electrostatic interaction between glutamate and lysine analogs leads to a very different self-assembly morphology as well as peptide arrangements. For instance, N-isobutyl-Aβ(16-22)Lys16 and N-isobutyl-Aβ(16-22)Lys16Orn form fibrils (Figure 2-9e, f), while N-isobutyl-Aβ(16-22)Lys16Dab and N-isobutyl-Aβ(16-22)Lys16Dpr tend to form tubes and sheets (Figure 2-9g-h) instead of fibrils.
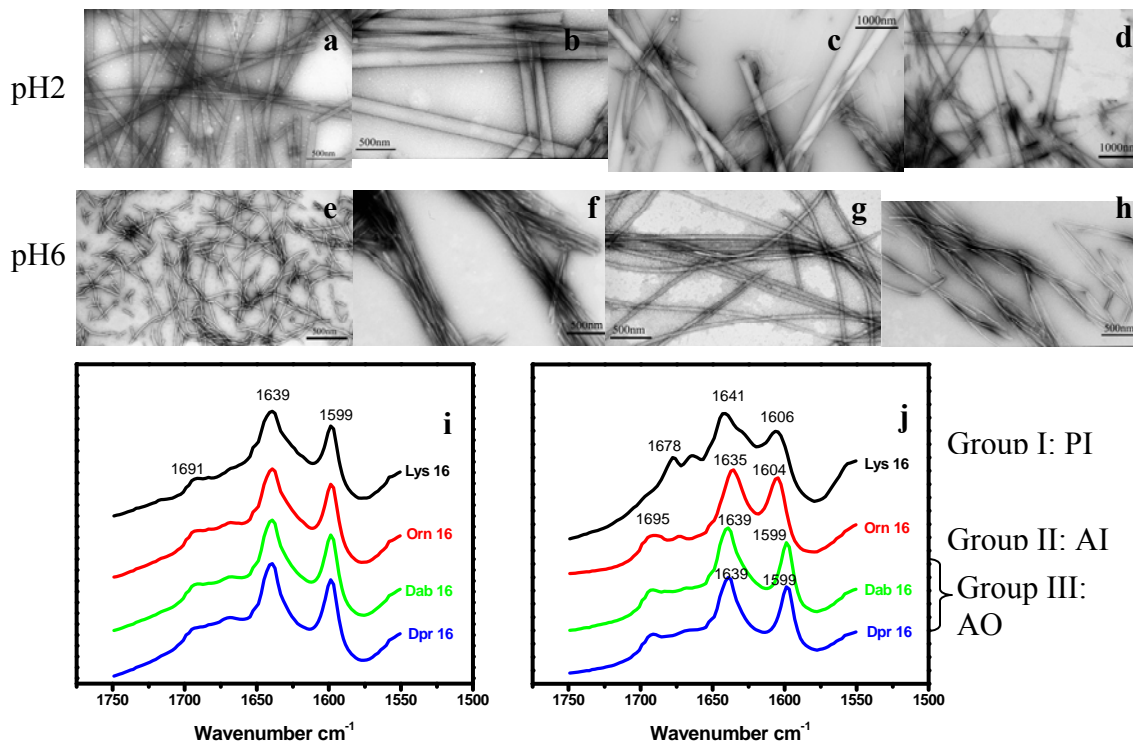
Figure 2-9. TEM images of lysine substituted self-assemblies and the corresponding FT-IR spectra.
TEM images of negatively stained N-isobutyl-Aβ(16-22) Lys16X assemblies: nanotubes formed at acidic pH: (a) N-isobutyl-Aβ(16-22) Lys16, (b) N-isobutyl-Aβ(16-22) Lys16Orn, (c) N-isobutyl-Aβ(16-22) Lys16Dab, (d) N-isobutyl-Aβ(16-22) Lys16Dpr and fibrils at neutral (pH6) pH (e) N-isobutyl-Aβ(16-22) Lys16, (f) N-isobutyl-Aβ(16-22) Lys16Orn, (g) N-isobutyl-Aβ(16-22) Lys16Dab, (h) N-isobutyl-Aβ(16-22) Lys16Dpr. In each case, 1.5 mM peptide was incubated in 40% acetonitrile / water with either 0.1% TFA or 15 mM MES (pH6) for 2 weeks.
FT-IR spectra amide I region of [1-^{13}C] F19-labeled N-isobutyl-Aβ(16-22) Lys16X (i) nanotube and (j) fibrils. The preformed assemblies were pelleted, frozen and lyophilized to yield white powder, pressed with KBr for the spectra analysis. The peptide arrangement AI is the abbreviation of Antiparallel In-registry, AO is for Antiparallel Out-of registry and PI is for Parallel In-registry.

Interestingly, these self-assemblies display different FTIR amide I bands (Figure 2-9j), which can be categorized into three groups. Group I includes the N-isobutyl-Aβ(16-22)Lys16 fibrils with high wave number shoulder band at 1678 cm^{-1}, indicative of parallel peptide orientation. Group II comprises of N-isobutyl-Aβ(16-22)Lys16Orn fibrils with antiparallel diagnostic band at 1695 cm^{-1}. In addition, the amide I band of [1-^{13}C] F19-labeled N-isobutyl-Aβ(16-22)Lys16Orn fibrils splits into two components, one at 1604 cm^{-1} for ^{13}C and the other at 1635 cm^{-1} for ^{12}C, implying antiparallel in-registry β-sheets within fibrils. The group III, including N-isobutyl-Aβ(16-22)Lys16Dab tubes and N-isobutyl-Aβ(16-22)Lys16Dpr sheets, presents a weak shoulder at 1695 cm^{-1} with migration of ^{13}C component to 1599 cm^{-1}, characteristic of antiparallel with one residue out-of registry β-sheets (Mehta et al., 2008). The self-assembly morphologies and peptide arrangements in the final self-assemblies could be regulated by tuning the length between the opposite charged groups.

To further examine the general correlation between peptide arrangement and the distance of charged groups, the four lysine analogs have been synthetically incorporated into N-acetyl-Aβ(16-22) and N-lauryl-Aβ(16-22), respectively. At acidic pH, all eight peptide congeners formed nanotubes (Figure 2-10a-h). The [1-^{13}C] F19-labeled tubes have similar band patterns at the same position with ^{13}C component shifting to 1597 cm^{-1} (Figure 2-10i-j), which is assumed to be antiparallel one residue out-of registry β-sheets (Mehta et al., 2008).

The impact of lysine side chain length on the self-assembly at acidic pH was further evaluated by electron diffraction analysis of N-acetyl-Aβ(16-22)Lys16X nanotubes. As shown in Figure 2-11, all four tubes display the similar diffraction pattern with tilt angles

(half of the angle between two H-bonding arcs) of $52 \pm 1^{\circ}$, and H-bonding and lamination repeating distances of 4.7 Å and 9.8 Å, respectively.
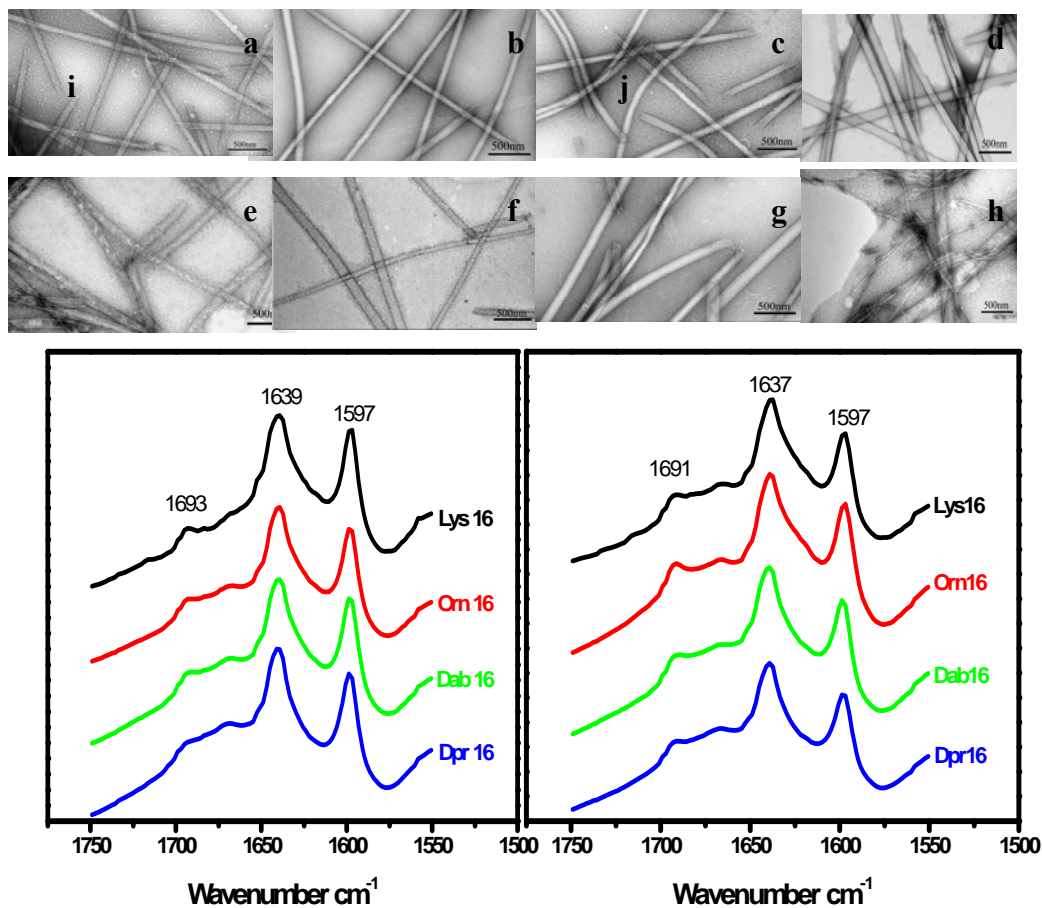
Figure 2-10. TEM images and FT-IR spectra amide I region of N-acetyl-Aβ(16-22)Lys16X and N-lauryl-Aβ(16-22) Lys16X at acidic pH.

TEM images of (a) N-acetyl-Aβ(16-22) Lys16, (b) N-acetyl-Aβ(16-22) Lys16Orn, (c) N-acetyl-Aβ(16-22) Lys16Dab, (d) N-acetyl-Aβ(16-22) Lys16Dpr, (e) N-lauryl-Aβ(16-22) Lys16, (f) N-lauryl-Aβ(16-22) Lys16Orn, (g) N-lauryl-Aβ(16-22) Lys16Dab and (h) N-lauryl-Aβ(16-22) Lys16Dpr. In each case, 1.5 mM peptide was incubated in 40% acetonitrile / water with 0.1% TFA for 2 weeks.

FTIR amid I band of [1-^{13}C] F19-labeled (i) N-acetyl-Aβ(16-22)Lys16X nanotube and (j) N-lauryl-Aβ(16-22)Lys16X nanotubes. The preformed nanotubes were bundled with sulfate with peptide to sulfate ratio of 1 to 10 before being pelleted, frozen and lyophilized and the yielded white powder was pressed with KBr for the spectra analysis.
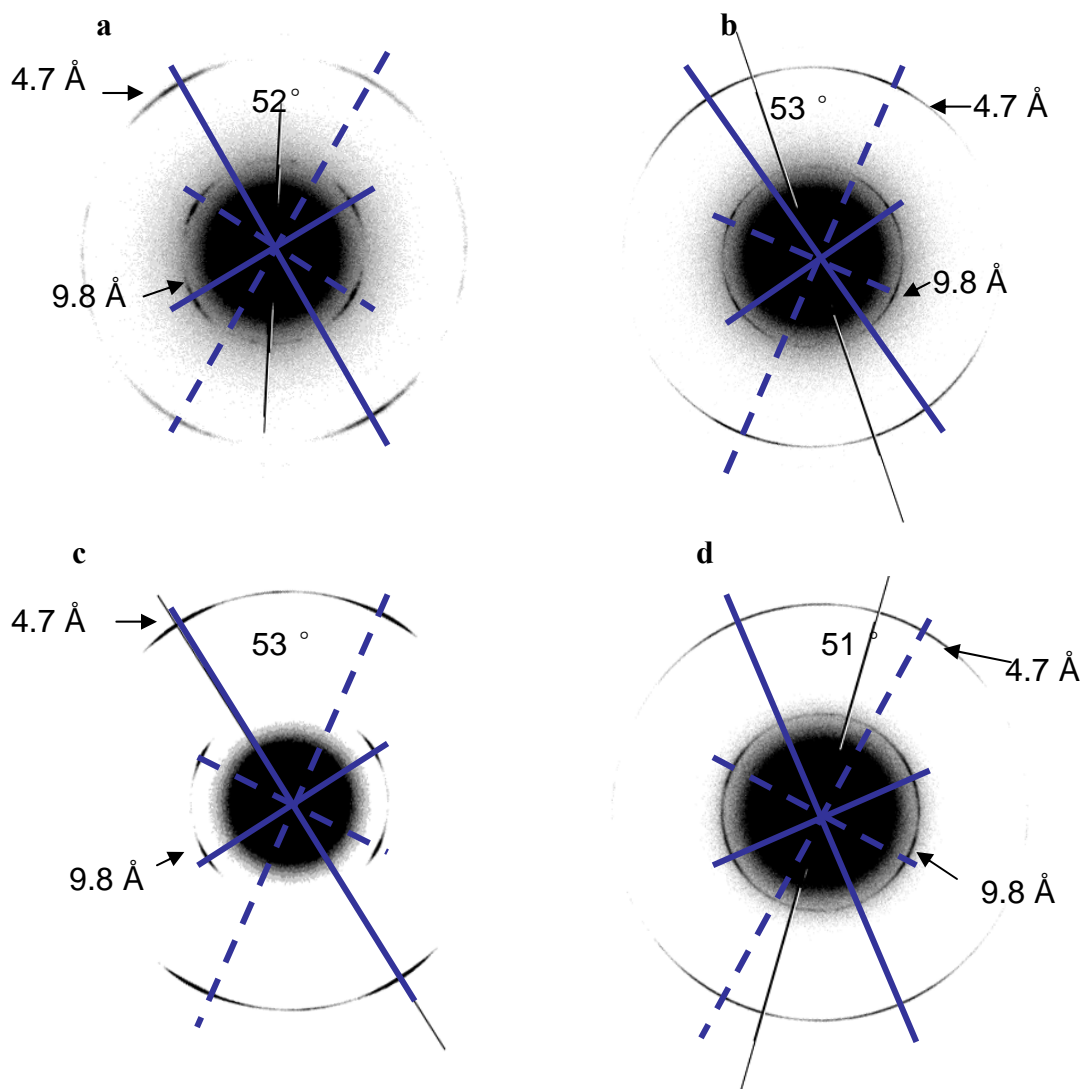
Figure 2-11. Electron diffraction of N-acetyl-Aβ(16-22)Lys16X nanotubes at acidic pH.
(a) N-acetyl-Aβ(16-22)Lys16, (b) N-acetyl-Aβ(16-22)Lys16Orn, (c) N-acetyl-Aβ(16-22)Lys16Dab, and (d) N-acetyl-Aβ(16-22)Lys16Dpr. The peptide repeating distances and tube tilt angles (the angle between two H-bonding direction) were labeled. Two pairs of orthogonal arcs were highlighted with solid and dashed lines, respectively. The black / white line cross the center is the technique artifact.

At neutral pH, different self-assembly morphologies (Figure 2-12a-h) and peptide arrangements (Figure 2-12i-j) have been observed. By shortening lysine side chain, both N-acetyl-Aβ(16-22)Lys16X and N-lauryl-Aβ(16-22)Lys16X make a transition from fibrils to sheets (Figure 2-12a-h). In addition, the IR spectra of [1-^{13}C] F19-labeled
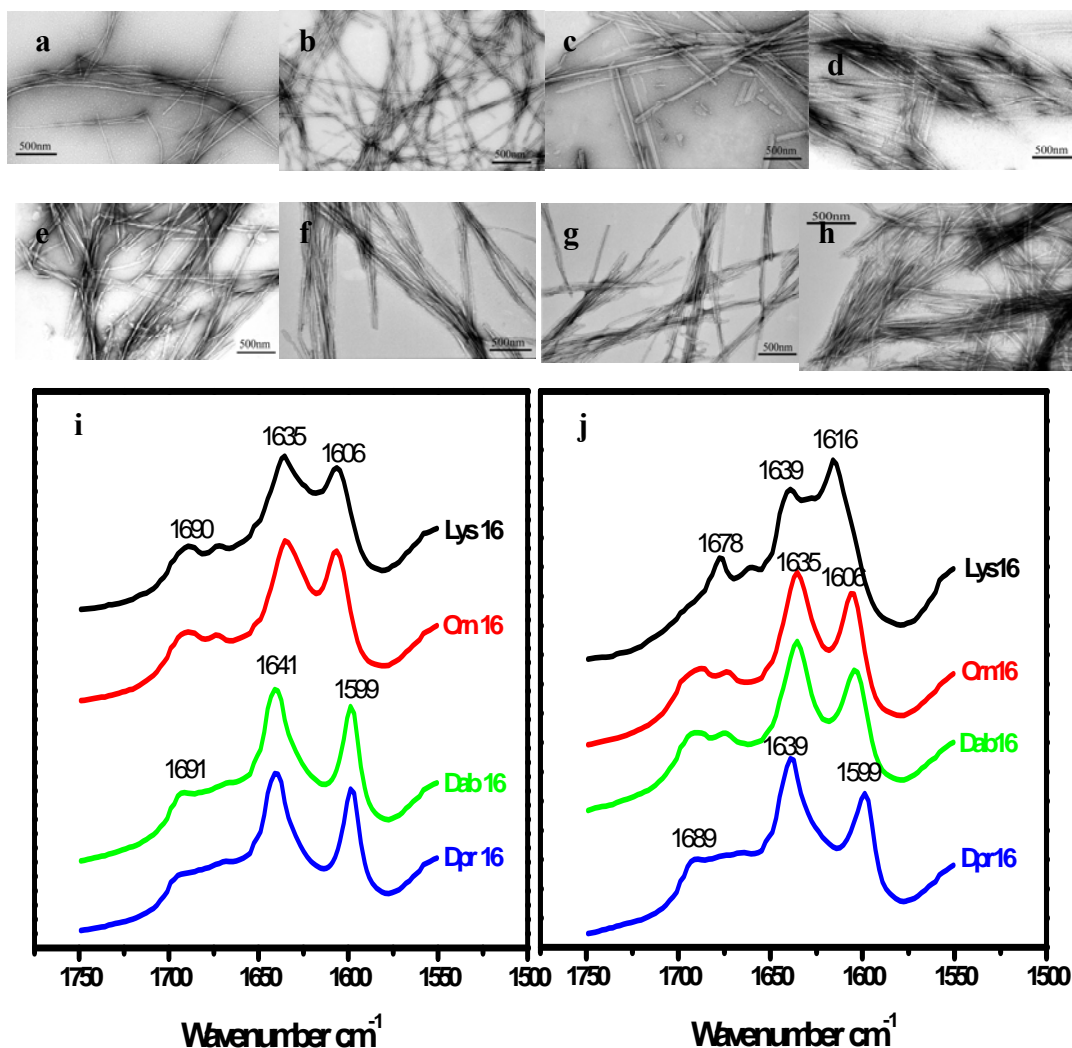
Figure 2-12. TEM images and FT-IR spectra amide I region of N-acetyl-Aβ(16-22)Lys16X and N-lauryl-Aβ(16-22) Lys16X at neutral pH.

TEM images of negatively stained N-acetyl- and N-lauryl-Aβ(16-22)Lys16X fibrils assembled at neutral pH. The first row from left to right is (a) N-acetyl-Aβ(16-22)Lys16, (b) N-acetyl-Aβ(16-22)Lys16Orn, (c) N-acetyl-Aβ(16-22)Lys16Dab and (c) N-acetyl-Aβ(16-22)Lys16Dpr. The bottom row is (e) N-lauryl-Aβ(16-22)Lys16, (f) N-lauryl-Aβ(16-22)Lys16Orn, (g) N-lauryl-Aβ(16-22)Lys16Dab and (h) N-lauryl-Aβ(16-22)Lys16Dpr. In each case, 1.0 mM peptide was incubated in 40% acetonitrile / water with 15 mM MES buffer (pH6) for 2 weeks.

FTIR amid I band of [1-^{13}C] F19-labeled (i) N-acetyl-Aβ(16-22)Lys16X and (j) N-lauryl-Aβ(16-22)Lys16X. The preformed nanotubes were pelleted, frozen and lyophilized and the yielded white powder was pressed with KBr for the spectral analysis.

The peptide arrangement AI is the abbreviation of Antiparallel In-registry, AO is for Antiparallel Out-of registry and PI is for Parallel In-registry.

peptides (Figure 2-12i) show that the peptide arrangement of N-acetyl-Aβ(16-22)Lys16X undergoes a switch from antiparallel in registry β-sheets (X = Lys and Orn) to antiparallel out-of registry β-sheets (X = Dab and Dpr). While the peptide arrangements in N-lauryl-Aβ(16-22)Lys16X self-assemblies could be classified into three groups (Figure 2-12j): 1) parallel in-registry (X = Lys), 2) antiparallel in-registry (X = Orn and Dab) and 3) antiparallel out-of registry (X = Dpr). The similar structure transitions of these three different peptides demonstrate that the cross-sheet charge interaction is critical to modulate the peptide arrangement within self-assemblies.

Do N-terminal alkyl chains alter the distribution of lysine on the fibril surface?

N-acetyl-Aβ(16-22) antiparallel β-sheet fibrils have been reported to bind specifically with negatively-charged gold colloids (Kun Lu, 2004). Lysine residues in the parallel β-sheet fibrils, however, may be completely buried interior of the fibril (Figure 2-1) or blocked from access to the solvent by the N-terminal long alkyl chain (Figure 2-2). To investigate the surface properties of parallel β-sheet fibrils, negatively-charged gold nanoparticles, prepared by following the protocol of Kun (Kun Lu, 2004), were mixed with these fibrils. Figure 2-13 shows images of fibrils containing different N-alkyl chains, in which very high gold-binding specificity was found for all fibrils. The N-long alkyl chains (N-lauryl, N-palmityl) have no apparent impacts on gold nanoparticle association with the fibril surface, which suggests that the N-terminal alkyl chains are not extended, but buried within fibrils.
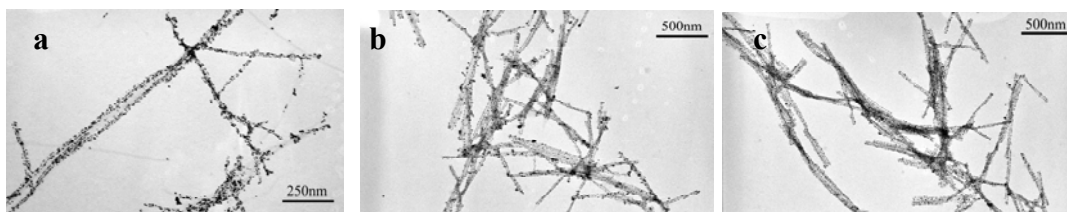
Figure 2-13. TEM images of gold-bound fibrils.

(a)N-acetyl-Aβ(16-22), (b) N-lauryl-Aβ(16-22) and (c) N-palmityl-Aβ(16-22) gold-bounded fibrils without uranyl acetate staining.

The preformed fibrils (1.0 mM in 40% acetonitrile with 15 mM pH6 MES buffer) were mixed with negatively charged gold colloids in a ratio of 1 : 10 (peptide : gold colloid). After one hour incubation at room temperature, the mixed sample was centrifuge to remove the unbounded gold particles in supernatant and the pellet was resuspended and prepared for EM analysis.

Does the N-terminal alkyl chain alter the peptide repeat distances?

If the N-terminal alkyl chains are buried between or within the sheets, the peptide repeat distances along lamination or the hydrogen-bonding distances should be different. The X-ray diffraction shows that 4.7 Å hydrogen-bonding distance d-spacing was conserved for all the samples (Figure 2-14). However, only one lamination repeating distance (LRD) was observed at 11.0 Å for short N-alkyl chain substitution such as N-propyl-Aβ(16-22). Two LRD d-spacings, one at 9.8 Å and another ranging from 11.0 Å to 13.3 Å (Figure 2-14) were found for the long alkyl chain capped fibrils, from N-butyl-Aβ(16-22) to N-palmityl-Aβ(16-22), consistent with two distinct sheets stacking interfaces.
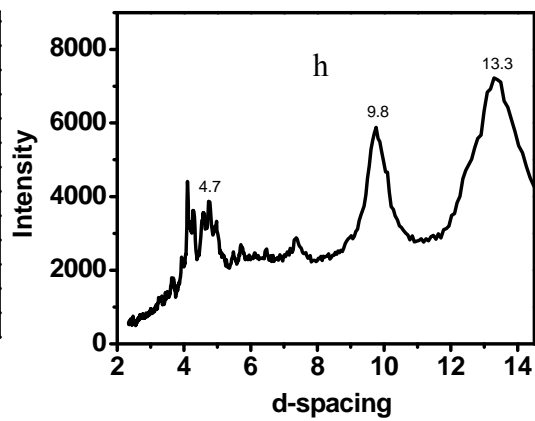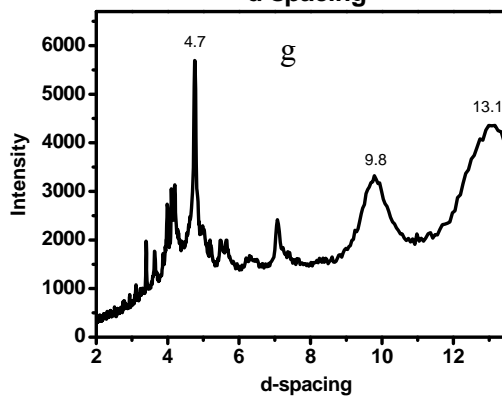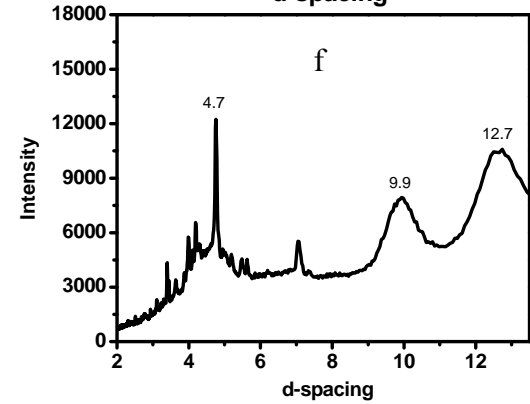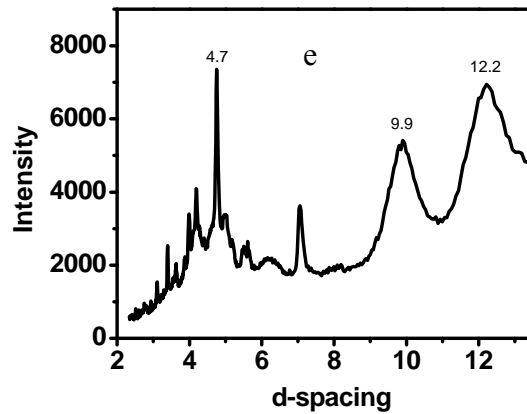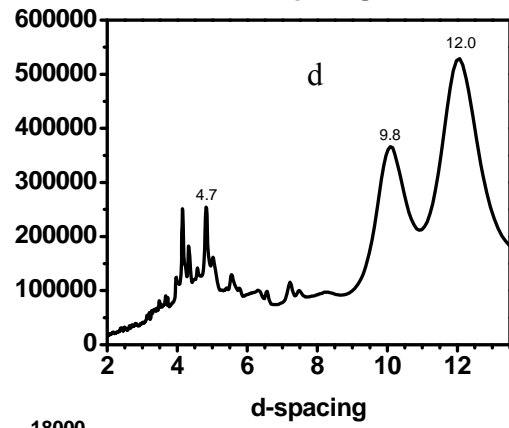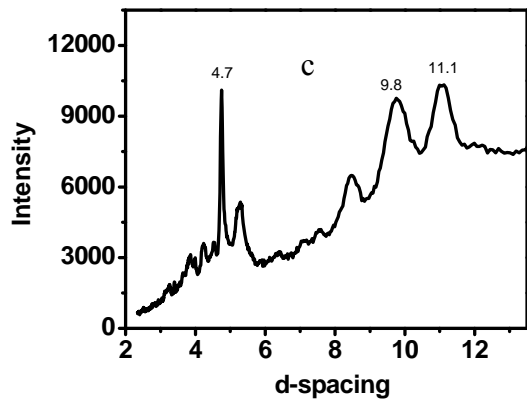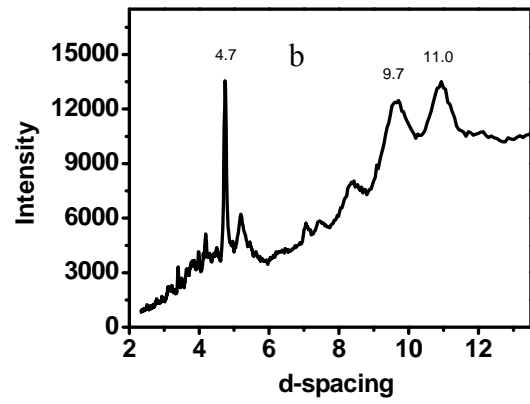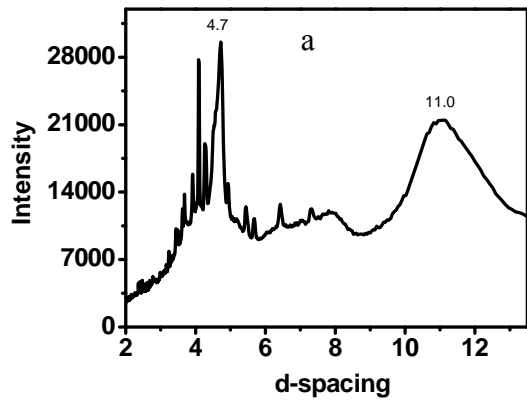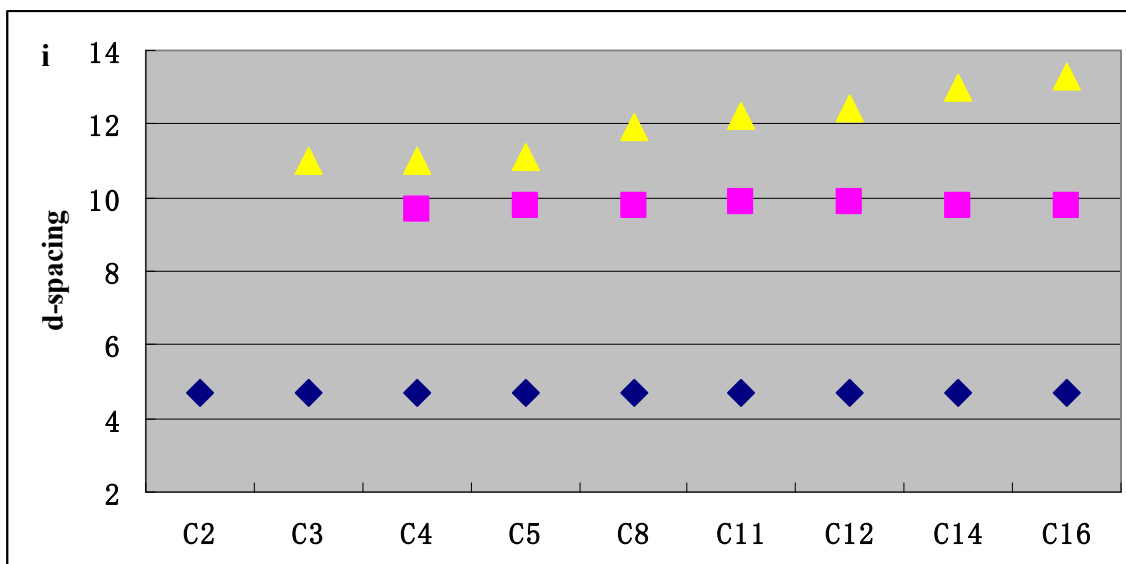
Figure 2-14. X-ray diffraction of N-substituted fibrils at neutral pH.

X-ray diffraction of the assemblies at neutral pH: (a) N-propyl-Aβ(16-22), (b) N-butyl-Aβ(16-22), (c) N-valeryl-Aβ(16-22), (d) N-octanoyl-Aβ(16-22), (e) N-decanoyl-Aβ(16-22), (f) N-lauryl-Aβ(16-22), (g) N-myristyl-Aβ(16-22) and (h) N-palmityl-Aβ(16-22).

(i) The plot of hydrogen-bonding (blue diamond) and lamination distances (purple square and yellow triangle for the short and long lamination distance, respectively) as function of the N-terminal capping group carbon number.

In each case, 1.0 mM peptide was incubated in in 40% acetonitrile with 15 mM pH6 MES buffer for 1 week.

ssNMR characterization of β-sheet stacking

The data obtained from above three experiments (shortening lysine side chain, gold-binding and X-ray diffraction) strongly suggest the antiparallel sheets stacking with proximity between lysine and glutamate in the parallel β-sheet fibrils (Figure 2-15). To further evaluate this crude structural model, solid-state NMR is essential to measure the distance between sheets. However, the lamination backbone distance in fibrils ranging from 9.8 Å to 13.3 Å (Figure 2-14) is far beyond the detection limitation of the rotational-echo double-resonance (REDOR), which is usually employed to measure the distance between [1-^{13}C] to [^{15}N] (Mehta et al., 2008). In order to overcome REDOR detection

limits, the new strategy employing isotope-labeling on the side chains instead of backbone is developed. As shown in the model in Figure 2-15, the Leu17 side chain is close to Ala21 backbone so that the side chain at the 17th position was labeled by substitution of leucine with ^{13}C-labeled N-methyl glutamine due to its easier access. The other isotope is introduced at A21 backbone with commercially available [^{15}N] Ala. Since N-isobutyl group capped fibrils (N-isobutyl-Aβ(16-22)) have been fully characterized, this capping group was also selected for the synthesis of N-isobutyl-Aβ(16-22)[N-methyl ^{13}C]L17N-methyl-Q [^{15}N] A21 (Figure 2-16).
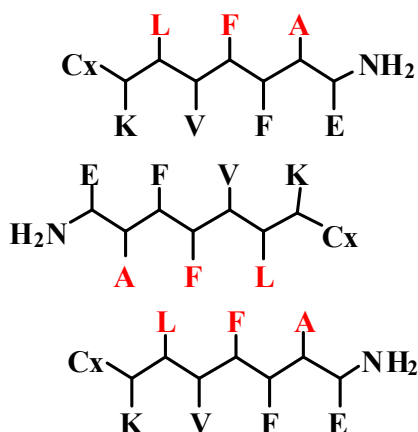
Figure 2-15. The crude model of parallel β-sheets stacking with antiparallel sheet-sheet orientation. Two faces of sheets are color coded in red and black, respectively. The same face stacks together to afford two different sheet-sheet interfaces (black / black and red / red).
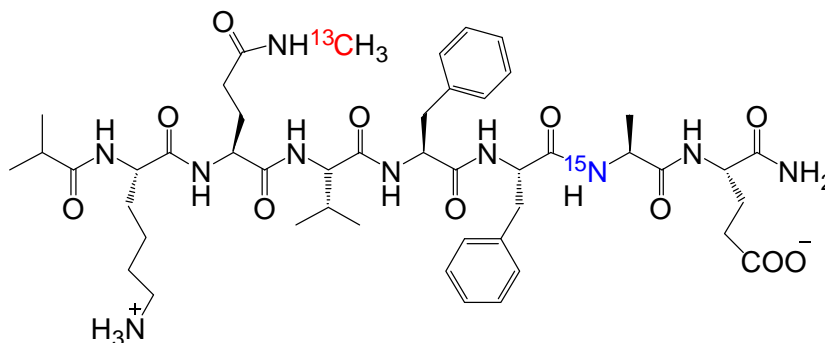
Figure 2-16. Chemical structure of N-isobutyl-Aβ(16-22) [N-methyl ^{13}C]L17N-methyl-Q [^{15}N] A21. ^{13}C is highlighted with red color and ^{15}N with blue.

Does N-isobutyl-Aβ(16-22) L17N-methyl-Q maintain the self-assembly properties as N-isobutyl-Aβ(16-22)?

At neutral pH, N-isobutyl-Aβ(16-22) L17N-methyl-Q self-assembles to homogenous fibrils (Figure 2-17a). The FT-IR spectra amide I region shows the high wave number band and main amide I stretch at 1676 cm^{-1} and 1630 cm^{-1}, respectively, same as those of N-isobutyl-Aβ(16-22) fibrils, suggesting parallel β-sheets.
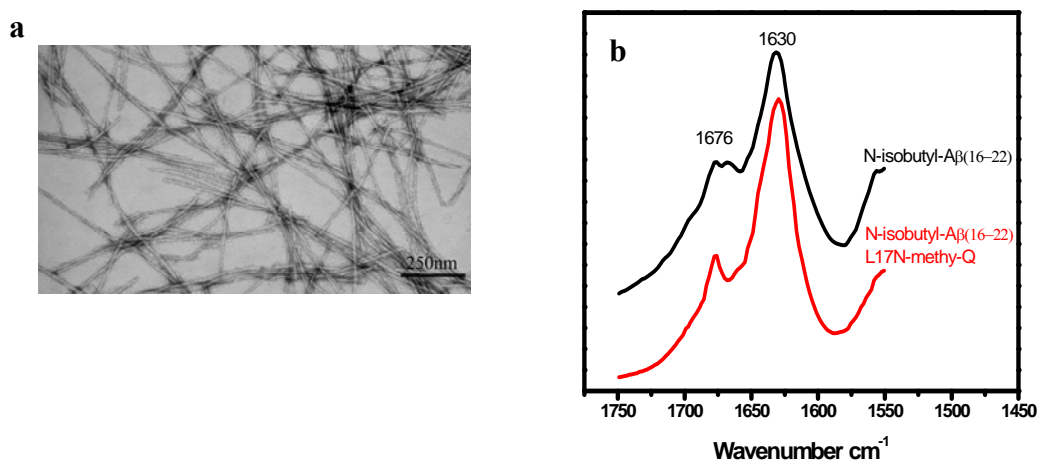
Figure 2-17. TEM image and FT-IR spectra amide I region of N-isobutyl-Aβ(16-22) L17N-methyl-Q fibrils at neutral pH.

(a) Electron micrograph of N-isobutyl-Aβ(16-22) L17N-methyl-Q fibrils formed in 20% acetonitrile / water with 15 mM pH6 MES buffer at room temperature for 1-2 weeks.

(b) FTIR amide I band of N-isobutyl-Aβ(16-22) fibrils (black line) and N-isobutyl-Aβ(16-22)L17 N-methyl-Q fibrils (red line) at neutral pH. The preformed fibrils were pelleted, frozen, lyophilized to yield white powder, pressed with KBr for spectra analysis.

To further evaluate the impacts of L17N-methyl-Q substitution of N-isobutyl-Aβ(16-22) on peptide registry within fibrils, FT-IR spectra of four single-[1-^{13}C]-labeled N-isobutyl-Aβ(16-22) and N-isobutyl-Aβ(16-22)L17N-methyl-Q were analyzed (Figure 2-18). Each labeled residue in both fibrils displays similar band splitting, suggesting the similar environment of each residue in both fibrils. Therefore, N-isobutyl-Aβ(16-

22)L17N-methyl-Q fibrils have the same peptide arrangement as other parallel β-sheet fibrils.
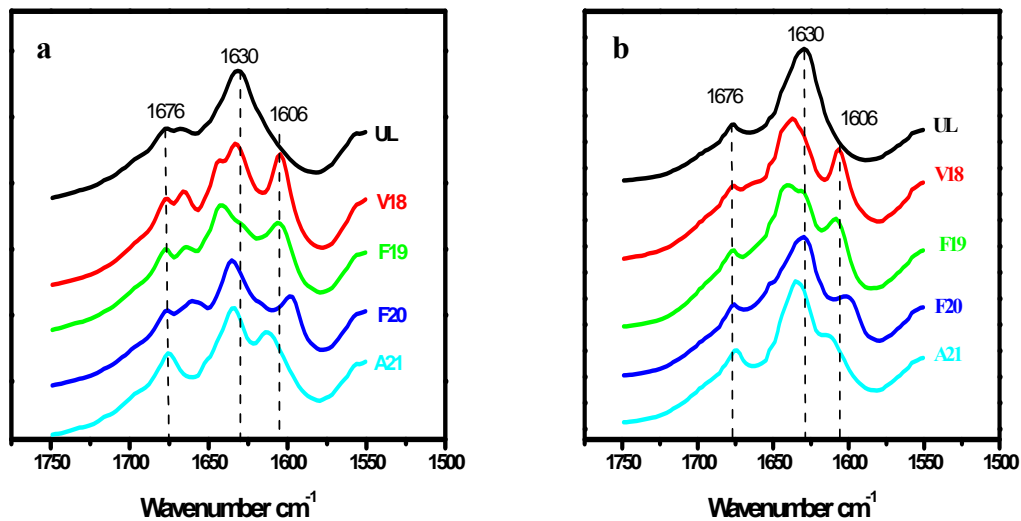
Figure 2-18. Stacked IE-IR amide I spectra of L17N-methyl-Q substituted fibrils at neutral pH.
The unlabeled (UL) and single isotope-labeled amyloid fibrils formed from (a) N-isobutyl-Aβ(16-22) and (b) N-isobutyl-Aβ(16-22)L17N-methyl-Q at neutral pH. The [1-^{13}C]-labeled residue is specified on the right side of each line. For clarification, the bands located at 1676 cm^{-1}, 1630 cm^{-1} and 1606 cm^{-1} are highlighted with dashed lines, respectively.

Characterization of sheets orientation through measuring the ^{13}C-^{15}N cross-sheet distance with solid-state NMR (ssNMR) REDOR technique

The ^{13}C-^{15}N distance in N-isobutyl-Aβ(16-22)[N-methyl-^{13}C]L17N-methyl-Q [^{15}N]A21 fibrils was determined with REDOR technique. The dephasing is well-fit to intermolecular distance of 6.6 Å between A21 backbone [^{15}N] and L17 N-methyl-Q side chain [N-methyl-^{13}C] (Figure 2-19), strongly supporting the antiparallel sheets arrangement in the parallel β-sheet fibrils (Figure 2-15).
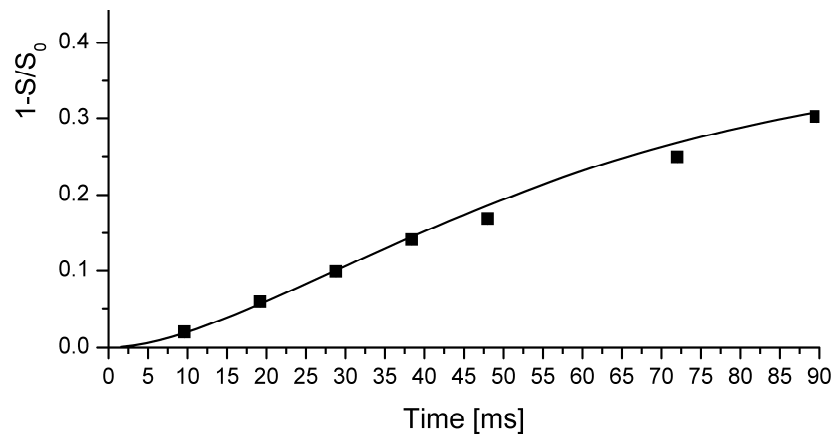
Figure 2-19. Characterization of sheet orientation by ssNMR REDOR technique.
ssNMR ^{13}C-^{15}N REDOR measurements of N-isobutyl-Aβ(16-22)[N-methyl-^{13}C]L17N-methyl-Q [^{15}N]A21 fibrils. Shaded squares are the experimental results and the solid line is the fit REDOR curve for antiparallel sheets packing with ^{13}C-^{15}N distance of 6.6 Å. X = 0.0 Å, y = 6.6 Å, σ_x = 0.4 Å, σ_y = 2.0 Å.

Discussion

The interaction between amyloid and membrane phospholipids has been implicated in membrane disruption and cell death, including hydrophobic interaction, charge repulsion, and charge attraction (McLaurin and Chakrabartty, 1997; Seelig et al., 1995; Terzi et al., 1995). The contribution of these interactions to amyloid formation has been systematically studied through the covalent linkage of the lipid alkyl chains containing different length with amyloid fragment Aβ(16-22). The synergic interaction of these forces leads to formation of parallel-β-sheet fibrils with a specific structure (Figure 2-20): 1) the positively-charged lysines and negatively-charged glutamates form cross-sheets salt-bridge, stabilizing the parallel β-sheets; 2) the alternating stacking of parallel-β-sheets creates two non-equivalent laminates with one hydrophobic environment to de-solvate and accommodate N-terminal alkyl chains; 3) the small residue A21 in the hydrophobic laminate creates a cavity to accommodate long alkyl chains such as palmityl group (C16) (Figure 2-20).
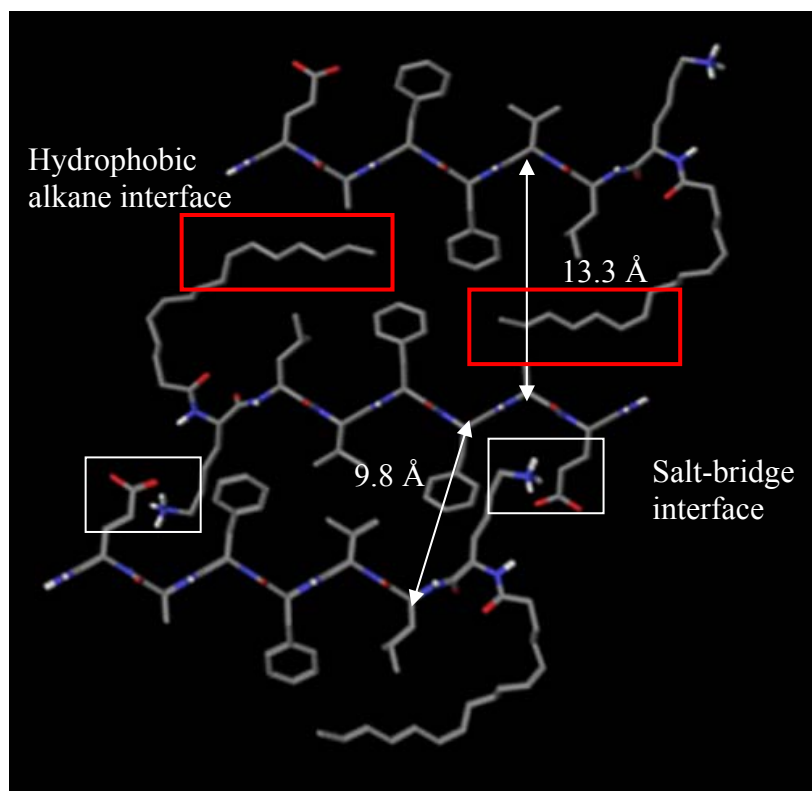
Figure 2-20. Structural model of parallel β-sheet fibrils in lamination dimension.
Three parallel β-sheets of N-palmityl-Aβ(16-22) stacks together with antiparallel orientation, resulting in two unsymmetrical lamination interfaces with lamination distances of 13.3 Å and 9.8 Å. The N-alkanes (in red box) are buried in the hydrophobic grove composed of L17, F19 and A21 residues, expanding the lamination distance to 13.3 Å. And the cross-sheet salt-bridge between lysine and glutamate (in white rectangle box) is located in another laminate, maintaining the lamination distance of 9.8 Å. H-bonding direction is pointing toward the paper plane.

The specific sequence properties of peptide region in the peptide-amphiphiles are critical for the formation of unique structured-fibrils. The parallel β-sheets formed from N-X-Aβ(16-22) (x = propyl to palmityl group) is distinct different from the literature reported peptide-amphiphile fibril models such as cylindrical fibrils formed from N-palmityl-S_4G_3S(P)RGD (S-PA) in Stupp's lab (Beniash et al., 2005; Bull et al., 2005; Hartgerink et al., 2001; Hartgerink et al., 2002). In Stupp's model (S-PA), the hydrophobic cluster of alkanes drives the cylindrical parallel β-sheet fibril formation with

all the alkanes buried in the interior of fibrils. However, in our model (L-PA), the parallel β-sheets stacked with antiparallel orientation with placing the alkanes at both end of peptides by insertion into hydrophobic laminates. The following several reasons may account for these different peptide-amphiphile fibril structures. 1) Peptide segments have different self-assembly capability. For example, Aβ(16-22) itself in L-PA can assemble to fibrils or tubes at different pHs, but $S_4G_3S(P)RGD$ in S-PA can not. 2) Both peptides have different molecular shape. Seven residues in Aβ(16-22) forms rectangular shape due to the similar residue size distributions (Figure 2-21b), while the amino acids in $S_4G_3S(P)RGD$ form a cone-shape with sizes gradually increased from N to C terminus (Figure 2-21a). 3) Both peptides have different charge distributions. In L-PA, the opposite charges are located at both ends of the peptide, but in S-PA, all the charges are situated at the head group (C-terminus). 4) Both peptides have the different sheet-stacking interface. The central five hydrophobic residues in L-PA have longer or larger side chains, which could create a hydrophobic environment to bury alkyl chains (Figure 2-21b). In contrast, the hydrophobic residues in S-PA are short and small, which can not form a hydrophobic pocket to de-solvate alkyl chains. Therefore, for the same length alkyl chain capped peptide-amphiphiles, the specific molecular geometry, charge distribution and hydrophobic residue size within the peptide region are important factors to drive the unique architecture formation.
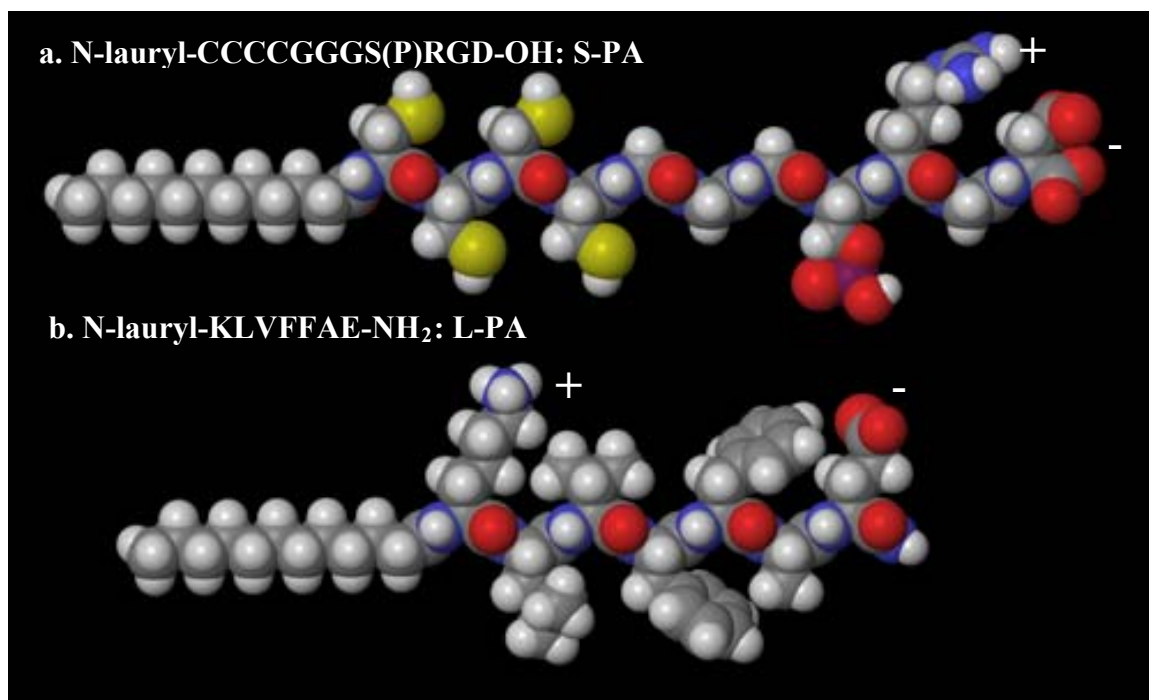
Figure 2-21. Molecular structure of two peptide-amphiphile monomers.

(a) Stupp's molecule N-lauryl-C_4G_3S(P)RGD-OH (S-PA: Stupp's peptide-amphiphile) (Hartgerink et al., 2001); and (b) the N-lauryl-Aβ(16-22) studied in this chapter (L-PA: Lynn's peptide-amphiphile). The charge of lysine and arginine are labeled with + and the aspartate and C-terminal carboxylic acid are labeled with −. The color code is red for Oxygen (O), blue for Nitrogen (N), gray for Carbon (C), white for Hydrogen (H) and yellow for Sulfur (S).

These exclusive parallel β-sheet fibrils are primarily formed through the cross-sheet electrostatic interaction between N-lysine and C-glutamate residues, instead of the N-terminal alkyl chain interaction. In this study, we found that the shortest N-terminal alkyl chain which could switch the β-sheet orientation from antiparallel to parallel is propyl group (C3) (Figure 2-4). Even though the long N-alkane substitutions such as N-octanoyl-Aβ(16-22) and N-lauryl-Aβ(16-22) formed parallel β-sheets at neutral pH, the same N-alkane substitutions without cross-sheet salt-bridge formation capability, such as N-octanoyl-Aβ(16-22)E22L and N-lauryl-Aβ(16-22)Lys16X (X = Orn, Dab and Dpr), could not form parallel β-sheets under the same conditions (Figure 2-7 and 2-12). Since

the control experiments of the lysine substitutions at acidic pH show that without electrostatic interaction, shortening lysine side chain has less impact on the peptide self-assembly properties at acidic pH (Figure 2-9, 2-10 and 2-11), it could be concluded that shortening the lysine side chain to disrupt the cross-sheet electrostatic interaction is the main reason to eliminate the parallel β-sheet formation at neutral pH. The parallel β-sheet structure observed in our study is consistent with the literature report, but the underneath driving force is different from the amphiphilicity argument claimed by Meredith et al. (Gordon et al., 2004). The possible reason may be that they proposed this argument by only based on β-sheet structure without sheet-sheet stacking information.

The strength of electrostatic interaction between lysine and glutamate could modulate the peptide arrangement and amyloid morphology. With Lys substitution, the cross-sheet electrostatic interaction is strong enough to stabilize the parallel β-sheets of N-isobutyl and N-lauryl-Aβ(16-22)Lys (Figure 2-22a). When lysine is substituted with Orn or Dab, the resulting longer distance between opposite charges on adjacent sheets weakens cross-sheet electrostatic interactions, but the cross-strand electrostatic interaction is strong enough to promote antiparallel in-registry fibril formation (Figure 2-22b). When lysine is replaced with shortest side chain Dpr, the electrostatic interaction between glutamate and Dpr is weaker than other forces such as V18 / A21 β-branched cross-strand paring (Liang et al., 2008) and phe-phe packing (Mehta et al., 2008; Waters, 2002), which drive formation of the antiparallel one-residue out-of register β-sheets (Figure 2-22c). This length dependence of electrostatic interaction is consistent with previous observation of the intra-helical glutamate-lysine ion-pairing (Cheng et al., 2007). Cheng et al. found that only lysine residue supported lysine-glutamate (i, i+3) interaction

with lower energy conformation and even shortening one methylene group significantly altered the peptide property by losing electrostatic interaction capability.
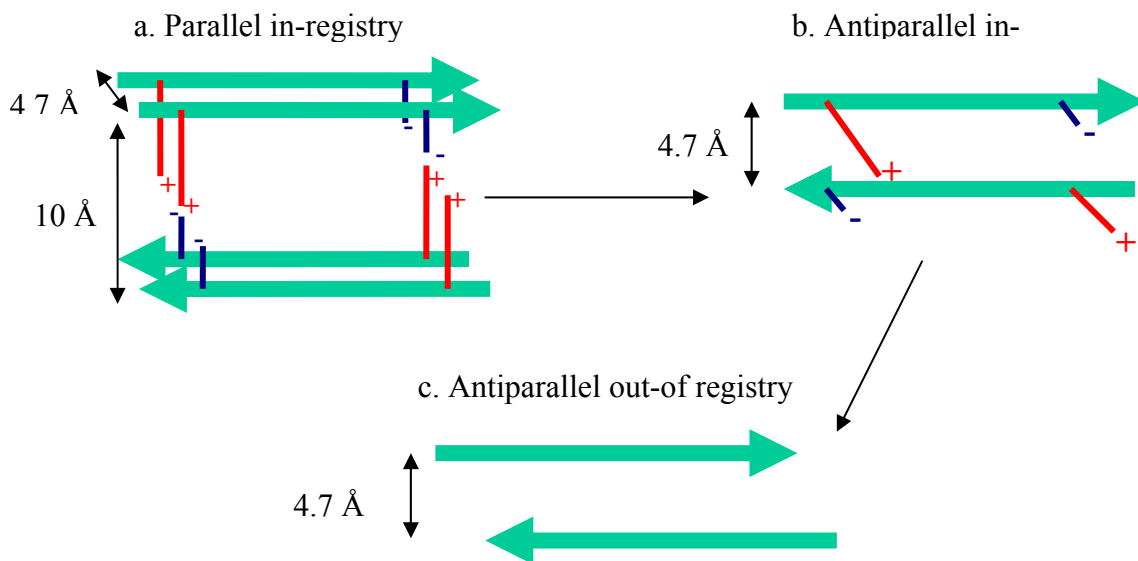
Figure 2-22. Illustration of peptide arrangement switch modulated by electrostatic interaction.
(a) Parallel in-register β-sheets with cross-sheet electrostatic interaction. Two peptide strands within sheets stack with distance of 4.7 Å and lysine (red +) and glutamate (blue -) are separated at both ends. Two parallel β-sheets pack with antiparallel orientation with lysine and glutamate pointing toward each other to form cross-sheet salt-bridge.
(b) Antiparallel in-register β-sheet with cross-strand electrostatic interaction.
(c) Antiparallel out-of registry β-sheets with cross-strand pairing between V18 and A21 and Phe-Phe aromatic stacking. The peptide hydrogen-bonding distance is 4.7 Å, and lamination distance is 10 Å. The light blue arrow represents peptide strand from N to C terminus. Res + and blue − stand for the lysine and glutamate side chain, respectively.

In this study, we discovered an unexpected peptide-amphiphile self-assembly structure, complementary to the existed literature models. The interaction between alkane and amyloid peptide may occur in cells and contribute to the toxicity of amyloid oligomers / fibrils through extracting lipid from phospholipid membranes. In addition, the cross-sheet electrostatic interaction, the underneath driving force for the parallel β-sheet formation, is complementary to the existed library and changing the strength of this

interaction by controlling the side chain length of charged residues is able to be applied to modulate the self-assembly structure and morphology, which may find applications in many fields such as nanomaterials and catalysis through adjusting the surface properties of self-assemblies.

Since the primary force to drive this specific parallel β-sheet fibril formation comes from the cross-sheet electrostatic interaction between lysines and glutamates, suppression of this interaction by mutating glutamate to leucine inhibits the formation of parallel β-sheets, leading to antiparallel β-sheet tubes. What would the Aβ(16-22) self-assembled structure be when this charge complementary interaction is simply reduced by acidifying the incubation solution to acidic pH? Will the interaction between lipid and peptide be altered without cross-sheet electrostatic interaction?

Materials and methods

Peptide synthesis and purification

The peptides N-X-Aβ(16-22) (X = propyl to palmityl group) were synthesized through standard FMOC/HBTU chemistry with FMOC Rink-amide polystyrene resin (Anaspec, Inc.) on a Rainin Symphony Quartet peptide synthesizer. The peptide region was automatically synthesized on the machine with the first 5 residues (VFFAE) single coupled for 2 hr and the last two residues (Lys16 and Leu17) double coupled for 4 hr. The peptide N-terminus was capped manually by coupling the corresponding acid with resin overnight with HBTU/NMM activation. The dried resin was mixed with cleavage cocktail (90 vol% TFA, 5 vol% thioanisole, 3 vol% ethanedithiol and 2 vol% anisole) over 1.5 hr at room temperature to cleave the peptide from the resin. The cleavage was

treated with cold diethylether 4 times to extract the crude peptide. The peptide was purified by reverse-phase HPLC (Waters Delta 600) using a Waters Atlantis C-18 preparative column (19 x 250 mm) and employed a linear gradient at 10 ml/min starting at 20% acetonitrile and ending with 95% acetonitrile over 75 min. After removing acetonitrile *in vacuo*, the peptide fractions were frozen and lyophilized to yield a peptide powder that was stored at 4 °C. The product mass was always confirmed by MALDI-TOF (a Voyager-DETM STR Biospectrometry Workstation) analysis with a-Cyano-4-hydroxycinnamic acid (CHCA) as matrix. For Isotope-labeled peptides, the same procedure was applied except the isotope-labeled amino acid was manually coupled for 4 hr.

Fibril Assembly

The weighted peptide powder was dissolved in 40% acetonitrile/water mixture with vortexing, and the sample was neutralized with 15 mM pH 5.6 MES buffer or acidified with 0.1 vol% TFA for fibril and tube sample preparation, respectively. Incubation at room temperature for 1-3 weeks was generally required for the sample maturation.

Transmission Electron Microscopy (TEM)

A TEM copper grid with a 200 mesh carbon supported (from Electron Microscopy Sciences) was covered with 10 μL of a diluted sample (0.05 mM to 0.1 mM) for 1 min before removing excess solution with filter paper. A 10 μL of staining solution (2% uranyl acetate, Sigma-Aldrich) was added and incubated for 2 min. After wicking away,

the sample grids were placed in desiccators to dry under vacuum overnight. A Hitachi H-7500 transmission electron microscope was used to image the samples at 75 kV.

Fourier Transform Infrared (FTIR)

Spectra were collected on a Nicolet MAGNA-IR 560 Spectrometer with 4 cm^{-1} resolution and generally 100 scans were averaged. For sample preparation, the matured fibrils were pelleted at 16,100 xg for 5 min, frozen at -80 ºC, and lyophilized to a dry powder. The dried sample was mixed well with grounded KBr (at a ratio of 1 : 10 (w / w)) and pressed into a transparent disk. Isotope-edited IR sample preparation was identified.

X-ray powder diffraction sample preparation

The matured fibrils were centrifuged at 16,100 xg for 10 min and the pellet was collected, frozen and lyophilized to yield dry powder for X-ray diffraction.

Electron Diffraction

The sample (15.0 μL, 0.2 mM to 0.5 mM) was applied on a TEM grid and incubated for 1min. To prepare an aligned sample on grids, the excess solution was slowly wicked away with filter paper at one direction. These micrographs were recorded on Philips 4500 transmission electron microscope in diffraction mode. A d-spacing, where $d = \lambda L/R$, was calculated, where R is half the distance (mm) between two opposite arcs, λ is the electron wavelength (75 kV), and L is the camera length (distance in mm between specimen and photographic film), calibrated using an aluminum polycrystalline standard (Electron Microscopy Sciences, Hartfield, PA).

REDOR and DRAWS sample preparation

The preformed fibrils, prepared according to aforementioned procedure, were centrifuged, frozen and lyophilized to yield dry powder.

Gold binding

For gold binding studies, 200 μL of preformed negative-charged gold colloid (0.3 mM, 3-5 nm diameter) was mixed with 5 μL of matured tubes (1.2 mM) to get the final ratio of gold to peptide 10 : 1. The mixture was incubated at room temperature for 1 hour, until a purple red precipitate gradually formed. After centrifugation, the collected pellet was resuspended in freshly prepared 40% acetronitrile / water with 0.1% TFA. Then 10 μL of sample was applied to TEM grid for 2 min, and excess solvent was removed with filter paper. The sample grid was stored in desiccators overnight before imaging.

References

Anguiano, M., Nowak, R. J., and Lansbury, P. T. (2002). Protofibrillar islet amyloid polypeptide permeabilizes synthetic vesicles by a pore-like mechanism that may be relevant to type II diabetes. Biochemistry *41*, 11338-11343.

Beniash, E., Hartgerink, J. D., Storrie, H., Stendahl, J. C., and Stupp, S. I. (2005). Self-assembling peptide amphiphile nanofiber matrices for cell entrapment. Acta Biomater *1*, 387-397.

Benzinger, T. L., Gregory, D. M., Burkoth, T. S., Miller-Auer, H., Lynn, D. G., Botto, R. E., and Meredith, S. C. (1998). Propagating structure of Alzheimer's beta-amyloid(10-35) is parallel beta-sheet with residues in exact register. Proc Natl Acad Sci U S A *95*, 13407-13412.

Benzinger, T. L., Gregory, D. M., Burkoth, T. S., Miller-Auer, H., Lynn, D. G., Botto, R. E., and Meredith, S. C. (2000). Two-dimensional structure of beta-amyloid(10-35) fibrils. Biochemistry *39*, 3491-3499.

Bower, P. V., Oyler, N., Mehta, M. A., Long, J. R., Stayton, P. S., and Drobny, G. P. (1999). Determination of torsion angles in proteins and peptides using solid state NMR. J Am Chem Soc *121*, 8373-8375.

Bull, S. R., Guler, M. O., Bras, R. E., Meade, T. J., and Stupp, S. I. (2005). Self-assembled peptide amphiphile nanofibers conjugated to MRI contrast agents. Nano Lett *5*, 1-4.

Cheng, R. P., Girinath, P., and Ahmad, R. (2007). Effect of lysine side chain length on intra-helical glutamate--lysine ion pairing interactions. Biochemistry *46*, 10528-10537.

Demuro, A., Mina, E., Kayed, R., Milton, S. C., Parker, I., and Glabe, C. G. (2005). Calcium dysregulation and membrane disruption as a ubiquitous neurotoxic mechanism of soluble amyloid oligomers. Journal of Biological Chemistry *280*, 17294-17300.

Domanov, Y. A., and Kinnunen, P. K. (2008). Islet amyloid polypeptide forms rigid lipid-protein amyloid fibrils on supported phospholipid bilayers. J Mol Bio *376*, 42-54.

Gordon, D. J., Balbach, J. J., Tycko, R., and Meredith, S. C. (2004). Increasing the amphiphilicity of an amyloidogenic peptide changes the beta-sheet structure in the fibrils from antiparallel to parallel. Biophys J *86*, 428-434.

Gregory, D. M., Mehta, M. A., Shiels, J. C., and Drobny, G. P. (1997). Determination of local structure in solid nucleic acids using double quantum nuclear magnetic resonance spectroscopy. J Chem Phys *107*, 28-42.

Halverson, K. J., Sucholeiki, I., Ashburn, T. T., and Lansbury, P. T. (1991). Location of Beta-Sheet-Forming Sequences in Amyloid Proteins by Ftir. J Am Chem Soc *113*, 6701-6703.

Hartgerink, J. D., Beniash, E., and Stupp, S. I. (2001). Self-assembly and mineralization of peptide-amphiphile nanofibers. Science *294*, 1684-1688.

Hartgerink, J. D., Beniash, E., and Stupp, S. I. (2002). Peptide-amphiphile nanofibers: a versatile scaffold for the preparation of self-assembling materials. Proc Natl Acad Sci U S A *99*, 5133-5138.

Janson, J., Ashley, R. H., Harrison, D., McIntyre, S., and Butler, P. C. (1999). The mechanism of islet amyloid polypeptide toxicity is membrane disruption by intermediate-sized toxic amyloid particles. Diabetes *48*, 491-498.

Lu, K., Conticello, V. P., and Lynn, D. G. (2004). Templating colloidal metal nanoparticle assemblies: use of the Aβ amyloid peptide nanotube. Mater Res Soc Synp Proc *1.6*.

Liang, Y., Pingali, S. V., Jogalekar, A. S., Snyder, J. P., Thiyagarajan, P., and Lynn, D. G. (2008). Cross-strand pairing and amyloid assembly. Biochemistry *47*, 10018-10026.

Lu, K. (2005). Discovery of diverse peptide nanotube architecture from the self-assembly of designed amyloid-beta cassettes. pHD thesis, Emory University, Atlanta, Georgia.

Lu, K., Jacob, J., Thiyagarajan, P., Conticello, V. P., and Lynn, D. G. (2003). Exploiting amyloid fibril lamination for nanotube self-assembly. J Am Chem Soc *125*, 6391-6393.

McLaurin, J., and Chakrabartty, A. (1997). Characterization of the interactions of Alzheimer beta-amyloid peptides with phospholipid membranes. European journal of biochemistry / FEBS *245*, 355-363.

Mehta, A. K., Lu, K., Childers, W. S., Liang, Y., Dublin, S. N., Dong, J., Snyder, J. P., Pingali, S. V., Thiyagarajan, P., and Lynn, D. G. (2008). Facial symmetry in protein self-assembly. J Am Chem Soc *130*, 9829-9835.

Miyazawa, T. (1960). Perturbation Treatment of the Characteristic Vibrations of Polypeptide Chains in Various Configurations. J Chem Phys *32*, 1647-1652.

Paul, C., and Axelsen, P. H. (2005). beta Sheet structure in amyloid beta fibrils and vibrational dipolar coupling. J Am Chem Soc *127*, 5754-5755.

Paul, C., Wang, J., Wimley, W. C., Hochstrasser, R. M., and Axelsen, P. H. (2004). Vibrational coupling, isotopic editing, and beta-sheet structure in a membrane-bound polypeptide. J Am Chem Soc *126*, 5843-5850.

Seelig, J., Lehrmann, R., and Terzi, E. (1995). Domain formation induced by lipid-ion and lipid-peptide interactions. Molecular membrane biology *12*, 51-57.

Terzi, E., Holzemann, G., and Seelig, J. (1995). Self-association of beta-amyloid peptide (1-40) in solution and binding to lipid membranes. J Mol Bio *252*, 633-642.

Vauthey, S., Santoso, S., Gong, H., Watson, N., and Zhang, S. (2002). Molecular self-assembly of surfactant-like peptides to form nanotubes and nanovesicles. Proc Natl Acad Sci U S A *99*, 5355-5360.

Waters, M. L. (2002). Aromatic interactions in model systems. Curr Opin Chem Biol *6*, 736-741.

CHAPTER 3

Accommodating Alkyl Chains within Amyloid Nanotubes

Introduction

The data presented in Chapter 2 have established that for N-alkyl substitution from propyl to palmityl group on Aβ(16-22), when assembled at neutral pH, the cross-sheet electrostatic interaction between lysine and glutamate directs parallel β-sheet fibril formation. Further, the N-terminal alkyl chains bend to occupy the hydrophobic laminates created by antiparallel sheet stacking. This β-sheet fibril structure, unprecedented in the existing literature, is not formed when the electrostatic attraction between sheets is reduced by either substitution of the glutamate with leucine or shortening of the lysine side chain. Alternatively, protonation of the glutamate reduces the salt bridge energy and the resulting assembly is known to be dominated by the cross-strand pairing interaction between Val and Ala to shift in registry within the antiparallel β-sheet to give N-acetyl-Aβ(16-22) nanotubes (Liang et al., 2008b; Mehta et al., 2008). The question to be explored here is whether acidic pH is sufficient to override the self-assembly registry and morphology of the peptide-amphiphiles with N-alkyl substitution. This question is particularly relevant given the required placement of the alkyl chains within the bilayer and along the surface of the amyloid tubes. We show that alkyl chains

promote the self-assembly of peptides (Hartgerink et al., 2001; Hartgerink et al., 2002) and define how the inclusion in N-X-Aβ(16-22) (X= propyl to palmityl group) alters the tube structure and is accommodated within the nanotube β-sheet structure.

Results

Is the self-assembled morphology at acidic pH altered by addition of alkyl chains?

The N-acetyl-Aβ(16-22) assembled to homogenous nanotubes with diameter of 44 ± 4 nm (Figure 3-1, Group I) (Lu et al., 2003; Mehta et al., 2008) in 40% acetonitrile / water at acidic pH. Under the same incubation conditions, all other alkyl chain-conjugated peptides self-assembled to various morphologies, including nanotubes, sheets and fibrils revealed by the series of electron micrographs (Figure 3-1). According to the final morphologies, these peptides can be categorized into four groups. In Group I, the N-acetyl- to N-butyl-Aβ(16-22) peptides formed nanotubes (Figure 3-1). Relative to the diameter of the N-acetyl-Aβ(16-22) tubes (44 ± 5 nm), the nanotubes formed from N-propyl-Aβ(16-22) are slightly smaller with diameter of 39 ± 6 nm and those prepared with N-butyl-Aβ(16-22) peptides are 50% larger (68 ± 4 nm) (Table 3-1). In Group II, including the N-valeryl- to N-decanoyl-Aβ(16-22) peptides, these assemblies are no longer tubes, but instead sheets and small ribbons (Figure 3-1). Interestingly, with alkyl chains of N-undecyl to N-tridecyl in Group III, the tube morphology reappeared. N-undecyl and N-lauryl substituted tubes have homogenous diameter of 53 ± 5 nm (Table 3-1), slightly larger than N-acetyl-Aβ(16-22) tubes, while the N-tridecyl substituted nanotubes are more heterogeneous with a slightly smaller average diameter of 35 ±10 nm.
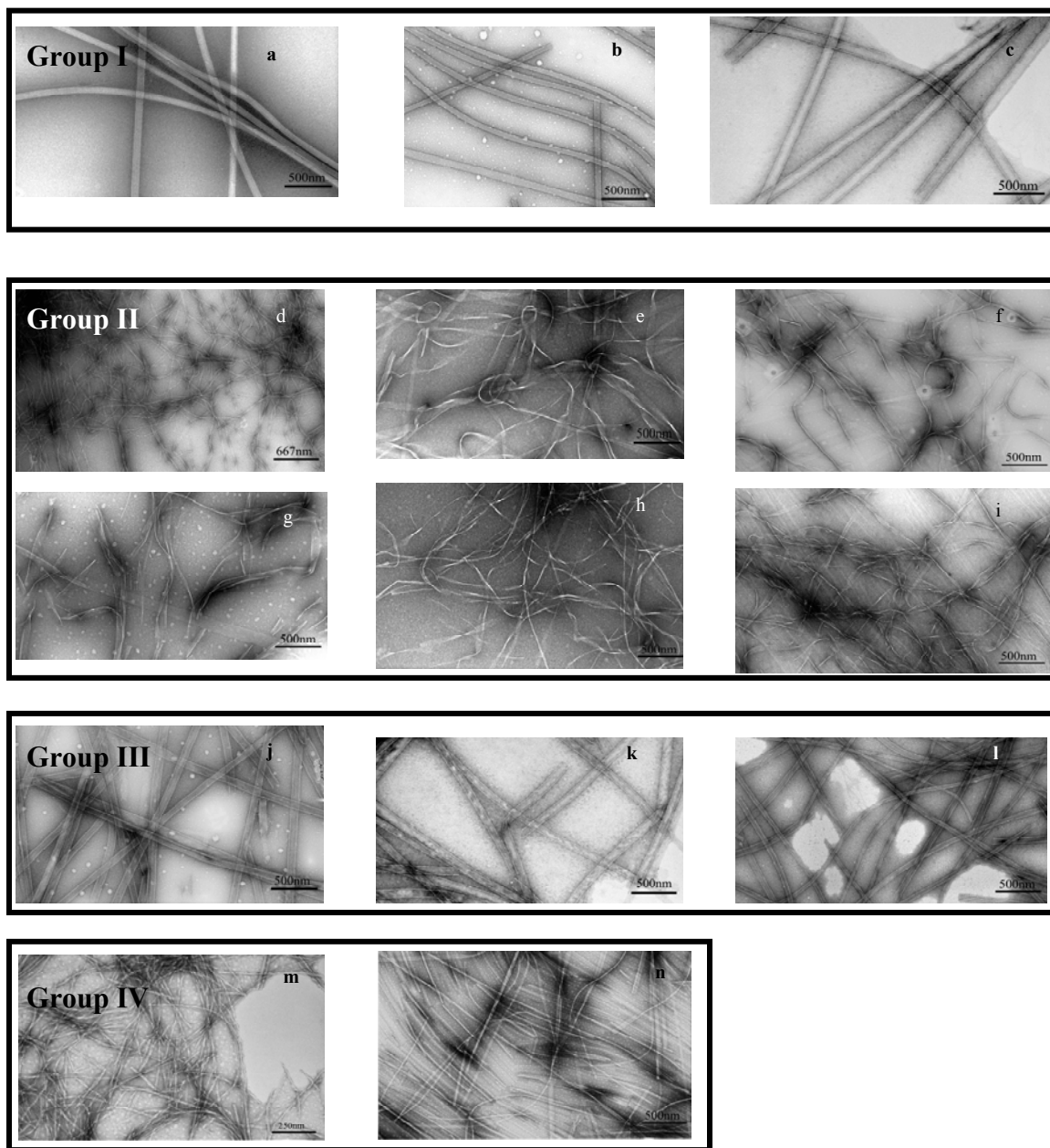
Figure 3-1. Electron micrographs of the N-X-Aβ(16-22) (X=acetyl to palmityl) peptide assembled at acidic pH.

(a)N-acetyl-Aβ(16-22), (b) N-propyl-Aβ(16-22), (c) N-butyl-Aβ(16-22), (d) N-valeryl-Aβ(16-22), (e) N-caproyl-Aβ(16-22), (f) N-enanthyl-Aβ(16-22), (g) N-octanoyl-Aβ(16-22), (h) N-pelargyl-Aβ(16-22), (i) N-decanoyl-Aβ(16-22), (j) N-undecyl-Aβ(16-22), (k) N-lauryl-Aβ(16-22), (l) N-tridecyl-Aβ(16-22), (m) N-myristyl-Aβ(16-22) and (n) N-palmityl-Aβ(16-22). In each case, 1.2 mM peptide was incubated in 40% acetonitrile / water with 0.1% TFA at room temperature for 2-3 weeks before imaging.

In group IV (Figure 3-1, N-myristyl to N-palmityl group), the morphology switched back to fibrils.

Table 3-1. Estimated nanotube diameters at acidic pH.

The tube dimension is measured from the dried nanotubes in Figure 3-1 and the calculation is based on the equation $d = c/\pi$ (d is the tube diameter and c is the tube intersection circumstance). The measured value is the average of twenty tubes, and the tube size measured on the dried samples may be slightly smaller than that measured in solution due to the drying artifacts (Lu et al., 2003).

N-X-Aβ(16-22)	acetyl-	propyl	isobutyl-	butyl-	undecyl-	lauryl-	tridecyl-
Diameter (nm)	44 ± 5	39 ± 6	44 ± 5	68 ± 4	53 ± 5	53 ± 5	35 ± 10

Do N-terminal alkyl chains impact peptide secondary structure in the assembly?

The wide range of self-assembled morphologies observed above might result from the impact of N-alkanes on peptide secondary structure. As an initial test, the matured N-X-Aβ(16-22) (X = acetyl to lauryl) self-assemblies were studied with circular dichroism (CD) and found to contain negative ellipticity ranging from 212 nm to 222 nm (Figure 3-2), consistent with β-sheet secondary structure. The N-myristyl- and N-palmityl-Aβ(16-22) fibrils were precipitated, but the amide I band of their powder samples also gave an amide I band stretch at 1632 cm^{-1} (data not show), suggesting β-sheet secondary structure is maintained in all these N-terminal modified self-assemblies at acidic pH (Zandomeneghi et al., 2004).
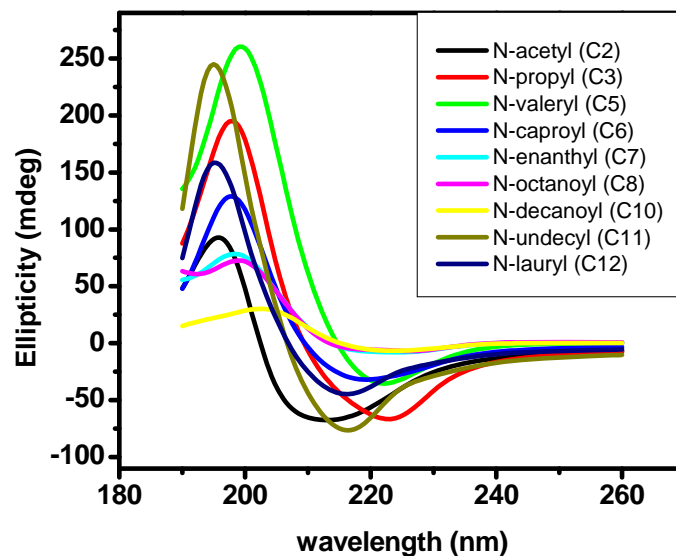
Figure 3-2. CD spectra of N-X-Aβ(16-22) (X= acetyl to lauryl) assemblies at acidic pH.
All samples were assembled in 40% acetonitrile / water with 0.1% TFA at room temperature for 3 weeks at a peptide concentration of 1.2 mM and analyzed directly.

By following the CD negative ellipticity change with time, the effect of N-alkanes on the peptide self-assembly kinetics has been determined. Figure 3-3 shows the kinetic curves of five different alkane-capped Aβ(16-22) peptides through 700 hr of assembly. N-acetyl-Aβ(16-22) remained as random coil during the first 100 hr, then gradually developed the β-sheet signature at 215 nm. The N-propyl to N-caproyl- peptides developed relatively strong β-sheet signature within 100 hr of incubation, and after 400 hr appeared to plateau. N-octanoyl-Aβ(16-22) reached a plateau within 20 hr, but the ellipticity is quite low. Overall, it appears that the longer alkane substituents mediate in the faster self-assembly rate, but the nature of this assembly will need to be determined.
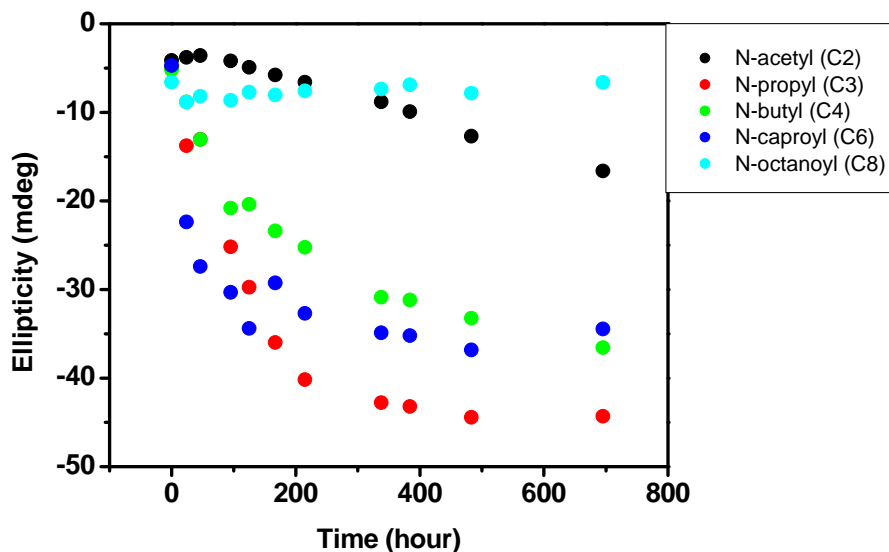
Figure 3-3. Self-assembly kinetics of N-alkane substituted assemblies at acidic pH.
Each peptide (1.5 mM) was incubated in 40% acetonitrile / water with 0.1% TFA at room temperature and aliquots were taken at the indicated time point and the ellipticity at 215 nm was plotted.

Do the N-alkanes alter the peptide arrangement within β-sheets?

To probe the peptide arrangement within these assemblies, [1-^{13}C] F19 was incorporated for isotope-edited infrared (IR) analysis. In the fourier transform infrared (FTIR) spectra amide I region (Figure 3-4a), a diagnostic band at 1690 cm^{-1} for antiparallel β-sheets is observed and the pattern of ^{12}C at 1639 cm^{-1} and ^{13}C at 1597 cm^{-1} is undistinguishable from N-acetyl-Aβ(16-22) (Figure 3-4a, b), suggesting the peptides in Group I to III share the same peptide β-sheet arrangement within self-assemblies. In contrast to this antiparallel out-of-registry arrangement, the IR spectra of N-myristyl- and N-palmityl-Aβ(16-22) fibrils show a higher wave number band at 1678 cm^{-1} independent of incubation pH (Figure 3-4a-c), suggesting parallel β-sheets. The detailed structure characterization and proposed models for these assemblies are discussed in Chapter 2.
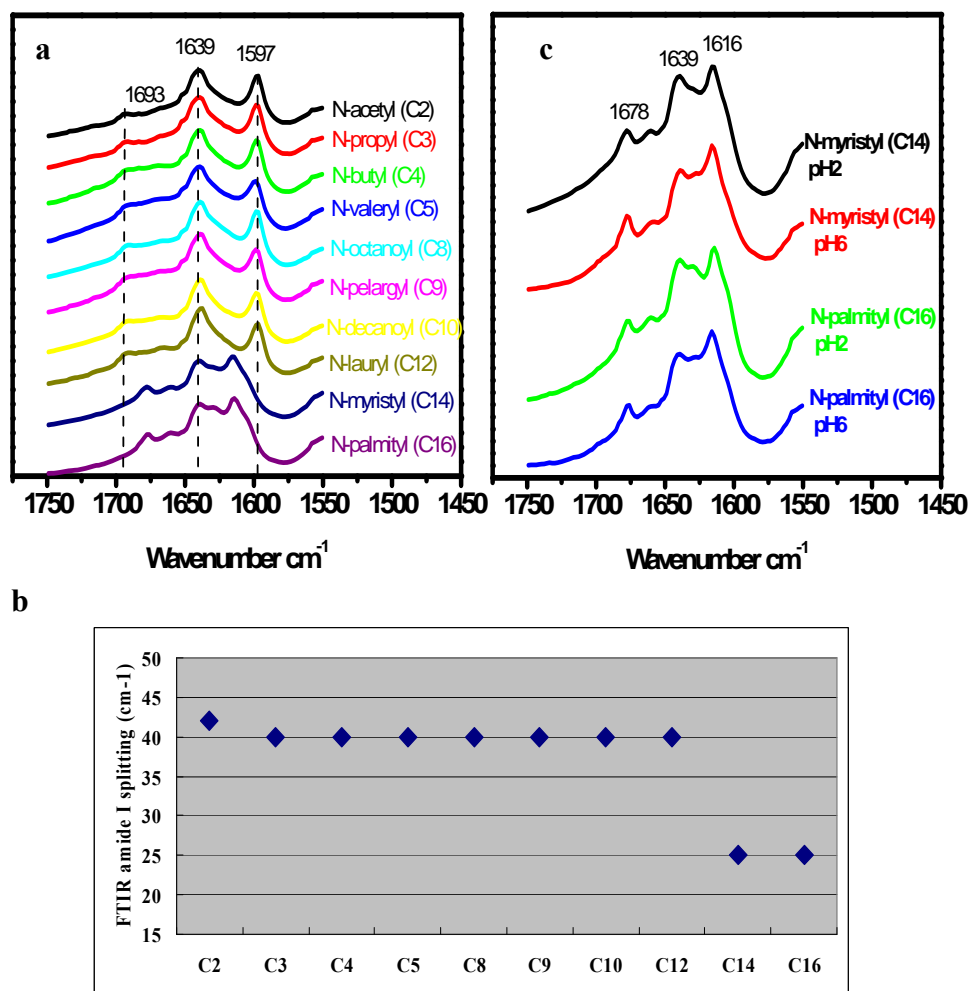
Figure 3-4. Isotope-edited IR amide I band of [1-¹³C] F19-labeled assemblies at acidic pH.

(a) Stacked plot of the individual spectra with the alkane name and carbon number indicated at the right side and the band assignments shown with dashed lines.

(b) Plot of the wave number difference between ^{12}C and ^{13}C amide I stretches as function of then-alkane carbon number.

(c) FTIR amide I band of [1-^{13}C] F19-labeled N-myristyl-Aβ(16-22) and N-palmityl-Aβ(16-22) fibrils assembled at acidic or neutral pHs with major bands highlighted.

Does a N-terminal alkyl chain impact tube wall thickness and tube surface property?

The TEM images presented in Figure 3-1 are most consistent with the N-undecyl to N-tridecyl capped Aβ(16-22) peptides forming tubular self-assemblies, which share the same peptide arrangement as N-acetyl-Aβ(16-22) tubes. To further test the hollow nanotube assignment, the N-lauryl-Aβ(16-22) nanotubes were analyzed under cryo-etch SEM conditions (Mehta et al., 2008). Surveys of the cryo-SEM images of the N-lauryl-Aβ(16-22) tubes identified remarkably similar hollow tubes (Figure 3-5b) to those seen with the N-acetyl-Aβ(16-22) assemblies (Figure 3-5a). These images also suggested remarkably similar dimensions, both size and wall thickness, to the N-acetyl-Aβ(16-22) tubes, raising fundamental questions about the positioning of the additional mass from N-lauryl substitution.
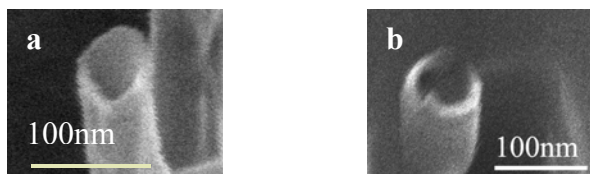
Figure 3-5. Cryo-SEM images of peptide nanotubes formed from (a) **N-acetyl-Aβ(16-22) and (b) N-lauryl-Aβ(16-22)** (Mehta et al., 2008)**.**

In each case, peptide was incubated in 40% acetonitrile / water (1.5mM) with 0.1% TFA for 3 weeks at room temperature. 1.5 μL tube sample was plunge-frozen in liquid ethane at -180 ºC, and then transferred into chromium-coater to etch for 10 min at -105 ºC before coating with 4.5 nm thickness of Cr. After that, the coated sample were transferred into cryo-stage and imaged at -120 ºC. To illustrate the hollow feature, the vertical tubes with the visible intersection were recorded and shown here.

To further evaluate the positioning of the N-terminal alkyl chains within the tubes, tube wall thickness was measured using AFM. As shown in Figure 3-6 and Table 3-2, the

tube wall thickness is unchanged at 4 nm for all four nanotubes, consistent with the similar wall thickness shown in SEM images (Figure 3-5).
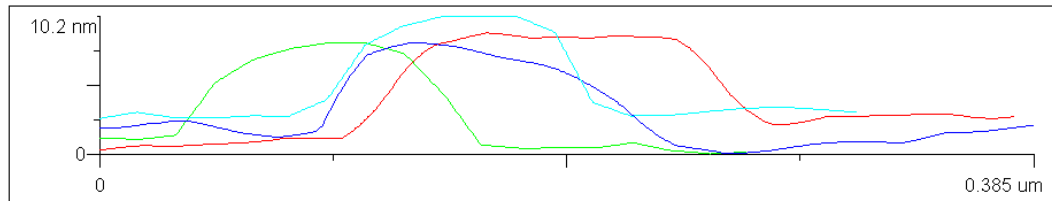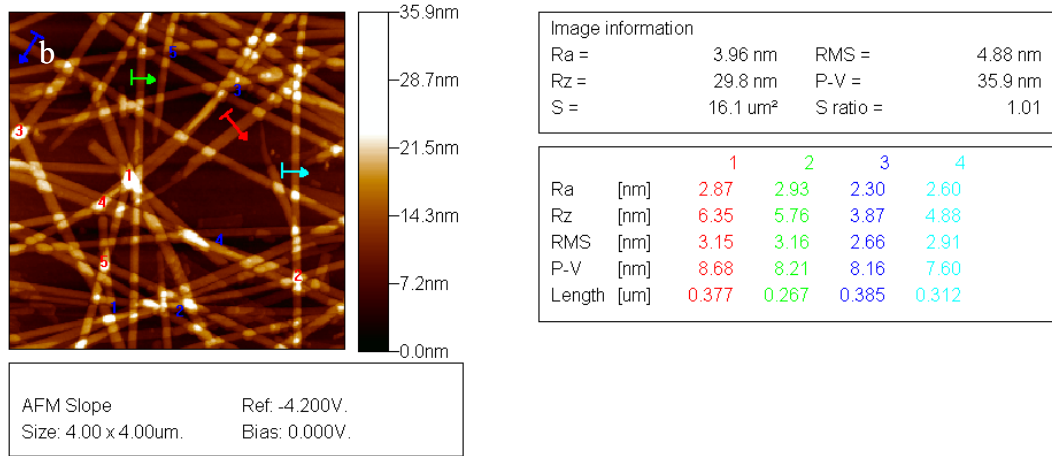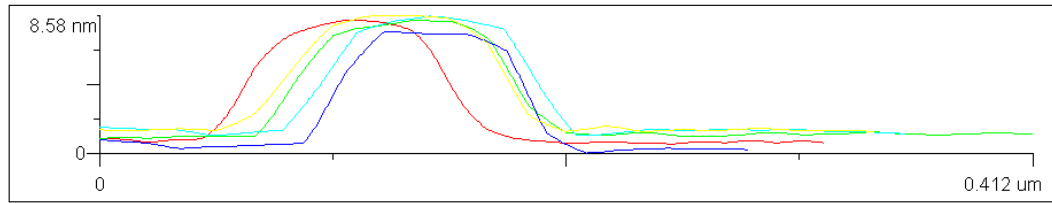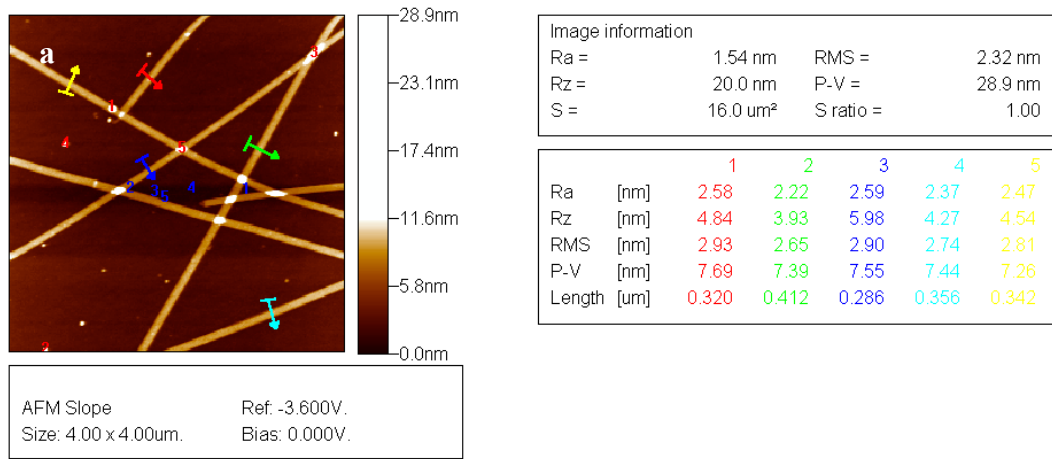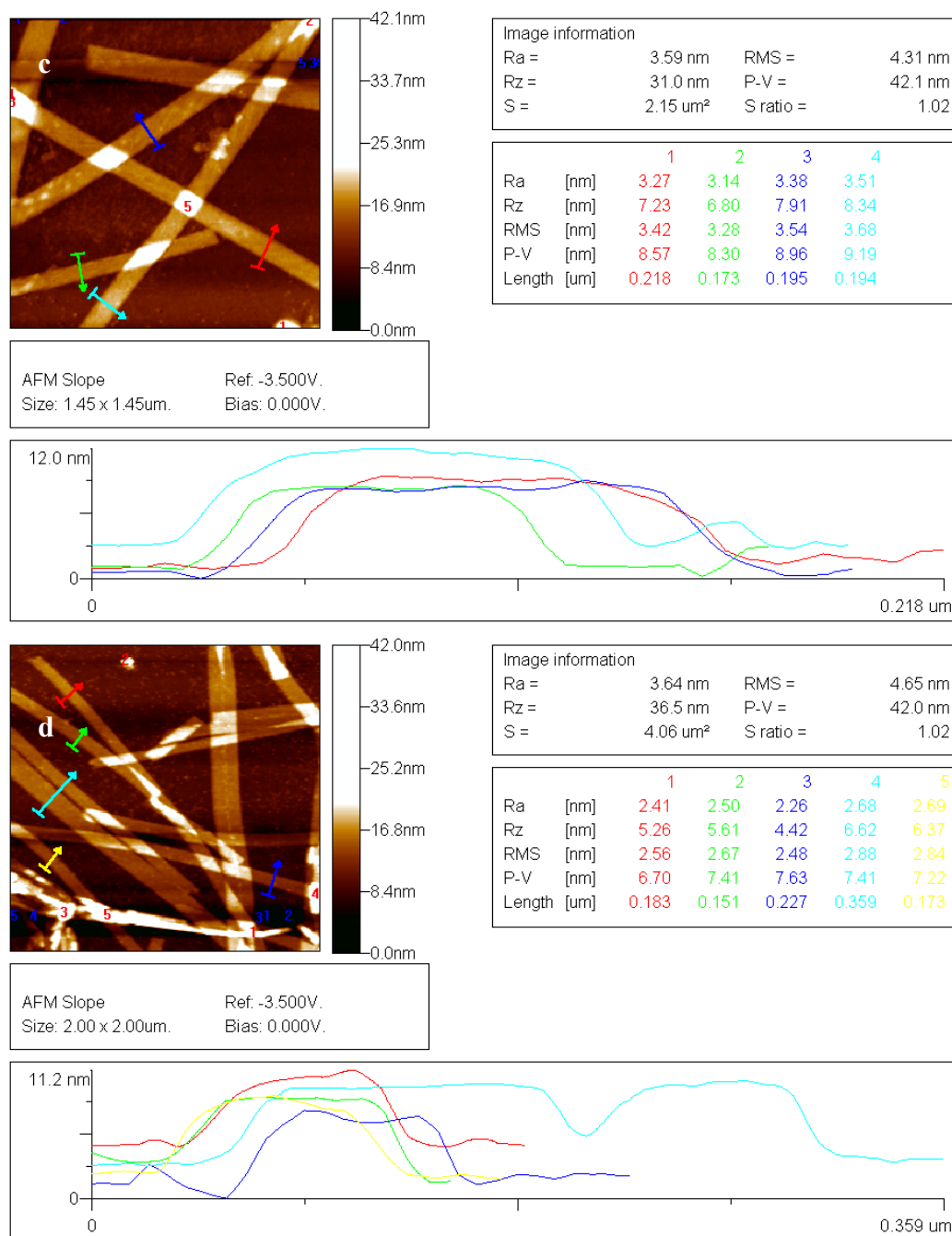
Figure 3-6. AFM images of nanotubes with measurement profiles.

Assemblies prepared with (a) N-acetyl-Aβ(16-22), (b) N-propyl-Aβ(16-22), (c) N-lauryl-Aβ(16-22), and (d) N-tridecyl-Aβ(16-22) were imaged in topography by non-contact mode under the dry condition.

In each case, 1.2 mM peptide was incubated in 40% acetonitrile / water with 0.1% TFA at room temperature for 3 weeks. The AFM samples were prepared by applying 20 µL diluted preformed tubes (0.2 mM) on the freshly cleaned silica chips. After 1min incubation, the extra solvent was wicked off with a piece of wedged filter paper, followed by storing silica chips in a desiccator overnight. The final AFM images shown here were background subtracted and brightness adjusted.. The tube height shown as the

value (P-V nm) was measured with WinSPM data analysis software.

Table 3-2. Tube wall thickness obtained using AFM.

The tube height is the average of 10 separate height measurements, expressed as ± SD.

N-X-Aβ(16-22)	acetyl	propyl	lauryl	tridecyl
Tube wall thickness (nm)	3.8 ± 0.3	4.1 ± 0.3	4.2 ± 0.3	3.8 ± 0.3

In the bilayer model of the nanotube, antiparallel arrangement of N-acetyl-Aβ(16-22) peptides places half of the lysine residue inside the bilayer and half contributing to a positively-charged inside and outside tube surface (Mehta et al., 2008). This arrangement has been previously tested by the tube binding affinity to negatively-charged gold colloidal (Kun Lu, 2004). Since the N-alkanes are covalently attached to the lysine residues, it is possible that the lysine side-chains might be less accessible to the nanoparticles. The images shown in Figure 3-7 are consistent with that N-lauryl-Aβ(16-22) assembled tubes have the same specific gold binding as the N-acetyl-Aβ(16-22) tubes.
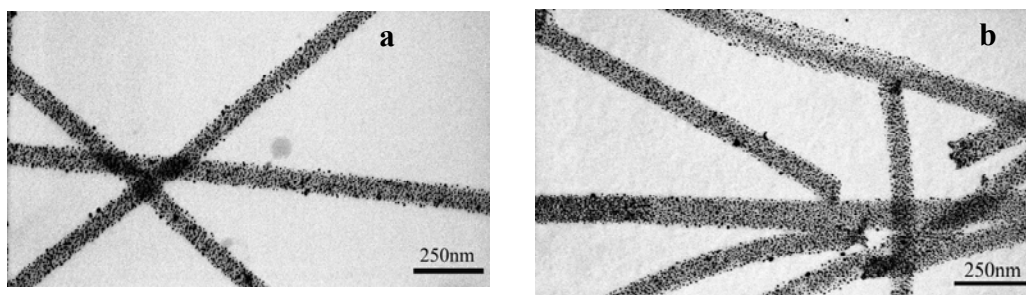
Figure 3-7. TEM images of gold-bound nanotubes.

(a) N-acetyl-Aβ(16-22) nanotubes or (b) N-lauryl-Aβ(16-22) nanotubes were mixed with negatively charged gold colloids at a peptide to gold colloid ratio of 1: 10 and incubated at room temperature for 1 hour. Then the purple precipitant was pelleted to remove the unbound gold particles, following by resuspension of pellet and TEM imaging without uranyl acetate staining.

Congo red (CR) is now known to bind end–to-end as J-aggregates in the laminate groves of N-acetyl-E22L tubes (Childers et al., 2009a). If the laminate groves are

occupied by the alkyl chains, i.e., allowing the lysine side chains to associate with the gold nanoparticles, CR's ability to line the laminate surface may be compromised. Due to the pKa of CR, binding is limited to neutral or slightly basic pH, so N-octanoyl-E22L tubes whose self-assemble is pH-independent, were selected for analysis. As a control (Figure 3-8), when CR bound to the N-acetyl-E22L tubes, the λ_{max} intensity increased and red-shifted, consistent with J-aggregation of CR in the lamination grove (Childers et al., 2009a). However, the binding of CR with N-octanoyl-E22L tubes resulted in a CRλ_{max} intensity decrease and blue-shift (Figure 3-8, blue dotted line). This change in the transition might be consistent with CR association with the alkanes, but certainly suggests that the arrangement of CR on the tube surface is altered.
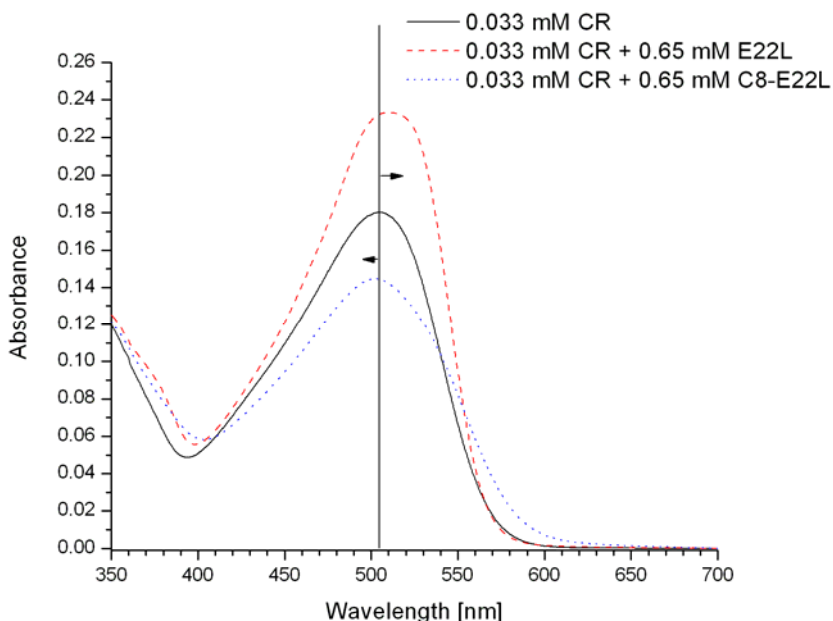
Figure 3-8. UV spectra of Congo red binding to nanotubes.
The mature nanotubes, prepared in 40% acetonitrile with 15 mM MES buffer at neutral pH, were mixed with CR with ratio of 20:1 (CR / peptide) and incubated overnight to ensure equilibrium binding. In the figure, the solid black line represents 0.033 mM CR only; red dashed line means 0.033 mM CR + 0.65 mM N-acetyl-E22L tubes and blue dotted one stands for 0.033 mM CR + 0.65 mM N-octanoyl-E22L tubes.

Do the N-terminal alkyl chains alter the peptide repeat distances?

Amyloid self-assemblies usually display two orthogonal diffraction d-spacings, assigned as the hydrogen-bonded peptide strand spacing of 4.7 Å (Geddes, 1968; Krejchi, 1997; Sikorski, 2003) and the sheet laminate spacing, which is side chain size-dependent and ranges from 3.4 Å (Fraser, 1973) to 14 Å (Keith et al., 1969). To evaluate the possible perturbation of the tube structure by the N-terminal long alkanes, x-ray and electron diffraction were used to measure the d-spacings within these assemblies. As shown in the Figure 3-9 and Table 3-3, all the self-assemblies display same hydrogen-bonding distance of 4.7 Å by both X-ray and electron diffractions, while the lamination distance appears to depend on the N-terminal alkyl chain length. Distinct from two lamination distances observed for N-X-Aβ(16-22) (X = propyl to palmityl) fibrils assembled under neutral conditions (Figure 2-3), at acidic pH single lamination spacing of 10.4±1 Å, increasing with the N-terminal alkyl chain length, is obtained for tubes and sheets in Group I to III (Figure 3-9 and Table 3-3). Remarkably, two more extra bands with distance of 5.8 Å (X-ray diffraction) and 4.4 Å (electron diffraction) were observed for N-lauryl tubes, which may be from the arrangement of N-alkanes and the new peptide plane (Childers et al., 2009b), respectively. While, the longer alkane substituent N-myristyl- and N-palmityl-Aβ(16-22) fibrils display two lamination distances, 9.8 Å and 13.2 ± 0.2 Å (Figure 3-9a) reflected by X-ray diffraction, suggesting two distinct sheet-sheet stacking interfaces, consistent with parallel β-sheets. These two lamination distances may give the corresponding bands in electron diffraction micrographs, which require further investigation.
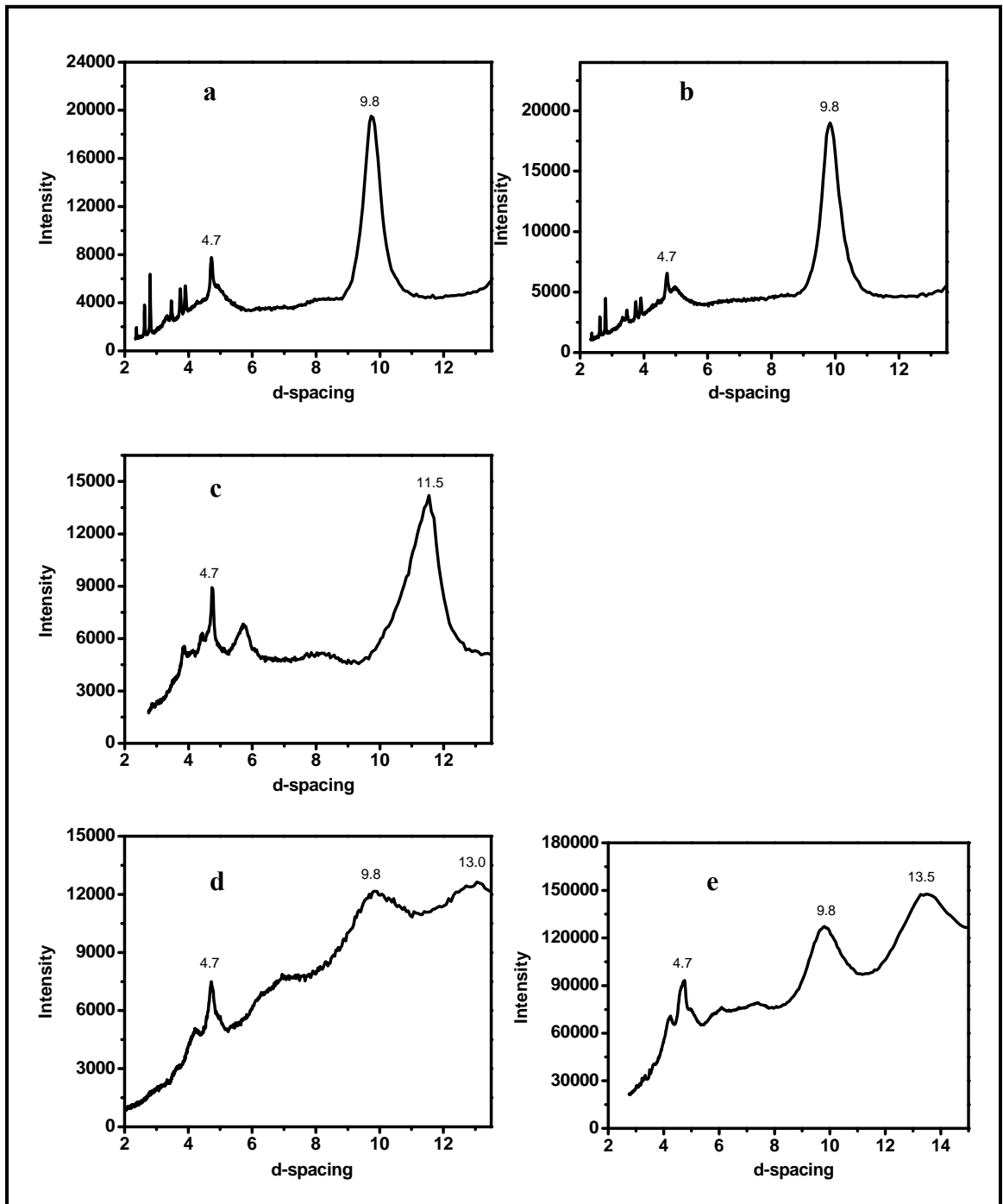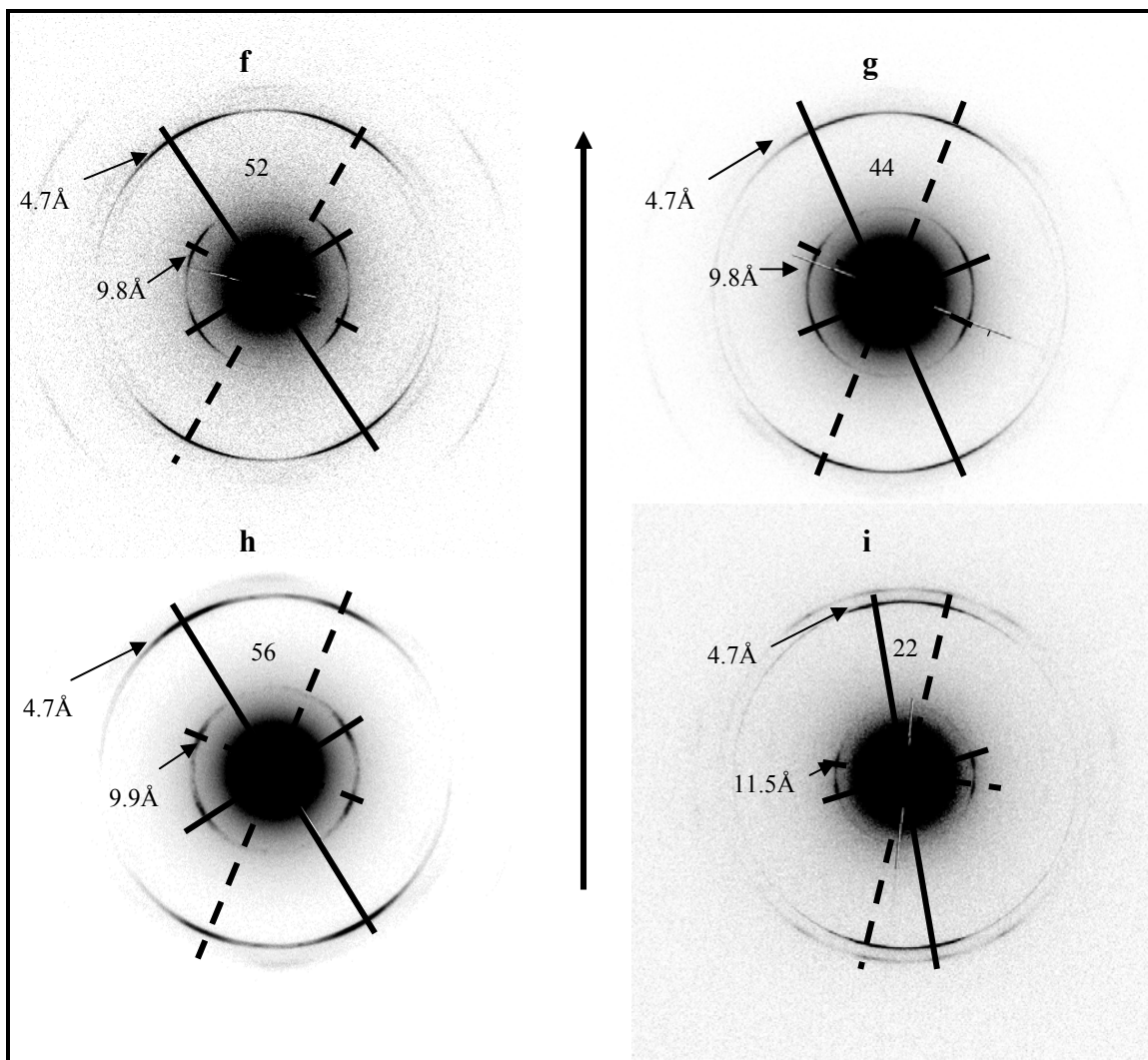
Figure 3-9. X-ray and electron diffractions of the peptide assemblies at acidic pH.

X-ray powder diffraction of selected (a) N-acetyl, (b) N-propyl, (c) N-lauryl, (d) N-myrityl and (e) N-palmityl-Aβ(16-22) peptide assemblies at acidic pH.

The electron diffraction of aligned (f) N-acetyl, (g) N-propyl, (h) N-butyl and (i) N-lauryl-Aβ(16-22) nanotubes at acidic pH. Dashed and solid crossed-lines represent the two sets of hydrogen-bonding and lamination distance reflections from each nanotube wall. The offset between hydrogen-bonding arcs of each cross-β pattern is 26° ± 2°, 28° ± 2°, 22° ± 1° and 11° ± 1° for N-acetyl, N-propyl, N-butyl and N-lauryl nanotubes, respectively. The small arrows specify the d-spacing for each arc, and the number between the cross-β patterns specifies the angles, while the thick black arrow indicates the direction of aligned tubes. The white thin line across the center is the technique artifact.

Table 3-3. Peptide repeat distances.

The assignments are based on X-ray and/or electron diffraction micrographs from the H-bonding and lamination d-spacings.

N-X-Aβ(16-22))	acetyl C2	propyl C3	butyl C4	valeryl C5	caporyl C6	ocantoyl C8	lauryl C12	palmityl C16
H-bonding (Å)	4.7	4.7	4.7	4.7	4.7	4.7	4.7	4.7
Lamination (Å)	9.8	9.8	9.9	10.0	10.2	10.4	11.5	9.8 / 13.5

Relative to X-ray powder diffraction, electron diffraction micrographs of oriented tubes give extra information to assign the offset between hydrogen-bonding arcs in the top and bottom of tube walls, half of which is called tube tilt angle. As shown in Figure 3-9b, the tube tilt angle decreases with increasing alkyl chain length from 25° ± 3° for N-acetyl- to N-butyl-Aβ(16-22) tubes to 11° ± 1° for N-lauryl-Aβ(16-22) tubes. Significant decrease of the tube tilt angle may suggest that the inclusion of N-lauryl impact on the bilayer packing and tube persistent length.

What is the conformation of N-lauryl chain within nanotubes?

The N-acetyl-Aβ(16-22) and N-lauryl-Aβ(16-22) tubes are remarkably similar, maintaining the same peptide β-sheet secondary structure, the relative peptide arrangement within tubes, identical hydrogen-bonding peptide repeat distances, and a positively-charged tube surface. However, the N-lauryl-Aβ(16-22) assembly has a longer lamination distance, a smaller tilt angle, and a wider lamination grove that is no longer accessible to CR. To probe whether both peptides are able to co-assemble, the N-acetyl-
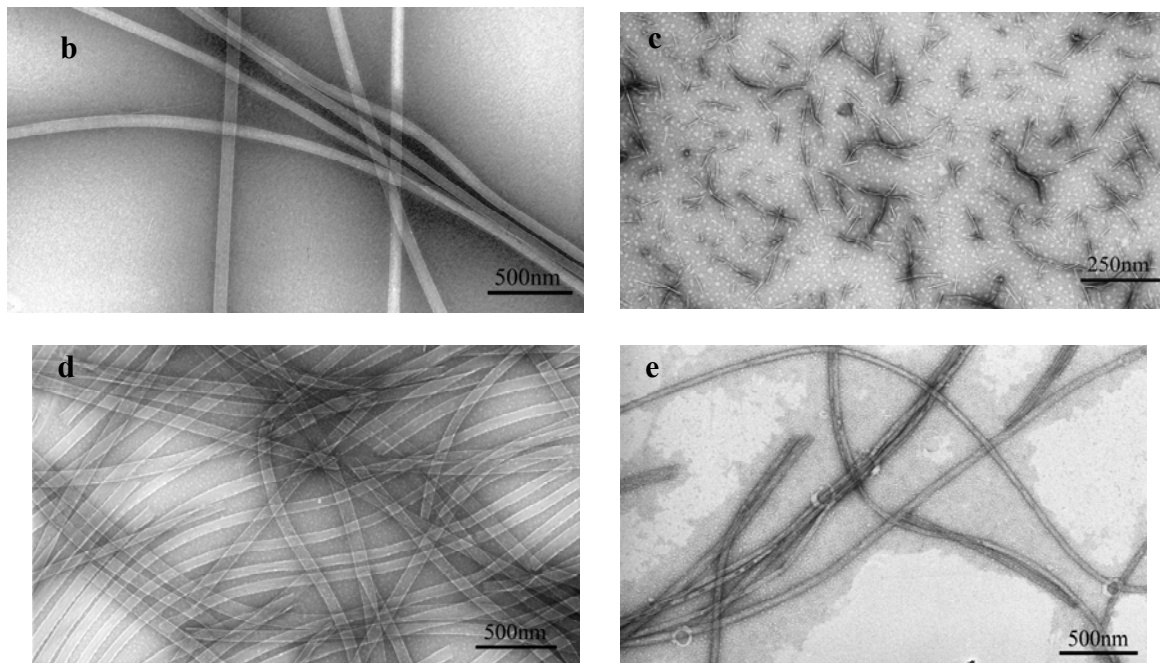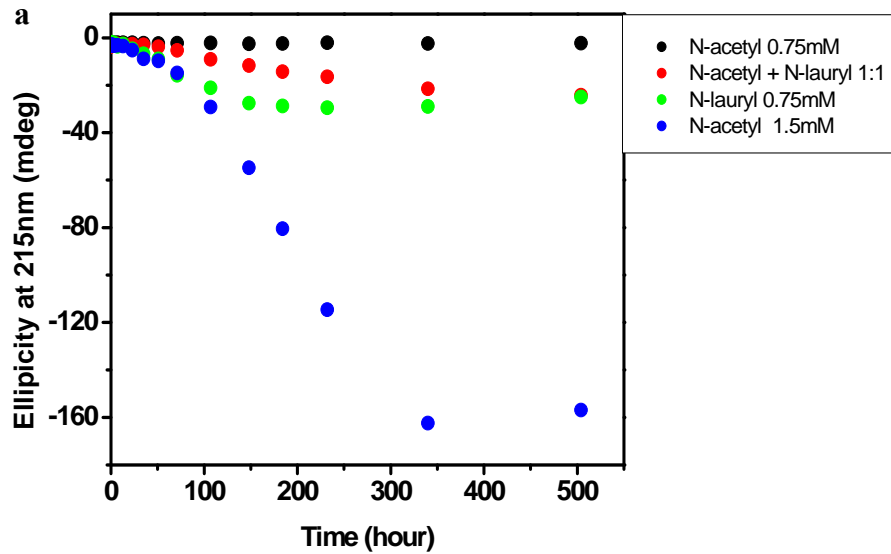
Figure 3-10. Co-assembly of N-acetyl-Aβ(16-22) and N-lauryl-Aβ(16-22).

(a) The kinetic curve by following the negative ellipticity at 215 nm with time. The peptide with specific concentration was incubated in 40% acetonitrile/water with 0.1% TFA and the aliquots were taken for CD analysis. The graph is plotted by the ellipticity intensity at 215 nm over time.

Electron micrographs of (b) 1.5 mM N-acetyl-Aβ(16-22), (c) 0.75 mM N-acetyl-Aβ(16-22), (d) 0.75 mM N-lauryl-Aβ(16-22) and (e) 0.75 mM N-acetyl-Aβ(16-22) + 0.75 mM N-lauryl-Aβ(16-22). The EM was taken after 3 weeks incubation.

Aβ(16-22) and N-lauryl-Aβ(16-22) peptides were mixed 1:1 to a final peptide concentration of 1.5 mM (Fig 3-10). N-acetyl-Aβ(16-22) with concentration of 1.5 mM formed homogenous nanotubes with diameter of 44 ± 4 nm (Figure 3-10b) and the CD analysis showed that it developed strong negative ellipticity at 215 nm and reached the plateau at about 350 hr. However, half of N-acetyl-Aβ(16-22) (0.75 mM) only assembled to thin filaments with diameter of 5 ± 1 nm, which displayed random coil CD signal (Figure 3-10b). At this concentration (0.75 mM), N-lauryl-Aβ(16-22) self-assembled to slightly larger nanotubes with diameter of 53 ± 5 nm, reaching the plateau after 120 hr even though the negative ellipticity was relatively low. However, the mixing of 0.75 mM N-acetyl-Aβ(16-22) and 0.75 mM N-lauryl-Aβ(16-22) peptide monomers significantly increased the maturation time from 120 hr to 400 hr and the EM established that this mixture formed smaller nanotubes with diameter of 25 ± 6 nm. This suggests that the structure difference of N-acetyl-Aβ(16-22) and N-lauryl-Aβ(16-22) tubes slow down the peptide recognition process, but the structure similarity between them allows the coassembly of both peptide to different-sized nanotubes. The distribution of both peptides within final assemblies requires further ssNMR investigation.

We hypothesized that the greatest impact of N-terminal long alkanes on the recognition of these two peptides would occur at the bilayer leaflet packing interface. While diffraction defined the lamination distance and hydrogen-bonding distance quite nicely, no reflections were expected for a bilayer arrangement. Accordingly we sought to measure the distance across the leaflets of the bilayer with ssNMR dipolar recoupling with a windowless sequence (DRAWS) technique (Benzinger et al., 1998; Benzinger et al., 2000). Since DRAWS is able to measure ^{13}C-^{13}C distance which is shorter than 6.5 Å,

with the previously assigned antiparallel one-residue out-of registry configuration, placing a [1-^{13}C] label at the N-terminal alkyl chain carbonyl would isolate spins along both the hydrogen-bonding dimension (separated by 9.4 Å) (Figure 3-11a) and β-sheet lamination (11.5 Å in Figure 3-9), hopefully allowing direct interrogation of the leaflet bilayer interface. The DRAWS data of [1-^{13}C]N-acetyl-Aβ(16-22) nanotubes fit to a 5.3 Å bilayer distance (W. Seth Childers, 2010), while the same labeling scheme of [1-^{13}C]N-lauryl-Aβ(16-22) nanotubes yielded, at best, a very weak coupling between leaflets (Figure 3-11b), suggesting incorporation of N-lauryl group altered leaflet packing and somehow positioned the ends of the adjacent leaflets outside DRAWS range (6.5 Å).
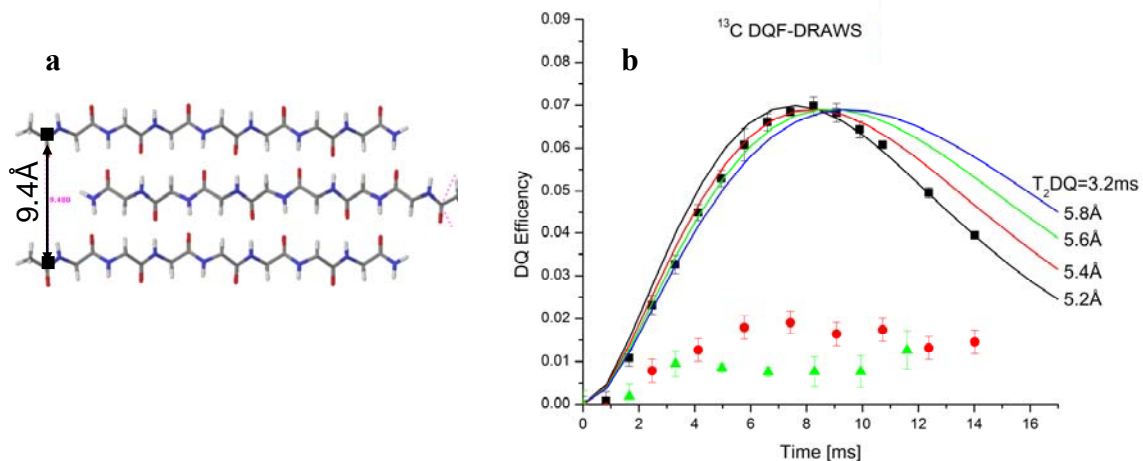
Figure 3-11. ^{13}C DQF DRAWS for [1-^{13}C]N-acetyl-Aβ(16-22) and [1-^{13}C]N-lauryl-Aβ(16-22) nanotube.

(a) Structural model of the antiparallel one-residue out-of register   -sheet with the distance of 9.4 Å between every other acetyl carbonyls.

(b) The DRAWS data and fitting curves for both [1-^{13}C]N-acetyl-Aβ(16-22) (black square), [1-^{13}C]N-lauryl-Aβ(16-22) nanotubes (red circle) and natural abundance N-acetyl-Aβ(16-22) fibers (green triangle) as the control.

To evaluate the different conformations of the N-acetyl and N-lauryl chains, [^{15}N]L17 was incorporated together with [1-^{13}C]N-acetyl or [1-^{13}C]N-lauryl to measure the intrastrand distances with ^{13}C{^{15}N} rotational-echo double-resonance (REDOR) experiments (Saalwachter and Schnell, 2002). Boltzmann statistics REDOR analysis (BS-REDOR) (Gehman et al., 2007), one of the solid-state NMR techniques, offers the way to measure the hetero-nucleus distance between ^{13}C-^{15}N within the range of 7.0 Å. BS-REDOR provides an unbiased fit of REDOR dephasing data to isolated ^{13}C-^{15}N spin pairs, and in this case, displayed two ^{13}C-^{15}N distance distributions for [1-^{13}C]N-acetyl-Aβ(16-22)[^{15}N]L17 nanotubes centered at 3.6 Å for 24% and 4.5 Å for 73% of the sample (Figure 3-13b) . In contrast, the BS-REDOR fits for the N-lauryl-Aβ(16-22) assembly were consistent with 94% of the sample with a ^{13}C-^{15}N distance of 3.8 Å (Figure 3-13c), indicating that the majority of the carbonyl carbons have the same conformation.

MD simulations on a block of 6 laminated β-sheets of 6 H-bonded peptides each in explicit water (Mehta et al., 2008) suggests that the acetyl (C2) capping group can adopt two conformations, one adopting α-helical conformation (Figure 3-12), which positions the N-terminal acetyl with a ^{13}C-^{15}N distance of 3.6 Å. The second conformation places the lysine backbone in a typical extended β -sheet conformation (Figure 3-12) with a
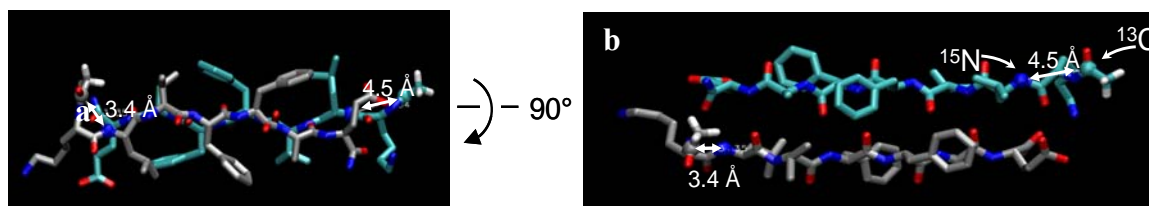
Figure 3-12. MD simulation of N-acetyl-Aβ(16-22) with different terminal conformation.
(a) Side view of two peptide strands with antiparallel organization and lysine backbone adopts *trans* and *cis* conformation in blue and gray strands, respectively.
(b) Top view of the same peptides after 90° rotation from (a). The distances of 3.4 Å and 4.5 Å between [^{15}N]L17 and [1-^{13}C]N-acetyl are specified in Figure.

longer ^{13}C-^{15}N distance of 4.5 Å. One possible rationalization of these dramatic differences between the N-acetyl and N-lauryl groups is that the increased hydrophobicity of N-lauryl substituent demands burial in the hydrophobic grove and this burial distorts the carbonyl carbon to adopt a single conformation.
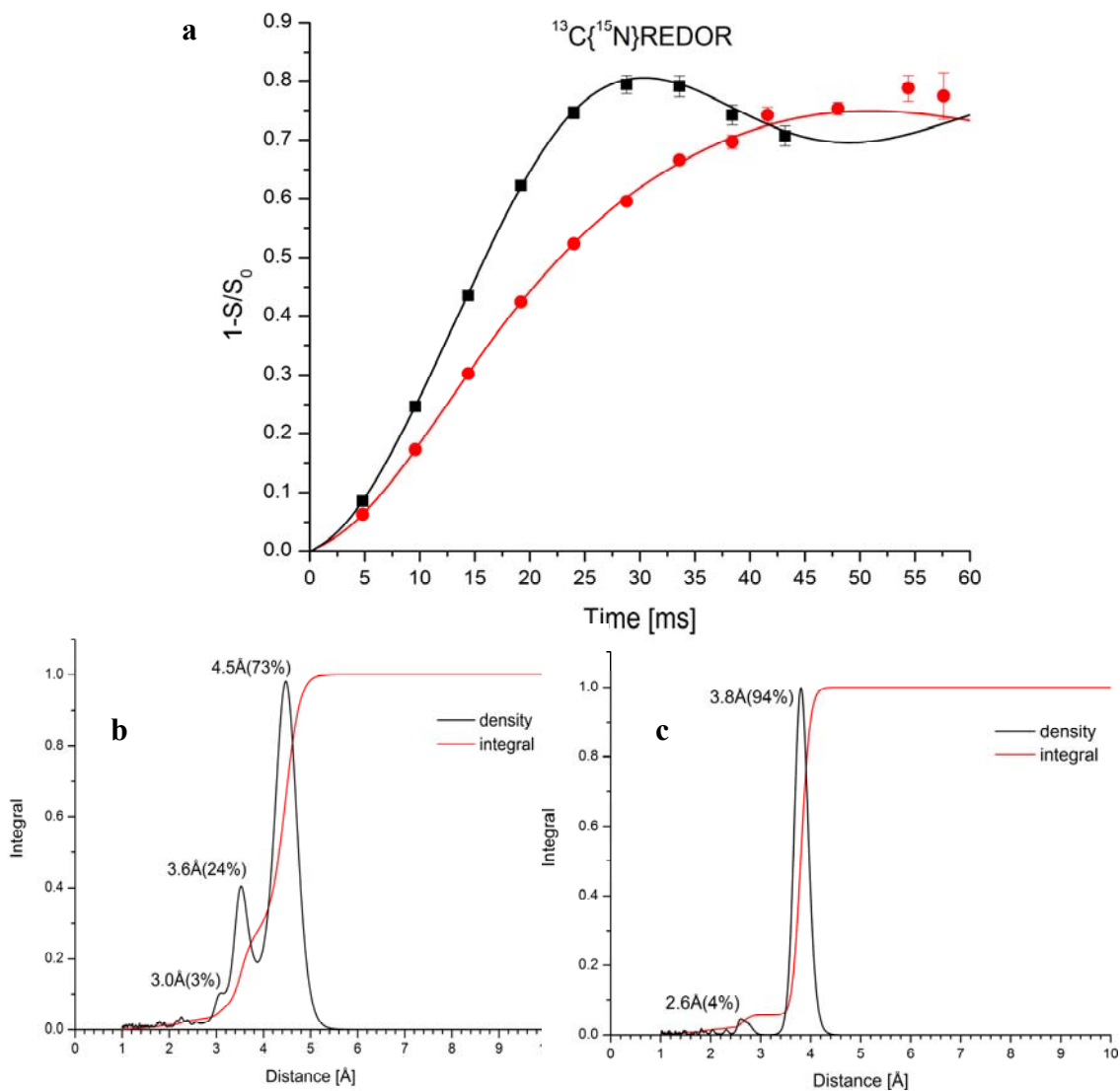
Figure 3-13. REDOR analyses of [^{15}N]L17 and [1-^{13}C]N-alkyls in self-assembled nanotubes.
(a) REDOR measurements of [1-^{13}C]N-acetyl-Aβ(16-22)[^{15}N]L17 (red circle) and [1-^{13}C]N-lauryl-Aβ(16-22)[^{15}N]L17 nanotubes (black square).
The solid lines are the fitted REDOR curves by calculation. The distance fitting curve for (b) N-acetyl-Aβ(16-22) nanotubes and (c) N-lauryl-Aβ(16-22) nanotubes.

To further constrain the lauryl chain, the distance from lauryl group's methyl ^{13}C to ^{15}N of valine was measured by ^{13}C{^{15}N}REDOR. The dephasing data can be fitted to two roughly equivalent populations with distances of 5.0 Å and 6.8 Å (Figure 3-14). Together with the uniform intrastrand distance of [1-^{13}C]N-lauryl-Aβ(16-22)[^{15}N] L17, the result here further constraints the location of N-lauryl groups in laminated β-sheets (Figure 3-15).
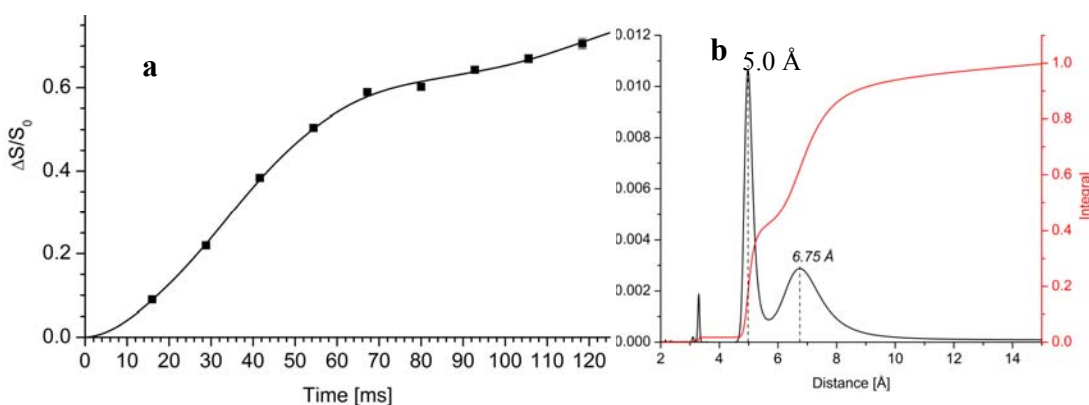
Figure 3-14. REDOR measurement of peptide terminal intrastrand distance.
(a) REDOR dephasing and (b) BS-REDOR fitting curve of [12-^{13}C]N-lauryl-Aβ (16-22) [^{15}N]V18 nanotubes.

Discussion

We show that alkyl chains promote the self-assembly of peptides (Hartgerink et al., 2001; Hartgerink et al., 2002) and define how the N-alkanes are accommodated within the nanotube β-sheet structure and how the inclusion alters the tube structure.

This study demonstrates that the Aβ-lipid chimeric assembly is a useful *in vitro* model system to investigate membrane/protein interaction. The introduction of N-alkanes does not change the dominant role of peptide segment on assembly morphology and

peptide arrangement. In addition, this study shows the direct view of Aβ-lipid interaction, defined by ssNMR relative to the previous neutron scattering and fluorescence studies (Ashley et al., 2006; Kremer et al., 2001). Therefore, with the investigation of N-lauryl-Aβ(16-22), we have taken the first steps to elucidating the molecular-level interaction between Aβ-peptide and lipid alkanes in this hybrid architecture. The N-lauryl-Aβ(16-22) structural model highlights the potential coupled interaction between alkanes and the cross-β structure. Molten-globule like oligomers at the membrane surface have the potential to interact and bury the lipid alkanes within cross-β laminates. In contrast, the buried cross-β laminates of mature fibrils are inaccessible. Indeed, the automatic insertion of lipid alkanes into hydrophobic β-sheet laminates is consistent with experimental evidence that soluble Aβ-aggregates may insert into lipid bilayer (Ashley et al., 2006; Kremer et al., 2001) or extract lipid from bilayer (Jayasinghe and Langen, 2007; Sparr et al., 2004) disrupting membrane organization (D'Errico et al., 2008; Dante et al., 2006; Friedman et al., 2009).

Understanding the interaction between lipid and amyloid peptide is critical to uncovering the mechanism of the cytotoxicity and neurological dysfunction in amyloid diseases (Ashley et al., 2006; Bystrom et al., 2008; Kremer et al., 2001). To extend the study of Aβ-lipid interaction at neutral pH in Chapter 2, this chapter presents a systematic study of the chimera self-assemblies (N-X-Aβ(16-22) (X = acetyl to palmityl)) at acidic pH, which further demonstrates that the Aβ-lipid chimeric assembly is a useful *in vitro* model system to investigate membrane/protein interaction. Suppression of the cross-sheet electrostatic interaction by protonation of Glu22 at acidic pH, the self-assembly registry and morphology is able to be overridden by peptide segment, independent of alkane

length in the range of N-acetyl to N-tridecyl substituents. This is distinctly different from the hydrophobic clustering of alkanes in conventional peptide-amphiphiles (Hartgerink et al., 2001; Hartgerink et al., 2002), which may attribute to the inherent hydrophobic property of Aβ peptide and size-distribution of amino acid residues (Hartgerink et al., 2001; Hartgerink et al., 2002; Lu et al., 2003; Mehta et al., 2008). The structural model of N-lauryl-Aβ(16-22) nanotubes proposed in this study (Figure 3-15) now argues the unique capacity of the hydrophobic interior of amyloid's cross-β laminate to bury alkyl chains (Figure 3-15), which shows the different ways to desolvate alkyl chains from that occurring in parallel β-sheet fibrils (neutral pH) and conventional peptide-amphiphiles (Hartgerink et al., 2001; Hartgerink et al., 2002).
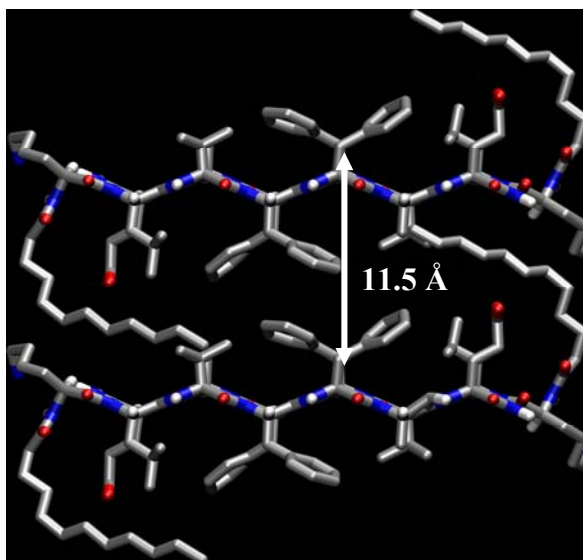
Figure 3-15. Structural model of β-sheet-stacking within N-lauryl-Aβ(16-22) tubes.
Two peptides represent the front strands of each sheet. Two sheets pack with a distance of 11.5 Å, highlighted with the white arrow. The color code is red (oxygen), blue (nitrogen) and gray (carbon).

V18-A21 cross-strand pairing interaction overwhelms the electrostatic interaction and alkane hydrophobic clustering at acidic pH to direct antiparallel one-residue out-of register β-sheet formation. In this study, the assemblies of N-acetyl to N-tridecyl

substituent all adopt antiparallel out-of registry, independent of N-alkane length (Figure 3-4). Previous study suggests that this peptide arrangement is driven by V18-A21 cross-strand pairing (Mehta et al., 2008), consistent with the assemblies of N-octanoyl-E22L at both acidic and neutral pHs (Figure 2-7) in the absence of electrostatic interaction. The antiparallel β-sheets directed by V18/A21 cross-strand pairing interaction create a unique hydrophobic environment to accommodate N-alkanes up to tridecyl chain. Firstly, the uniform hydrophobic sheet-sheet interface allows the insertion of N-alkanes without bias, which gives one single lamination distance (Figure 3-9), instead of two found in parallel β-sheet fibrils (Figure 2-14). Of the diverse morphologies generated in this study, the nanotubes from the Group III N-undecyl to N-tridecyl peptides (Figure 3-1) appear to represent an optimal match between the alkyl chain and the β-sheet laminates, consistent
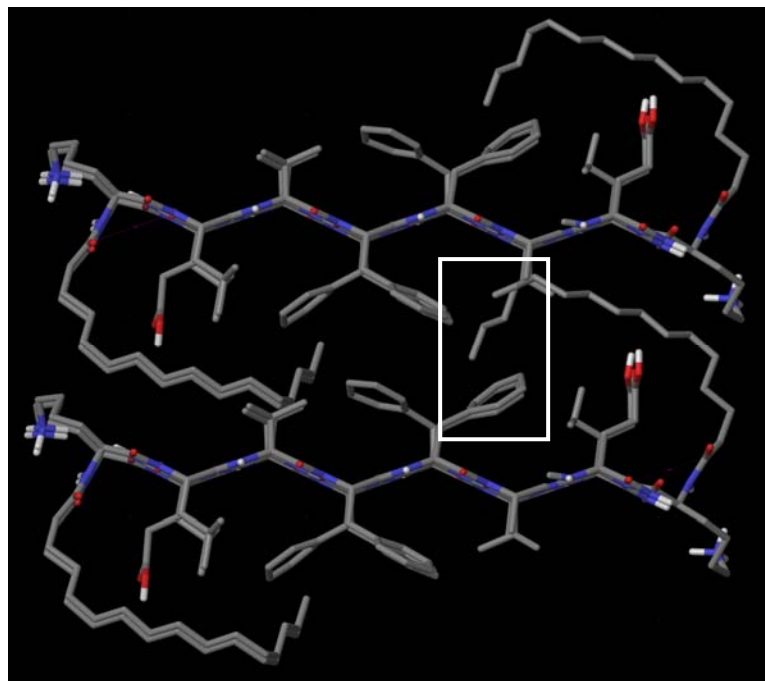
Figure 3-16. Model of antiparallel β-sheets of N-palmityl-Aβ(16-22) at acidic pH.

Two sheets of 3 strands each constructed with a possible configuration of the N-palmityl chain buried in the antiparallel β-sheet laminates. White box highlights the hydrophobic clash between the tails of palmityl group with aromatic residues in the laminates.

with the small cavity created by residue V18 and A21 in the laminates. While for the longer N-alkanes, the structure model shows the unfavorable hydrophobic clash between the extra alkane tail with the larger aromatic residues Phe19 and Phe20 (highlighted in white box Figure 3-16), which may account for the peptide arrangement switch of N-myristyl and N-palmityl-Aβ(16-22) β-sheets from antiparallel to parallel under this condition (Figure 3-4b). However, together with the parallel β-sheets formed by N-X-Aβ(16-22) (X = propyl to palmityl) at neutral pH (Gordon et al., 2004), the antiparallel β-sheets assembled at acidic pH here also argue that the peptide with high assembly propensity could override the hydrophobic clustering interaction of alkanes in the peptide-amphiphile assemblies (Hartgerink et al., 2001; Hartgerink et al., 2002).

Inclusion of two portions (tail and head) of alkanes at different positions in antiparallel β-sheets alters some of the tube structure and property, even though the tube morphology and peptide arrangement are maintained. As shown in the bilayer structure model (Figure 3-17), the tail portion of alkanes (in blue box) located in the laminates interacts with residues V18/A21, expanding the β-sheets (Figure 3-9). The head portion of N-alkanes located at the tube bilayer interface (in red box) slightly expands the bilayer distance within measurement error by AFM (Figure 3-6). However, the introduced hydrophobic interaction between bilayer may increase the bilayer rigidity, accounting for the tube pitch and size increase (Figure 3-9, 3-19 and Table 3-4). The head of N-alkanes at the tube outer surface (in yellow box) may alter the tube surface property by blocking the lamination grove, resulting in the different Congo red binding fashion illustrated in Figure 3-18. This study establishes the cavities within peptide nanotubes with limited space to accommodate the extra small groups, consistent with the peptide arrangement

and assembly morphology switch by the attached large groups (such as rhodamine and biotin) (Liang et al., 2008a; Lu, 2005). Also, these small cavities may be able to hold small drug molecules, which may find potential application as a drug delivery carrier.
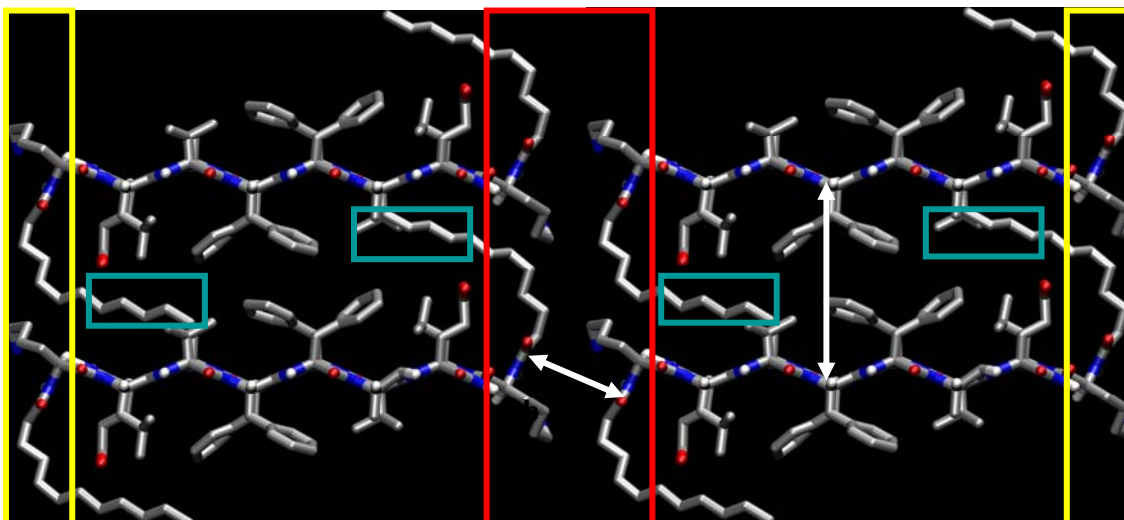
Figure 3-17. Bilayer structure model of N-lauryl-Aβ(16-22) nanotubes.

The lamination distance is 11.5 Å and bilayer distance of 6.5 Å is indicated. The different portion of N-alkanes located at different places is highlighted in colored box: red for N-alkane head in the bilayer interface and the yellow for it at tube outer surface; he blue for N-alkane tail in the laminates.

Table 3-4. Summary of the parameters related to nanotube size.

These parameters are determined from the TEM tube widths and electron diffraction data (Dong et al., 2006).

N-X-16-22	Radius ρ (nm)	Tilt angle α (º)	Pitch angle Ψ (º)	Pitch p (nm)	Ribbon width W (nm)	Laminate number
acetyl-	22 ± 2	26 ± 2	64	283	124	127
propyl-	20 ±3	22 ± 1	68	311	116	118
butyl-	34 ± 2	28 ± 1	62	402	189	191
undecyl-	27 ± 2	17 ± 1	73	555	162	141
lauryl-	27 ± 2	11 ± 1	79	872	166	144

a. N-acetyl-Aβ(16-22)E22L

b. N-octanoyl-Aβ(16-22)E22L
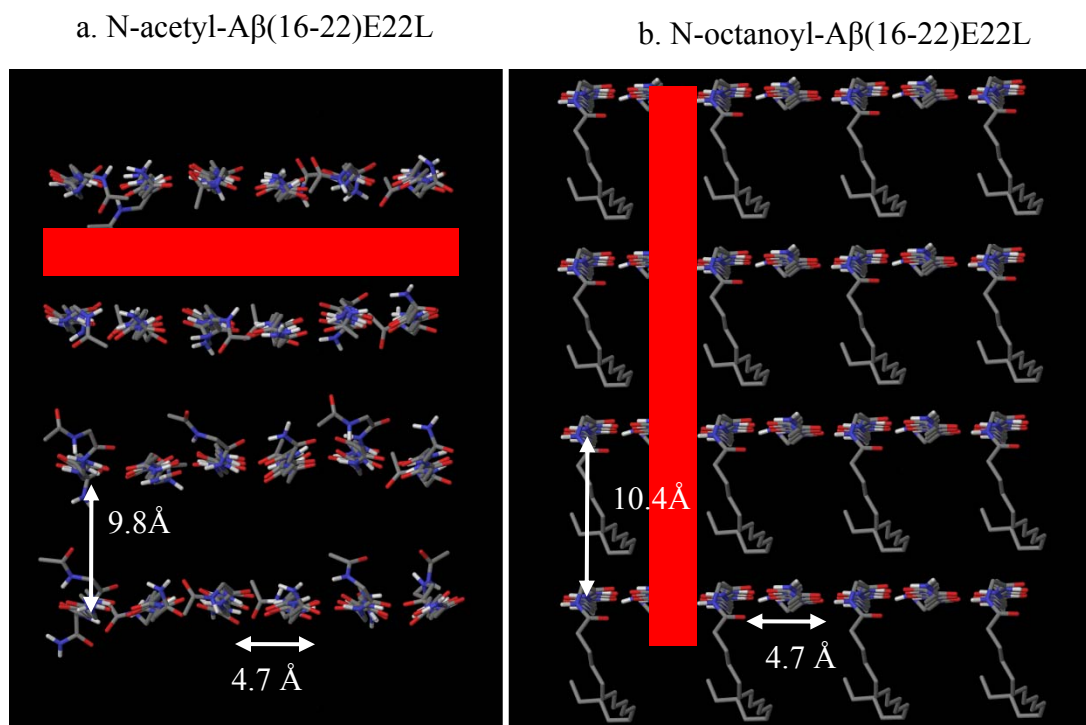
Figure 3-18. Illustration of Congo Red binding on the nanotubes surface.
(a) A congo red molecule (reb bar) binds in N-acetyl-Aβ(16-22)E22L β-sheet lamination grove. Four sheets, each contains 6 peptide strands with H-bonding distance of 4.7 Å stack with lamination distance of 9.8 Å.
(b) The Congo red molecule (reb bar) may bind across β-sheet laminats of N-octanoyl-Aβ(16-22)E22L, because the lamination grove has already been blocked by N-alkanes. Four sheets, each contains 6 peptide strands with H-bonding distance of 4.7 Å stack with lamination distance of 10.4 Å.

The identification of this cavity created by V18 / A21 in amyloid may well prove to be critically important to our understanding of these assemblies at membrane surfaces. How these covalently derivatized peptides may differ from the intermolecular association with phospholipid alkyls, the degree of double bond functionality that can be accommodated, and how such integration between lipids and peptide impacts membrane function and memory will now need to be understood. Additionally, this novel self-assembly architecture is complementary to the existing peptide-amphiphile library,

expanding our view for the peptide-amphiphile assembly. Moreover, these findings clearly establish that N-terminal alkyl chains are able to tune the amyloid self-assembled morphology, peptide orientation, tube / fibril surface properties and the distance between specific residues such as lysine at the outer surface. The tuning capability could be utilized to design distinct materials with properties that range from novel self-assembling surfaces, robust compartments, and other components for building supermolecular self-assemblies. And most importantly, the findings in this chapter uncovered many complementary aspects of the rules that govern amyloid interaction with alkyl chains, which is critical to rational design of amyloid-based nanomaterials and amyloid-related disease inhibitors.

Materials and Methods

Circular dichroism spectroscopy

Jasco-810 CD spectropolarimeter was used to record circular dichroism (CD) spectra of 20 μL of sample in 0.1 mm path length cell at room temperature. The presented spectra represent the average of three scans between 260 nm to 190 nm with a step size of 0.2 nm and a speed of 100 nm/s.

Kinetics measurement

Since the peptide was purified with mixtures of acetonitrile and water with 0.1% TFA, which is the same solvents used for the tube sample preparation, there are preformed seeds after purification and lyophilization. Therefore, in order to better compare the self-assembly kinetics, the peptide powder sample should be treated with

hexafluoroisopropanol (HFIP) to disaggregate the preformed seeds (Hirota-Nakaoka et al., 2003) before the sample preparation. The weighted peptide powder was dissolved with HFIP with about 10 mg/mL for 30 min on ice, and then HFIP was gently evaporated under dry argon atmosphere. The eppendorf tube with formed transparent peptide film was placed on lyophilizer to remove any trace of HFIP. The peptide film was dissolved in 60% acetonitrile / water mixture by vortexing for 2 min, and then more water was added to render the ratio of acetonitrile / water in the final sample solution to be 40%. Then right after the sample solution was acidified with 0.1 vol% TFA, it was taken for the CD measurement to count for the time zero.

Coassembly of N-acetyl-Aβ(16-22) and N-lauryl-Aβ(16-22)

The weighted peptide powder was firstly dissolved in HFIP with concentration about 10 mg/mL. After 30 min treatment, an aliquot of each peptide HFIP solution was taken to other two vials. The mixing peptide in HFIP was further incubate for additional 20 min, and then dried under dry argon atmosphere.

Congo red binding

The matured E22L and N-octanoyl-Aβ(16-22)-E22L tubes (1.3 mM) were incubated in 40% acetonitrile / water with 15 mM pH6 MES buffer for 2 weeks. Then one aliquot of matured tubes and one aliquot of CR (0.066 mM) were mixed together and incubated overnight to reach the equilibrium. Then the mixed sample was taken UV with 1.0 cm length UV curvette. And the UV spectra were recorded from 700 nm to 350 nm.

Cryo-etch high-resolution SEM

The nanotube solution (2.0 μL, 0.2 mM) on the gold plunchet was plunge-frozen in liquid ethane. Then the frozen sample was transferred and mounted in a precooled (-180 °C) Gatan 500 CT cryostage, following by fracturing the sample surface with a prechilled blade. The cryostage was transferred to a Denton DV-602 Cr coater, where the sample temperature was gradually increased to -105 °C over 70 min and hold at that temperature to sublime ice for 10 min at 0.3 μTorr. The etched sample was quickly cooled to -170 °C. The Cr coater was flushed with 5 mTorr nitrogen for 5 min to remove the air. Then the sample was sputter-coated with 4.5 nm Cr at a rate of 0.3 Å/s and a current of 50 mA under 2 mTorr. After the coated sample was transferred to a DS-130F scanning electron microscope, the cryostage was heated slowly to -120 °C and equilibrated for 30 min before imaging.

Fourier Transform Infrared (FTIR)

Spectra were collected on a Nicolet MAGNA-IR 560 Spectrometer with 4 cm^{-1} resolution and generally 100-time scans were averaged. For sample preparation, the mature tubes were protected by bundling with Na_2SO_4 in a 1:10 ratio of peptide to sulfate (Lu et al., 2007). After 1 hour incubation, the bundled sample was pelleted at 16,100 xg for 5 min to remove un-assembled material. The fibril samples were pelleted without bundling, frozen at -80 ℃, and lyophilized to a dry powder. The dried sample was mixed well with grounded KBr (at a ratio of 1:10 (w/w)) and pressed into a transparent disk. Isotope-edited IR sample preparation was identified.

X-ray powder diffraction sample preparation

Nanotube sample was prepared according to the aforementioned procedure. The matured nanotubes were bundled with sulfate or nicotinamide adenine dinucleotide (NADH) with the ratio of peptide to sulfate 1:10 or peptide to NADH 1:4. The white precipitate was collected by centrifugation. The pellet was frozen and lyophilized to yield dry powder for X-ray diffraction.

REDOR and DRAWS sample preparation

The preformed nanotubes, prepared according to aforementioned procedure, were bundled with NADH with peptide to NADH ratio of 1 : 4. The concentration of peptide and NADH stock solution is 1.2 mM and 40 mM, respectively. The 5 separated aliquots of NADH was titrated into tubes solution every 5 min. The white precipitated was collected, frozen and lyophilized to yield dry powder.

References

Ashley, R. H., Harroun, T. A., Hauss, T., Breen, K. C., and Bradshaw, J. P. (2006). Autoinsertion of soluble oligomers of Alzheimer's A beta(1-42) peptide into cholesterol-containing membranes is accompanied by relocation of the sterol towards the bilayer surface. BMC Struct Biol *6* (21) (http://www.biomedcentral.com/content/pdf/1472-6807-6-21.pdf)

Benzinger, T. L., Gregory, D. M., Burkoth, T. S., Miller-Auer, H., Lynn, D. G., Botto, R. E., and Meredith, S. C. (1998). Propagating structure of Alzheimer's beta-amyloid(10-35) is parallel beta-sheet with residues in exact register. Proc Natl Acad Sci USA *95*, 13407-13412.

Benzinger, T. L., Gregory, D. M., Burkoth, T. S., Miller-Auer, H., Lynn, D. G., Botto, R. E., and Meredith, S. C. (2000). Two-dimensional structure of beta-amyloid(10-35) fibrils. Biochemistry *39*, 3491-3499.

Bystrom, R., Aisenbrey, C., Borowik, T., Bokvist, M., Lindstrom, F., Sani, M. A., Olofsson, A., and Grobner, G. (2008). Disordered Proteins: Biological Membranes as Two-Dimensional Aggregation Matrices. Cell Biochem Biophys *52*, 175-189.

Childers, W. S., Mehta, A. K., Lu, K., and Lynn, D. G. (2009). Templating Molecular Arrays in Amyloid's Cross-beta Grooves. J Am Chem Soc *131*, 10165-10172

Childers, W. S., Ni, R., Mehta, A. K., and Lynn, D. G. (2009b). Peptide membranes in chemical evolution. Curr Opin Chem Biol *13*, 652-659.

D'Errico, G., Vitiello, G., Ortona, O., Tedeschi, A., Ramunno, A., and D'Ursi, A. M. (2008). Interaction between Alzheimer's A beta(25-35) peptide and phospholipid bilayers: The role of cholesterol. Biochim Biophys Acta: Biomembranes *1778*, 2710-2716.

Dante, S., Hauss, T., and Dencher, N. A. (2006). Cholesterol inhibits the insertion of the Alzheimer's peptide Abeta(25-35) in lipid bilayers. Eur Biophys J *35*, 523-531.

Dong, J., Lu, K., Lakdawala, A., Mehta, A. K., and Lynn, D. G. (2006). Controlling amyloid growth in multiple dimensions. Amyloid *13*, 206-215.

Fraser, R. D. B. M., T. P. (1973). Conformation in fibrous proteins and related synthetic polypeptides. In. (New York: Academic Press).

Friedman, R., Pellarin, R., and Caflisch, A. (2009). Amyloid Aggregation on Lipid Bilayers and Its Impact on Membrane Permeability. J Mol Biol *387*, 407-415.

Geddes, A. J. P., K. D.; Atkinds, E. D. T.; Beighton, E. (1968). "Cross-beta" conformation in proteins. J Mol Biol *32*, 343.

Gehman, J. D., Separovic, F., Lu, K., and Mehta, A. K. (2007). Boltzmann statistics rotational-echo double-resonance analysis. J Phys Chem B *111*, 7802-7811.

Gordon, D. J., Balbach, J. J., Tycko, R., and Meredith, S. C. (2004). Increasing the amphiphilicity of an amyloidogenic peptide changes the beta-sheet structure in the fibrils from antiparallel to parallel. Biophys J *86*, 428-434.

Hartgerink, J. D., Beniash, E., and Stupp, S. I. (2001). Self-assembly and mineralization of peptide-amphiphile nanofibers. Science *294*, 1684-1688.

Hartgerink, J. D., Beniash, E., and Stupp, S. I. (2002). Peptide-amphiphile nanofibers: a versatile scaffold for the preparation of self-assembling materials. Proc Natl Acad Sci USA *99*, 5133-5138.

Hirota-Nakaoka, N., Hasegawa, K., Naiki, H., and Goto, Y. (2003). Dissolution of beta(2)-microglobulin amyloid fibrils by dimethylsulfoxide. J Biochem *134*, 159-164.

Jayasinghe, S. A., and Langen, R. (2007). Membrane interaction of islet amyloid polypeptide. Biochim Biophys Acta: Biomembranes *1768*, 2002-2009.

Keith, H. D., Giannoni, G., and Padden, F. J. (1969). Single Crystals of Poly(L-Glutamic Acid). Biopolymers *7*, 775

Krejchi, M. T. C., S. J.; Deguchi, Y.; Atkins, E. D. T.; Fournier, M. J.; Mason, T. L.; Tirrell, D. A. (1997). Crystal structures of chain folded antiparallel beta-sheet assemblies from sequence-designed periodic polypeptides. Macromolecules *17*, 5012.

Kremer, J. J., Sklansky, D. J., and Murphy, R. M. (2001). Profile of changes in lipid bilayer structure caused by beta-amyloid peptide. Biochemistry *40*, 8563-8571.

Liang, Y., Guo, P., Pingali, S. V., Pabit, S., Thiyagarajan, P., Berland, K. M., and Lynn, D. G. (2008a). Light harvesting antenna on an amyloid scaffold. Chem Commun (Camb), 6522-6524.

Liang, Y., Pingali, S. V., Jogalekar, A. S., Snyder, J. P., Thiyagarajan, P., and Lynn, D. G. (2008b). Cross-strand pairing and amyloid assembly. Biochemistry *47*, 10018-10026.

Lu, K. (2005) Discovery of diverse peptide nanotube architecture from the self-assembly of designed amyloid-beta cassettes.

Lu, K., Conticello, V. P. and Lynn, D. G. (2004). Templating colloidal metal nanoparticle assemblies: use of the Abeta amyloid peptide nanotube. Mater Res Soc Synp Proc *Vol(1.6)* (http://www.chemistry.emory.edu/faculty/lynn/pubs/amyloid_pubs/MRS%20procee dings.pdf)

Lu, K., Guo, L., Mehta, A. K., Childers, W. S., Dublin, S. N., Skanthakumar, S., Conticello, V. P., Thiyagarajan, P., Apkarian, R. P., and Lynn, D. G. (2007). Macroscale assembly of peptide nanotubes. Chem Commun (Camb), 2729-2731.

Lu, K., Jacob, J., Thiyagarajan, P., Conticello, V. P., and Lynn, D. G. (2003). Exploiting amyloid fibril lamination for nanotube self-assembly. J Am Chem Soc *125*, 6391-6393.

Mehta, A. K., Lu, K., Childers, W. S., Liang, Y., Dublin, S. N., Dong, J., Snyder, J. P., Pingali, S. V., Thiyagarajan, P., and Lynn, D. G. (2008). Facial symmetry in protein self-assembly. J Am Chem Soc *130*, 9829-9835.

Saalwachter, K., and Schnell, I. (2002). REDOR-based heteronuclear dipolar correlation experiments in multi-spin systems: rotor-encoding, directing, and multiple distance and angle determination. Solid State Nucl Magn Reson *22*, 154-187.

Sikorski, P. A., E. D. T.; Serpell, L. C. (2003). Structure and texture of fibrous crystals formed by Alzheimer's abeta(11-25) peptide fragment. Structure *11*, 915.

Sparr, E., Engel, M. F. M., Sakharov, D. V., Sprong, M., Jacobs, J., de Kruijff, B., Hoppener, J. W. M., and Killian, J. A. (2004). Islet amyloid polypeptide-induced membrane leakage involves uptake of lipids by forming amyloid fibers. Febs Lett *577*, 117-120.

Childers, W. S., Mehta, A. K., Ni, R., Taylor, J. V. and Lynn, D G. (2010). Peptides Organized as Bilayer Membranes. submitted.

Zandomeneghi, G., Krebs, M. R. H., Mccammon, M. G., and Fandrich, M. (2004). FTIR reveals structural differences between native beta-sheet proteins and amyloid fibrils. Protein Sci *13*, 3314-3321.

CHAPTER 4

Exploiting Amyloid Plasticity for
Architectural Control I

Introduction

Chapters 2 and 3 have demonstrated that linear N-alkyl chains of various lengths can be readily accommodated within the amyloid fold. In the nanotubes, the alkanes pack between the β-sheets, widening the laminate distances significantly, but do not really compromise the robust cross-β structure. Solid-state NMR experiments further suggest an expansion of the bilayer leaflets, and the Congo red binding data is consistent with some changes in lamination grove structure. More sterically bulky substitutions, including Biotin (Lu, 2005) and Rhodamine (Liang et al., 2008a), have been shown to destabilize nanotube formation, but still the robust cross-β fold is maintained.

Previous investigations have identified several amino acid combinations in which cross-strand pairing contributes significantly to amyloid assembly. For example, the protonation state of N-acetyl-Aβ(16-22) modulates the strength of the K-E bridges and dictates the registry of the β-sheet (Figure 4-1) and the corresponding assembled morphology. Stabilizing the K-E bridges at neutral pH directs antiparallel in-register β-sheet fiber assembly (Mehta et al., 2008), While when the salt bridge is weakened at acidic pH, V18 / A21 cross-strand pairing dictates a staggered registry and drives

nanotube assembly (Liang et al., 2008b). Indeed, placing a *t-butyl* substituent L-*tert-*leucine as the side-chain at V18 position, dictates nanotube architecture independent of pH (Liang et al., 2008b).

Our basic hypothesis is that through appropriate combinations of these energetic constraints, amyloid morphology and architecture can be controlled. More specifically, these examples suggest that simple modification of the peptide termini may be sufficient for this control. To test this hypothesis, we have systematically altered the N-acetyl cap of N-acetyl-Aβ(16-22) with branched alkyl chains (N-isobutyl and N-pivaloyl in Figure 4-2) and evaluated their assembly at acidic and neutral pHs. We now demonstrate that these simple modifications can indeed be used to control parallel / antiparallel sheet architecture, peptide registry, and nanotube diameter.

Staggered interface   Blunt interface

```
    KLVFFAE  KLVFFAE           KLVFFAE  KLVFFAE
     EAFFVLK  EAFFVLK           EAFFVLK  EAFFVLK
    KLVFFAE  KLVFFAE           KLVFFAE  KLVFFAE
     EAFFVLK  EAFFVLK           EAFFVLK  EAFFVLK
```
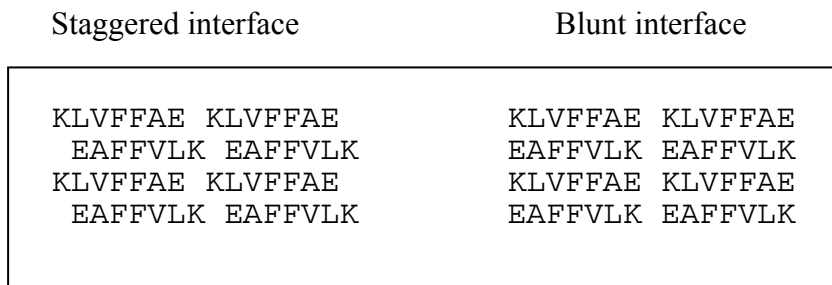
Figure 4-1. The staggered and blunt peptide bilayer interfaces containing antiparallel peptide β-sheets.
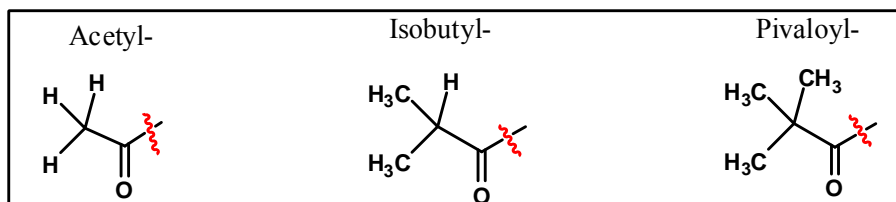
Figure 4-2. Chemical structure of the N-terminal capping groups used in this study.

Results

Is morphology controlled by the N-terminal cap?

The N-acetyl-, N-isobutyl- and N-pivaloyl-Aβ(16-22) derivatives were synthesized via standard solid-phase Fmoc chemistry with overnight N-terminal capping. In 20% acetonitrile / water at acidic pH, all three peptides assembled as homogenous nanotubes, established by the electron micrographs (Figure 4-3). The N-acetyl- and N-isobutyl-Aβ(16-22) tubes show indistinguishable diameters of 44 ± 4 nm (Figure 4-3a, b), slightly smaller than that measured in solution for the N-acetyl peptide with SAXS (Lu et al., 2003), that may be the result of the variability of nanotube collapse on the EM grids

e

1000nm

45.9nm
36.7nm
27.6nm
18.4nm
9.2nm
0.0nm

Image information				
Ra =	4.02 nm	RMS =	5.01 nm
Rz =	33.9 nm	P-V =	45.9 nm
S =	16.1 um²	S ratio =	1.01

		1	2	3
Ra	[nm]	2.24	2.55	2.34
Rz	[nm]	4.28	6.85	5.37
RMS	[nm]	2.59	2.87	2.66
P-V	[nm]	7.42	7.82	7.38
Length	[um]	0.386	0.410	0.387

AFM Slope Ref: -3.600V.
Size: 4.00 x 4.00um. Bias: 0.000V.

9.17 nm

0

0   0.410 um

f

1000nm

40.4nm
32.3nm
24.2nm
16.1nm
8.1nm
0.0nm

Image information				
Ra =	2.62 nm	RMS =	3.34 nm
Rz =	31.5 nm	P-V =	40.4 nm
S =	16.1 um²	S ratio =	1.00

		1	2	3
Ra	[nm]	2.55	2.64	2.87
Rz	[nm]	5.86	5.12	6.58
RMS	[nm]	2.67	2.79	2.99
P-V	[nm]	7.74	7.89	7.45
Length	[um]	0.330	0.335	0.342

AFM Slope Ref: -3.500V.
Size: 4.00 x 4.00um. Bias: 0.000V.

9.95 nm

0

0   0.342 um

Figure 4-3. TEM and AFM images of N-substituted assemblies at acidic pH.

TEM images of (a) N-acetyl-Aβ(16-22) nanotubes, (b) N-isobutyl-Aβ(16-22) nanotubes, and (c) N-pivaloyl-Aβ(16-22) nanotubes.

AFM images of (d) N-acetyl-Aβ(16-22) nanotubes, (e) N-isobutyl-Aβ(16-22) nanotubes, and (f) N-pivaloyl-Aβ(16-22) nanotubes.

Nanotube samples were prepared by incubation of 1.5 mM peptide in 20% acetonitrile / water with 0.1% TFA at room temperature for 2 weeks prior to imaging.

(Lu et al., 2007; Mehta et al., 2008). The N-pivaloyl-Aβ(16-22) tubes have a diameter of more than twice the size, 104 ± 10 nm (Figure 4-3c and Table 4-1). Despite the size variability, these tubes all have a wall thickness of just under 4 nm as measured by AFM (Table 4-1), and these numbers are consistent with previous neutron and x-ray scattering measurement on the N-acetyl-Aβ(16-22) tubes (Lu et al., 2003).

Table 4-1. Estimated nanotube diameter and tube wall thickness.
The nanotube dimensions were measured from the TEM and AFM images shown in Figure 4-3. The average tube diameter is obtained according to the equation of $d = c/\pi$ (d: diameter; c: circle circumstance) and c is converted from the tube width (15 separate measurements) of dry tubes in EM images. The tube wall thickness is expressed as half the measured AFM height of 10 individual measurements and expressed as ±SD.

Peptide: N-X-Aβ(16-22)	acetyl-	isobutyl-	pivaloyl-
Diameter (nm)	44 ± 4	44 ± 4	104 ± 10
Wall thickness (nm)	3.8 ± 0.1	3.8 ± 0.1	3.9 ± 0.1

At neutral pH (Figure 4-4), both N-acetyl- and N-isobutyl-Aβ(16-22) peptides assemble as unbranched twisted fibrils, but the N-isobutyl-Aβ(16-22) peptides have a high propensity for assembly, as shown in the dense fibrils in Fig 4-4b, and are 50% larger, diameters of 15nm, than N-acetyl-Aβ(16-22) fibrils (Figure 4-4a, and Table 4-2). Under the same conditions, N-pivaloyl-Aβ(16-22) still forms nanotubes with diameter of 94 ± 8 nm (Figure 4-4c). This pH-independence is similar to that reported for the peptide containing the V18L-*tert*-leucine substitution (Liang et al., 2008b).
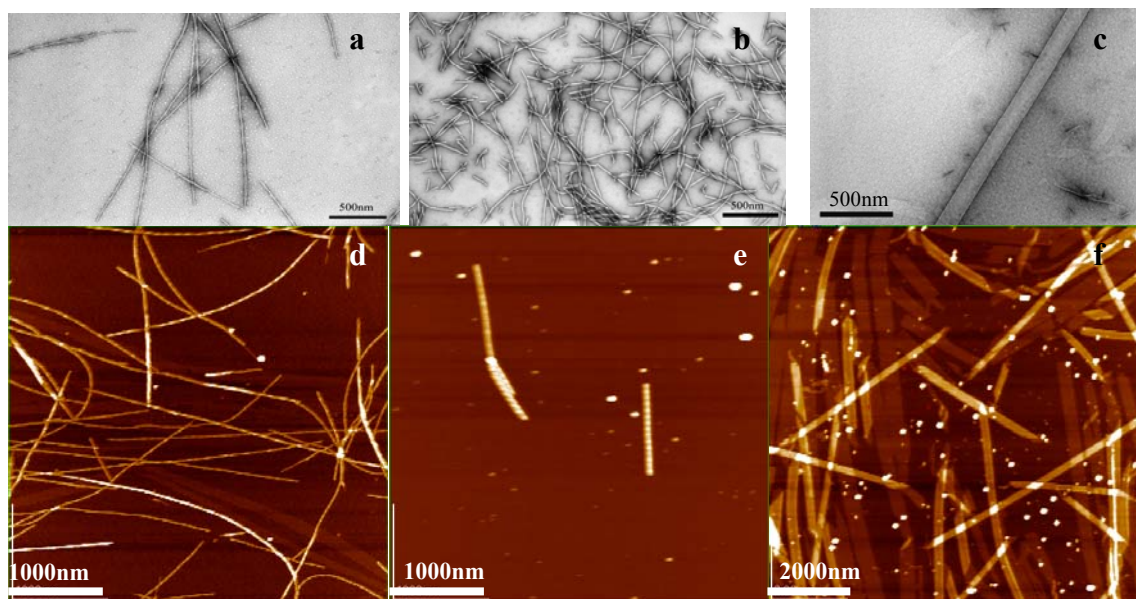
Figure 4-4. TEM and AFM images of N-substituted assemblies at neutral pH.

TEM images of (a) N-acetyl-Aβ(16-22) fibrils, (b) N-isobutyl-Aβ(16-22) fibrils, and (c) N-pivaloyl-Aβ(16-22) nanotubes.

AFM images of (d) N-acetyl-Aβ(16-22) fibrils, (e) N-isobutyl-Aβ(16-22) fibrils, and (f) N-pivaloyl-Aβ(16-22) nanotubes.

In each case, the peptide (1.0 mM) was incubated in 20% acetonitrile/water with 15 mM pH6 MES buffer at room temperature for 2 weeks prior imaging.

Table 4-2. Estimated Fibril width and tube wall thickness.

The nanotube and fibril dimensions were measured from the TEM and AFM images shown in Figure 4-4. The final values represent the average of 10 measurements ± SD.

Peptide: X-Aβ(16-22)	Acetyl-	Isobutyl-	Pivaloyl-
Fibril width or tube diameter (nm)	10 ± 1	15 ± 2	94 ± 8
Fibril height or tube wall thickness (nm)	10.0 ± 1.0	16.0 ± 1.0	4.0 ± 1.0

Impact on assembled secondary structure

By circular dichroism (CD) analyses at acidic pH, the N-acetyl- and N-isobutyl-Aβ(16-22) peptides mature to give signature β-sheet spectra with negative ellipticity centered at 214 and 212 nm, respectively (Figure 4-5). The N-pivaloyl-Aβ(16-22) peptide develops relatively weaker β-sheet signals that are red-shift to 220 nm (Figure 4-5). FT-

IR confirmed the β-sheet assignment with the appearance of amide I band at 1627 cm^{-1} for all three tubes (Figure 4-6a). In addition, the characteristic weak shoulder at 1693 cm^{-1} suggested that all three peptides form antiparallel β-sheets at acidic pH (Blout and Lenormant, 1957; Elliott et al., 1950; Miyazawa, 1960).
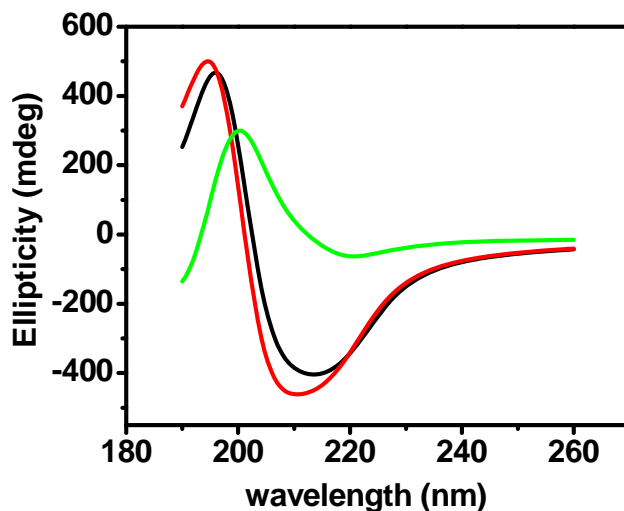
Figure 4-5. CD analyses of Aβ(16-22) congener nanotubes.
The N-acetyl-Aβ(16-22) (black), N-isobutyl-Aβ(16-22) (red), or N-pivaloyl-Aβ(16-22) (green) peptides (1.5 mM) were individually incubated in 20% acetonitrile / water with 0.1% TFA at room temperature for 2 weeks prior to analysis.

At neutral pH, the amide I stretches range from 1628 cm^{-1} to 1632 cm^{-1}, again consistent with β-sheet structure (Figure 4-6b) (Haris and Chapman, 1995). N-acetyl-Aβ(16-22) fibrils and N-pivaloyl-Aβ(16-22) tubes both display the diagnostic antiparallel shoulder at 1693 cm^{-1}, but this band shifts to 1678 cm^{-1} in N-isobutyl-Aβ(16-22) fibrils, more consistent with parallel β-sheets (Chapter 3). Precipitation of N-isobutyl-Aβ(16-22) fibrils at more neutral pHs prevented further analysis by CD.
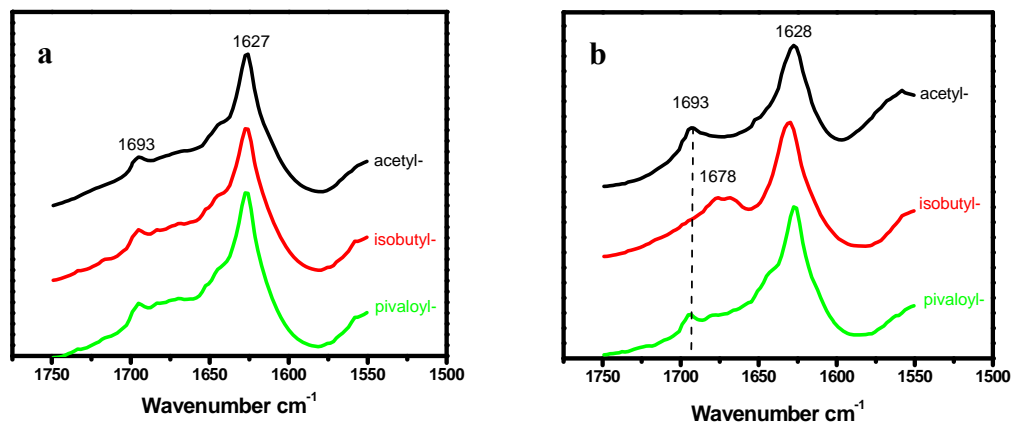
Figure 4-6. FT-IR analyses of Aβ(16-22) congener assemblies at (a) acidic pH, and (b) neutral pH.
The preformed tubes in 20% acetonitrile / water containing 0.1% TFA were bundled with sulfate with peptide to sulfate ratio of 1 to 8, followed by the centrifugation and lyophilization. The resulted white powders were mixed and compressed with anhydrous KBr for IR analysis with IR spectra collected from 4000 cm^{-1} to 400 cm^{-1}. The IR sample of the matured fibrils in 20% acetonitrile / water with 15 mM pH6 MES buffer was prepared with the same procedure without sulfate bundling.

Impact on assembled peptide registry

Peptide registry in amyloid assemblies have been assigned definitively by ssNMR analyses (Benzinger et al., 1998; Burkoth et al., 2000) and shown to correlate specifically with isotope edited (IE) FT-IR analyses (Mehta et al., 2008). The magnitude of the $^{12}C/^{13}C$ band splitting is a function of where the isotopic substitutions are positioned within the β-sheet array (Decatur, 2006; Hiramatsu and Kitagawa, 2005; Kubelka and Keiderling, 2001; Paul and Axelsen, 2005; Petty and Decatur, 2005). For example, in the N-acetyl Aβ(16-22)[1-^{13}C]F19-labeled peptides assembled under acidic conditions give a ^{12}C band at 1639 cm^{-1} and the^{13}C band at 1597 cm^{-1} (Figure 4-7a), consistent with well-alignment of F19 carbonyls (Mehta et al., 2008; Halverson et al., 1991; Paul and Axelsen, 2005; Paul et al., 2004) and antiparallel one-residue out-of registry β-sheet. If the carbonyl is shifted away from resonance alignment, the magnitude of the splitting is

attenuated as seen for [1-^{13}C] L17-labeled N-acetyl-Aβ(16-22) tubes (Figure 4-7b). All three peptide assemblies show identical splitting patterns for either [1-^{13}C] F19 or [1-^{13}C] L17 labels (Figure 4-7), confirming the same registry shifted β-sheets in all of these tubes.
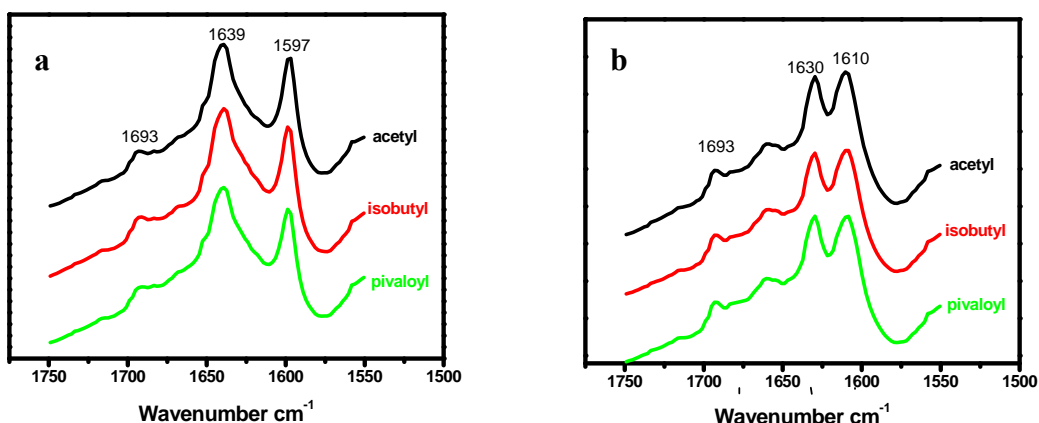
Figure 4-7. Isotope-edited FT-IR of the nanotube assemblies at acidic pH with (a) [1-^{13}C] F19 or (b) [1-^{13}C] L17 labels.
The major peaks within amide I region are specified and the name of the samples is presented at the right side of each corresponding line.

At more neutral pHs (Figure 4-8a), the N-acetyl-Aβ(16-22) peptide assembles as antiparallel in-register β-sheet fibrils with their ^{13}C stretch at 1606 cm^{-1} and ^{12}C at 1635 cm^{-1} in the amide I region when the carbonyl of F19 was isotope labeled. In contrast, the 35 cm^{-1} splitting observed for the N-isobutyl-Aβ(16-22)[1-^{13}C] F19-labeled fibrils are more consistent with parallel carbonyl alignments in a parallel in-register β-sheet (Liang et al., 2008b). In contrast, the stretching modes of the N-pivaloyl-Aβ(16-22) tubes are the same, independent of pH, and similar enough to those of the N-acetyl-Aβ(16-22) peptide nanotubes assembled at acidic pH (Figure 4-8b) to assign them as antiparallel one-residue out-of registry β-sheets.
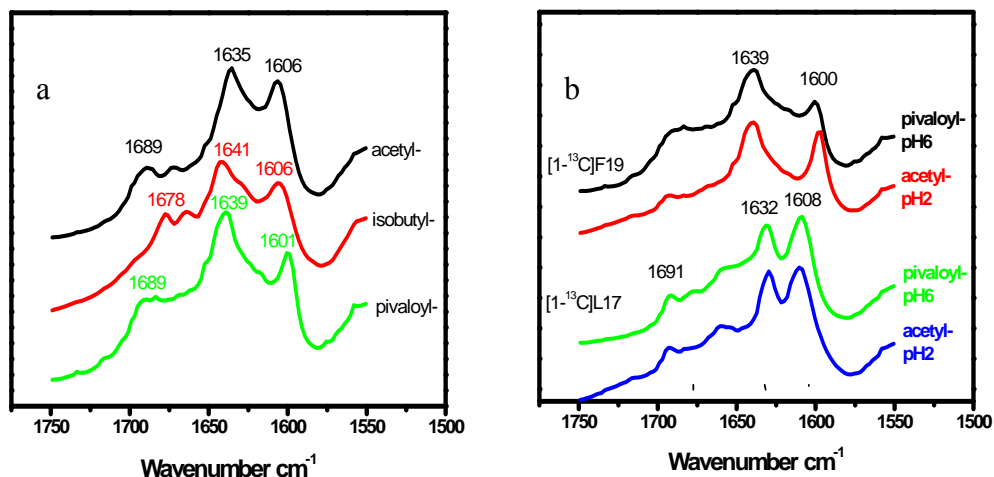
Figure 4-8. Isotope-edited FT-IR of assemblies formed at neutral pH.

(a) Amide I band region of the assemblies with [1-^{13}C] F19-labeles.

(b) [1-^{13}C] F19- (top) or [1-^{13}C] L17-labeled (bottom) N-pivaloyl- and N-acetyl-Aβ(16-22) at acidic or neutral pHs.

In both figure, the major peaks within amide I region are specified and the peptide name corresponding to each line is presented. The neutral assembly conditions involved incubation of 1.0 mM peptide in 20% acetonitrile / water with 15 mM pH6 MES buffer for 2 weeks.

Impact on the cross-β amyloid structure

For assemblies prepared under acidic conditions, the nanotubes were oriented with fluid flow and electron diffraction(Childers et al., 2009; Mehta et al., 2008) showed two sets of orthogonal d-spacing arcs at 4.7 Å and 9.8 Å for all three tubes (Figure 4-9) (Childers et al., 2009; Lu et al., 2007; Mehta et al., 2008). Even though the nanotubes differ in diameter, the overall hydrogen bonding repeats, lamination distances and pitch angles are the same (Table 4-3). The small lamination number precluded detection of the 9.8 Å arcs in the fibrils but a single reflection arc corresponding to a d-spacing of 4.7 Å is apparent for the N-acetyl and N-isobutyl-Aβ(16-22) fibrils (data not shown), while the N-pivaloyl-Aβ(16-22) tubes show the nanotube pattern (Table 4-3).

131
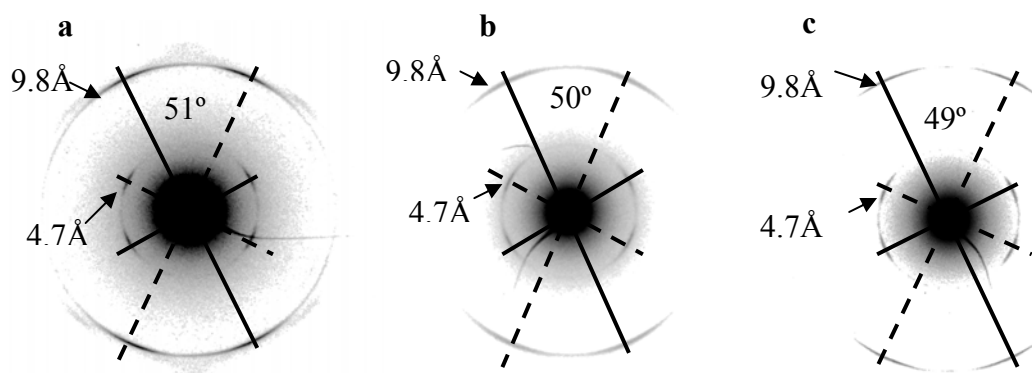
Figure 4-9. Electron diffraction of oriented nanotubes at acidic pH.

N-acetyl-Aβ(16-22), (b) N-isobutyl-Aβ(16-22), and (c) N-pivaloyl-Aβ(16-22) tubes oriented vertically along the page as presented.

The preformed tubes at acidic pH were applied to TEM grids, and were aligned by removing the excess solution with filter paper at one direction.

Table 4-3. Measured d-spacing of these assemblies at both pHs.

These reported values were determined from the electron diffraction micrographs shown in Figure 4-9.

N-X-Aβ (16-22)	Acidic pH		Neutral pH	
	H-bonding (Å)	H-bonding (Å)	H-bonding (Å)	Lamination (Å)
acetyl-	4.7	4.7	4.7	n/a
isobutyl-	4.7	4.7	4.7	n/a
pivaloyl-	4.7	4.7	4.7	9.8

Structure modeling

The assembled structural constraints set all the nanotubes as classic cross-β amyloid composed of antiparallel, one residue out of register β-sheets. Having measured the radius and the pitch angle, and using the d-spacing to define the ribbon width and the number of laminates, it is possible to calculate the pitch P of each nanotube using the following geometric relationship (Dong et al., 2006): $P = 2\pi\rho\tan\psi$ and $\delta = W/\cos\psi$ (Table 4-4). We propose that this greater than two fold increase in pitch and corresponding change in diameter arises from the packing of the bulky pivaloyl capping group both

along the β-sheet in a cross-strained pairing sense as well as the packing between the leaflets of the nanotube bilayer. Computer modeling is now being pursued to better understand the energetic surfaces of these structures and extend the predictive potential for the control of nanotube size.

Table 4-4. Nanotube parameters and dimensions.

These parameters (tube radius ρ, pitch P, pitch angle ψ, ribbon width W and laminates #) were calculated based on experimentally determined TEM images (Figure 4-3) and electron diffraction constraints (Figure 4-9) (Dong et al., 2006).

N-X-Aβ(16-22)	Radius, ρ (nm)	Pitch angle Ψ (°)	Pitch P (nm)	Ribbon width W (nm)	Laminate #
acetyl-	22 ± 2	65	296	125	128
isobutyl-	22 ± 2	65	296	125	128
pivaloyl-	52 ± 5	66	717	297	303

The transitional control between fibril and nanotube assemblies is even more sensitive to the N-capping substituent. The addition of single methyl carbons mediates transitions from typical fibrils, to large fibril assemblies, to nanotubes; and these changes are probably driven from a shift from antiparallel in-registry, to parallel in-registry, to antiparallel one-residue out-of registry sheets. These sheet structures are depicted in Figure 4-10.
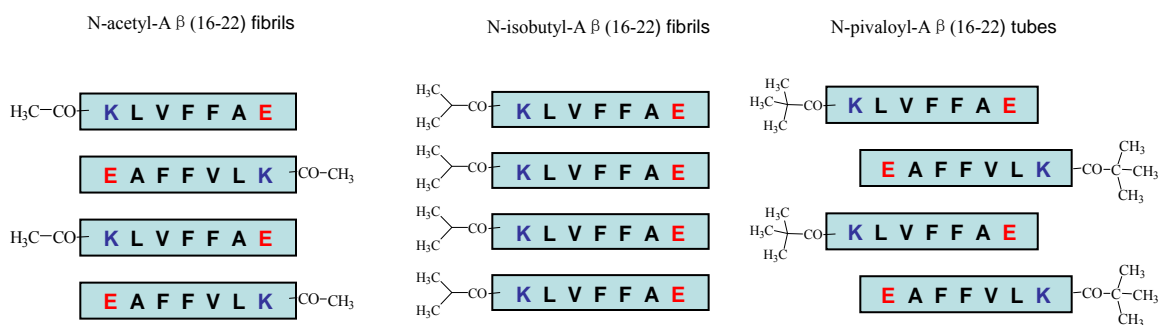
Figure 4-10. Peptide arrangements accessed under neutral assembly conditions.

The peptide sequence (light blue rectangle), side chain charge (dark blue means positively-charged and red means negatively-charged), and capping group are shown.

Assuming that these differences may be the result of the exposed alkyl chains, the water exposed surface area (WESA) of these models within a six-peptide-strand β-sheet was calculated, in which both peptide N- and C-terminal groups (grey part in Figure 4-11) were included and the calculated surface area was listed in Table 4-5. For N-acetyl, there is no significant difference between the antiparallel and parallel in-register models (Table 4-5) and previous analyses attributed the stability of the antiparallel in-registry orientation to cross-strand salt-bridge formation (lysine16 and glutamate22) (Mehta et al., 2008). However, both N-isobutyl and N-pivaloyl caps have significantly less WESA in the parallel in-register β-sheets, consistent with the parallel β-sheet fibrils formed from octanoyl-Aβ(16-22) at neutral pH as discussed in Chapter 2 (Gordon et al., 2004). However, the hydrophobic clash between N-alkyl chains, denoted as Van der Waals contact in this study, with adjacent peptide strands also modulates the peptide orientation/registry. By constraining the full hydrogen-bonding interaction within peptide region, the terminal Van der Waals contact was shown in Figure 4-12. The average three bad contacts (hydrophobic clash) were detected for N-pivaloyl groups, much more than that for N-isobutyl groups. As with side chain cross-strand pairing, the modeling suggests that minimizing the packing of the pivaloyl group forces antiparallel out of registry arrangement and nanotube formation even at neutral pH.
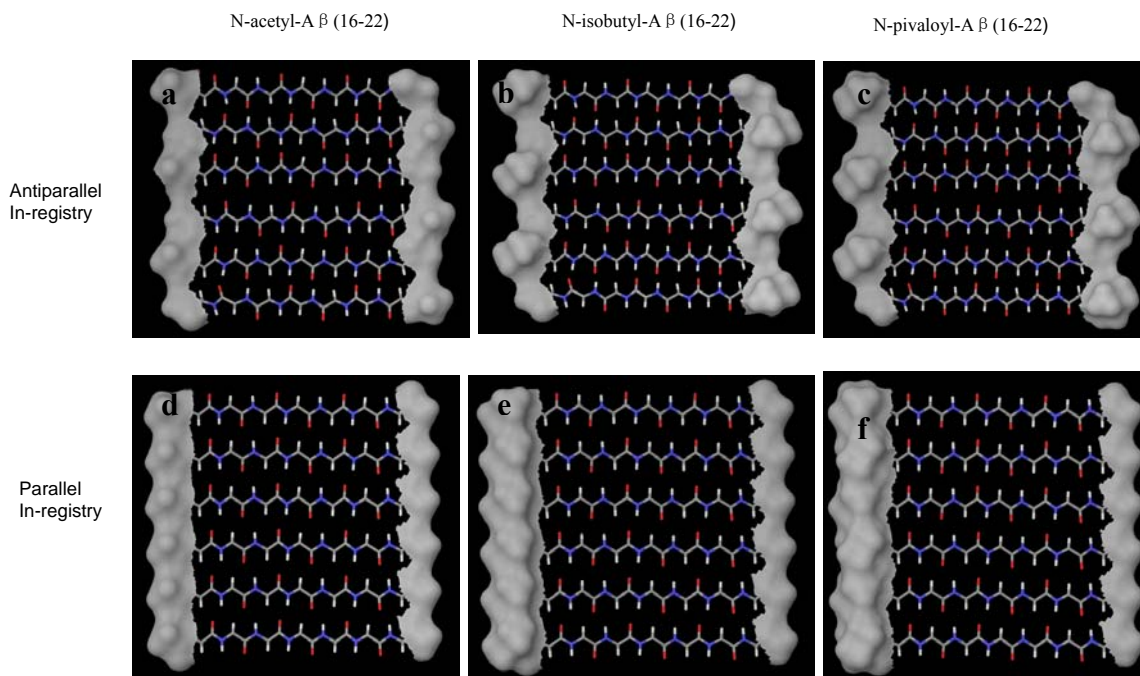
Figure 4-11. Water exposed surface for antiparallel and parallel β-sheets through conformational search.

Upper panel (antiparallel in-register β-sheet): (a) N-acetyl-Aβ(16-22), (b) N-isobutyl-Aβ(16-22) and (c) N-pivaloyl-Aβ(16-22).

Lower panel (parallel in-register β-sheet): (e) N-acetyl-Aβ(16-22), (f) N-isobutyl-Aβ(16-22) and (g) N-pivaloyl-Aβ(16-22).

The six-peptide-strand β-sheet was treated with energy minimization and to get the fair comparison between parallel and antiparallel β-sheets, the calculated water exposed surface area is the sum of both N and C-terminal groups, highlighted with grey color.

Table 4-5. Water exposed surface area (WESA) of the β-sheets corresponding to each model in Figure 4-11.

peptide	Water exposed surface area (WESA)		Surface area difference
	Antiparallel in-register	Parallel in-register	
N-acetyl-Aβ(16-22)	509	507	2
N-isobutyl-Aβ(16-22)	702	641	61
N-pivaloyl-Aβ(16-22)	729	665	64

a   N-isobutyl-Aβ(16-22)   **b**   N-pivaloyl-Aβ(16-22)
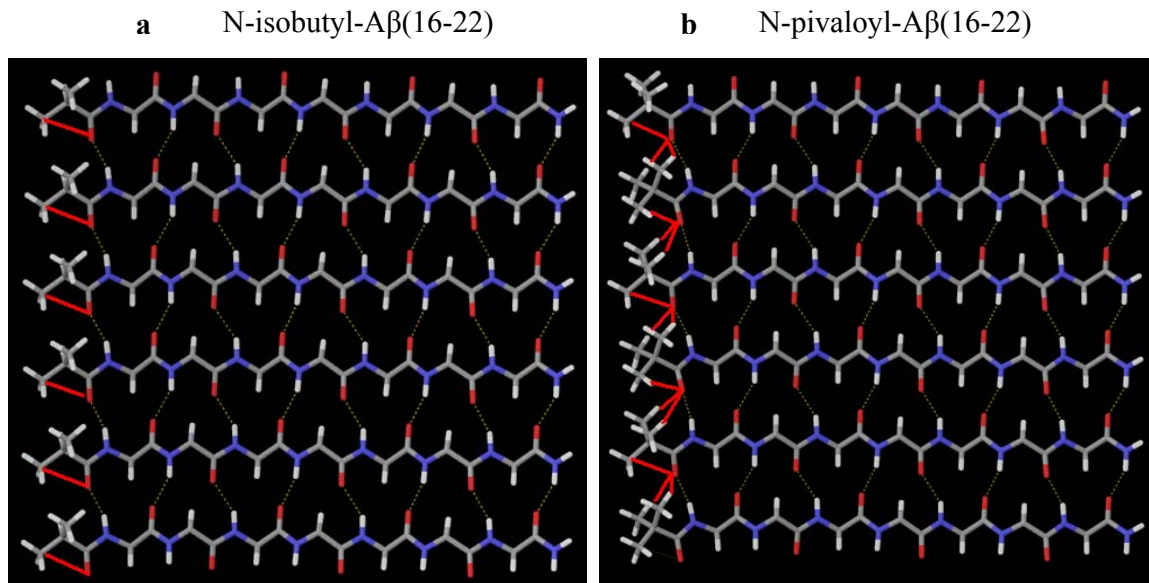
Figure 4-12. Van der Waals contact between N-terminal alkyl chain and the adjacent peptide strands within parallel in-register β-sheets.

(a) N-isobutyl-Aβ(16-22) β-sheet , (b) N-pivaloyl-Aβ(16-22) β-sheet.

By constraining the peptide backbone hydrogen-bonding interaction (yellow dotted line), the Van der Waals contacts between parallel β-sheets after energy minimization were shown with red lines. Color code for the atoms: red for oxygen, blue for nitrogen and grey for carbon.

Discussion

Peptide terminal modification has frequently been employed as the strategy to functionalize peptide-based nanomaterials (Lu, 2005; Liang et al., 2008a), but the structure alteration has not been fully understood. Previous studies have already established that the interaction of different amino acid combinations (K-E salt-bridge or V18/A21 cross-strand pairing) at different pHs directs peptide orientation/registry within β-sheets and the corresponding self-assembled morphology (Liang et al., 2008b; Lu et al., 2003; Mehta et al., 2008). Therefore, peptide termini interaction may regulate amyloid morphology and architecture through the simple modification.

Peptide terminal modification may impact the self-assembly by rebalancing the

preexisting driving forces through the introduced new ones. As aforementioned, the self-assembly driving forces (K-E or V-A), as well as the resulted peptide registry (in-registry vs out-of registry) within antiparallel β-sheets is dependent on the protonation state of glutamate (Liang et al., 2008b; Lu et al., 2003; Mehta et al., 2008), in other words, the incubation solution pH, which provides different local environments for peptide terminal caps. Therefore, we hypothesize that terminal interaction at the specific local environment will have distinct impacts on amyloid morphology and architecture under different incubation pHs. At acidic pH, antiparallel out-of registry β-sheets could not only create a cavity but also avoid hydrophobic clash between N-alkyl chains and the adjacent peptide strands through the N-terminal dangling. Therefore, the cavity created by the out-of registry β-sheets may be able to accommodate these short/bulky alkyl chains, resulting in less impact on self-assembly architecture. In contrast, the antiparallel in-registry β-sheets at neutral pH neither build a cavity to hold N-alkyl chains, nor circumvent the unfavorable Van der Waals interaction caused by the increased size of N-alkyl chains. To bury these hydrophobic alkyl chains in the suitable environment, subtle terminal modification may cause significant structure alteration. The impacts of N-bulky alkyl chains on amyloid architecture will be discussed individually in the following sections.

At acidic pH, N-bulky alkyl chains maintain majority of amyloid self-assembly properties, indicating high plasticity of amyloid cross-β structure under this condition. Substitution of N-acetyl with isobutyl and pivaloyl groups not only keeps nanotube morphology (Figure 4-3), but also antiparallel out-of register peptide arrangements (Figure 4-7). This demonstrates that antiparallel out-of register β-sheets are able to accommodate these N-bulky alkyl chains without structure perturbation. However,

different from N-linear alkyl chains, these branched ones are short and rigid, which limit their bending to laminates. Therefore, the only place to hold them in nanotubes is in the terminal cavity, as supported by the constant peptide-repeat d-spacing along both hydrogen-bonding and lamination direction (Figure 4-9). When the size of N-alkyl chains exceeds this terminal cavity, these alkyl chains either keep self-assembly morphology by bending to fit themselves in laminates such as N-linear alkyl chains (Chapter 3) or change the self-assembly morphology by switching peptide arrangements such as N-Biotin (Lu, 2005) and N-Rhodamine (Liang et al., 2008a). Therefore, these short/bulky alkyl chains are able to isolate the peptide terminal interaction, offering a simple and efficient strategy to probe peptide terminal structure.

Even though these bulky alkyl chains maintain the majority of self-assembly properties at acidic pH, the increase of N-terminal bulkiness could control nanotube size by regulating the strength of peg-hole interaction at the bilayer interface. N-acetyl and N-isobutyl tubes have similar size, but N-pivaloyl substituent dramatically increases tube size (Figure 4-3). This transition may attribute to the alkyl chains – cavity interaction in the bilayer interface. Increase the N-alkyl chains size may decrease bilayer freedom, resulting in the increase of peptide persistent length and the corresponding tube pitch and tube size (Figure 4-9 and Table 4-4). Shortly, the study at acidic pH demonstrates that the cavity created by out-of registry β-sheets is critical to accommodate N-bulky alkyl chains to maintain the amyloid architecture, while the peg-hole interaction is able to modulate tube size, which further supports the bilayer structure in Aβ(16-22) nanotubes (Lu et al., 2003; Mehta et al., 2008; W. Seth Childers, 2010).

At neutral pH, simple modification of N-terminal alkyl chains modulates the

amyloid morphology and architecture, while the cross β-structure is conserved (Figure 4-6b). With the substitution of N-acetyl with N-isobutyl or pivaloyl group, the self-assembled morphologies transit from typical to larger fibrils and to tubes (Figure 4-4), at the same time the corresponding peptide orientation/registry also switches from antiparallel in-registry to parallel in-registry and antiparallel out-of registry, respectively (Figure 4-8). Different from that at acidic pH, at neutral pH the in-registry β-sheets build a flat peptide terminal surface, which does not have space to accommodate N-bulky alkyl chains. As illustrated by structure modeling, to minimize water exposed surface area, the peptide strands have to switch orientation or shift the registry through balancing the introduced hydrophobic cluster and hydrophobic clash (Figure 4-12 and 4-13), which is consistent with the peptide orientation switch observed for N-octanoyl-Aβ(16-22) at neutral pH (Gordon et al., 2004).

However, N-pivaloyl, the bulkiest alkyl chain, drives the antiparallel out-of registry β-sheets formation at neutral pH. This pH-independence has ever been reported for V18L-*tert*-leucine substitution, which is directed by the cross-strand size-complementary pairing interaction, instead of K-E electrostatic interaction (Liang et al., 2008b). Therefore, the pH-independence of self-assembly observed for N-pivaloyl substitution suggests that peg-hole interaction overwhelms the K-E salt bridge formation in antiparallel in-registry β-sheets, further supporting the important role of peptide terminal interaction in amyloid self-assembly. These pH-dependence studies demonstrate that the regulation capability of N-terminal alkyl chains on amyloid morphology and architecture is highly correlated with the original terminal surface structure and the bulkiness of N-alkyl chains.

139

In summary, the defined plasticity of amyloid cross-β structure and the modulating effects of N-bulky alkyl chains on amyloid self-assemblies not only identify the role of peptide terminal interaction on amyloid self-assembly, but also shed light on amyloid self-assembly mechanism. In addition, these short/bulky alkyl chains could efficiently isolate the peptide terminal interaction, which offers a useful probe to study peptide terminal structures. Further, the variety of self-assembled architectures achieved by simply modification of bulkiness of N-alkyl chains presents an efficient way to manipulate self-assembly morphology/architecture; and the identified peg-hole cross-leaflet interaction is complementary to the existed amino acid combinations, which could be adapted for novel nanomaterial applications. Whereas, deep understanding the specific interactions involved in peg-hole bilayer interface, as well as the role of peptide C-terminal backbone alkyl substitutions in amyloid self-assembly are critical for the morphological control, which will be explored in the next chapter.

Materials and methods

Peptide synthesis and purification

The peptide region (KLVFFAE) was automatically synthesized through standard FMOC/HBTU chemistry with FMOC Rink-amide polystyrene resin (Anaspec, Inc.) on a Rainin Symphony Quartet peptide synthesizer. The peptide N-terminus was capped manually by coupling the corresponding acid with resin overnight with HBTU/NMM activation. The cleavage (90 vol% TFA, 5 vol% thioanisole, 3 vol% ethanedithiol and 2 vol% anisole) of the resin was treated with cold diethyl ether 4 times to extract the crude peptide. The peptide was purified by reverse-phase HPLC (Waters Delta 600) using

Waters Atlantis C-18 preparative column (19 x 250 mm) and confirmed by MALDI-TOF (Voyager-DETM STR Biospectrometry Workstation) analysis with a-Cyano-4-hydroxycinnamic acid (CHCA) as matrix. For Isotope-labeled peptides, the same procedure was applied except that the isotope-labeled amino acid was manually coupled for 4 hr.

Fibril or nanotube assembly

The weighted peptide powder was dissolved in 40% acetonitrile/water mixture with vortexing, and the sample was neutralized with 15 mM pH5.6 MES buffer or acidified with 0.1 vol% TFA for fibril and tube sample preparation, respectively. Incubation at room temperature for 1-3 weeks was generally required for the sample maturation.

Transmission electron microscopy (TEM) and electron diffraction

A diluted sample (10 μL, 0.05 mM to 0.1 mM) was applied on a TEM copper grid (200 mesh carbon supported grid from Electron Microscopy Sciences) for 1 minute, following with removing excess solution with filter paper and addition of another 10 μL staining solution (2% uranyl acetate, Sigma-Aldrich for 2 min. After wicking away the staining solution, the sample grids were placed in desiccators to dry under vacuum overnight. A Hitachi H-7500 transmission electron microscope was used to image the samples at 75 kV.

The sample prepared for electron diffraction followed the above procedure without staining. To prepare an aligned sample on grids, the excess solution was slowly wicked away with filter paper at one direction. These micrographs were recorded on Philips 4500

transmission electron microscope in diffraction mode. A d-spacing, where d = λL/R, was calculated, where R is half the distance (mm) between two opposite arcs, λ is the electron wavelength (75 kV), and L is the camera length (distance in mm between specimen and photographic film), calibrated using an aluminum polycrystalline standard (Electron Microscopy Sciences, Hartfield, PA).

Fourier Transform Infrared (FTIR)

Spectra were collected on a Nicolet MAGNA-IR 560 Spectrometer with 4 cm^{-1} resolution and generally 100-time scans were averaged. For sample preparation, the matured fibrils were pelleted at 16,100 xg for 5 minutes, frozen at −80ºC, and lyophilized to a dry powder. The tube samples were bundled with NADH with peptide to NADH 1:4 ratio for 30 min before pelleting and drying. The dried sample was mixed well with grounded KBr (at a ratio of 1:10 (w/w)) and pressed into a transparent disk. Isotope-edited IR sample preparation was identified.

DRAWS sample preparation

The preformed fibrils, prepared according to aforementioned procedure, were centrifuged, frozen and lyophilized to yield dry powder.

References

Benzinger, T. L., Gregory, D. M., Burkoth, T. S., Miller-Auer, H., Lynn, D. G., Botto, R. E., and Meredith, S. C. (1998). Propagating structure of Alzheimer's beta-amyloid(10-35) is parallel beta-sheet with residues in exact register. Proc Natl Acad Sci USA *95*, 13407-13412.

Blout, E. R., and Lenormant, H. (1957). Reversible configurational changes in poly-L-lysine hydrochloride induced by water. Nature *179*, 960-963.

Burkoth, T. S., Benzinger, T. L. S., Urban, V., Morgan, D. M., Gregory, D. M., Thiyagarajan, P., Botto, R. E., Meredith, S. C., and Lynn, D. G. (2000). Structure of the beta-amyloid((10-35)) fibril. J Am Chem Soc *122*, 7883-7889.

Childers, W. S., Mehta, A. K., Lu, K., and Lynn, D. G. (2009). Templating Molecular Arrays in Amyloid's Cross-beta Grooves. J Am Chem Soc 131, 10165-10172

Childers, W. S., Mehta, A. K., Ni, R., Taylor, J. V., and Lynn, D. G. (2010) Peptides Organized as Bilayer Membranes. Angew Chem. Int. Ed. 2010, ASAP

Decatur, S. M. (2006). Elucidation of residue-level structure and dynamics of polypeptides via isotope-edited infrared spectroscopy. Acc Chem Res *39*, 169-175.

Dong, J., Lu, K., Lakdawala, A., Mehta, A. K., and Lynn, D. G. (2006). Controlling amyloid growth in multiple dimensions. Amyloid *13*, 206-215.

Elliott, A., Ambrose, E. J., and Robinson, C. (1950). Chain configurations in natured and denatured insulin: evidence from infrared spectra. Nature *166*, 194.

Gordon, D. J., Balbach, J. J., Tycko, R., and Meredith, S. C. (2004). Increasing the amphiphilicity of an amyloidogenic peptide changes the beta-sheet structure in the fibrils from antiparallel to parallel. Biophys J *86*, 428-434.

Halverson, K. J., Sucholeiki, I., Ashburn, T. T., and Lansbury, P. T. (1991). Location of Beta-Sheet-Forming Sequences in Amyloid Proteins by Ftir. J Am Chem Soc *113*, 6701-6703.

Haris, P. I., and Chapman, D. (1995). The conformational analysis of peptides using Fourier transform IR spectroscopy. Biopolymers *37*, 251-263.

Hiramatsu, H., and Kitagawa, T. (2005). FT-IR approaches on amyloid fibril structure. Biochim Biophys Acta *1753*, 100-107.

Kubelka, J., and Keiderling, T. A. (2001). The anomalous infrared amide I intensity distribution in (13)C isotopically labeled peptide beta-sheets comes from extended, multiple-stranded structures: an ab initio study. J Am Chem Soc *123*, 6142-6150.

Liang, Y., Guo, P., Pingali, S. V., Pabit, S., Thiyagarajan, P., Berland, K. M., and Lynn, D. G. (2008a). Light harvesting antenna on an amyloid scaffold. Chem Commun 6522-6524.

Liang, Y., Pingali, S. V., Jogalekar, A. S., Snyder, J. P., Thiyagarajan, P., and Lynn, D. G. (2008b). Cross-strand pairing and amyloid assembly. Biochemistry *47*, 10018-10026.

Lu, K. (2005). Discovery of diverse peptide nanotube architecture from the self-assembly of designed amyloid-beta cassettes. Ph.D. thesis, Emory University, Atlanta, GA, USA.

Lu, K., Guo, L., Mehta, A. K., Childers, W. S., Dublin, S. N., Skanthakumar, S., Conticello, V. P., Thiyagarajan, P., Apkarian, R. P., and Lynn, D. G. (2007). Macroscale assembly of peptide nanotubes. Chem Commun 2729-2731.

Lu, K., Jacob, J., Thiyagarajan, P., Conticello, V. P., and Lynn, D. G. (2003). Exploiting amyloid fibril lamination for nanotube self-assembly. J Am Chem Soc *125*, 6391-6393.

Mehta, A. K., Lu, K., Childers, W. S., Liang, Y., Dublin, S. N., Dong, J., Snyder, J. P., Pingali, S. V., Thiyagarajan, P., and Lynn, D. G. (2008). Facial symmetry in protein self-assembly. J Am Chem Soc *130*, 9829-9835.

Miyazawa, T. (1960). Perturbation Treatment of the Characteristic Vibrations of Polypeptide Chains in Various Configurations. J Chem Phys *32*, 1647-1652.

Paul, C., and Axelsen, P. H. (2005). beta Sheet structure in amyloid beta fibrils and vibrational dipolar coupling. J Am Chem Soc *127*, 5754-5755.

Paul, C., Wang, J., Wimley, W. C., Hochstrasser, R. M., and Axelsen, P. H. (2004). Vibrational coupling, isotopic editing, and beta-sheet structure in a membrane-bound polypeptide. J Am Chem Soc *126*, 5843-5850.

Petty, S. A., and Decatur, S. M. (2005). Experimental evidence for the reorganization of beta-strands within aggregates of the Abeta(16-22) peptide. J Am Chem Soc *127*, 13488-13489.

CHAPTER 5

Exploiting Amyloid Plasticity for

Architectural Control II

Introduction

Chapter 4 detailed the precise control afforded by N-terminal bulky alkyl substitution on amyloid morphology and architecture. The control comes from manipulating the energetic costs associated with either exposure of the peptide ends to solvent or packing these ends between the leaflets of the bilayer (Lu et al., 2003; Mehta et al., 2008). In both cases, very simple alkylation strategies were sufficient to control global architecture. With these results in mind, the H-bonding potential of the C-terminus should also contribute significantly to stability, and manipulating these associations should impact final architecture. We therefore proposed that systematic replacement of each N-H with an N-alkane at C-terminus could destabilize bilayer assembly and constrain cross-strand pairing while still being limited by the hydrophobic penalty of solvent exposure. By exploring this energetic tension and combining those lessons with the C-terminal constraints, we will greatly extend the range of architectures available to the amyloid fold.

To test this hypothesis, we prepared a series of C-terminal modified N-acetyl-$A\beta$(16-22)-NH_2 peptides replacing one C-terminal amide hydrogen with either methyl,

ethyl, or lauryl chains. In addition, both H atoms were replaced with methyl to remove all H-bonding potential. We further modified some of the N-terminal structures developed in Chapter 2/3 to probe the complementarity of functionalized two ends, which we now propose to associate in the bilayer model (Lu et al., 2003; Mehta et al., 2008). We will show that indeed these simple substitutions can have a profound and predictable impact on assembly architecture independent of peptide sequence and that these assemblies further diversity the rich array of architectural morphologies available to amyloid assemblies.

Results

Is morphology controlled by the C-terminal cap?

The C-terminal modified peptides were achieved by coupling the corresponding primary amine with side chain protected and C-terminal free peptide (N-acetyl-K(Boc)LVFFAE(tButyl)-COOH). Accordingly, the N-acetyl side chain protected peptide was synthesized on 2-Chlorotrityl resin with the normal Fmoc chemistry, and the peptide was cleaved from the resin with weak acid (TFE : ACE : DCM = 1 : 1 : 8) to yield N-acetyl-K(Boc)LVFFAE(tButyl)-OH, which was amidated in solution with the appropriate alkyl amines overnight. The peptides were deprotected with cleavage cocktail (90% TFA+ 5% EDT + 3% Thioanisol + 2% Anisol), purified via RP-HPLC, and their molecular weight was confirmed by MALDI-mass.

When incubated at room temperature in 20% acetonitrile/water at acidic pH for 2-3 weeks, both N-acetyl-Aβ(16-22)-NH$_2$ and N-acetyl-Aβ(16-22)-NHCH$_3$ assembled as nanotubes with diameters of 44 $\pm$ 5 nm and 43 $\pm$ 6 nm, respectively (Figure 5-1a, b). The
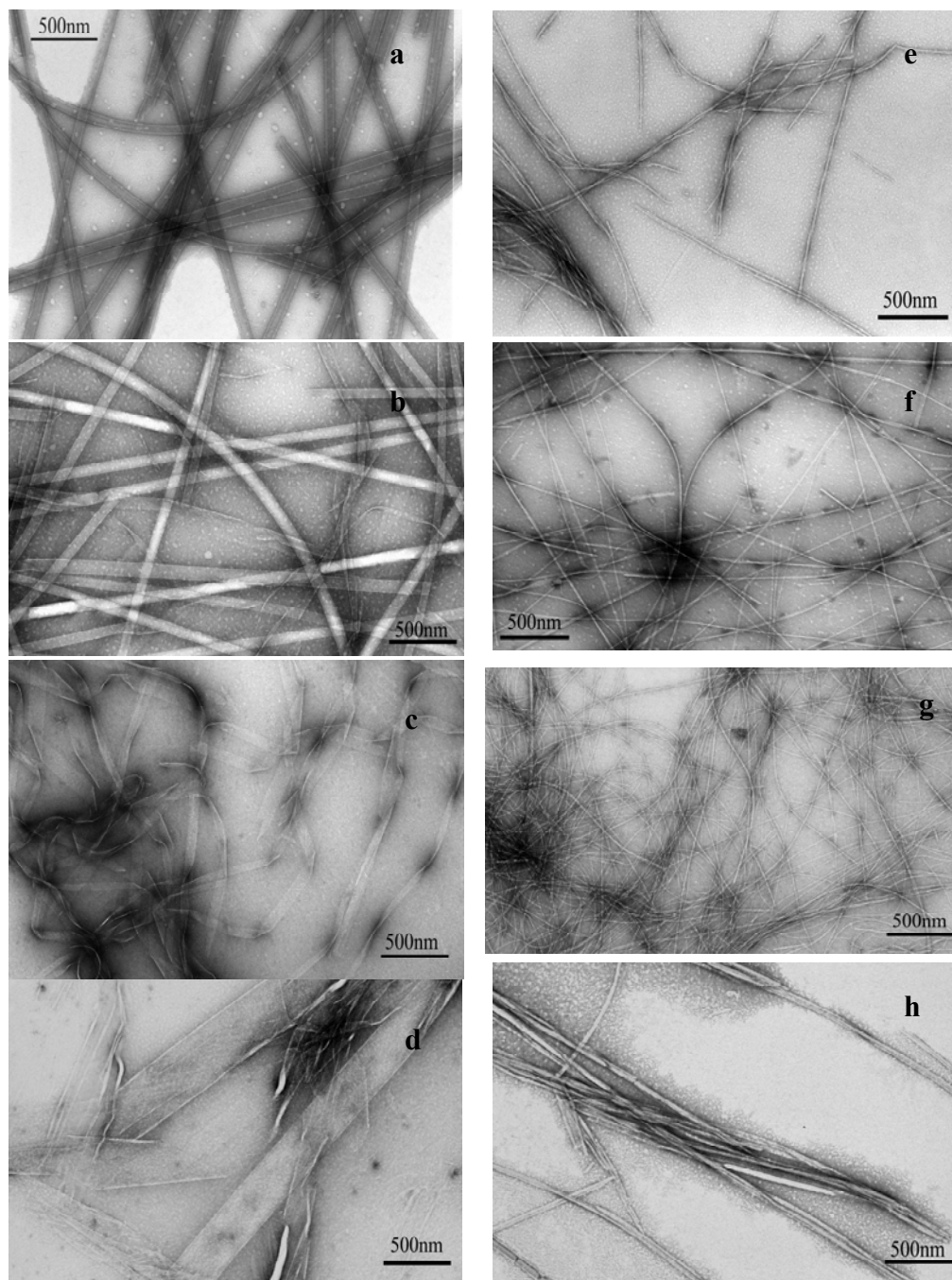
Figure 5-1. Transmission electron micrographs of self-assemblies of C-terminal modified N-acetyl-Aβ(16-22)-NH₂ at both acidic and neutral pHs.

Assemblies formed at acidic pH: (a) N-acetyl-Aβ(16-22)-NH$_2$, (b) N-acetyl-Aβ(16-22)-NHCH$_3$, (c) N-acetyl-Aβ(16-22)-NHCH$_2$CH$_3$, (d) N-acetyl-Aβ(16-22)-NH(CH$_2$)$_{11}$CH$_3$.

Assemblies formed at neutral pH: (e) N-acetyl-Aβ(16-22)-NH$_2$, (f) N-acetyl-Aβ(16-22)-NHCH$_3$, (g) N-acetyl-Aβ(16-22)-NHCH$_2$CH$_3$, (h) N-acetyl-Aβ(16-22)-NH(CH$_2$)$_{11}$CH$_3$. All peptides (1.2 mM) were

incubated in 20% acetonitrile / water containing either 0.1% TFA or 15 mM MES buffer at pH6 for 2-3 weeks at room temperature prior to imaging. Representative micrographs are shown.

N-acetyl-Aβ(16-22)-NHCH$_2$CH$_3$ formed small ribbons (Figure 5-1c), but did not assemble into tubes, whereas the N-acetyl-Aβ(16-22)-NH(CH$_2$)$_{11}$CH$_3$ assembled to the mixed species with tubes and sheets (Figure 5-1d).

At neutral pH, all these C-terminal modified peptides formed fibrils, independent of C-alkane length. N-acetyl-Aβ(16-22)-NH$_2$ and N-acetyl-Aβ(16-22)-NHCH$_2$CH$_3$ fibrils are twisted with diameter of 10 nm (Figure 5-1e), while N-acetyl-Aβ(16-22)-NHCH$_3$ and N-acetyl-Aβ(16-22)-NH(CH$_2$)$_{11}$CH$_3$ fibrils are more rigid and flat with less twisted pattern. Moreover, N-acetyl-Aβ(16-22)-NH(CH$_2$)$_{11}$CH$_3$ fibrils are tend to bundle together.

Impact on assembled secondary structure

As shown in Figure 5-2, the amide I region of the IR spectra, independent of the substitution on the C-terminal amide, show the diagnostic signature band for antiparallel sheets at 1690 cm^{-1} at neutral pH (Halverson et al., 1991; Mehta et al., 2008; Paul and Axelsen, 2005; Paul et al., 2004); while this band appears at slightly higher energy, 1693 cm^{-1}, in the homogeneous nanotubes formed at acidic pH. This difference also appears in the isotope-edited IR (IE-IR) spectra, as is most easily seen in the [1-^{13}C] F19-labeled spectra shown in Figure 5-2a. The ^{13}C oscillator appears at 1597 cm^{-1} in the -NH$_2$ and -NHCH$_3$ tubes as well as the -NHCH$_2$CH$_3$ sheets, consistent with perfectly aligned ^{13}C carbonyls, but the ^{12}C bands of the N-acetyl-Aβ(16-22)-NHX (X = CH$_3$, CH$_2$CH$_3$ and (CH$_2$)$_{11}$CH$_3$) are shifted to lower energy at 1635 cm^{-1}, 4 cm^{-1} less than that in the N-

acetyl-Aβ(16-22)-NH$_2$ tubes, most consistent with the strands being more loosely packed within the β-sheet. This compression of the ^{13}C/^{12}C splitting is even more pronounced in the fibers assembled at more neutral pHs, consistent with the confirmed in-register sheets of the N-acetyl-Aβ(16-22)-NH$_2$ fibers. The N-acetyl-Aβ(16-22)-NH(CH$_2$)$_{11}$CH$_3$ peptides, even though they formed nanotubes, show ^{13}C stretching bands at 1605 cm^{-1} and ^{12}C at 1633 cm^{-1}, which may be the results of more weakly assembled β-sheets or in-register antiparallel sheets. The precise assignment requires the further characterization by ssNMR.
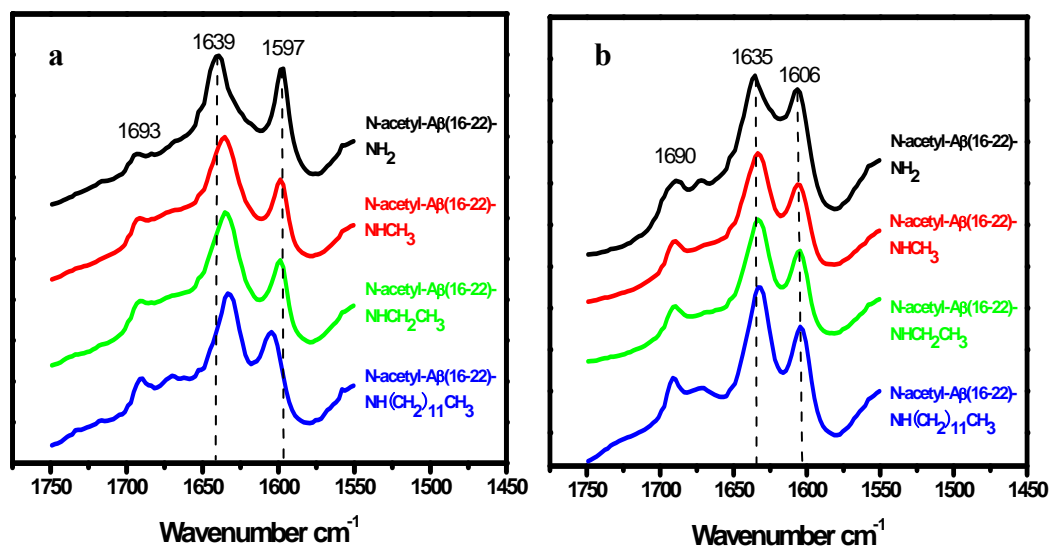
Figure 5-2. Isotope-edited IR amide I band of [1-^{13}C] F19-labeled assemblies.

Assemblies formed (a) at acidic pH, (b) at neutral pH. The major bands are specified and the sample names corresponding to each line are presented at the right side.

In each case, 1.2 mM peptide was allowed to mature in 20% acetonitrile / water with either 0.1% TFA or 15 mM MES (pH6) for 2-3 weeks. The preformed assemblies were pelleted directly (for fibrils) or after bundled with 10-fold sulfate (tubes/sheets). The white sample powder, yielded after being frozen and lyophilization, was mixed and pressed with KBR for IR spectra analysis.

Impact on β-sheet laminates

The X-ray diffraction shown in Figure 5-3, displays 4.7 Å H-bonding distance for both N-acetyl-Aβ(16-22)-NH(CH$_2$)$_{11}$CH$_3$ assemblies, independent of incubation pH, but at acidic pH the main lamination d-spacing is 11.7 Å, 1.9 Å wider than N-acetyl-Aβ(16-22)-NH$_2$, suggestive of the insertion of C-(CH$_2$)$_{11}$CH$_3$ into laminates (Chapter 2 and 3). The noteworthy is that broad peak at neutral pH with maximum of 12.0 Å may suggest two unresolved lamination distances or one uniform laminates with high dynamics.
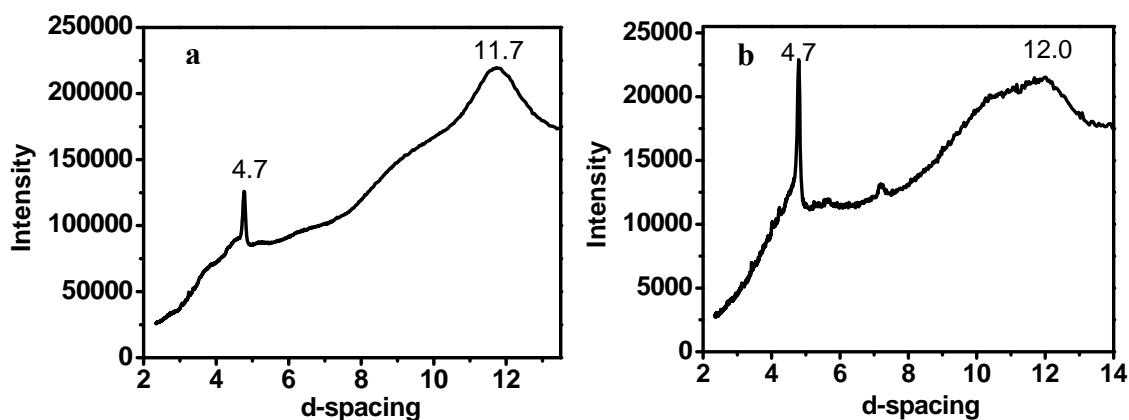
Figure 5-3. X-ray diffraction of N-acetyl-Aβ(16-22)-NH(CH$_2$)$_{11}$CH$_3$ at (a) acidic and (b) neutral pH. The spectra were collected as white powder prepared by pelleting, freezing and lyophilizing matured (2-3 weeks) assemblies at each pH.

Impact of the C-N(CH$_3$)$_2$ substitution on morphology

The N-acetyl-Aβ(16-22)-NH$_2$ C-terminus has two hydrogen-bond sites to associate within the β-sheets or across the bilayer leaflets. In 20% acetonitrile/water at acidic pH, N-acetyl-Aβ(16-22)-NH$_2$ assembled to homogenous nanotubes (Figure 5-4a) with

diameters of 44 ± 5 nm and characteristic β-sheet negative ellipticity at 212 nm (Figure 5-4e). Both N-acetyl-Aβ(16-22)-NHCH$_3$ and N-acetyl-Aβ(16-22)-N(CH$_3$)$_2$ self-assembled
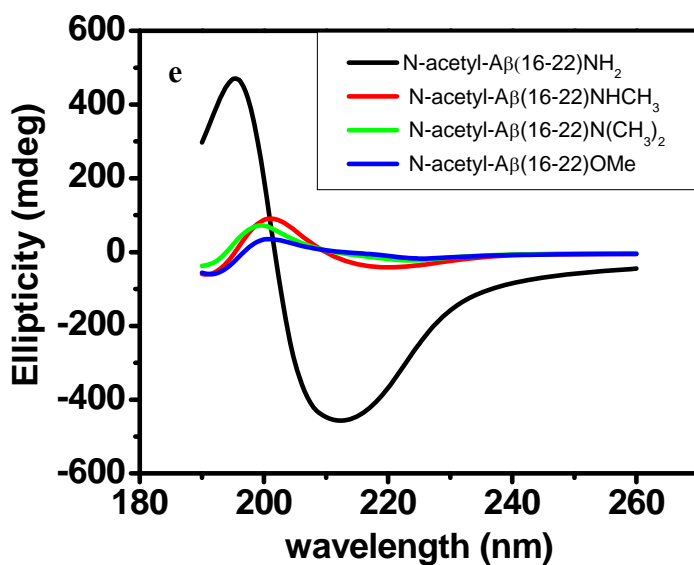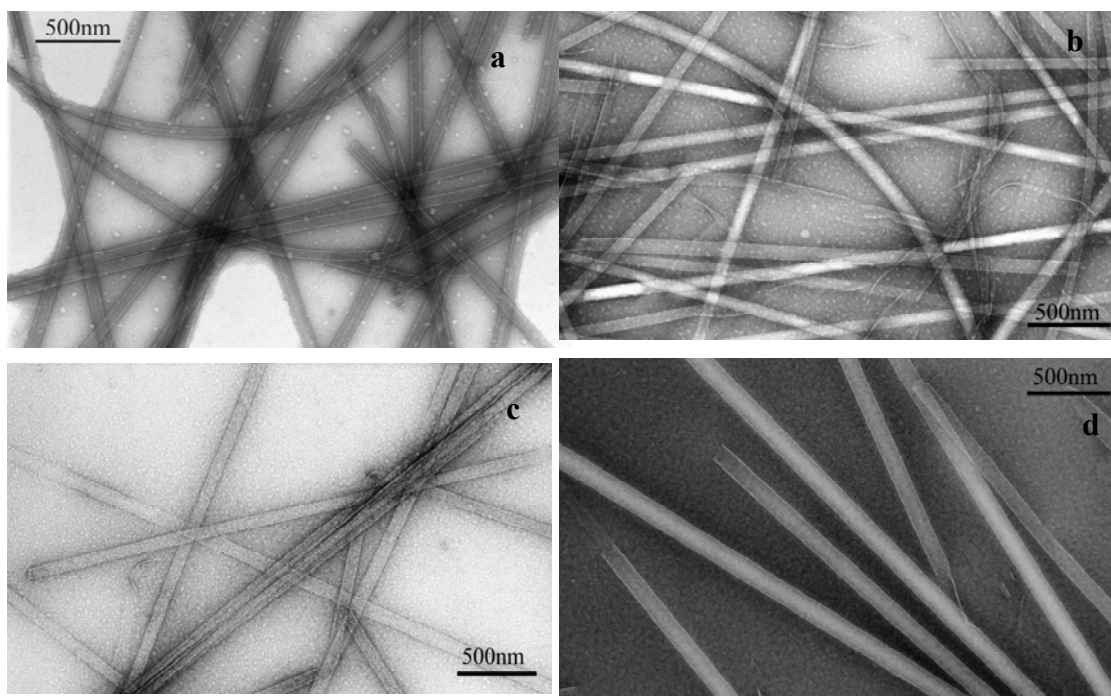
Figure 5-4. TEM images and CD spectra of C-terminal methylated peptides at acidic pH.
Negatively stained self-assemblies of (a) N-acetyl-Aβ(16-22)-NH$_2$, (b) N-acetyl-Aβ(16-22)-NHCH$_3$, (c) N-acetyl-Aβ(16-22)-N(CH$_3$)$_2$ and (d) N-acetyl-Aβ(16-22)-OMe.

(e) CD spectra of the matured samples in 20% acetonitrile / water with 0.1% TFA.

For each case, 1.5 mM peptide solution was incubated in 20% acetonitrile / water with 0.1% TFA at room temperature for 3 weeks to ensure maturation.

by TEM analyses into nanotubes with diameters of 43 ± 6 nm and 50 ± 2 nm, respectively (Figure 5-4b, c), and show weak negative ellipticity ranging from 217 nm to 226 nm (Figure 5-4e), most consistent with β-sheet secondary structure. The controlled peptide N-acetyl-Aβ(16-22)-OMe (Figure 5-4d), with one methyl group but without hydrogen-bond donor at the peptide C-terminus, assembled into homogenous tubes with diameter of 73 ± 7 nm (Figure 5-4d) with weak β-sheet signal at 226 nm (Figure 5-4e) in 20% acetonitrile/water at acidic pH, indicating the similar assembly propensity with N-acetyl-Aβ(16-22)-N(CH$_3$)$_2$.

Impact of the C-N(CH$_3$)$_2$ substitution on bilayer

The AFM images with the measurement profiles shown in Figure 5-5 indicate the tube wall layers by the tube-wall thickness analysis (Lu et al., 2003). N-acetyl-Aβ(16-22)-NHCH$_3$ tubes have the wall thickness of 3.7 nm, similar to that of N-acetyl-Aβ(16-22)-NH$_2$ tubes (Figure 5-5 and Table 5-1), suggestive of bilayer structure (Lu et al., 2003; W. Seth Childers, 2010). However, N-acetyl-Aβ(16-22)-X (X = N(CH$_3$)$_2$ and OMe) tubes without C-terminal H-donor have a reduced wall thickness of around 2.5 nm, very close to a single peptide length, suggesting monolayer tube wall in the latter two nanotubes.

a
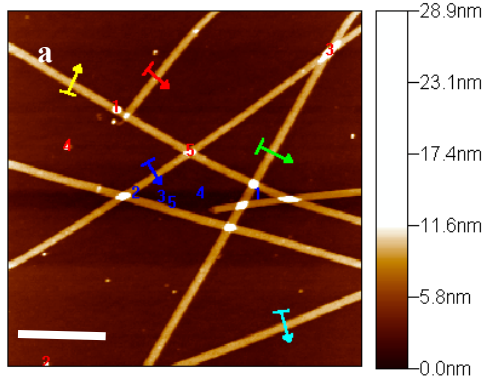
		1	2	3	4	5

Image information
Ra = 1.54 nm   RMS = 2.32 nm
Rz = 20.0 nm   P-V = 28.9 nm
S = 16.0 um²   S ratio = 1.00

		1	2	3	4	5
Ra	[nm]	2.58	2.22	2.59	2.37	2.47
Rz	[nm]	4.84	3.93	5.98	4.27	4.54
RMS	[nm]	2.93	2.65	2.90	2.74	2.81
P-V	[nm]	7.69	7.39	7.55	7.44	7.26
Length	[um]	0.320	0.412	0.286	0.356	0.342

AFM Slope   Ref: -3.600V.
Size: 4.00 x 4.00um.   Bias: 0.000V.

b
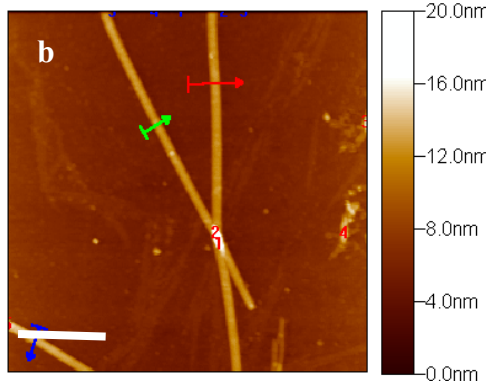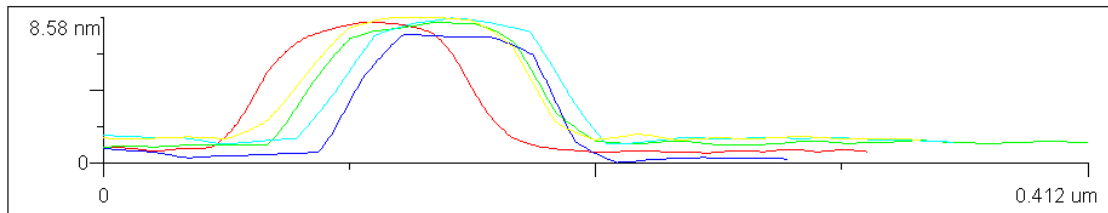
Image information
Ra = 1.12 nm   RMS = 1.68 nm
Rz = 17.4 nm   P-V = 20.0 nm
S = 16.0 um²   S ratio = 1.00

		1	2	3
Ra	[nm]	1.84	2.41	2.21
Rz	[nm]	3.35	3.97	3.88
RMS	[nm]	2.41	2.74	2.56
P-V	[nm]	7.60	7.58	7.29
Length	[um]	0.593	0.350	0.395

AFM Slope   Ref: -3.200V.
Size: 4.00 x 4.00um.   Bias: 0.000V.

153
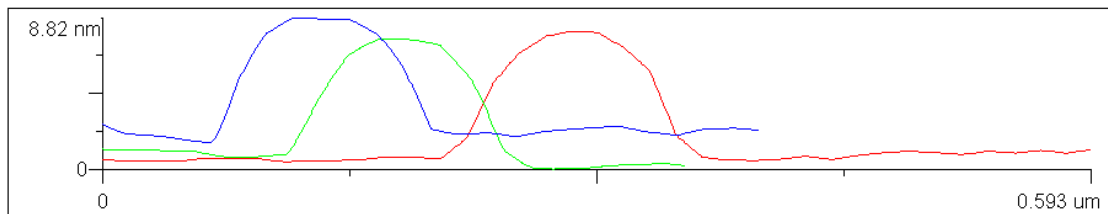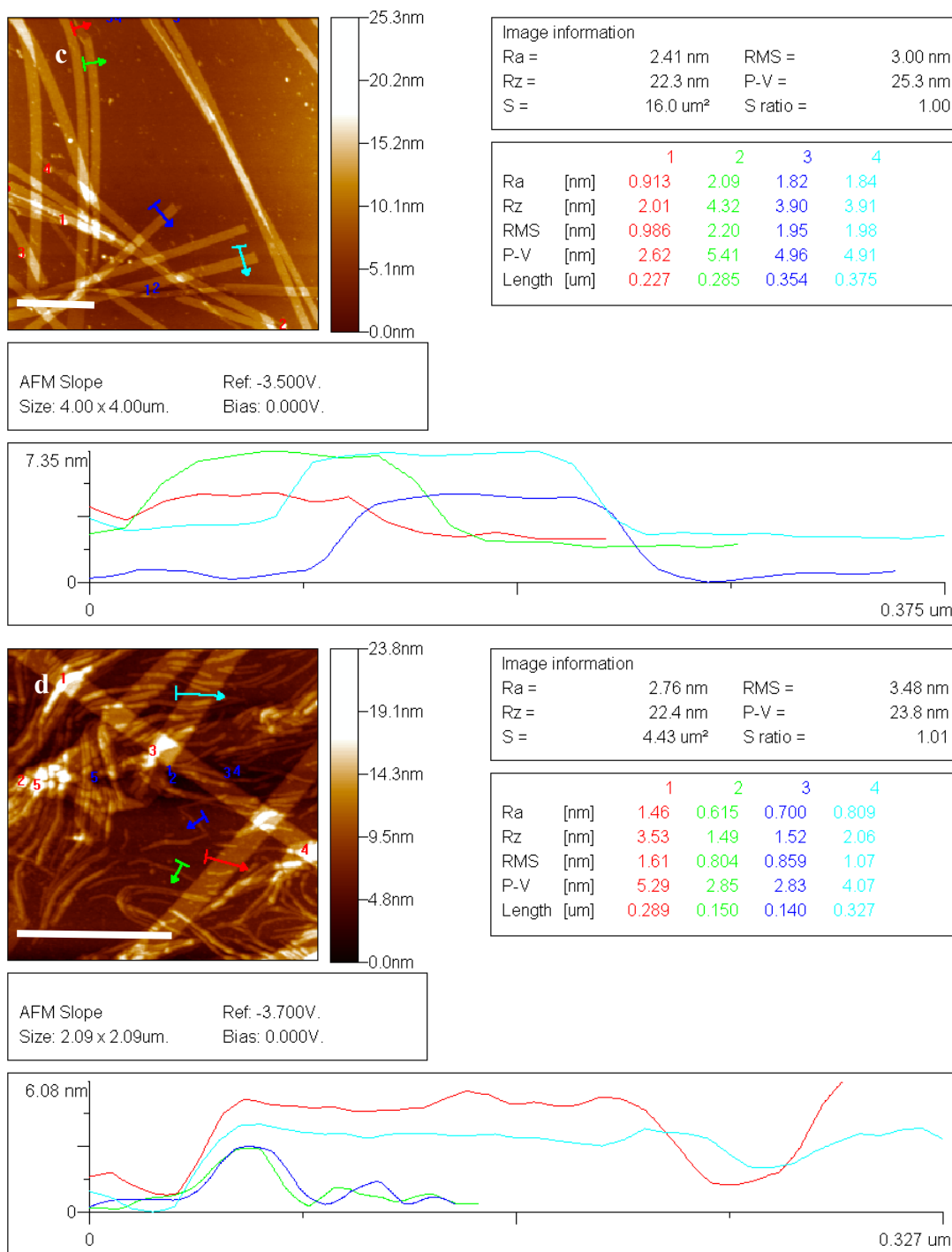
Figure 5-5. AFM images with height measurement of C-terminal modified assemblies.

(a) N-acetyl-Aβ(16-22)-NH$_2$, (b) N-acetyl-Aβ(16-22)-NHCH$_3$, (c) N-acetyl-Aβ(16-22)-N(CH$_3$)$_2$, (d) N-acetyl-Aβ(16-22)-OMe.

In the first three cases, 1.5 mM peptide was incubated in 20% acetonitrile / water at acidic pH for 3 weeks and the last one is the one week sample with the mixture of tube and filaments. The scale bar represents 1000 nm.

154

Table 5-1. Estimated tube-wall thickness.

The wall thickness is determined by averaging ten measurements of dry tubes on silica chip by AFM, expressed as ± sd. Here, the tube wall thickness is roughly estimated to be half of the dry tube height obtained from AFM.

N-acetyl-Aβ(16-22)-X	-NH$_2$	-NHCH$_3$	-N(CH$_3$)$_2$	-OMe
Tube wall thickness (nm)	3.8 ± 0.1	3.7 ± 0.1	2.5 ± 0.1	2.3 ± 0.4

Impact of the C-N(CH$_3$)$_2$ substitution on peptide arrangement

As shown in Figure 5-6, the amide I region of IE-IR spectra including [1-^{13}C] F19-labeles shows the high wave number antiparallel diagnostic band at 1693 cm^{-1} for all tubes, along with the red-shift of ^{13}C oscillators to 1597 / 1599 cm^{-1}, indication of antiparallel one-residue out-of registry for N-acetyl-Aβ(16-22)-NH$_2$ and N-acetyl-Aβ(16-22)-NHCH$_3$ β-sheets (Miyazawa, 1960). However, ^{13}C stretch in N-acetyl-Aβ(16-22)-
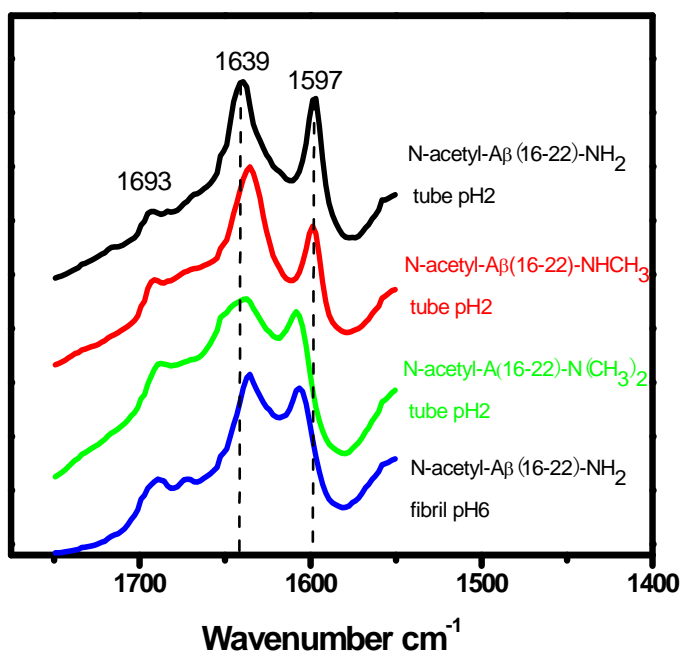
Figure 5-6. Isotope-edited IR amide I band of [1-^{13}C] F19-labeled C-terminal modified tubes under acidic conditions.

In each case, the 1.5 mM peptide was incubated in 20% acetonitrile / water with 0.1%TFA for 3 weeks.

N(CH$_3$)$_2$ nanotubes is at 1608 cm^{-1} with ^{12}C at 1637 cm^{-1}, which is very close to the amide I bands of N-acetyl-Aβ(16-22)-NH$_2$ fibrils with antiparallel in-register β-sheets (Figure 5-6, blue line). The precise assignment of N-acetyl-Aβ(16-22)-N(CH$_3$)$_2$ arrangement within nanotubes requires further structure characterization with ssNMR.

Impact of the C-N(CH$_3$)$_2$ substitution on β-sheet laminates

In addition, the electron diffraction was performed for aligned N-acetyl-Aβ(16-22)-N(CH$_3$)$_2$ tubes to evaluate the impacts of C-terminal dimethyl groups on the peptide
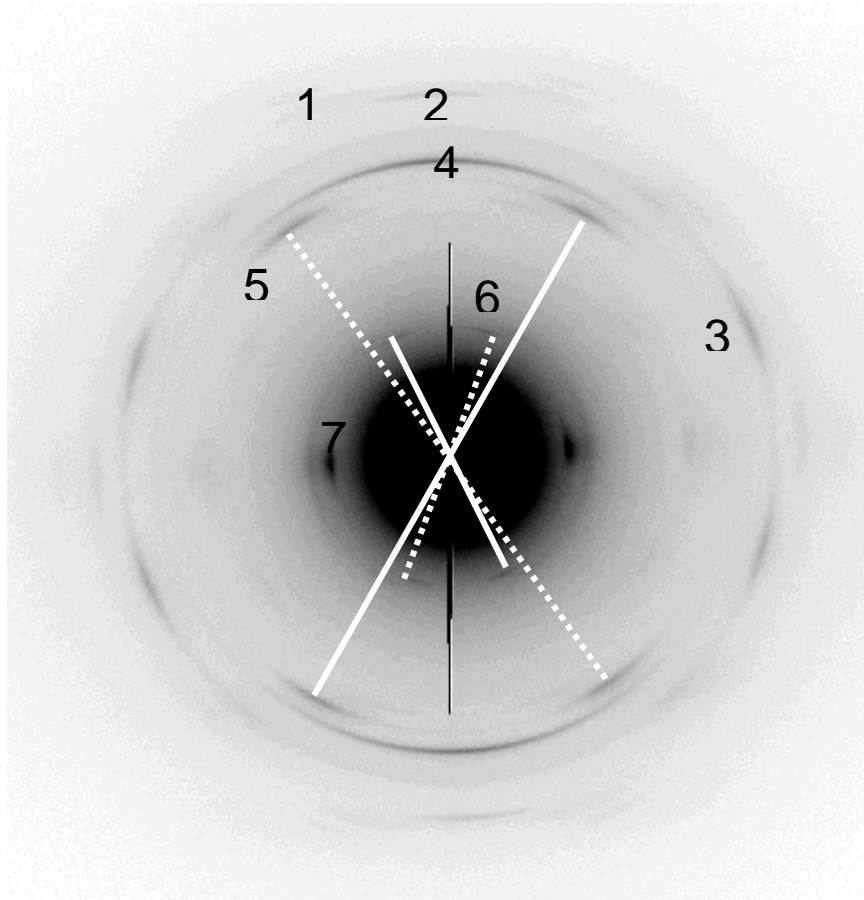
Figure 5-7. Electron diffraction of N-acetyl-Aβ(16-22)-N(CH$_3$)$_2$ nanotubes.
The electron diffraction micrograph was collected from the aligned nanotubes on TEM grids prepared by wicking off the extra solution of matured tubes (3-week incubation at pH2) with a piece of filter paper at one direction. The right black arrow points to the aligned tube axis and the black line cross the center is the instrument artifact.

stacking within tubes. In deed, the diffraction shows very abnormal patterns from that of N-acetyl-Aβ(16-22)-NH$_2$ and other mutated tubes at acidic pH. Most strikingly, several arcs with variable distances were obtained (Figure 5-7 and Table 5-2) with the hydrogen-bonding distance of 4.7 Å and lamination distance of 10.0 Å. Interestingly, the angle between H-bonding and lamination is 51º, instead of 90º, frequently observed in other cross β-sheet amyloids (Childers et al., 2009; Mehta et al., 2008). In addition, there are single arc 4 and 7 with distance of 4.4 Å and 10.6 Å, respectively, which have not been assigned yet. The further assignment of this tube structure requires more characterization information.

Table 5-2. The peptide repeat distances corresponding to each arc in Figure 5-7.

| Arc	1	2	3	4	5	6	7
Distance (Å)	3.3	3.6	3.9	4.4	4.7	10.0	10.6

Impact of mixing N- and C-terminal alkyl substitutions on assembled morphology and peptide arrangement

As one of the representatives to evaluate the impact of N- and C-terminal interaction on amyloid self-assembly, the simple methyl group was chosen as the C-terminal substitution and fatty acids of different length were coupled at the N-terminus of H$_2$N-Aβ(16-22)-NHCH$_3$. At acidic pH, N-acetyl-Aβ(16-22)-NHCH$_3$ assembled to majority nanotubes with few ribbons, while N-isobutyl-Aβ(16-22)-NHCH$_3$ only formed ribbons as TEM analysis (Figure 5-8b). The longer N-substitution N-lauryl-Aβ(16-22)-NHCH$_3$ resumed the formation of nanotubes with larger size, but N-palmityl-Aβ(16-22)-NHCH$_3$ with even longer N-alkane substitution formed bundled fibrils. At neutral pH, N-acetyl-Aβ(16-22)-NHCH$_3$ assembled to rigid, flat fibrils with well-separation (Figure 5-
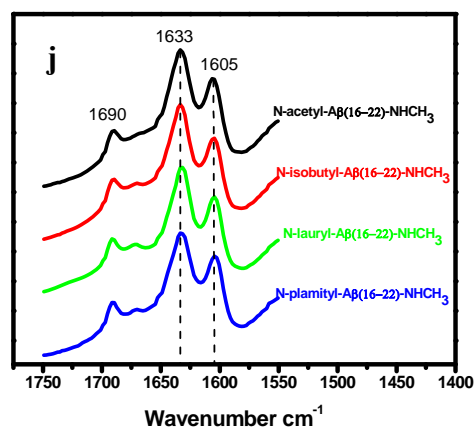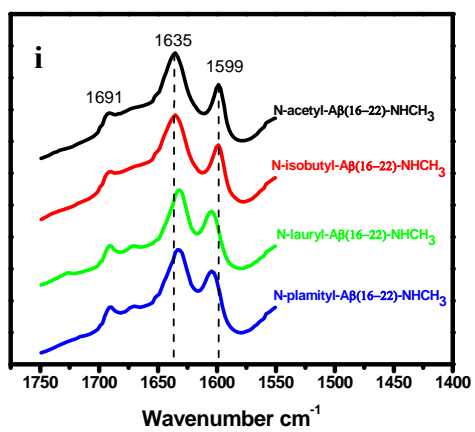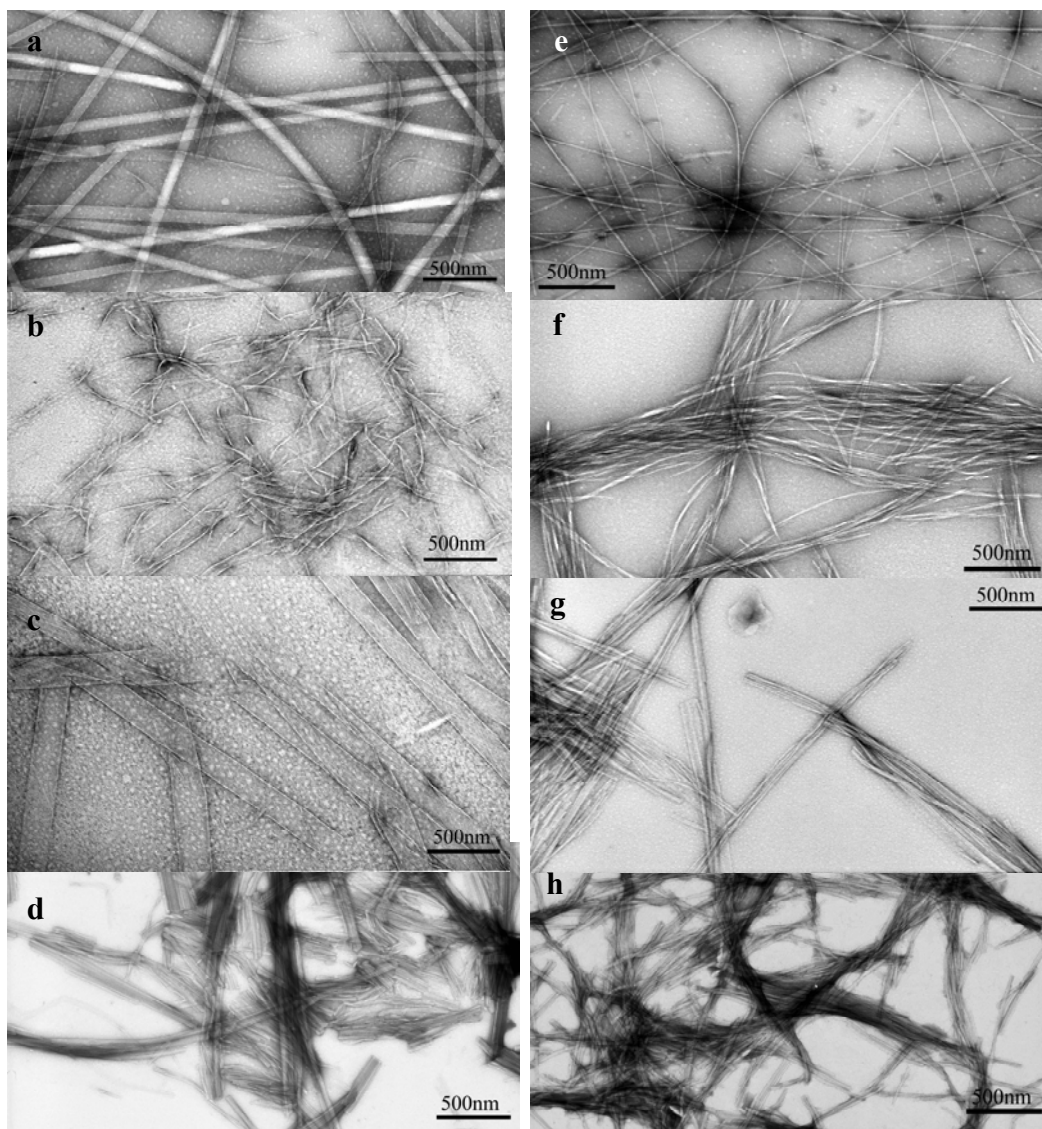
Figure 5-8. TEM and Isotope-edited IR spectra of X-Aβ(16-22)-NHCH₃ (X = N-acetyl, -isobutyl, -lauryl and -palmityl).

The TEM images of self-assemblies formed at acidic pH: (a) N-acetyl-Aβ(16-22)-NHCH₃, (b) N-isobutyl-Aβ(16-22)-NHCH₃, (c) N-lauryl-Aβ(16-22)-NHCH₃, and (d) N-palmityl-Aβ(16-22)-NHCH₃; and fibrils assembled at neutral pH: (e) N-acetyl-Aβ(16-22)-NHCH₃, (f) N-isobutyl-Aβ(16-22)-NHCH₃, (g) N-lauryl-Aβ(16-22)-NHCH₃, and (h) N-palmityl-Aβ(16-22)-NHCH₃.

Stacked FT-IR spectra amide I region of [1-^{13}C] F19-labeled X-Aβ(16-22)-NHCH₃ (X = N-acetyl, -isobutyl, -lauryl and -palmityl) at (i) acidic pH and (j) neutral pH, with peptide name presented at the right side of each line.

In each case, 1.2 mM peptide was incubated in 20% acetonitrile / water with either 0.1% TFA or 15 mM (pH6) MES buffer for 2-3 weeks to allow for maturation.

8e), while N-acetyl-Aβ(16-22)-NHCH₃ formed fibrils with loosely bundled thin filaments (Figure 5-8f). For the longer N-alkanes, N-lauryl-Aβ(16-22)-NHCH₃ and N-palmityl-Aβ(16-22)-NHCH₃ assembled to fibrils with high tendency to bundle together (Figure 5-8g-h).

In the FT-IR spectra amide I region (Figure 5-8i), N-acetyl-Aβ(16-22)-NHCH₃ tubes and N-isobutyl-Aβ(16-22)-NHCH₃ ribbons assembled at acidic pH both show the amide I stretches of ^{13}C component at 1599 cm^{-1} and ^{12}C at 1635 cm^{-1}, along with 1691 cm^{-1} high wave number shoulder band, suggestive of antiparallel one-residue out-of register β-sheets (Mehta et al., 2008). However, for the long N-alkanes, the amide I bands of N-lauryl-Aβ(16-22)-NHCH₃ tubes and N-palmityl-Aβ(16-22)-NHCH₃ fibrils display same stretches for ^{13}C and ^{12}C oscillators at 1605 cm^{-1} and 1632 cm^{-1}, respectively (Figure 5-8i), which is exactly same as the amide I spectra of N-acetyl-Aβ(16-22) fibrils with antiparallel in-registry β-sheets (Mehta et al., 2008). At neutral pH, independent of N-alkyl substitutions, the amide I bands of all four assemblies show antiparallel diagnostic shoulder band at 1690 cm^{-1} and the major stretches at 1605 cm^{-1} and 1633 cm^{-1}, respectively (Figure 5-8j), suggestive of antiparallel in-registry β-sheets (Mehta et al.,

2008). This initial structure information provides the basic clue for the further characterization, such as isotope-labels for ssNMR.

Another series of N- and C- double substitution N-X-Aβ(16-22)-N(CH$_3$)$_2$ (X = acetyl, isobutyl, lauryl and palmityl) were also studied, as comparison to the significant impacts of C-terminal dimethyl on amyloid architecture. When incubated in 20% acetonitrile/water at acidic pH, N-acetyl-Aβ(16-22)-N(CH$_3$)$_2$ assembled to homogenous tubes with diameter of 50 ± 2 nm (Figure 5-9a), while N-isobutyl-Aβ(16-22)-N(CH$_3$)$_2$ only formed small ribbons with width of 25 ± 6 nm (Figure 5-9b). For the longer N-alkane substitutions, N-lauryl-Aβ(16-22)-N(CH$_3$)$_2$ resumed the formation of homogenous nanotube with diameter of 54 ± 8 nm (Figure 5-9c) and N-palmityl-Aβ(16-22)-N(CH$_3$)$_2$ formed the mixed species of tubes and ribbons (Figure 5-9d). At more neutral pH, N-acetyl-Aβ(16-22)-N(CH$_3$)$_2$ assembled to flat and rigid fibrils without twisting pattern, while N-isobutyl-Aβ(16-22)-N(CH$_3$)$_2$ and N-lauryl-Aβ(16-22)-N(CH$_3$)$_2$ formed flat fibrils too, but these fibrils were more intent to bundle together (Figure 5-9e-h). Under the same conditions, N-palmityl-Aβ(16-22)-N(CH$_3$)$_2$ assembled to bundled fibrils, which may attribute to the N-long alkanes.

The peptide registry was defined by isotope-edited IR (Figure 5-9i-j). At acidic pH, the FTIR amide I bands show the diagnostic antiparallel high wave number shoulder at 1689 cm^{-1}, independent of the assembled morphologies and the N-alkane length. The stretches of ^{12}C and ^{13}C for N-acetyl-Aβ(16-22)-N(CH$_3$)$_2$ tubes are unique at 1643 cm^{-1} and 1608 cm^{-1} respectively; and the rest three assemblies, N-isobutyl-Aβ(16-22)-N(CH$_3$)$_2$ ribbons, N-lauryl-Aβ(16-22)-N(CH$_3$)$_2$ tubes and N-palmityl-Aβ(16-22)-N(CH$_3$)$_2$ tubes
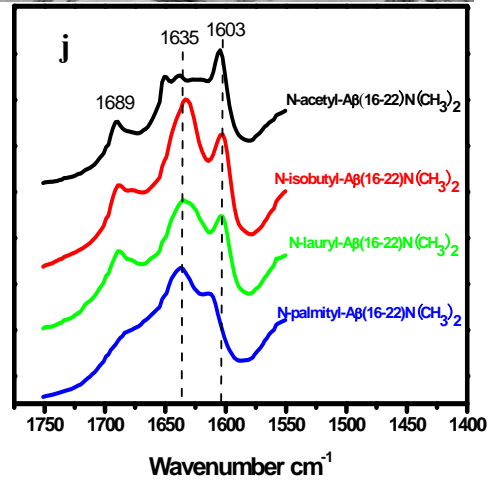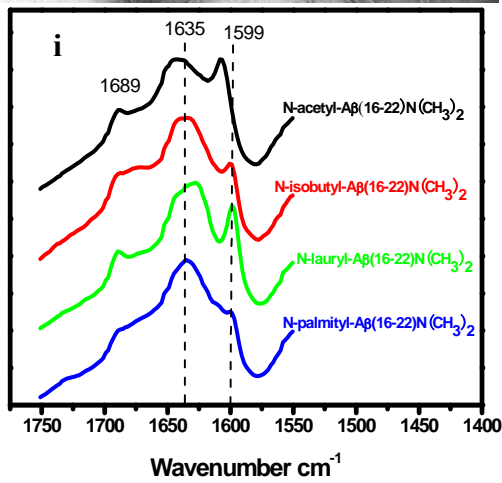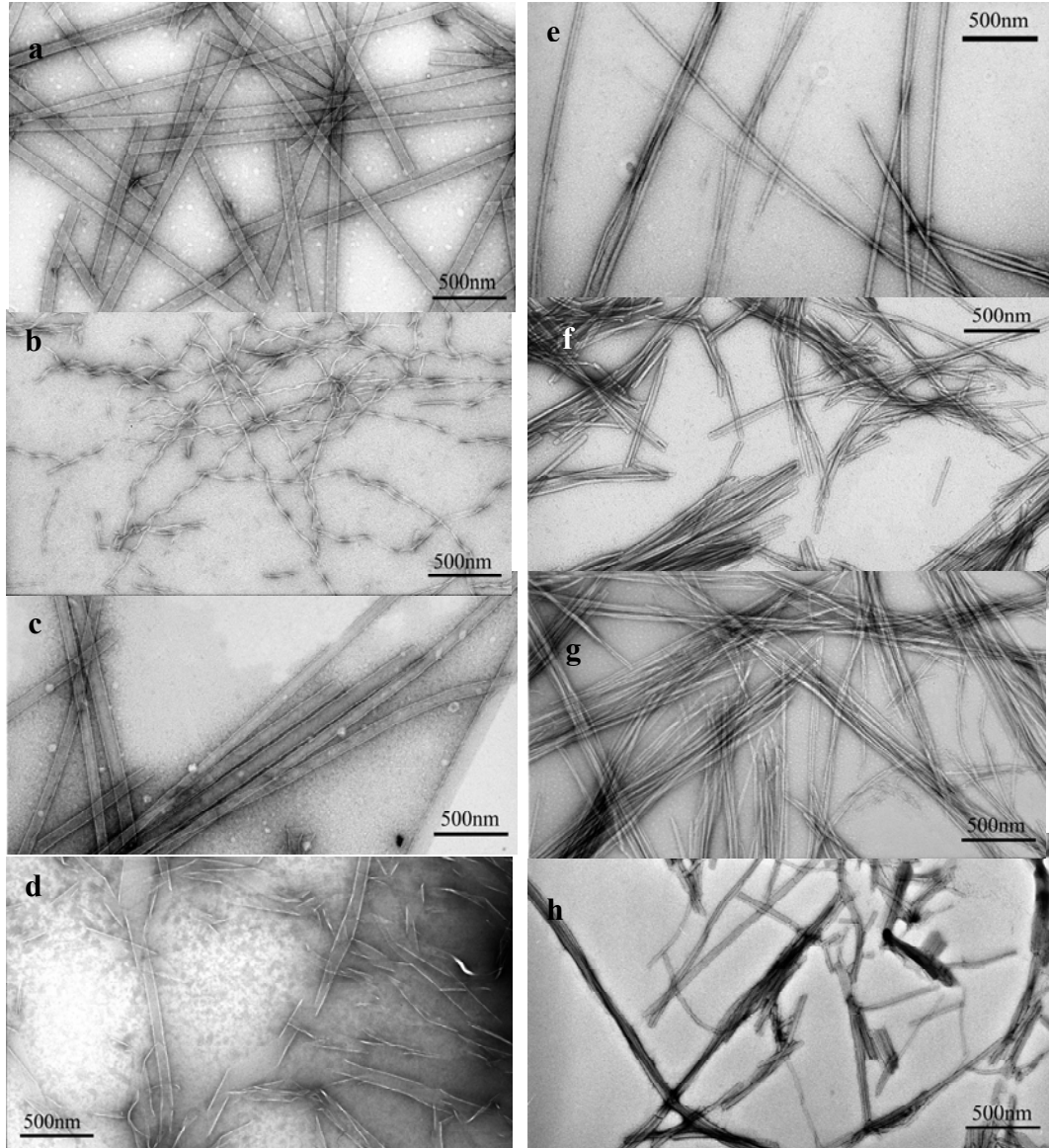
Figure 5-9. TEM and Isotope-edited IR spectra of N-X-Aβ(16-22)-N(CH$_3$)$_2$ (X= acetyl, isobutyl, lauryl and palmityl).

The electron micrographs of self-assemblies formed at acidic pH: (a) N-acetyl-Aβ(16-22)-N(CH$_3$)$_2$, (b) N-isobutyl-Aβ(16-22)-N(CH$_3$)$_2$, (c) N-lauryl-Aβ(16-22)-N(CH$_3$)$_2$, and (d) N-palmityl-Aβ(16-22)-N(CH$_3$)$_2$; and fibrils assembled at neutral pH: (e) N-acetyl-Aβ(16-22)-N(CH$_3$)$_2$, (f) N-isobutyl-Aβ(16-22)-N(CH$_3$)$_2$, (g) N-lauryl-Aβ(16-22)-N(CH$_3$)$_2$, and (h) N-palmityl-Aβ(16-22)-N(CH$_3$)$_2$.

Stacked FT-IR spectra amide I region of [1-^{13}C]F19-labeled N-X-Aβ(16-22)-N(CH$_3$)$_2$ (X=acetyl, isobutyl, lauryl and palmityl) at (i) acidic pH and (j) neutral pH, with peptide name presented at the right side of each line.

In each case, 1.2 mM peptide was incubated in 20% acetonitrile / water with either 0.1% TFA or 15 mM (pH6) MES buffer for 2-3 weeks to allow for maturation.

and ribbons, have the similar stretches with ^{12}C centered around 1635 cm^{-1} and ^{13}C at 1599 cm^{-1}, consistent with the well-alignment of ^{13}C carbonyls in the antiparallel one-residue out-of register β-sheets. At neutral pH, the amide I region of the first three fibrils, N-acetyl-Aβ(16-22)-N(CH$_3$)$_2$, N-isobutyl-Aβ(16-22)-N(CH$_3$)$_2$ and N-lauryl-Aβ(16-22)-N(CH$_3$)$_2$, display the antiparallel diagnostic band at 1689 cm^{-1}. In this region, ^{13}C stretch is at 1608 cm^{-1} for N-acetyl-Aβ(16-22)-N(CH$_3$)$_2$ fibrils with an unusual flat region between 1650 cm^{-1} to 1616 cm^{-1}. For N-isobutyl-Aβ(16-22)-N(CH$_3$)$_2$ and N-lauryl-Aβ(16-22)-N(CH$_3$)$_2$ fibrils, their amide I stretches are same with ^{13}C and ^{12}C at 1603 cm^{-1} and 1635 cm^{-1}, respectively, close to the ^{12}C/^{13}C splitting in N-acetyl-Aβ(16-22)-NH$_2$ antiparallel in-register fibrils (Mehta et al., 2008). However, the amide I region of N-palmityl-Aβ(16-22)-N(CH$_3$)$_2$ fibrils shows an intermediate shoulder band at 1681 cm^{-1} and two stretches of ^{12}C and ^{13}C at 1639 cm^{-1} and 1612 cm^{-1}, respectively, suggesting the mixed antiparallel and parallel β-sheets.

Impact of mixing N- and C-terminal alkyl substitution on β-sheet laminates

X-ray diffraction analysis of N-lauryl-Aβ(16-22)-NHCH$_3$ and N-lauryl-Aβ(16-22)-N(CH$_3$)$_2$ was preformed to evaluate the impact of N-lauryl group on the β-sheet laminates in the presence of C-terminal alkanes. As shown in Figure 5-10, all four assemblies
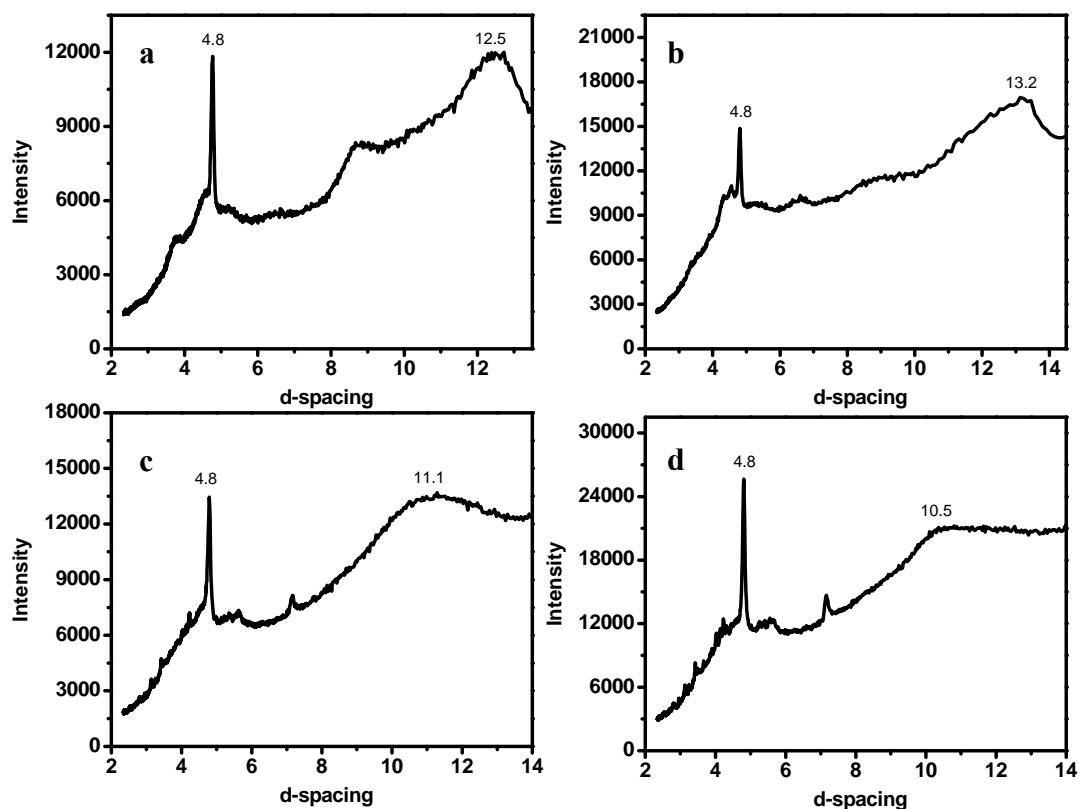
Figure 5-10. X-ray diffraction of N- and C- double-substituted peptide assemblies.
The X-ray of the assemblies formed at acidic pH: (a) N-lauryl-Aβ(16-22)-NHCH$_3$ tubes and (b) N-lauryl-Aβ(16-22)-N(CH$_3$)$_2$ tubes; the assemblies formed at neutral pH: (c) N-lauryl-Aβ(16-22)-NHCH$_3$ and (d) N-lauryl-Aβ(16-22)-N(CH$_3$)$_2$ fibrils.
In each case, 1.0 mM peptide was incubated in 20% acetonitrile / water with 0.1% TFA or with 15 mM pH6 MES buffer for 2 weeks to allow maturation. The preformed tubes were bundled with NADH with 1 to

4 ratio, then pelleted, frozen and lyophilized to yield white powder for X-ray analysis. The fibril samples followed the same procedure without bundling step.

conserve the H-bonding d-spacing of 4.8 Å, independent of incubation pH and the peptide terminal substitutions; while the lamination d-spacing is variable with broad peaks, suggesting the loosely sheets packing with high dynamic or the heterogeneity of the structure. The lamination d-spacing of N-lauryl-Aβ(16-22)-NHCH$_3$ tubes (acidic pH) is at 12.5 Å and that of fibrils (neutral pH) is slightly short with the d-spacing at 11.1 Å; whereas, the lamination d-spacing of N-lauryl-Aβ(16-22)-N(CH$_3$)$_2$ tubes (acidic pH) and fibrils (neutral pH) is at 13.2 Å and 10.5 Å, respectively. Comparing to the 11.5 Å lamination distance observed in N-lauryl-Aβ(16-22)-NH$_2$ tubes at acidic pH, the longer distances obtained here suggest that the C-terminal methyl and dimethyl groups may interact with N-lauryl group to expand the laminates, consistent with the loosely sheets packing.

Discussion

The energetic constraints from the amino acid pairing interactions, such as K / E cross-strand electrostatic interaction, V / A cross-strand pairing, F/F aromatic interaction and the new discovered cross-leaflets peptide terminal interaction, play a critical role to modulate amyloid morphology and architecture. Therefore, peptide C-terminus, one of the components in the bilayer interface, may contribute significantly to amyloid self-assemblies by regulating the cross-leaflets hydrogen-bonding and hydrophobic interaction.

Peptide C-terminus, due to two protons on the amide nitrogen, implies the potential different impacts on amyloid assembly from N-terminus. Substitution one of C-amide protons with alkanes will cause three possible impacts including 1) weakening cross-leaflets H-bonding interaction by eliminating one H-bond donor, 2) weakening cross-leaflets interaction by increasing the C-terminal steric effect, and 3) strengthening the bilayer interaction through increasing the overall peptide hydrophobic interaction. Substitution of both C-amide protons will totally eliminate the H-bonding interaction either cross-leaflets or cross-strand, which may destabilize the bilayer and β-sheet, resulting in different amyloid architecture. Introducing N-alkane to the C-mono or dimethylated peptide may result in new features by increasing possibility of N- and C-alkane interaction. The impacts of these modifications on amyloid structure and architecture will be discussed individually.

C-terminal mono-alkane substitution modulates amyloid architecture through the different way from N-terminal alkanes. With increasing the length of C-alkane, the morphologies assembled at acidic pH transit from tube to ribbons to tubes again, similar as but earlier (between C-methyl to C-dimethyl (Figure 5-1)) than the transition occurred for N-alkanes ((N-butyl to N-valeryl) (Figure 3-1)). At this pH, increasing C-terminal alkanes either makes the peptide packing within β-sheets weakening or renders peptide registry shifting from one-residue out-of registry to in-registry, which requires further confirmation (Figure 5-2a). However, within this alkane length range (shorter than lauryl), the N-alkanes maintain the same peptide arrangement (antiparallel one-residue out-of register β-sheets) in both tubes and sheets assembled at acidic pH (chapter 3). These differences may result from the different relative positions of N- and C-termini in

antiparallel out-of register β-sheets. The dangling-out and flexible N-terminus is more tolerant to the modification, but C-terminus is more constraint by burying inside, so amyloid architecture is more sensitive to the modification at C-terminus. This effect is consistent with the more significant impact of C-terminal amino acid mutation than N-terminal amino acid substitution on amyloid assembly (Lu, 2005). At neutral pH, C- and N-alkanes cause dramatical different impacts on amyloid architecture, such as maintaining the same peptide arrangement (Figure 5-2) by C-alkanes but altering the peptide orientation from antiparallel to parallel by N-alkanes (Figure 3-4) (from N-acetyl to N-propyl), even though both C- and N-alkanes maintain fibril morphology (Figure 5-1). This different impact may be correlated with the hydrophobic interaction between both terminal groups which will be discussed in detail in the following section.

Terminal H-bonding interaction plays critical role on modulating peptide registry/peptide layers within tube wall in the absence of other forces. Even though the electron diffraction of N-acetyl-Aβ(16-22)-N(CH$_3$)$_2$ tubes has not been fully assigned, the complicated diffraction patterns indicate unusual tube architecture. From the known structure information, we know that elimination of the potential terminal H-bonding interaction alters tube architecture by shifting the peptide registry from out-of registry to in-registry and by changing tube wall from bilayer to monolayer. This architecture switch may correlate with the number of H-bonds required to stabilize peptide stands within β-sheets. With antiparallel out-of registry, there are seven hydrogen-bonds between two adjacent peptide strands within N-acetyl-Aβ(16-22)-X (X = NH$_2$, or NHCH$_3$) β-sheets (Figure 5-11 and Table 5-3), but only six in N-acetyl-Aβ(16-22)-N(CH$_3$)$_2$ β-sheets. Shifting of N-acetyl-Aβ(16-22)-N(CH$_3$)$_2$ to in-register β-sheets would gain one more

hydrogen-bond (Figure 5-11). Therefore, we speculate that seven hydrogen-bonds may be required to form stable β-sheets for seven-residue peptides in the absence of other favorable forces. It is noteworthy to mention that terminal hydrogen-bonding interaction is critical but not necessarily required for the bilayer formation since by introducing other favorable force such as hydrophobic interaction, the peptide out-of registry and bilayer structure are able to be recovered (N-lauryl-Aβ(16-22)-N(CH$_3$)$_2$, data not shown). The role of N-lauryl group on this structure switch requires further investigation.
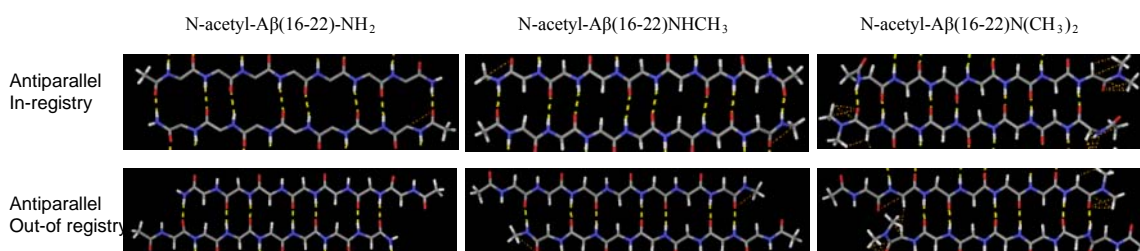
Figure 5-11. The illustration of H-bonding interaction of three C-terminal modified peptides in two different peptide β-sheets.
The two peptide strands stack together with antiparallel in-registry (upper panel) and antiparallel one-residue out-of registry (lower panel) with distance of 4.7 Å. Color codes: red for oxygen, blue for nitrogen, grey for carbon and yellow dot represents hydrogen-bonds.

Table 5-3. Average number of hydrogen-bonds between two adjacent peptide strands within β-sheets (Figure 5-11).

# of Hydrogen-bond	N-acetyl-Aβ(16-22)-NH$_2$	N-acetyl-Aβ(16-22)-NHCH$_3$	N-acetyl-Aβ(16-22)-N(CH$_3$)$_2$
Antiparallel in-registry	8	8	7
Antiparallel out-of registry	7	7	6

Mixed substitutions of simple C-alkanes with N-linear alkanes are able to regulate amyloid architectures in a different way from either C- or N-alkanes through terminal interaction. As established in Chapter 2 and 3, N-linear alkanes renders the parallel β-sheets formation for N-myristyl to N-palmityl at acidic pH and from N-propyl to N-palmityl at neutral pH, but in the presence of C-terminal mono or dimethyl groups, the

self-assemblies within these alkane length ranges at either acidic pH or neutral pH maintain antiparallel β-sheets. The interaction between N- and C-alkanes is one of the possibilities to keep this antiparallel orientation, consistent with the literature report that N- and C-alkyl chain interaction directs peptide orientation (Iqbal et al., 2008). The underneath mechanism of how this interaction between N-long alkanes and C-short alkanes directs peptide arrangements remain unclear and the further study is undergoing.

The elucidation of the role of peptide C-terminal alkyl chains and terminal backbone hydrogen-bonds on amyloid self-assembled morphologies and architectures further clarifies the underneath mechanism of molecular self-assembly. Regardless of final peptide orientation and registry within β-sheets, the lipid alkyl chains at either peptide terminus tend to interact with amyloid peptides by bending to fit in laminates. This phenomenon may imply the inherent capability of Aβ to interact with lipid, shedding light on the underneath mechanism of amyloid neurotoxicity through *in vivo* amyloid/membrane interaction. Moreover, the C-terminal modification extends our current strategies for the rational design of nanomaterials with desired structure through modulating the N-and C-terminal alkyl chains or hydrogen-bonding interactions.

The finding in this chapter also raises a question about the role of side chain hydrogen-bonding interaction for amyloid assembly, which will be addressed in the following chapter.

Materials and methods

Synthesis of side chain protected and C-terminal free peptide: Ac-K(Boc)LVFFAE(*t*Bu)-OH

The peptide was synthesized on a peptide synthesizer with 2-Chlorotrityl resin. The same procedure for Rank amide resin was followed except no capping with acetic anhydride. After the synthesis was completed, the resin was collected from the synthesizer, and dried with dichloromethane. The resin was placed in the Sigmacote treated glass round bottle and the cleavage cocktail (DCM : ACD : TFE = 8 : 1 : 1) was added. The reaction mixture was allowed to gently stir at room temperature for 1 hour, followed by filtration to remove the resin. The filtrate was collected and concentrated on rotavap under reduced pressure. The high boiling point solvents were removed via azeotropic evaporation of its hexane mixture with rotavap. After repeated addition of hexane and evaporation, dry powder or peptide film was obtained, which was used for the next step without further purification

Amidation of peptide C-terminus

The side chain protected peptide (1.0 equiv.) was dissolved in the minimum amount of Dimethylformamide (DMF). To the peptide solution were then added N,N-Diisopropylethylamine (DIPEA) (7.8 equiv.), 2-(1H-Benzotriazol-1-yl)-1,1,3,3-TetramethylUronium hexafluorophosphate (HBTU) (3 equiv.) and methylamine hydrochloride or dimethylamine hydrochloride or C12 amine hydrochloride (3.3 equiv.). The reaction mixture was stirred at room temperature overnight. Then the reaction mixture was concentrated on rotavap with vacuum to remove some DMF. The residue was precipitated in cold ether with drop-wise fashion and the white precipitate was washed with cold ether two more times and air-dried.

Deprotection of the peptide

The peptide powder was treated with the cleavage cocktail (TFA : EDT : Thioanisol : anisol 90 : 5 : 3 : 2, volume ratio) and allowed to stir for 2 hr. The reaction mixture was titrated in cold ether to precipitate out the desired peptide. The crude peptide was washed three more times with cold ether and centrifuged to yield the pellet, which was dried in hood prior to the HPLC purification.

Synthesis of Ac-KLVFFAE-OMe

To synthesize the peptide C-terminal backbone methyl ester, the following synthetic strategy was developed. The side chain free carboxylic acid of Fmoc-Glu-OMe was coupled to Wang resin, providing the desired solid-supported Fmoc-Glu-OMe for the Fmoc solid phase synthesis (FSPS).
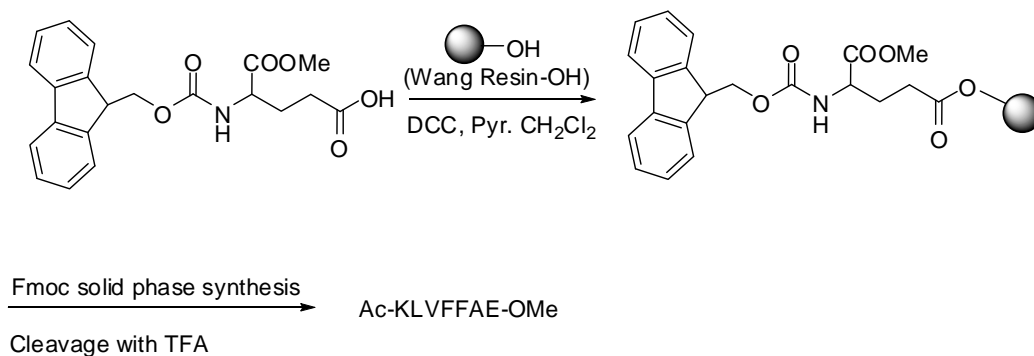
Coupling of the Fmoc-Glu-OMe to Wang resin

To a round-bottomed flash was charged with stir bar, Wang resin (204 mg, 0.2 mmol, 1.0 equiv.) and CH_2Cl_2 (5 mL). To this suspension were added Fmoc-Glu-OMe (GL Biochem Ltd. 115 mg, 0.3 mmol, 1.5 equiv.), pyridine (24.3 μL, 0.3 mmol, 1.5 equiv.) and N,N'-Dicyclohexylcarbodiimide (DCC) (62 mg, 0.3 mmol, 1.5 equiv.). The

reaction mixture was gently stirred for 24 hr at room temperature. The reaction mixture was filtered and the resin was washed with methanol and CH_2Cl_2 and allowed air dry. In order to determine the loading efficiency, small amount of dry resin was used as follows. The dry resin (2.12 mg) was added to 1.0 mL solution of 20% piperidine / DMF and incubated for 30 min with occasional agitation. The resin was removed by centrifugation and the supernatant was analyzed with UV at 295 nm to determine the loading efficiency to be 0.6 mmol/g.

To prevent the rest of hydroxyl group on wang resin for the further reaction, above loaded resin was acetylated by mixing with 4.0 mL CH_2Cl_2, acetic anhydride (2.0 mL) and triethylamine (1.0 mL) at room temperature. After 2 hr, the suspension was filtered and the resin was collected, washed with CH_2Cl_2 and dried in air for the solid phase peptide synthesis.

References

Childers, W. S., Mehta, A. K., Lu, K., and Lynn, D. G. (2009). Templating Molecular Arrays in Amyloid's Cross-beta Grooves. J Am Chem Soc, 131, 10165-10172

Halverson, K. J., Sucholeiki, I., Ashburn, T. T., and Lansbury, P. T. (1991). Location of Beta-Sheet-Forming Sequences in Amyloid Proteins by Ftir. J Am Chem Soc *113*, 6701-6703.

Iqbal, S., Miravet, J. F., and Escuder, B. (2008). Biomimetic self-assembly of tetrapeptides into fibrillar networks and organogels. Eur J Org Chem, 4580-4590.

Lu, K. (2005) Discovery of diverse peptide nanotube architecture from the self-assembly of designed amyloid-beta cassettes, Ph.D. Thesis, Emory university, Atlanta, GA, USA.

Lu, K., Jacob, J., Thiyagarajan, P., Conticello, V. P., and Lynn, D. G. (2003). Exploiting amyloid fibril lamination for nanotube self-assembly. J Am Chem Soc *125*, 6391-6393.

Mehta, A. K., Lu, K., Childers, W. S., Liang, Y., Dublin, S. N., Dong, J., Snyder, J. P., Pingali, S. V., Thiyagarajan, P., and Lynn, D. G. (2008). Facial symmetry in protein self-assembly. J Am Chem Soc *130*, 9829-9835.

Miyazawa, T. (1960). Perturbation Treatment of the Characteristic Vibrations of Polypeptide Chains in Various Configurations. J Chem Phys *32*, 1647-1652.

Paul, C., and Axelsen, P. H. (2005). beta Sheet structure in amyloid beta fibrils and vibrational dipolar coupling. J Am Chem Soc *127*, 5754-5755.

Paul, C., Wang, J., Wimley, W. C., Hochstrasser, R. M., and Axelsen, P. H. (2004). Vibrational coupling, isotopic editing, and beta-sheet structure in a membrane-bound polypeptide. J Am Chem Soc *126*, 5843-5850.

Childers, W. S., Mehta, A. K., Ni, R., Taylor, J.V., and Lynn, D. G. (2010). Peptides Organized as Bilayer Membranes. Angew Chem Int Ed, ASAP

CHAPTER 6

Glutamine Cross-Strand Pairing in Amyloid Assembly

Introduction

Mutations of the glutamate residue at position 22 in the amyloid β-peptide are known to aggravate Alzheimer's disease onset, and substitutions with glutamine, the Dutch mutation, most significantly impacts symptoms (Davis and VanNostrand, 1996). This specific substitution has been studied in both full length (Aβ(1-40)E22Q) (Davis and VanNostrand, 1996) as well as shorter peptide models (Aβ(13-26)E22Q) (Clements et al., 1993) to understand the role of glutamine. In fact, glutamine residues seem to be important in other neurodegenerative etiologies, most notably Huntington's disease (Kvam et al., 2009; Rousseau et al., 2009), where long tracks of glutamines appear to optimize hydrogen-bonding between side-chains to drive aggregation (Perutz, 1999a; Perutz, 1999b; Perutz et al., 1994). Our previous results have continued to implicate side chain interactions, both along the sheet and between individual sheets, as important to amyloid assembly (Dong et al., 2006; Lu et al., 2003; Mehta et al., 2008). In this chapter, I have combined these observations of glutamine with my previous results that the residues at the C-terminus of N-acetyl-Aβ(16-22) offers a very sensitive site for exploring cross strand pairing interactions.

Our basic hypothesis is that the E22Q (N-acetyl-Aβ(16-22)E22Q) substitution would not stabilize the cross-sheet interactions that are so important for the cytosine substituted (Liu et al., 2008) and Zn^{+2} associated (Dong et al., 2006) nanotubes. However, E22Q would specifically strengthen the cross-strand associations along the β-sheet much as the Aβ(13-21)H14A do in their association with metals (Dong, 2006). To test this hypothesis, I have determined the impacts of glutamine residues on amyloid self-assemblies and focus on the self-assembly of a series of glutamine side-chain alkyl substitutions. By defining the morphology, peptide secondary structure, peptide orientation/registry and peptide repeat distances, I have determined the factors that drive glutamine-directed peptide assembly.

Results

Impact of Q substitution on the self-assembly of N-acetyl-Aβ(16-22)

As previously reported, N-acetyl-Aβ(16-22) formed homogenous nanotubes with a diameter of 44 ± 5 nm (Figure 3-1a) and twisted fibrils with diameter of 8 to 10 nm (Figure 2-3a) at acidic and neutral pH, respectively (Lu et al., 2003; Mehta et al., 2008). To interrogate the impact of substitution, a glutamine scanning approach sequentially replaced six residues (L17, V18, F19, F20, A21, and E22) with glutamine. K16 was required for the N-terminal charge that maintained solubility and was not replaced in this study. At acidic pH, all six glutamine-substituted peptides assembled as fibrils (Figure 6-1a-f), with E22Q and L17Q giving the most homogeneous assemblies (Figure 6-1a, f).
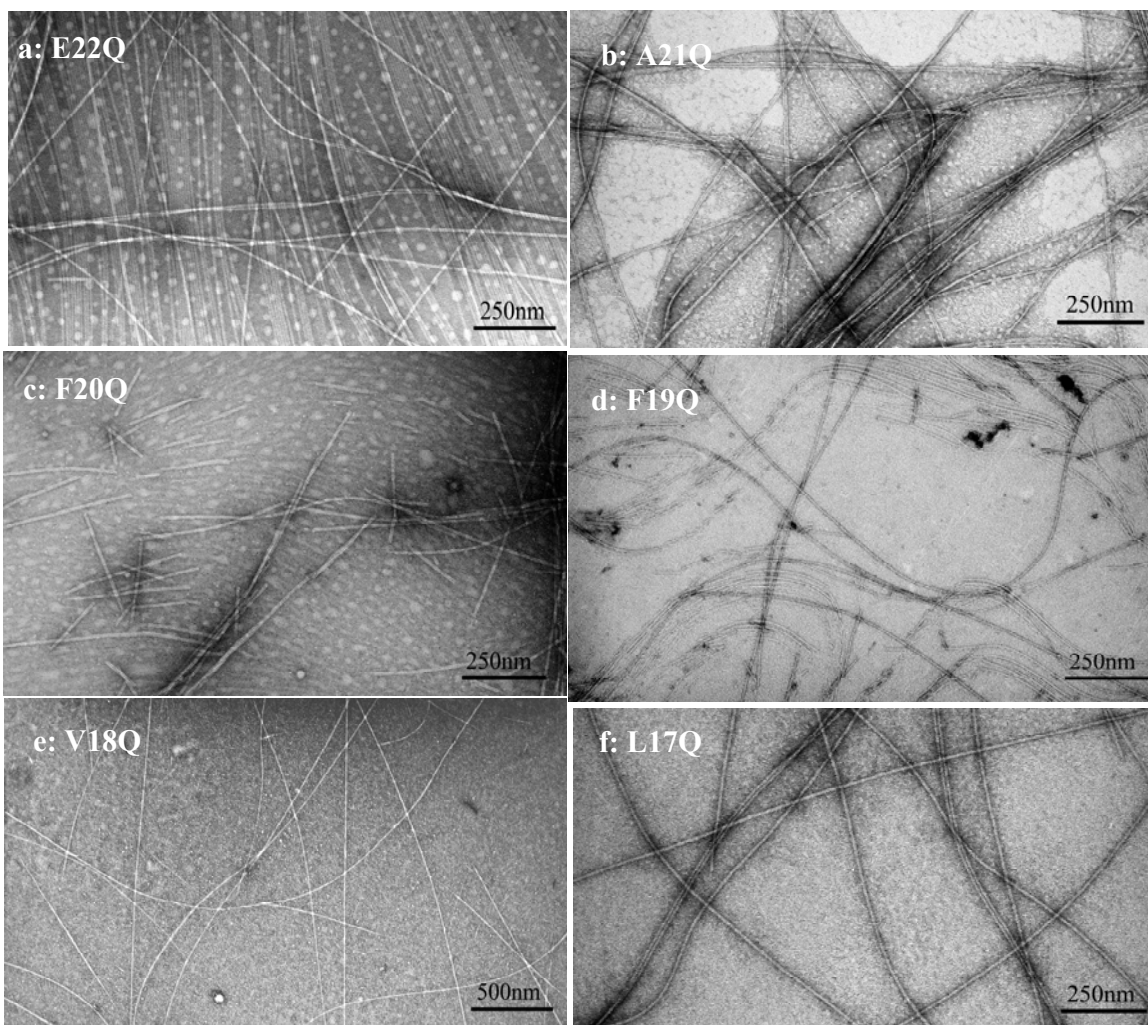
Figure 6-1. TEM images of glutamine substituents assembled at acidic pH.

Negative-staining of (a) E22Q, (b) A21Q, (c) F20Q, (d))F19Q, (e) V18Q and (f) L17Q fibrils with 2% uranyl acetate.

In each case, 2.5 mM peptide was incubated in 20% acetonitrile / water with 0.1% TFA for 1 month at room temperature prior to imaging.

The isotope-edited Infrared (IE-IR) analyses of these assemblies across the amide I region using [1-^{13}C] F19–labeled peptides are shown in Figure 6-2. E22Q and L17Q fibrils display clear ^{12}C/^{13}C band splitting and an apparent shoulder at 1676 cm^{-1}, a feature characteristic of parallel β-sheets (Chapter 2). The A21Q, F20Q, F19Q and V18Q fibrils show significantly broader bands between 1700 cm^{-1} to 1660 cm^{-1}, and a shoulder

that suggests parallel peptide arrangements, but the contributions of assembled heterogeneity within fibrils (Liang et al., 2008; Mehta et al., 2008) could not be readily determined.
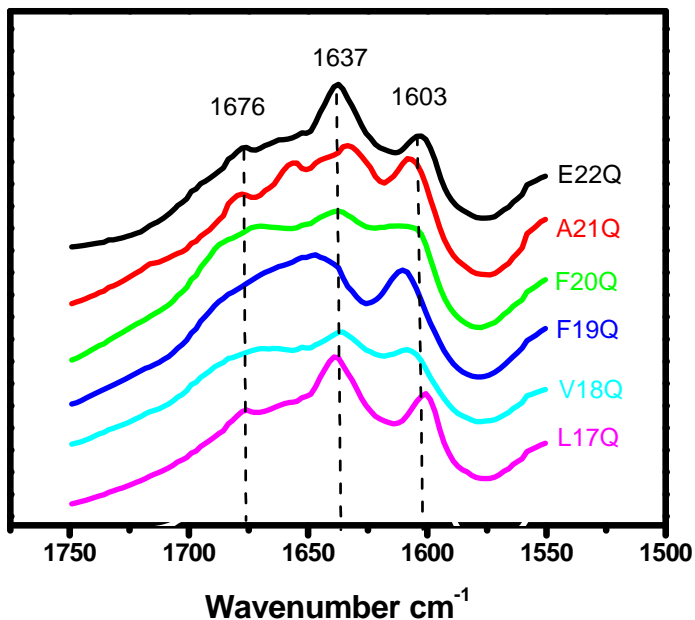

Figure 6-2. Stacked isotope-edited IR spectra amide I bands of carbonyl ^{13}C labeled fibrils at acidic pH.

Five samples: E22Q, A21Q, F20Q, V18Q and L17Q were [1-^{13}C] F19-labeled, while to compare the high frequency shoulder peak, F19Q was [1-^{13}C] L17-labeled. In the figure, the main amide I bands were specified and the sample name was presented at the right side of each line.

In each case, the matured fibrils in 20% acetonitrile / water with 0.1% TFA were pelleted, frozen and lyophilized to yield white powder, which was mixed and pressed with KBr for IR analysis.

Since both E22 and L17 are tolerant of Q substitution, the di-glutamine analog, L17QE22Q (N-acetyl-Aβ(16-22)L17QE22Q), was prepared. Interestingly, in this case the glutamines could be cross-strand paired across adjacent peptide in both antiparallel out of register and parallel in register β-sheet orientations as shown in Figure 6-3.
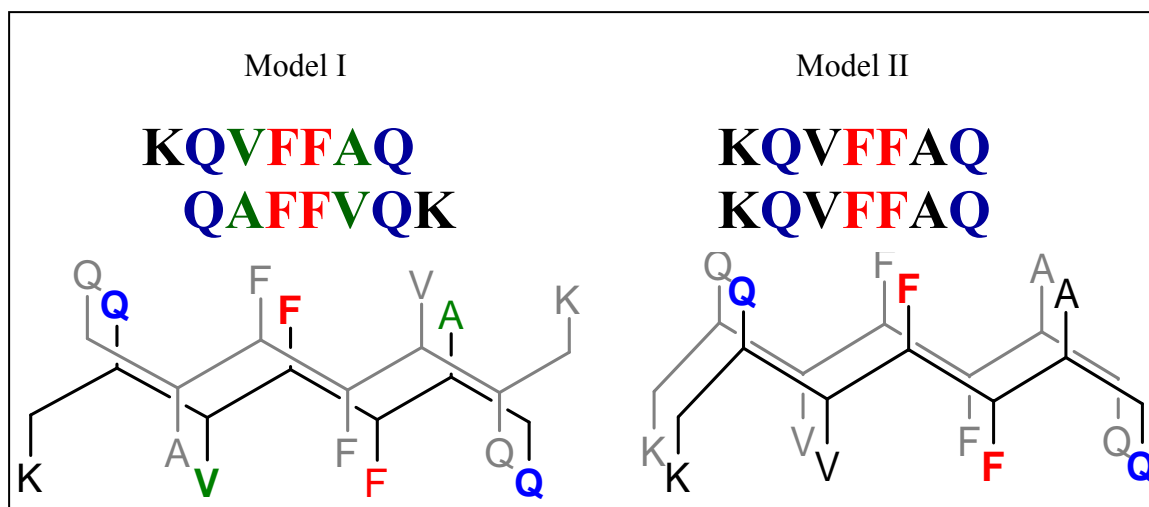
Figure 6-3. Structure model of L17QE22Q with antiparallel out-of registry (model I) and parallel in-registry (Mode II).

For both models, the two peptide strands are H-bonded along their backbones and the perspective at the bottom is the end view of each sheet. Phe19 and Phe20, which may involve aromatic interaction, were color-coded with red; Val18 and Ala21 were coded with green in model I, which might cross-strand pair with each other and Gln22 was coded with blue, which may form H-bonds with the adjacent strands.

At acidic pH, L17QE22Q self-assembled into rod-shape fibrils, 10 nm in width (Figure 6-4a, b). With its amide I major band at 1628 cm^{-1} and a high wavenumber band at 1678 cm^{-1} (Figure 6-4c), the assembly is likely to contain parallel β-sheets, same as E22Q assemblies, while the sharp band at 1653 cm^{-1} may derive from the random coil conformation. The solid state NMR experiments to confirm the peptide organization within sheets have not been completed at this point.
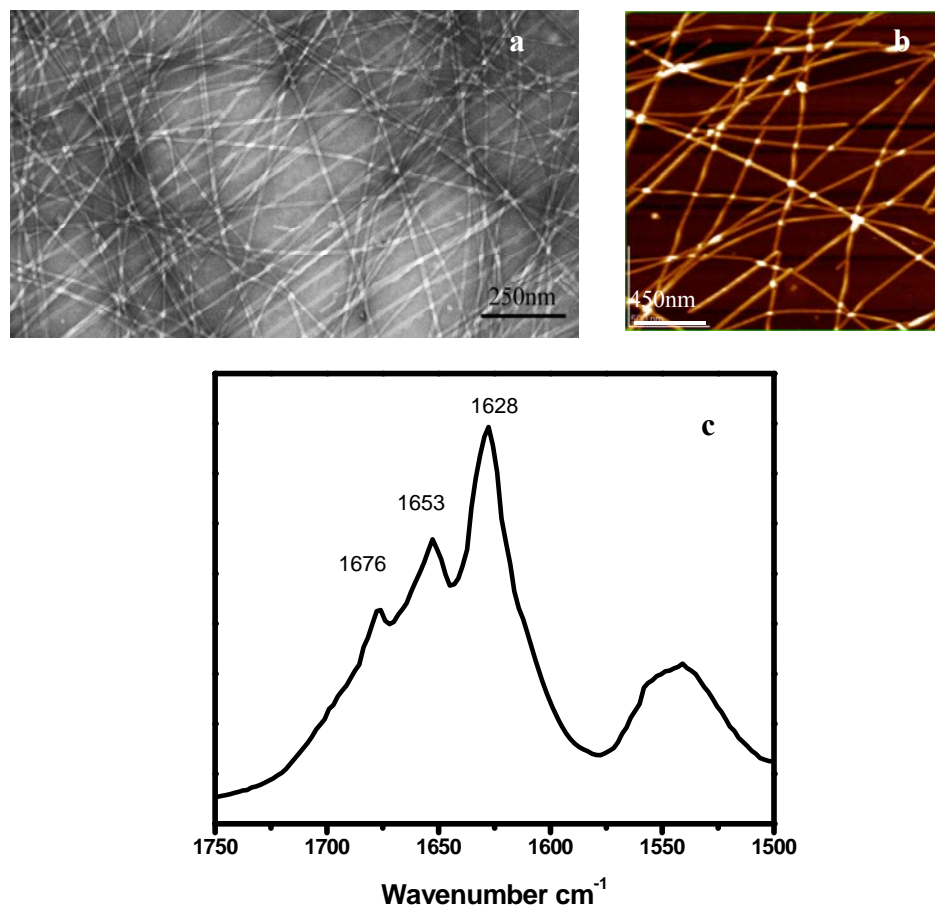
Figure 6-4. TEM/AFM images and FTIR amide I bands of L17QE22Q fibrils assembled at acidic pH.
(a) TEM image of negatively stained L17QE22Q fibrils and (b) the corresponding AFM image. The peptide was incubated in 20% acetonitrile / water with 0.1% TFA for 3 weeks to allow maturation.
(c) FT-IR amide I band of natural-riched L17QE22Q fibrils with the main bands presented. The preformed fibrils were pelleted with centrifugation and frozen, lyophilized to yield white powder for IR analysis.

The focus on position 22

The sensitivity of position 22 to substitution is nicely shown in Figure 6-5. E22A assembled as sheets, but with the same antiparallel peptide arrangement as Aβ(16-22). E22Q assembled as fibrils with parallel β-sheets, at least as evidenced by the different FT-IR amide I band spectra (chapter 2) even if assembled under slightly different conditions (Figure 6-5).
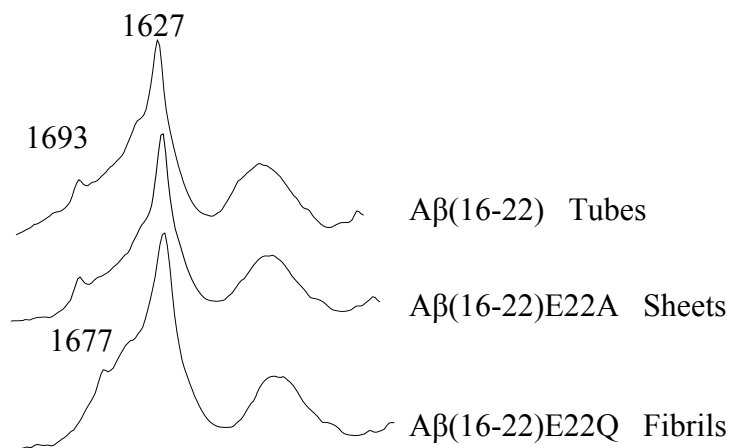
Figure 6-5. FTIR amide I spectra of the indicated N-acetyl-Aβ(16-22) analogs assembled under acidic conditions (Lu, 2005).

The peptides were assembled under acidic conditions in 40% acetonitrile / water for (N-acetyl-Aβ(16-22) and E22A, and in water for E22Q prior to analysis.

These rod-shape fibrils with diameters of 11 ± 1 nm are formed from E22Q peptide independent of pH (Figure 6-6d-f), and are flat and smooth with a unique weaven-like pattern (Figure 6-6d insertion), quite distinct from the twisted fibrils formed by N-acetyl-Aβ(16-22) (Figure 6-6c). Nevertheless, E22Q fibrils show X-ray diffraction characteristic of the cross-β pattern, Figure 6-8b, with hydrogen-bonding d-spacing of 4.7 Å, and a lamination d-spacing of 10.1 Å, slightly longer than 9.8 Å of the N-acetyl-Aβ(16-22) tubes (Figure 6-7a), indicating that glutamine does not strength the sheet-sheet interaction.
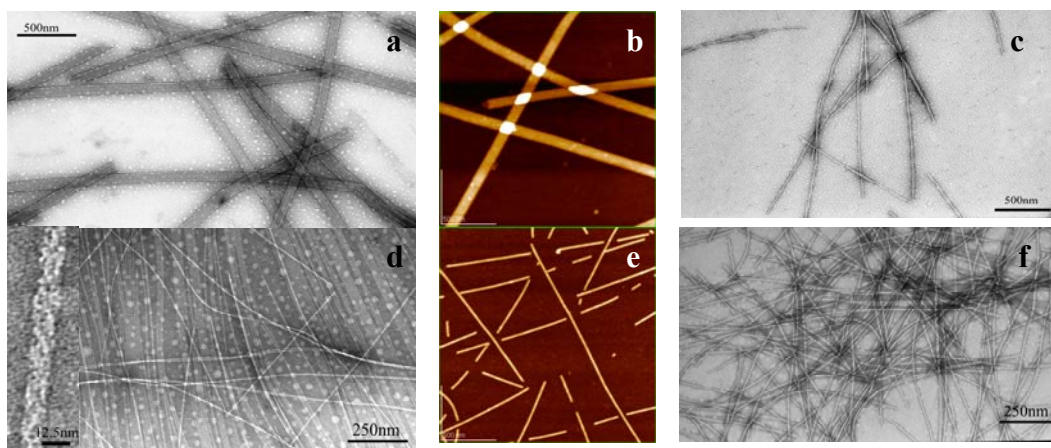
Figure 6-6. Electron micrographs of N-acetyl-Aβ(16-22) and E22Q assemblies at acidic and neutral pHs.

TEM images of negatively stained (a) N-acetyl-Aβ(16-22) nanotubes and (d) E22Q fibrils assembled at acidic pH, and (c) N-acetyl-Aβ(16-22) fibrils and (f) E22Q fibrils assembled at neutral pH.

AFM images of dry (b) N-acetyl-Aβ(16-22) nanotubes and (e) E22Q fibrils assembled under acidic conditions.

In each case, the peptide was incubated in 20% acetonitrile / water with either 0.1%TFA or in 15 mM pH 6 MES buffer at room temperature for 3 weeks.
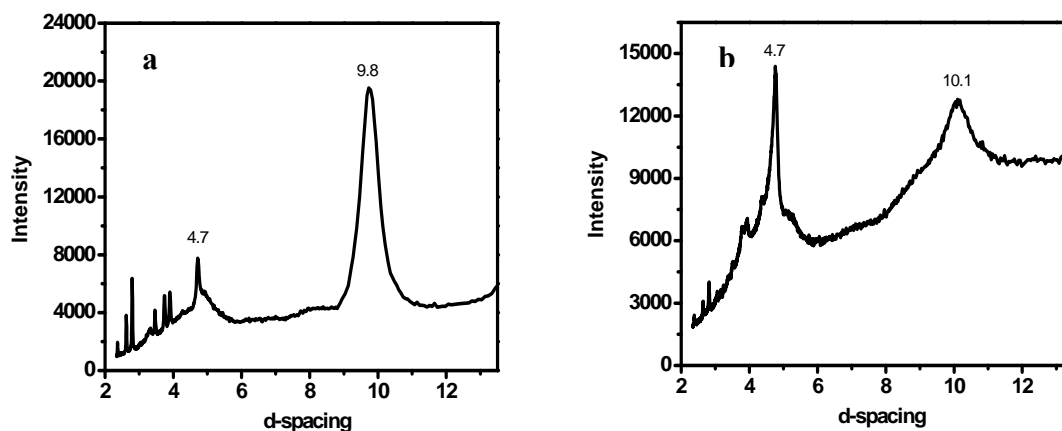
Figure 6-7. X-ray diffraction of (a) N-acetyl-Aβ(16-22) tubes and (b) E22Q fibrils at acidic pH.

The preformed tubes and fibrils were bundled with sulfate with ratio of peptide to sulfate 1 to 10, followed by pelleting, freezing and lyophilization to yield white powder for x-ray analysis.

CD and FTIR analysis were also typical to characterize the peptide secondary structure within assemblies. As shown in Figure 6-8, N-acetyl-Aβ(16-22) tubes and E22Q

fibrils have the same amide I bands at 1629 ± 1 cm^{-1}, as well as negative ellipticity at around 215 nm with the very intense and weak intensity, respectively. The one significant difference was the high wavenumber shoulder band at 1678 cm^{-1} in E22Q fibrils, indicating of parallel β-sheets (Chapter 2), as opposed to the 1693 cm^{-1} shoulder for the tubes, previously assigned to antiparallel β-sheets (Figure 6-8b) (Mehta et al., 2008).
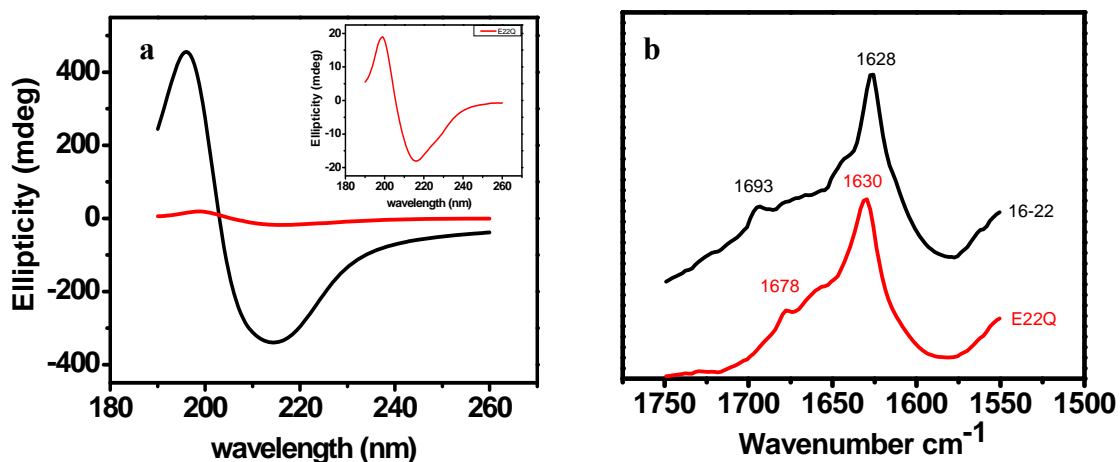

Figure 6-8. CD and FTIR analyses of N-acetyl-Aβ(16-22) tubes and E22Q fibrils at acidic pH.
(a) CD spectra of N-acetyl-Aβ(16-22) tubes (black curve) and E22Q fibrils (red curve, with the enlarged figure inserted) under acidic conditions. The matured fibrils were loaded in 0.1 mm path length quartz curvette and scanned three times between 260 nm to 190 nm.
(b) Stacked FTIR amide I bands of N-acetyl-Aβ(16-22) tubes and E22Q fibrils sampled from assemblies prepared under acidic conditions. The major bands were specified, with the sample name presented at the right side of each line.

To confirm this assignment and to evaluate the peptide registry, the amide I band splitting magnitudes were obtained from isotope-edited IR and compared with three known references (Figure 6-9): N-acetyl-Aβ(16-22) tubes containing antiparallel one-residue out-of register sheets, N-acetyl-Aβ(16-22) fibrils with antiparallel in-register sheets, and N-isobutyl-Aβ(16-22) fibrils with parallel in-registry sheets. The spectra for [1-^{13}C] L17-, [1-^{13}C] F19- and [1-^{13}C] F20-labeled E22Q fibrils are shown in Figure 6-9a,

and the band splitting magnitudes of 27 cm^{-1}, 36 cm^{-1} and 37 cm^{-1}, respectively are plotted in Figure 6-9b. As seen in Chapters 2-5, these values have proven to be a valuable indicator of the peptide arrangements within β-sheets and indeed the data for E22Q overlaps perfectly with the isotope-labeled N-isobutyl-Aβ(16-22) fibrils, suggesting E22Q adopts parallel in-register sheets within the fibrils.
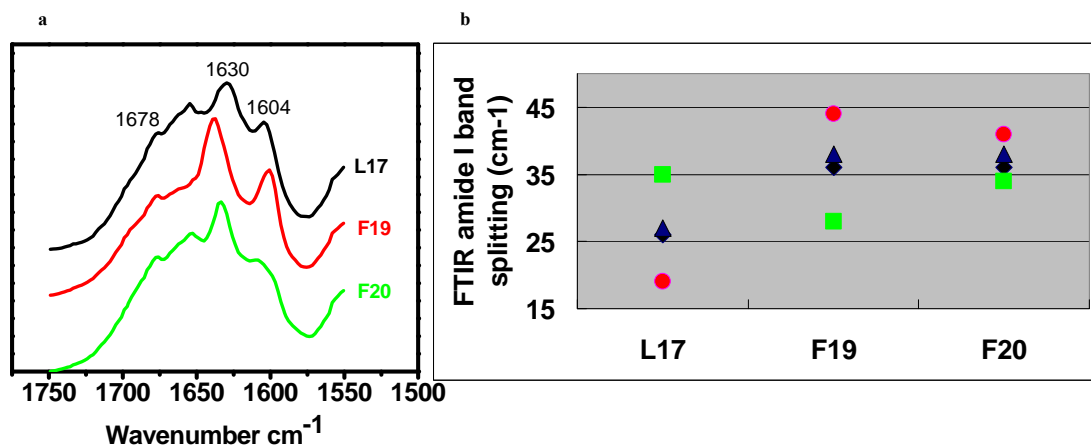
Figure 6-9. Isotope-edited IR spectra of E22Q fibrils and the band splitting magnitude comparison with the references.

(a) Stacked FTIR amide I band of the indicated single [1-^{13}C]-labeled E22Q at residues L17, F19 and F20 positions.

(b) The plot of the amide I band splitting magnitude versus the labeled residues in E22Q fibrils (black diamond), N-acetyl-Aβ(16-22) antiparallel out-of register sheet of the nanotubes (red circle), N-acetyl-Aβ(16-22) antiparallel in-register sheets of the fibrils (green square), and N-isobutyl-Aβ(16-22) parallel in-register sheets of the fibrils (blue triangle).

Analysis of the specific E22Q contribution to peptide self-assembly

Among all the tested N-acetyl-Aβ(16-22) 22 position substitutions, only glutamine and asparagine (Lu, 2005) now appear to switch the assembly to parallel peptide β-sheets. As is consistent with our initial hypothesis, this structural change may arise from H-bonding cross-strand pairing interactions stabilizing the sheets and accounting for the formation of fibrils and explaining the propensity for glutamine / asparagine-rich peptides

to self-assemble as fibers (Bousset et al., 2008; Perutz et al., 2002). We proposed that the hydrogen-bonding capability of glutamine side-chain could be gradually reduced by substitution of amide protons with one or two methyl groups, necessitating preparation of E22QNHCH$_3$ and E22QN(CH$_3$)$_2$ (Figure 6-10).
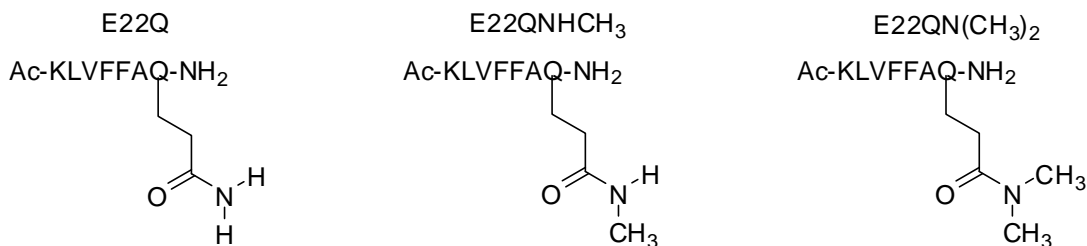
Figure 6-10. Three peptides with chemical structure of glutamine analogs specified.

E22Q fibrils are flat under both acidic and neutral conditions (Figure 6-11a, d), while under the same incubation conditions, E22QNHCH$_3$ formed larger fibrils with diameter ranging from 7 nm to 27 nm (Figure 6-11b, e and Table 6-1) and average height of 17 $\pm$ 1 nm (Figure 6-12). TEM established that E22QNHCH$_3$ fibrils are flat and fibril monomer associates to form dimmer, trimer, tetramer and pentamer (Table 6-1). In contrast, under both incubation conditions, the E22QN(CH$_3$)$_2$ peptides formed tubes and ribbons (Figure 6-11c, f), most similar in appearance to N-acetyl-Aβ(16-22) assemblies at acidic pH (Lu et al., 2003).
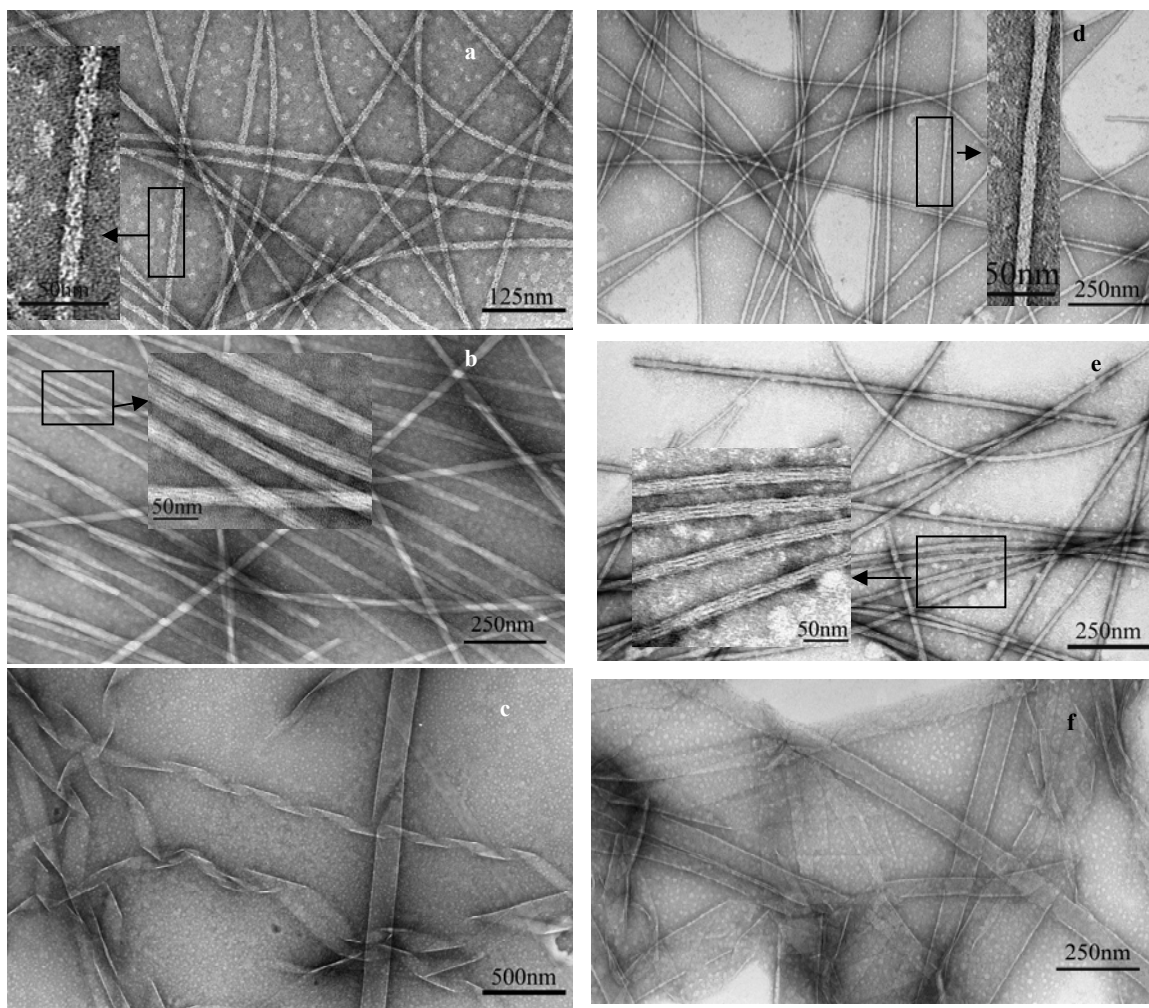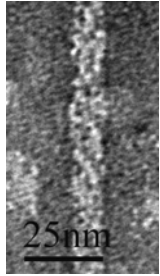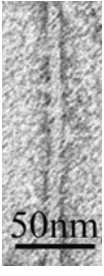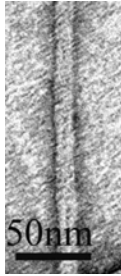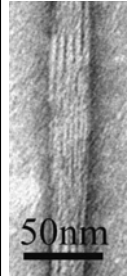
Figure 6-11. TEM images of side-chain substituted-glutamine analogs at acidic and neutral pHs.
Negatively stained assemblies formed at acidic pH: (a) E22Q fibrils, (b) E22QNHCH$_3$ fibrils and (c) E22QN(CH$_3$)$_2$ tubes and sheets, assemblies formed at neutral pH: (d) E22Q fibrils, (e) E22QNHCH$_3$ fibrils and (f) E22QN(CH$_3$)$_2$ tubes and sheets. The zoom in part is specified with black box.

Table 6-1. Estimated fibril width based on the high resolution TEM images.

peptides	E22Q	E22QNHCH$_3$				
Aggregation state	homogenous	monomer	dimer	trimer	tetramer	pentamer
	25nm	50nm	50nm	50nm	50nm	50nm
Width (nm)	12 ± 1	7 ± 1	12 ± 1	17 ± 1	22 ± 1	27 ± 1

Image information
Ra = 2.39 nm   RMS = 3.58 nm
Rz = 19.9 nm   P-V = 20.6 nm
S = 1.03 um²   S ratio = 1.03

		1	2	3	4
Ra	[nm]	3.76	4.35	5.18	5.09
Rz	[nm]	9.31	8.78	9.06	10.4
RMS	[nm]	4.47	4.91	6.03	5.91
P-V	[nm]	12.2	12.3	15.8	15.6
Length	[um]	0.180	0.161	0.174	0.170

AFM Slope   Ref: -3.100V.
Size: 1.00 x 1.00um.   Bias: 0.000V.
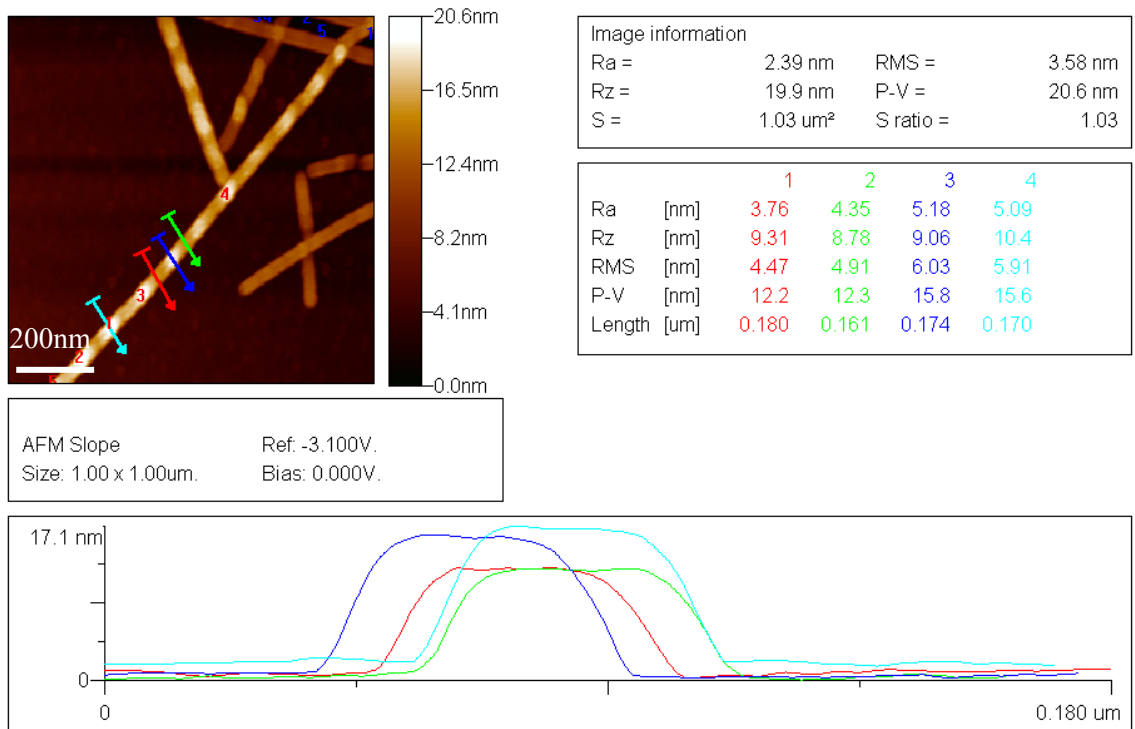
Figure 6-12. AFM image of E22QNHCH$_3$ fibrils.

The matured fibrils (20 μL) in 20% acetonitrile / water with 0.1% TFA was applied on freshly cleaned silica chip, followed by water rinsing to get rid of excess sample. The overnight dried sample in desiccator was viewed on AFM.
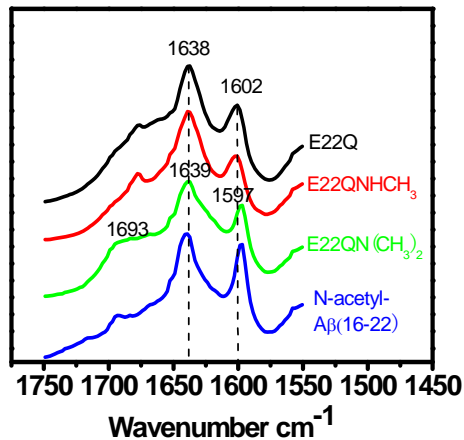
Figure 6-13. Stacked isotope-edited IR spectra of side-chain substituted-glutamine analogs. Amide I region of the FT-IR spectra of $[1-^{13}C]$ F19-labeled E22Q, E22QNHCH$_3$, E22QN(CH$_3$)$_2$ peptides and the control N-acetyl-Aβ(16-22) tubes assembled under acidic conditions.

The isotope-edited IR spectra obtained with $[1-^{13}C]$ F19-labled peptides assemblies again show virtually identical spectra for E22Q and E22QNHCH$_3$ fibrils, with ^{12}C and ^{13}C bands at 1638 cm^{-1} and 1602 cm^{-1}, respectively, and a high wavenumber band at 1678 cm^{-1}, most consistent with parallel β-sheets (Figure 6-13). The ^{12}C and ^{13}C components of E22QN(CH$_3$)$_2$ tubes are at 1639 cm^{-1} and 1597 cm^{-1}, respectively, along with antiparallel diagnostic band of 1692 cm^{-1}, indicative of antiparallel one residue out-of register assembly seen for the N-acetyl-Aβ(16-22) nanotubes (Mehta et al., 2008). Therefore, N, N-dimethyl substitution on 22Q side chain completely removes the impact of the side chain on assembly, suggesting the role of glutamine side chain H-bonding for the assembly morphology and peptide arrangements.

Discussion

In neurodegenerative diseases, glutamine-rich or asparagine-rich peptide segments appear critical for increasing the propensity of self-assembly. Accordingly, tremendous effort has focused on understanding the specific role that these side chains may play in amyloid assembly. Even though glutamine side-chain H-bonding interactions present the obvious energetic contributor (Bevivino and Loll, 2001; Perutz et al., 1994; Perutz et al., 1993), no solid experimental data have been reported to date, and in the existing structural studies, and the orientation of the side chains does not present a consistent pattern (Bevivino and Loll, 2001; Perutz et al., 1993).

In this chapter, we have investigated a mono-glutamine substitution in Aβ-peptide and provide experimentally evidence to support that glutamine side chain hydrogen-bonding interaction drives β-sheet switching from antiparallel one residue out-of registry to parallel in-registry. Glutamine scanning experiments have established that this peptide arrangement switch is substitution-position and substitution residue number-independent, suggesting that this is the general role for glutamine-substitutions. Moreover, at least one proton at glutamine side-chain amide (E22Q and E22QNHCH$_3$) is required for this peptide orientation and registry alteration, regardless of pH, and complete removal of glutamine side chain protons totally inhibits parallel β-sheet formation. Glutamine and asparagine have the strong potential to form H-bond with each other due to the H-bond donor and acceptor on their side chain amide, and the parallel in-register β-sheet is optimal for glutamine to form intra-sheet cross-strand H-bonds along a sheet with the peptide repeating distance of 4.7 Å, consistent with parallel β-sheets formed from several short glutamine/asparagine-contained peptides (Table 6-2) (Lu, 2005; Sawaya et al.,

2007). While due to the distribution of glutamine residue at one face of a sheet and the presence of lysine charge at N-terminus, cross-sheet H-bonding interaction between glutamines is impossible because this organization will place the positively-charged lysine residue together, which is energetically unfavorable. This suggests that glutamine residues mainly contribute to the intra-sheet interaction, consistent with fibril formation with limited laminates.

Table 6-2. The peptides with parallel peptide arrangements within β-sheets characterized by X-ray (Sawaya et al., 2007) or isotope-edited IR (Dong, 2006; Lu, 2005). Glutamine and asparagine are highlighted with red color.

source	Peptide segment
Sup35	GNNQQNY(Sawaya et al., 2007)
Sup35	NNQQNY(Sawaya et al., 2007)
Tau	VQIVYK(Sawaya et al., 2007) (Plumley and Dannenberg, 2010)
Sup35	NNQQ(Sawaya et al., 2007)
Prion protein	SNQNNF(Sawaya et al., 2007)
Amyloid β	KLVFFAN (Lu, 2005)
Amyloid β	HAQKLVFFA (Dong, 2006)

In addition, the glutamine side-chain hydrogen-bonding interaction along sheets may also account for the formation of flat fibrils. In current study and previous studies, we found that some glutamine and asparagine-contained peptides form flat fibrils, instead of typical twisted fibrils such as Aβ(16-22) (Mehta et al., 2008) and Aβ(10-35) (Benzinger et al., 2000; Burkoth et al., 2000) fibrils. According to the twisted fibril model, the single sheet is twisted due to the chirality of the amino acids (Burkoth et al., 2000; Mehta et al., 2008). Incorporation of proline in peptide strands has even been found to induce the formation of non-twisting sheets by influencing the twisting capability of single β-sheet (Lamm et al., 2005). Moreover, the molecular orbital studies suggest that glutamine side chain H-bonds along sheets is short and cooperative, which could force

the peptide backbone to be relatively flat (Figure 6-14) (Plumley and Dannenberg, 2010). Therefore, we conclude that the cross-strand glutamine side chain H-bonding interaction results in the less twisting sheet, which stacks to form the relatively flat fibrils. While E22QNHCH$_3$, substitution of one glutamine side chain amide proton with methyl group, has the compromised side chain H-bonding capability, hydrophobicity and steric hindrance. The balance of these interactions may decrease the packing density within sheets and between sheets, but the exposure of the side chain -NHCH$_3$ at the fibril surface may increase the chance for single fibril to associate to form fibril dimmer, trimer, tetramer or higher degree of aggregates.
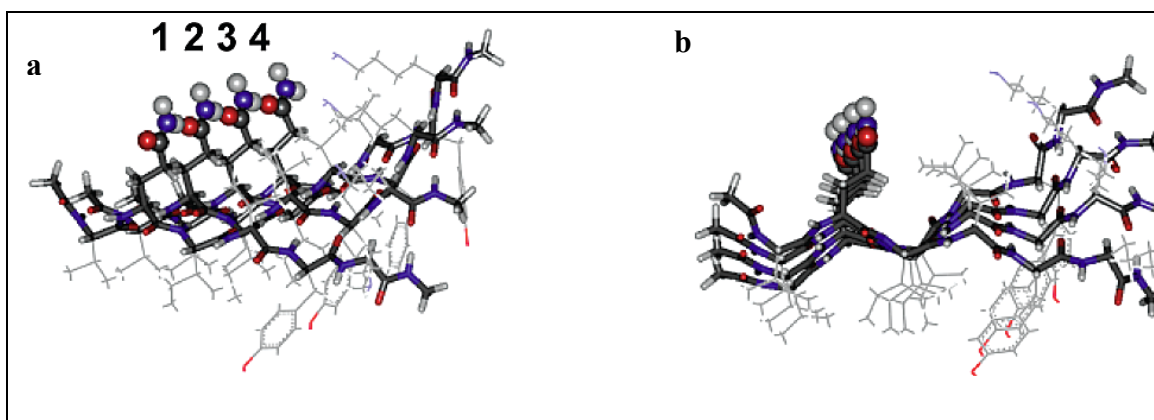
Figure 6-14. Parallel β-sheets of four (acetyl-VQIVYK-NHCH3) strands.
(a) Glutamine side chain amides form H-bonds along sheet; (b) the side view of this β-sheet and glutamine side chain amides are aligned well to lock the peptide N-terminal peptide backbone conformation. In both figures, the glutamine amide, peptide backbone and the rest residue side chain are shown with balls and sticks, tubes and wireframes, respectively (Plumley and Dannenberg, 2010). Copyright permission has been requested.

Since the stacking of these parallel in-registry β-sheets within fibril is uncertain, the different sheet-sheet stacking modes (parallel/antiparallel, in-registry or out-of registry) are possible. However, considering the distortion of individual β-sheet by glutamine side chain H-bonds, hydrophobic packing of the Phe dyads is required, due to its capability to

compensate the energetic penalty from β-sheets distortion. In addition, the specific gold binding on E22Q fibril surface (data not shown) indicates the exposure of lysine in aqueous phase. Therefore, six models have been proposed (Figure 6-15).

To clearly illustrate these models, the residues at one face of the sheet are highlighted with red color and another one with black color. In Model I, the same face of the sheets stacks to form two different interfaces (black/black and red/red), while orientation of the sheets could be antiparallel (Figure 6-15 Model Ia) or parallel (Figure 6-15 Model Ib). Clearly, the antiparallel sheet orientation in Model Ia is favorable because this sheet arrangement not only separates the lysine charge, but also let glutamine and lysine be close to form cross-sheet H-bonds, which may stabilize the parallel β-sheets. However, parallel sheet orientation in Model Ib forces lysines to be close to destabilize the sheet-sheet interaction. In Model II and III, the different face of sheets stacks to form uniform interface (black/red). In Model II, the sheets stack with antiparallel orientation, which separates lysine charge with either in-registry or out-of registry sheet-sheet stacking. In Model III, the parallel in-registry sheet orientation places all lysine residues at one side (Model IIIe), which may destabilize the assembly by charge repulsion; while the parallel out-of sheet stacking relieves this repulsion in some extent, but this organization loses the Phe-Phe aromatic interaction in the top sheet-sheet interface, which may destabilize the sheet stacking. Overall, there are three possible models (Model Ia, Model IIc, IId) left. According to the relative different distance between lysine and glutamine, these three models could be further differentiated by changing the length of lysine side chain (chapter 2). If the cross-sheet H-bonding interaction is critical for this parallel β-sheet fibril formation (chapter 2), shortening the

lysine side chain may have significant impact on Model Ia, but have little or no impact on Model II. To precisely define the sheet-stacking orientation, solid-state NMR experiments are necessary and ongoing. The following two isotope-labeling schemes have been proposed: 1) the information from the [^{15}N] Ala21 to [5-^{13}C] Leu17 could differentiate Model Ia, IIa from IIb, 2) the one from [3-^{13}C] Ala21 to [6-^{15}N] Gln22 could differentiate Model Ia and IIa.

According to the parallel β-sheet fibrils derived from short peptides, such as N-X-Aβ(16-22) (X = propyl to palmityl) (chapter 2) or the crystal structure of short glutamine-containing peptide fibril/crystals (Sawaya et al., 2007), we predict that the Model Ia is most reasonable for E22Q fibrils, because: 1) antiparallel sheet-sheet stacking in Model Ia could separate lysines to minimize the charge repulsion; 2) the hydrophobic residues (Red face) could interact with each other to form hydrophobic zipper, which could stabilize the laminates (Sawaya et al., 2007); 3) the proximity of the hydrophilic interfaces (black face) could lead to the hydrogen-bonding interaction across-sheets between C-glutamine and N-lysine, which could not only stabilize the sheet-sheet interaction, but also reduce the charge repulsion between lysines (Chapter 2).
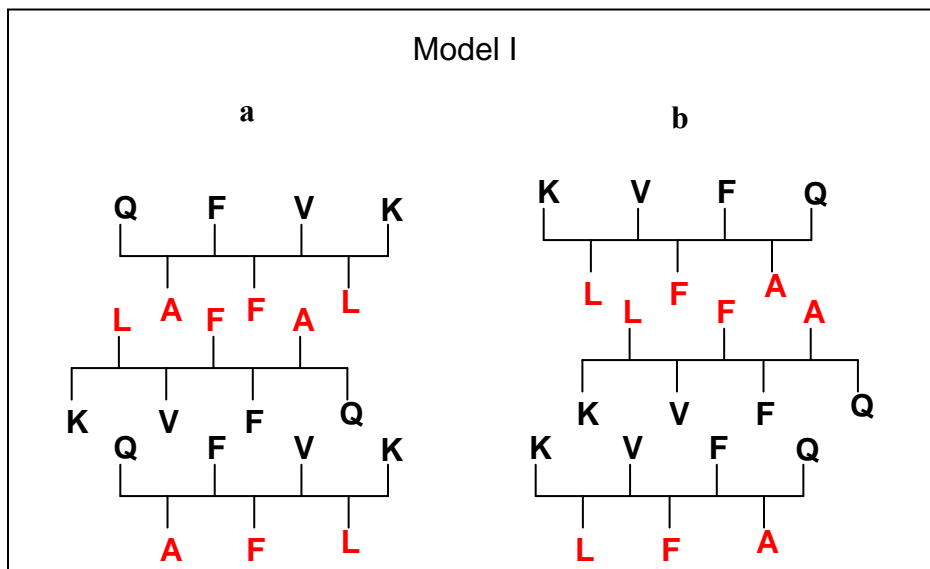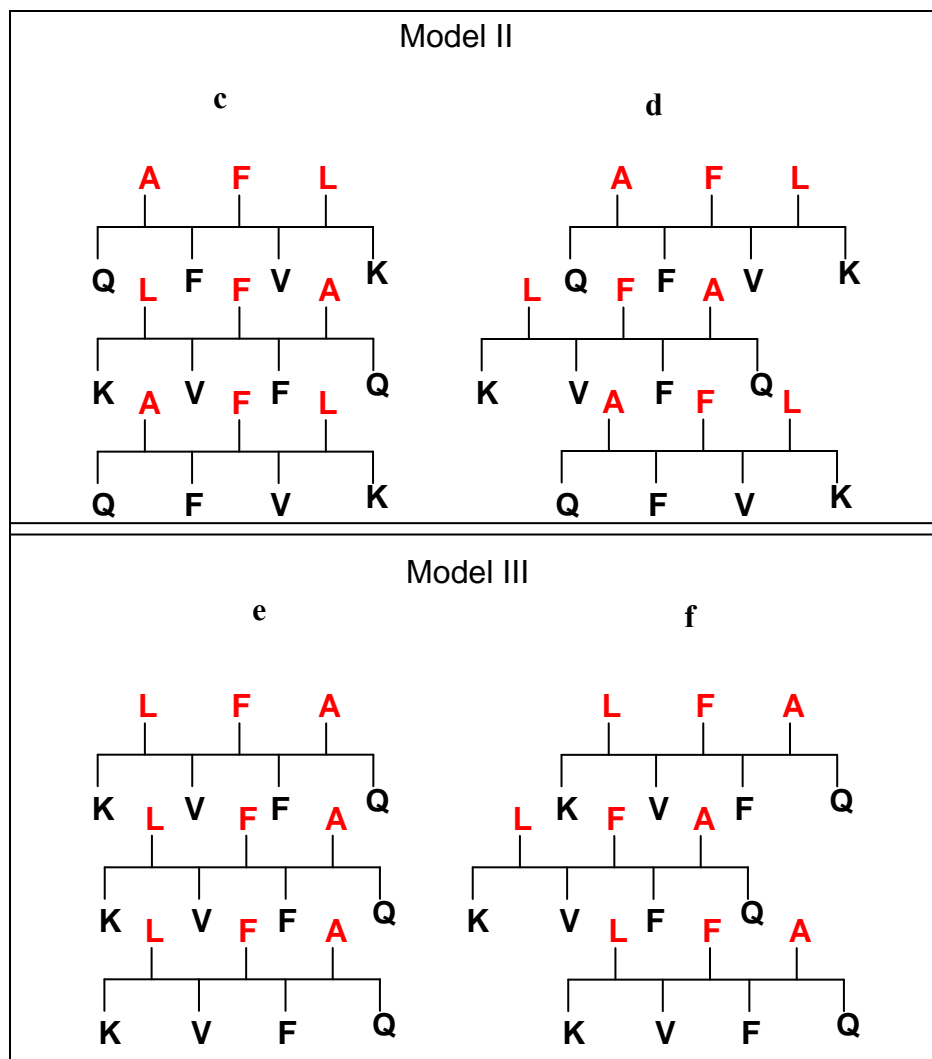
Figure 6-15. Six possible parallel β-sheet stacking models for E22Q fibrils.

Model I with same sheet face interaction: (a) antiparallel sheets stacking; (b) parallel sheets stacking;

Model II with antiparallel different sheet face stacking: (c) in-register sheets stacking; (d) out-of register sheets stacking.

Model III with parallel different sheet face stacking: (e) in-register sheets stacking; (f) out-of register sheets stacking.

To clarify sheet faces, the residues at one face are highlighted with red color and another one is black color. In all the models, the center peptide strand orientation keeps same.

The elucidation of the orientation of the glutamine side chains in amyloid reveals a specific energetic constraint for assemblies in neurodegenerative diseases, for a constraint that can now be used in the design of protein self-assemblies. This cross-strand pairing

interaction modulates parallel β-sheet formation, and may now be used in the rational design of new nanomaterials.

Materials and Methods

Synthesis of glutamine and glutamate analogs

**Amidation of Glutamate side chain carboxylic acid**: N-Fmoc-Glutamic acid t-Butyl ester (Anaspec, Inc.) (1equiv.) was dissolved in dry CH_2Cl_2 (treated with freshly microwave-dried molecular sieve overnight) and N,N-diisopropylethylamine (DIPEA, 2.6 equiv.), 2-(1H-Benzotriazol-1-yl)-1,1,3,3-TetramethylUronium hexafluorophosphate (HBTU, 1equiv.), and methylamine hydrochloride or dimethylamine hydrochloride (1.1 equiv.) were added sequentially. The reaction mixture was stirred under ambient temperature for 2 hr and monitored by thin layer chromatography (TLC) (hexane : ethyl acetate 1 : 1 (v/v), R_f = 0.25 and 0.3 for monomethyl and dimethyl substituents, respectively). After the reaction completed (starting material no longer observed on TLC plate), the reaction mixture was concentrated in vacuo and the residue purified with flash chromatography (hexane : ethylacetate 1 : 1 (v/v)) to give the amidation products as colorless oils.

Hydrolysis of *t*-Butyl esters: The above amidation product (0.3 mmol, 1 equiv.) was dissolved in dichloromethane (9.6 mmol, 32 equiv.). Then TFA (0.3 mL, 3.9 mmol, 13 equiv.) and triethylsilane (0.12mL, 0.75 mmol, 2.5 equiv.) were added to the solution. The reaction mixture was stirred until the starting material was completely consumed (~1 hr) as monitored by TLC (ethyl acetate, R_f = 0.25), the solvent was removed in vacuo. The resulting residue was triturated with cold ether and the white precipitate was

collected by centrifugation (16,100 xg) for 5 min and the pellet was air-dried in hood, followed by placing on the lyophilizer overnight for the peptide solid-phase synthesis without further purification.

Fmoc-Gln(NHMe)-O*t*Bu
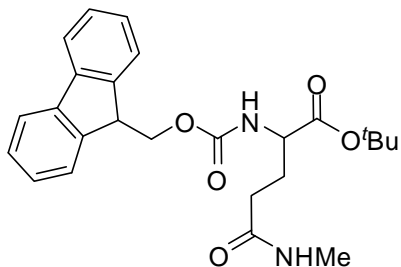
^{1}H NMR (400 MHz, CDCl$_3$) δ 7.74 (d, *J*=7.6 Hz, 2H), 7.58 (dd, *J*=6.8, 4.8 Hz, 2H), 7.37 (t, *J*= 7.6, 7.2 Hz, 2H), 7.29 (ddd, *J*= 7.2, 1.6 Hz, 2H), 6.14 (s, 1H), 5.72 (d, *J*=6.0 Hz, 1H), 4.36 (dd, *J*= 7.2, 2.4 Hz, 2H), 4.19 (dd, *J*=7.2, 6.8 Hz, 2H), 2.77 (d, *J*= 4.4 Hz, 3H), 2.44 (m, 2H), 2.21 (m, 3H), 1.91 (m, 1H), 1.44 (s, 9H). MS (ESI) m/z 439.6 (M+H)$^+$

Fmoc-Gln(NHMe)-OH
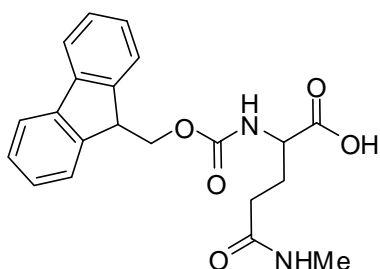
^{1}H NMR (400 MHz, CDCl$_3$) δ 7.77 (d, *J*=7.2 Hz, 2H), 7.60 (t, *J*= 7.2, 6.4 Hz, 2H), 7.41 (t, *J*= 7.6 Hz, 2H), 7.33 (dd, *J*= 7.6, 7.2 Hz, 2H), 6.16 (m, 1H), 6.05 (d, *J*= 6.0 Hz, 1H), 4.38 (m, 3H), 4.23 (t, *J*= 6.8 Hz, 1H), 2.87 (d, *J*= 4.4 Hz, 3H), 2.60-2.40 (m, 3H), 2.20 (m, 1H), 2.06 (s, 1H, OH). MS (ESI) m/z 383.5 (M+H)$^+$

Fmoc-Gln(NMe₂)-OtBu

^{1}H NMR (400 MHz, CDCl$_3$) δ 7.74 (d, J=7.6 Hz, 2H), 7.59 (dd, J= 8.0, 7.6 Hz, 2H), 7.37 (dd, J= 7.6, 7.2 Hz, 2H), 7.28 (dd, J= 7.6, 7.6 Hz, 2H), 5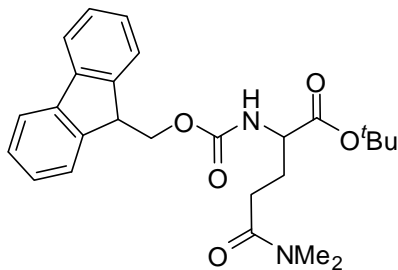.84 (d, J=8.0 Hz, 1H), 4.34 (m, 2H), 4.21 (m, 2H), 2.94 (s, 3H), 2.92 (s, 3H), 2.50-2.28 (m, 2H), 2.18 (m, 1H), 2.02 (m, 1H), 1.45 (s, 9H). MS (ESI) m/z 452.6 (M+H)$^+$

Fmoc-Gln(NMe₂)-OH
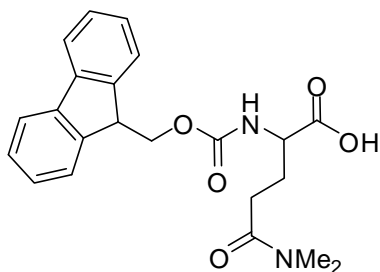
^{1}H NMR (400 MHz, CDCl$_3$) δ 9.20 (brs, 1H, OH), 7.77 (d, J=7.2 Hz, 2H), 7.60 (dd, J= 7.2, 6.4 Hz, 2H), 7.41 (t, J= 7.6 Hz, 2H), 7.32 (dd, J= 8.0, 7.2 Hz, 2H), 6.16 (d, J= 6.0 Hz, 1H), 4.38 (m, 2H), 4.27 (m, 1H), 4.22 (dd, J= 7.6, 5.6 Hz, 1H), 3.04 (s, 3H), 3.00 (s, 3H), 2.88 (m, 1H), 2.54 (ddd, J= 16.4, 6.0 Hz, 1H), 2.29 (m, 1H), 2.04 (m, 1H). MS (ESI) m/z 397.6 (M+H)$^+$

References

Benzinger, T. L., Gregory, D. M., Burkoth, T. S., Miller-Auer, H., Lynn, D. G., Botto, R. E., and Meredith, S. C. (2000). Two-dimensional structure of beta-amyloid(10-35) fibrils. Biochemistry *39*, 3491-3499.

Bevivino, A. E., and Loll, P. J. (2001). An expanded glutamine repeat destabilizes native ataxin-3 structure and mediates formation of parallel beta -fibrils. Proc Natl Acad Sci USA *98*, 11955-11960.

Bousset, L., Savistchenko, J., and Melki, R. (2008). Assembly of the asparagine- and glutamine-rich yeast prions into protein fibrils. Curr Alzheimer Res *5*, 251-259.

Burkoth, T. S., Benzinger, T. L. S., Urban, V., Morgan, D. M., Gregory, D. M., Thiyagarajan, P., Botto, R. E., Meredith, S. C., and Lynn, D. G. (2000). Structure of the beta-amyloid((10-35)) fibril. J Am Chem Soc *122*, 7883-7889.

Clements, A., Walsh, D. M., Williams, C. H., and Allsop, D. (1993). Effects of the mutations Glu22 to Gln and Ala21 to Gly on the aggregation of a synthetic fragment of the Alzheimer's amyloid beta/A4 peptide. Neurosci Lett *161*, 17-20.

Davis, J., and VanNostrand, W. E. (1996). Enhanced pathologic properties of Dutch-type mutant amyloid beta-protein. Proc Natl Acad Sci USA *93*, 2996-3000.

Dong, J. (2006) Metal Ions: a Probe of Amyloid Fibril Formation, Ph.D. dissertation, Emory University, Atlanta, GA, USA.

Dong, J., Shokes, J. E., Scott, R. A., and Lynn, D. G. (2006). Modulating amyloid self-assembly and fibril morphology with Zn(II). J Am Chem Soc *128*, 3540-3542.

Kvam, E., Nannenga, B. L., Wang, M. S., Jia, Z., Sierks, M. R., and Messer, A. (2009). Conformational targeting of fibrillar polyglutamine proteins in live cells escalates aggregation and cytotoxicity. PloS one *4*, e5727.

Lamm, M. S., Rajagopal, K., Schneider, J. P., and Pochan, D. J. (2005). Laminated morphology of nontwisting beta-sheet fibrils constructed via peptide self-assembly. J Am Chem Soc *127*, 16692-16700.

Liang, Y., Pingali, S. V., Jogalekar, A. S., Snyder, J. P., Thiyagarajan, P., and Lynn, D. G. (2008). Cross-strand pairing and amyloid assembly. Biochemistry *47*, 10018-10026.

Liu, P., Ni, R., Mehta, A. K., Childers, W. S., Lakdawala, A., Pingali, S. V., Thiyagarajan, P., and Lynn, D. G. (2008). Nucleobase-directed amyloid nanotube assembly. J Am Chem Soc *130*, 16867-16869.

Lu, K. (2005) Discovery of Diverse Peptide Nanotube Architecture from the Self-assembly of Designed Amyloid Cassettes, Ph.D. Thesis, Emory University, Atlanta, GA, USA.

Lu, K., Jacob, J., Thiyagarajan, P., Conticello, V. P., and Lynn, D. G. (2003). Exploiting amyloid fibril lamination for nanotube self-assembly. J Am Chem Soc *125*, 6391-6393.

Mehta, A. K., Lu, K., Childers, W. S., Liang, Y., Dublin, S. N., Dong, J., Snyder, J. P., Pingali, S. V., Thiyagarajan, P., and Lynn, D. G. (2008). Facial symmetry in protein self-assembly. J Am Chem Soc *130*, 9829-9835.

Perutz, M. F. (1999a). Glutamine repeats and neurodegenerative diseases. Brain Res Bull *50*, 467.

Perutz, M. F. (1999b). Glutamine repeats and neurodegenerative diseases: molecular aspects. Trends Biochem Sci *24*, 58-63.

Perutz, M. F., Johnson, T., Suzuki, M., and Finch, J. T. (1994). Glutamine Repeats as Polar Zippers - Their Possible Role in Inherited Neurodegenerative Diseases. P Natl Acad Sci USA *91*, 5355-5358.

Perutz, M. F., Pope, B. J., Owen, D., Wanker, E. E., and Scherzinger, E. (2002). Aggregation of proteins with expanded glutamine and alanine repeats of the glutamine-rich and asparagine-rich domains of Sup35 and of the amyloid beta-peptide of amyloid plaques. Proc Natl Acad Sci U S A *99*, 5596-5600.

Perutz, M. F., Staden, R., Moens, L., and De Baere, I. (1993). Polar zippers. Curr Biol *3*, 249-253.

Plumley, J. A., and Dannenberg, J. J. (2010). The importance of hydrogen bonding between the glutamine side chains to the formation of amyloid VQIVYK parallel beta-sheets: an ONIOM DFT/AM1 study. J Am Chem Soc *132*, 1758-1759.

Rousseau, E., Kojima, R., Hoffner, G., Djian, P., and Bertolotti, A. (2009). Misfolding of proteins with a polyglutamine expansion is facilitated by proteasomal chaperones. J Biol Chem *284*, 1917-1929.

Sawaya, M. R., Sambashivan, S., Nelson, R., Ivanova, M. I., Sievers, S. A., Apostol, M. I., Thompson, M. J., Balbirnie, M., Wiltzius, J. J., McFarlane, H. T., *et al.* (2007). Atomic structures of amyloid cross-beta spines reveal varied steric zippers. Nature *447*, 453-457.

CHAPTER 7

Probing Aβ(10-35) Fibril Structure by Fluorescence Resonance Energy Transfer (FRET)

Introduction

Previous chapters have focused on the elucidation of peptide terminal alkanes / amyloid peptide interaction on amyloid self-assemblies. These interactions are critical to amyloid peptide arrangement, sheet-sheet stacking and morphology. Similar intramolecular (peptide/peptide) interaction has been observed in protein folding and peptide aggregation (Liebman, 2005; Wasmer et al., 2008). In a longer segment of the Aβ peptide, Aβ(10-35), which is composed of several amphiphilic peptide segments, the intramolecular peptide-repeat interaction may direct amyloid fibril assembly. While there is good data constraining the relative arrangement of the peptide strands, at least three different models consistent with this data have been proposed for the Aβ(10-35) fibrils, including *extended β-sheet* model (Figure 7-1a) (Benzinger et al., 1998a; Benzinger et al., 2000; Burkoth et al., 2000), *β-helix* model (Figure 7-1b) (Lakdawala, 2003), and *turn* model (Figure 7-1c) (Petkova et al., 2002a).
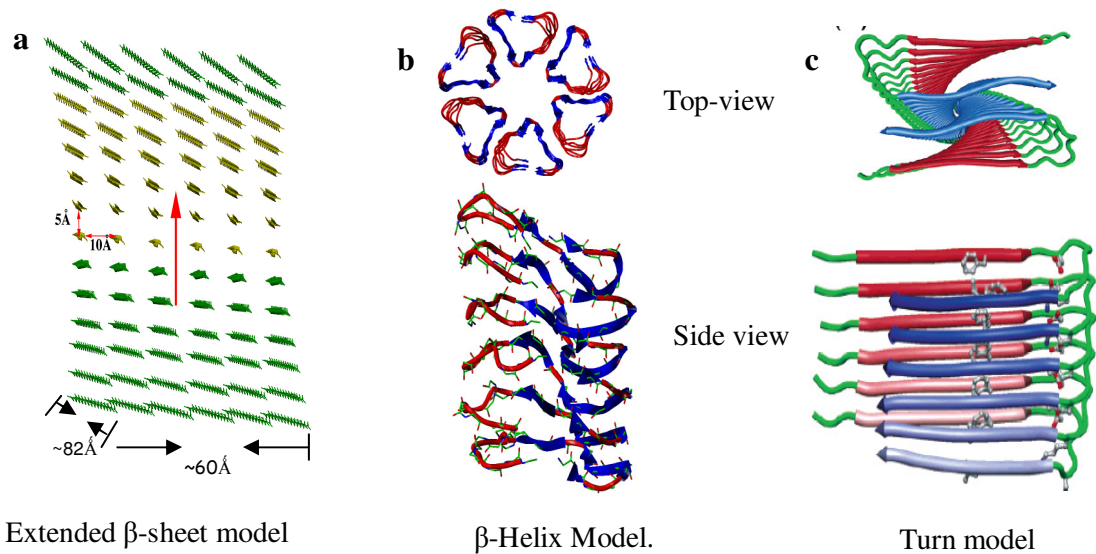
a — Extended β-sheet model

5Å
10Å
~82Å
~60Å

b — Top-view / Side view — β-Helix Model.

c — Top-view / Side view — Turn model

Figure 7-1. Three structural models of Aβ(10-35) fibrils.

(a) *Extended β-sheet* model with extended parallel in-register monomer conformation. The hydrogen-bond distance of 5 Å and sheets stacking distance of 10 Å give the fibril dimension of 60 Å ×80 Å (Benzinger et al., 1998a; Benzinger et al., 2000; Burkoth et al., 2000). (b) *β-helix* model with each monomer forming a triangle shape helical conformation (Lakdawala, 2003). (c) *Turn* model with the peptide forming a turn between residues 24 to 29 (Petkova et al., 2002b; Petkova et al., 2006).

To elucidate the possible intramolecular peptide interaction in Aβ(10-35) fibrils, it is necessary to determine the peptide strand conformation within fibrils. Unfortunately, without further structural constraints, it is hard to resolve peptide conformation with conventional structure characterization methods. However, Fluorescence Resonance Energy Transfer (FRET) can provide a long-distance molecular ruler and valuable structure information by measuring the relative distances between two specific residues (Decatur, 2000; Domanov, 2006; GarzonRodriguez et al., 1997; Hogue et al., 2009; Kinoshita et al., 2003; Kinoshita et al., 2001; Selvin, 2000).

In this chapter, we have elucidated the Aβ(10-35) strand conformation within fibrils by incorporation of a pair of small fluorophores at four different positions in Aβ(10-35). This approach provides additional structural constraints on the peptide strands and indeed develops a completely different structure model. We show that both peptide N- and C-termini bend to form turns and associate specifically with the peptide central region.

Results

Selection and placement of FRET pairs

FRET requires two fluorophores with overlapped fluorescence emission (donor) and absorption (acceptor) for energy transfer (Figure 7-2a) (Decatur, 2000; Domanov, 2006). In principle, when these two fluorophores are placed in the peptide with a specific distance, the emission energy of the donor will excite the acceptor, leading to a decrease of the donor emission intensity (Figure 7-2b). The difference of the donor emission intensity could be used to determine the donor/acceptor distance according to the equation in Figure 7-2b (Decatur, 2000; Domanov, 2006).
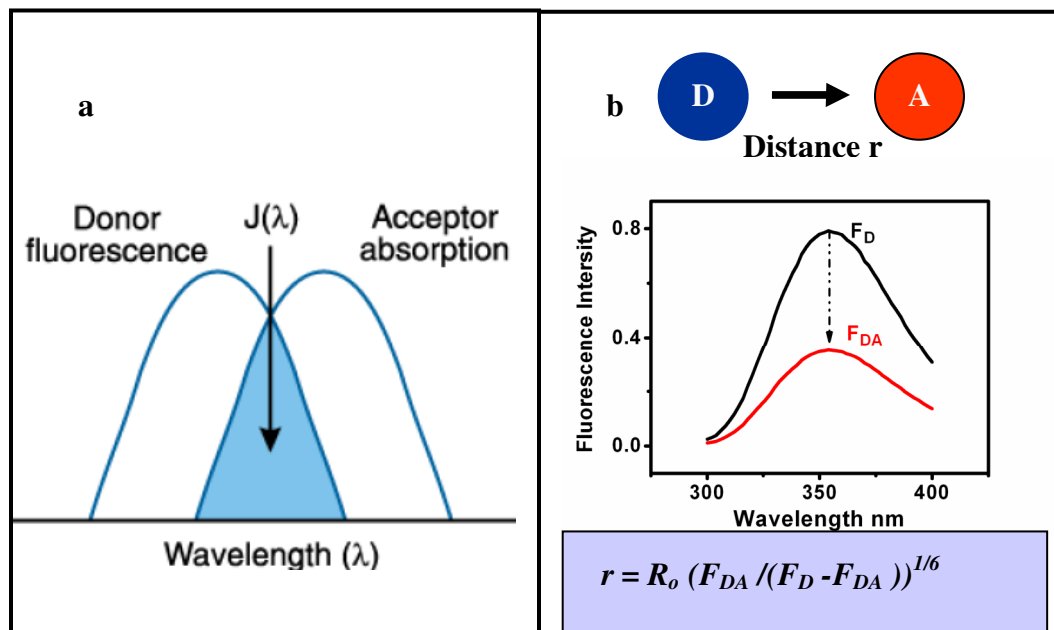
Figure 7-2. Mechanism of Fluorescence resonance energy transfer (Deeb, 2000).

(a) The donor emission overlaps with acceptor absorption. (b) When donor D and acceptor A are placed at distance r, the fluorescence intensity of donor (F_D) will decrease to F_{DA}. The value of r can be calculated according to the equation, where R_0 is the Förster distance, a distance between D and A when the energy transfer efficiency is 50%.

To minimize the perturbation of the introduced fluorophores on amyloid aggregation, tryptophan (Alston et al., 2008; Callis, 2001; Catherine A. Kraft1, 2009; Decatur, 2006) and N_ε-Dansyl-L-lysine were selected as the FRET pair. A Förster distance of 20 - 30 Å has been frequently utilized in peptide/protein systems where their small size and flexible linker have been advantageous (Munoz et al., 2006; Nannepaga et al., 2004). Several peptides were designed which contained both fluorophores in the Aβ(10-35) peptide. The first residues to place the D/A are at the termini (Figure 7-3), which should distinguish the three proposed models as shown in Figure 7-1.

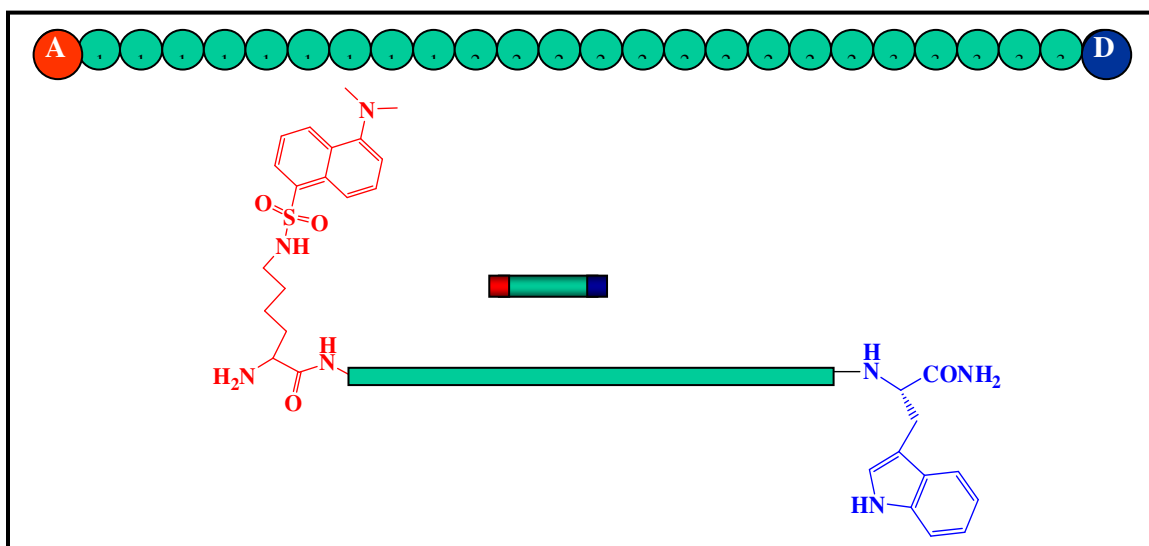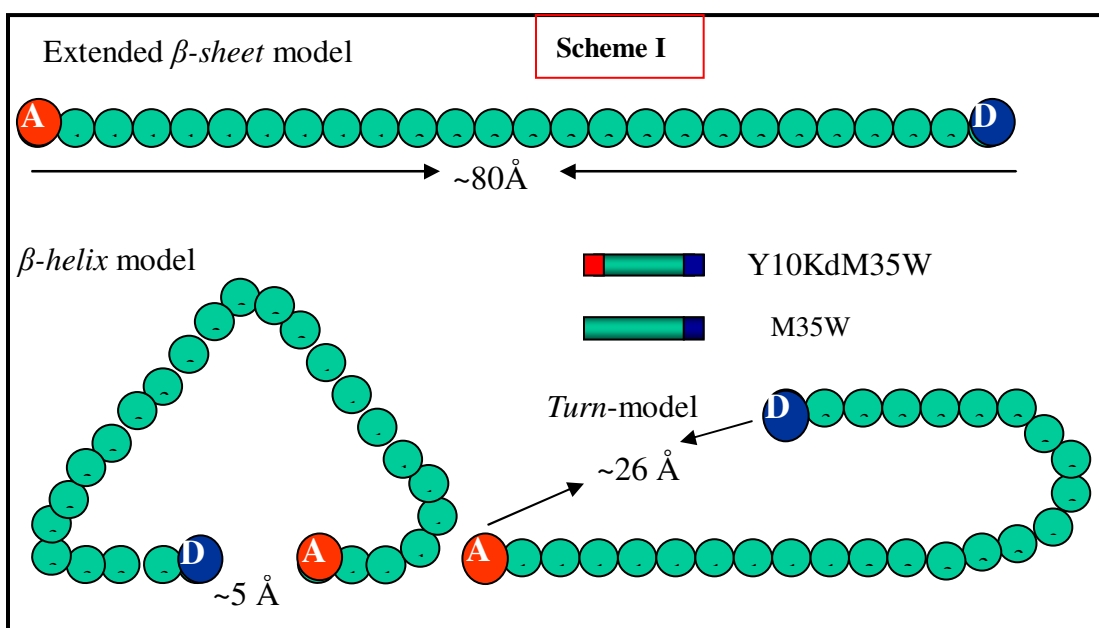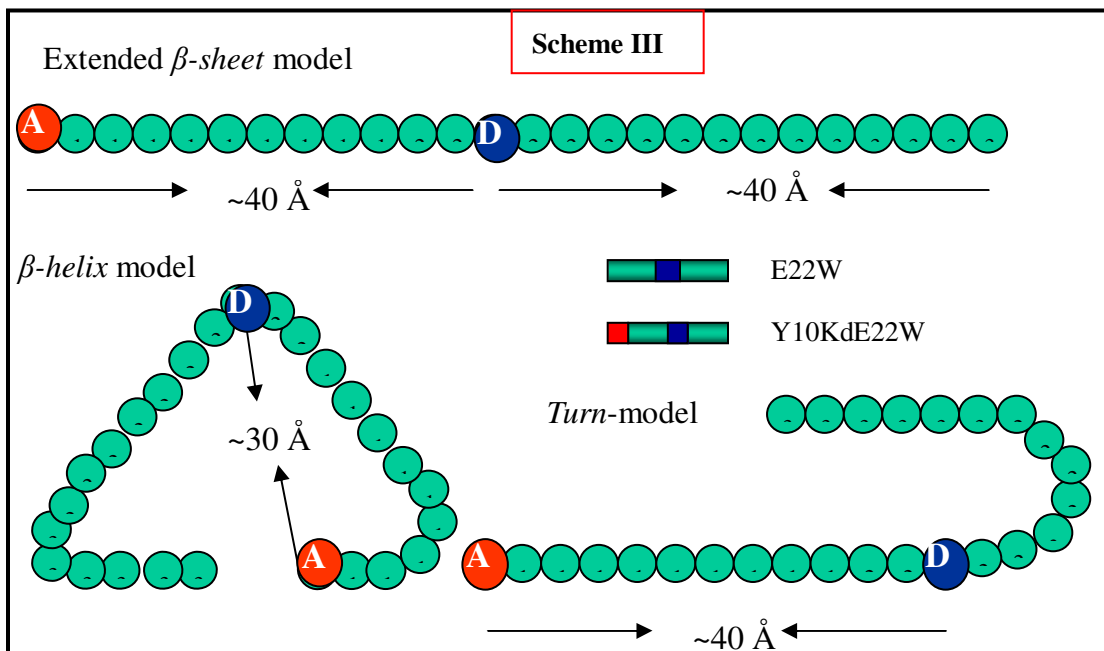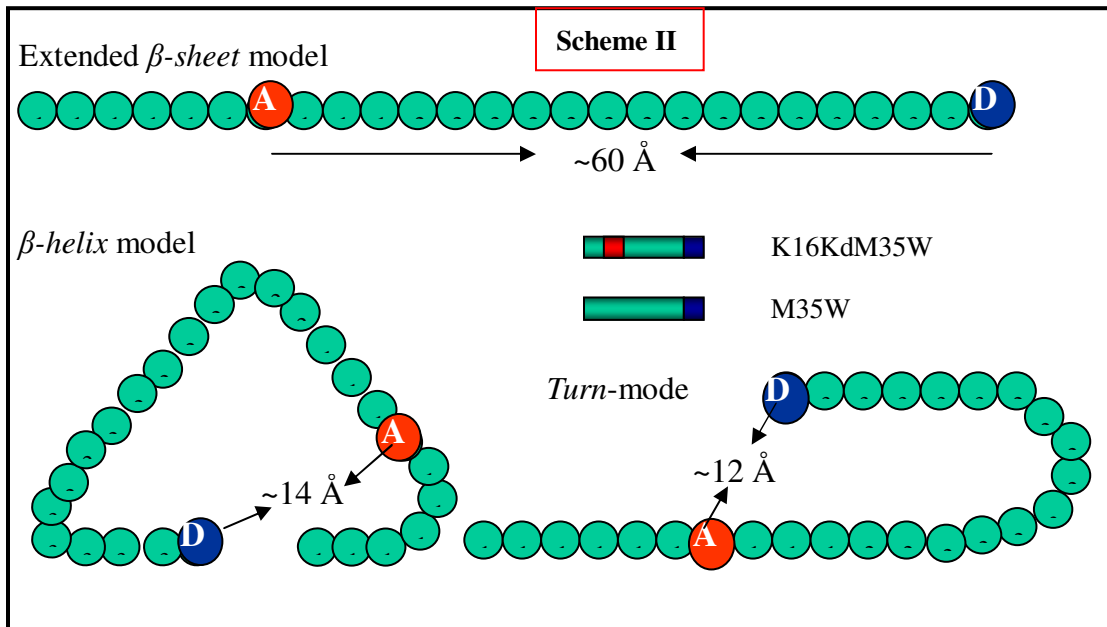**Figure 7-3. Structural cartoon of the Aβ(10-35) peptide containing both donor (tryptophan) and acceptor (dansyl).**

Further, the FRET pair was placed at four specific positions selected to test predictions regarding energy transfer efficiency for each model (Figure 7-4). According to the peptide length and peptide strand conformational geometry computer models, the
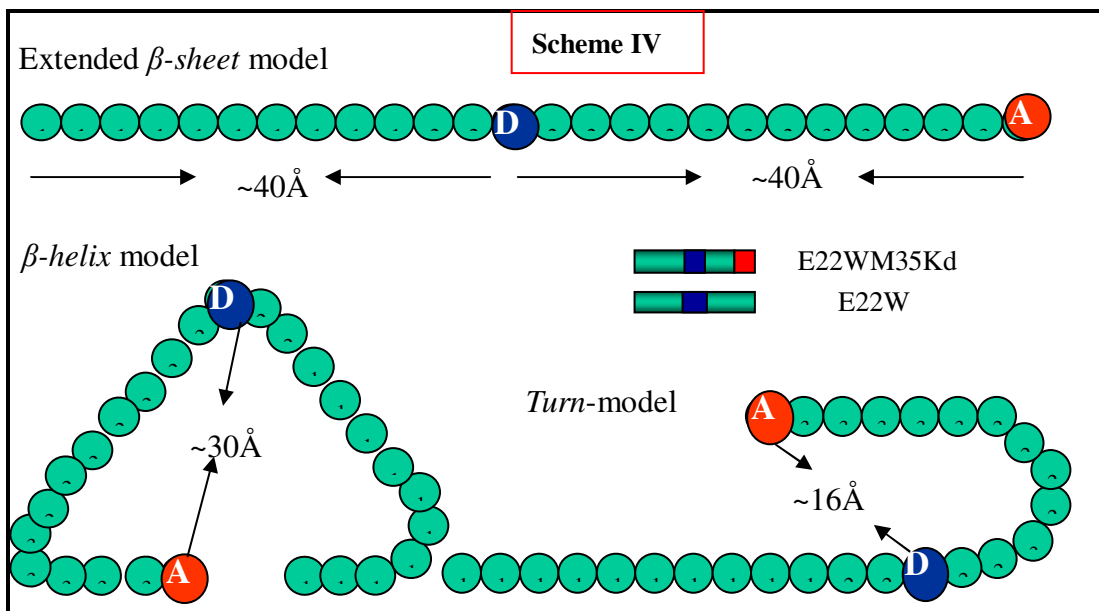
Figure 7-4. Each Scheme compares the predicted distances for a different donor (D) and acceptor (A) pair in the three proposed models.

The D (blue circle) and A (red circle) are placed at the C-terminus and the N-terminus in Scheme I, C-terminus and position 16 in Scheme II or position 22 and N-terminus in Scheme III and position 22 and C-terminus in Scheme IV, respectively. The distances are estimated from the backbone positions in the MD models.

Table 7-1. Estimated relative distances between D and A in different models shown in Figure 7-4.

Models		Extended *β-sheet* model (Å)	*β-helical* model (Å)	*Turn* model (Å)
Scheme I		80	5	26
Scheme II		60	14	12
Scheme III		40	30	40
Scheme IV		40	30	16

relative distance between D and A ranges from 40 Å to 82 Å in extended *β-sheet* model, 12 Å to 40 Å in *turn* model and 5 Å to 30 Å in *β-helical* model (Table 7-1).

Assembly of labeled peptides

The N_ε-Dansyl-L-lysine/tryptophan substituted peptides were prepared completely on solid supports using conventional solid-phase Fmoc chemistry with double-coupling (2×8 hr) at each synthetic step. After HPLC purification, the peptides were allowed to assemble at pH5.6 in 5.0 mM MES buffer containing 20% acetonitrile. The wild-type Aβ(10-35) peptide assembled as typical amyloid fibrils with diameters of about 10 nm (Figure 7-5a-c) (Benzinger et al., 1998a; Benzinger et al., 2000). Under the same incubation conditions, fluorophore-substituted M35W and Y10KdM35W peptides also assembled to typical amyloid fibrils (Figure 7-5d, e) with negative ellipticity ranging from 212 nm to 215 nm (Figure 7-5f-h), consistent with β-sheet secondary structure. However, when M35W and Y10KdM35W fibrils were excited at 295 nm, the maximum emission wavelength of tryptophan in both fibrils was at 352 nm and 358 nm, respectively (Figure 7-5i), suggesting different local environments of tryptophan in both fibrils (Callis, 2001).
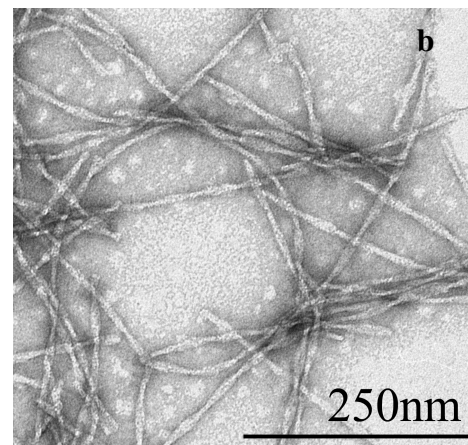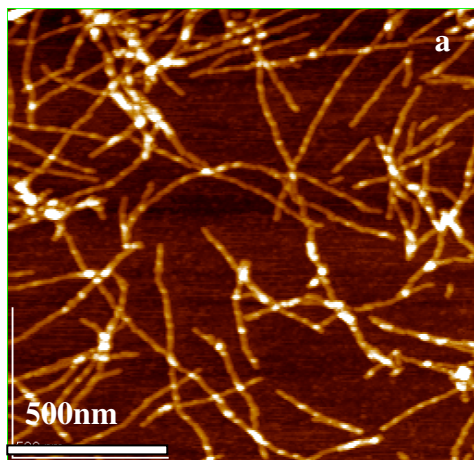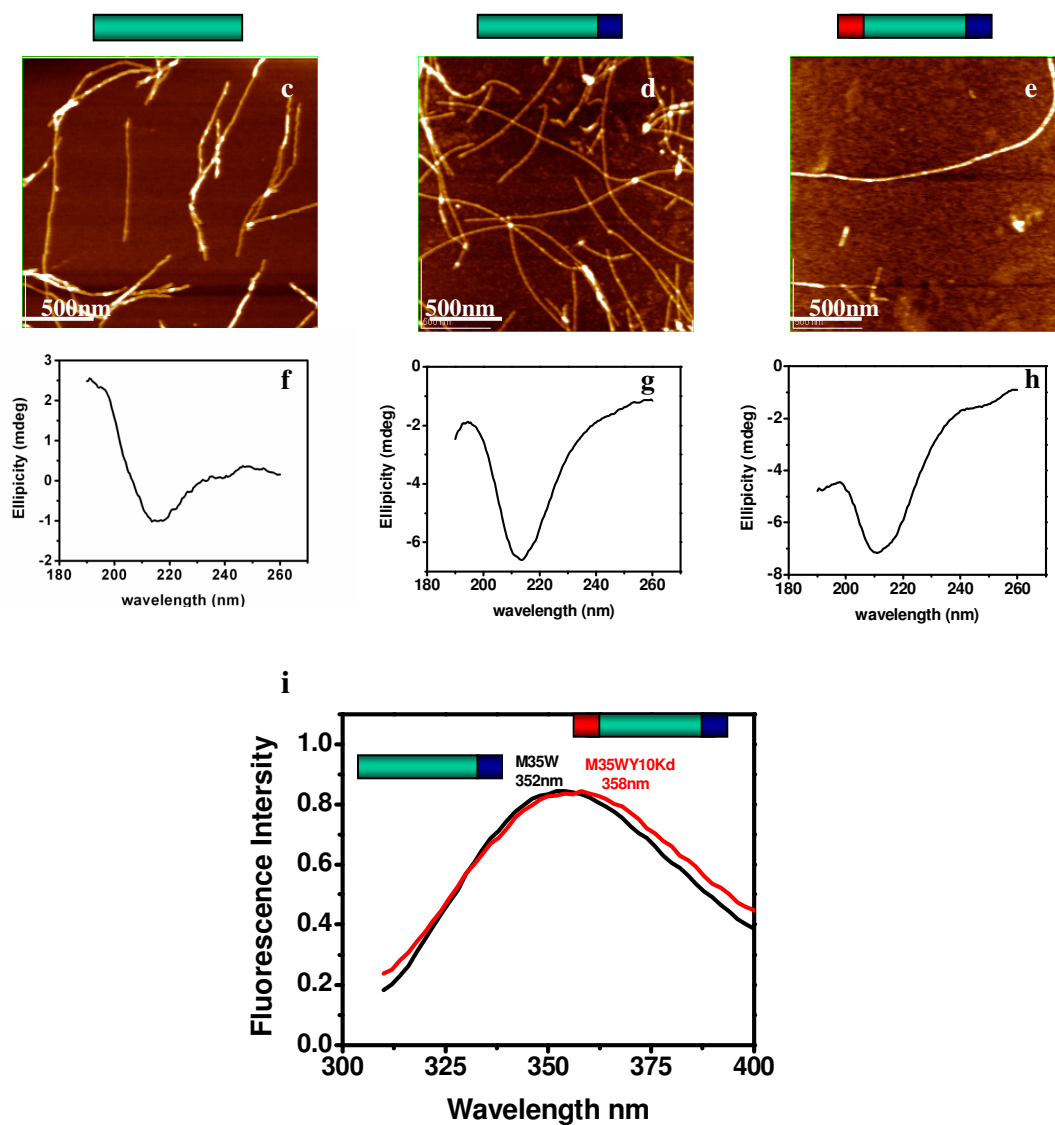
Figure 7-5. AFM images, CD secondary structure and fluorescence emission spectroscopy of fluorophore-substituted amyloid fibrils.

AFM images of (a, c) Aβ(10-35) fibrils, (d) M35W fibrils and (e) Y10KdlM35W fibrils. (b) TEM of Aβ(10-35) fibrils.

CD spectra of (f) Aβ(10-35) fibrils, (g) M35W fibrils and (h) Y10KdlM35W fibrils. Fluorescence emission spectra of (i) M34W (black) and Y10KdM35W (red) where the matured fibrils were excited at 295 nm, and the fluorescence emission spectra were collected between 310 nm to 400 nm.

In all cases, the fibrils were prepared by incubating 0.11 mM peptide at pH5.6 in 5.0 mM MES buffer containing 20% acetonitrile at room temperature for 2 weeks.

To isolate the tryptophan residues in both M35W and Y10KdM35W fibrils, each peptide was co-assembled with wild-type Aβ(10-35) at a molar ratio of 1 to 10. The mixed peptide self-assemblies were indistinguishable from Aβ(10-35) amyloid fibrils (Figure 7-6a-g), maintaining the same negative ellipticity at 215 nm (Figure 7-6h-k) and the same tryptophan maximum emission wavelength of 346 nm (Figure 7-6l). This approach ensures the same local environment for tryptophan in both M35W and Y10KdM35W fibrils, so that all subsequent fibril samples were prepared by mixing fluorophore-substituted peptides with wild-type Aβ(10-35) in a 1 to 10 molar ratio.
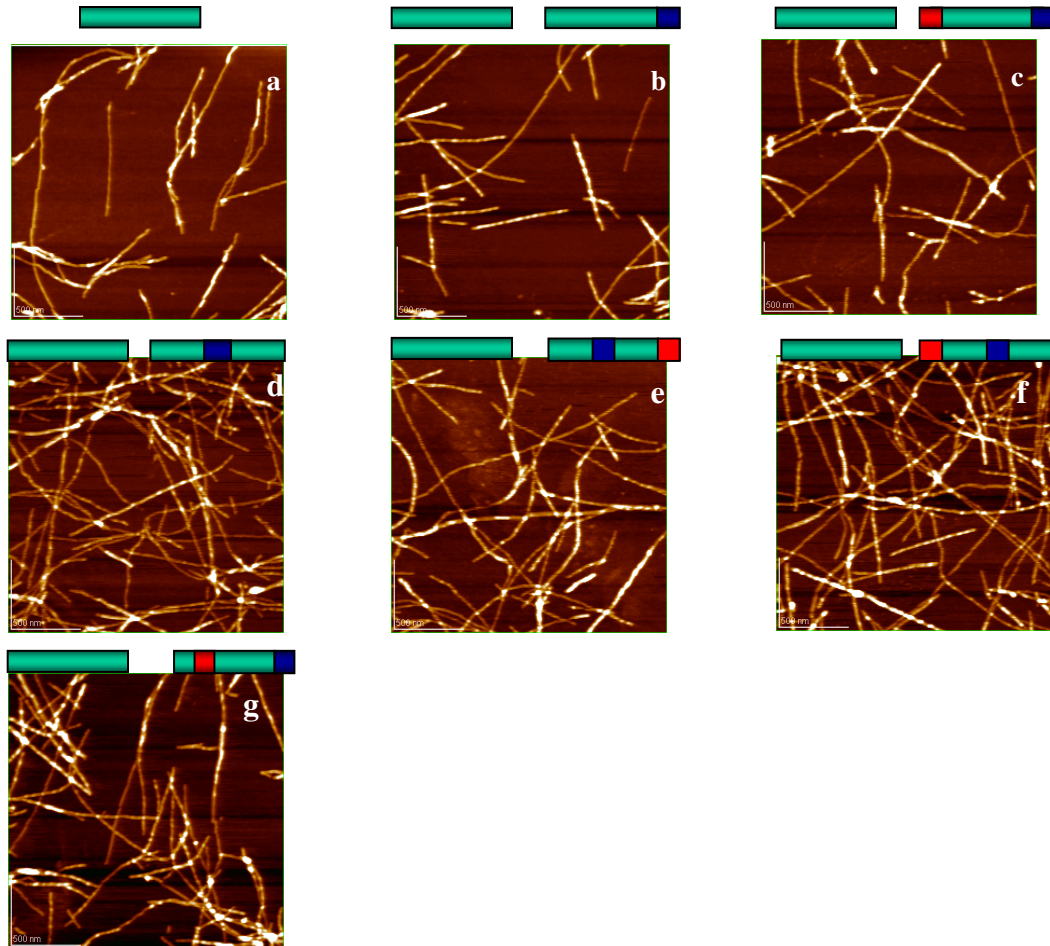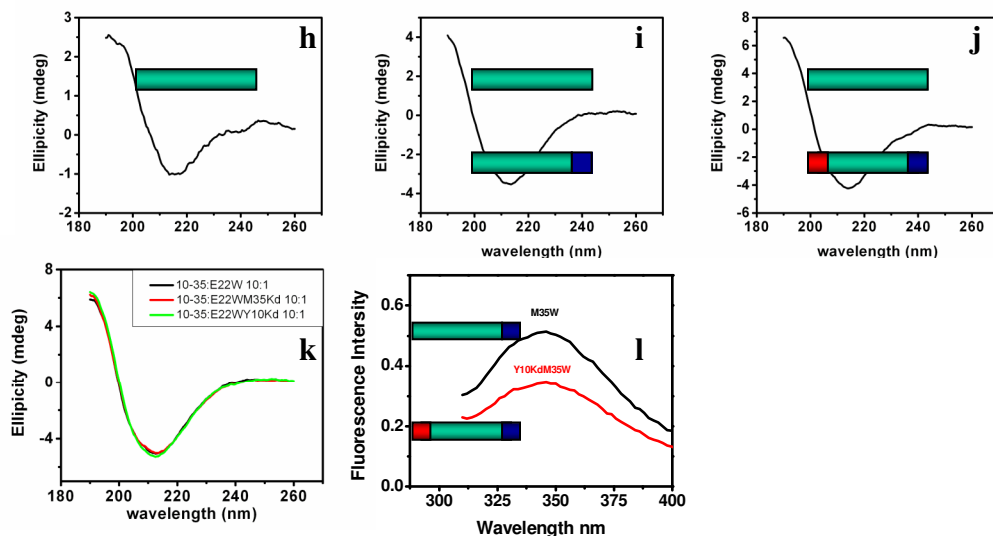
Figure 7-6. AFM images, CD analyses and fluorescence emission spectroscopy of co-assembled fibrils.

The AFM images of fibrils formed from (a) Aβ(10-35), (b) Aβ(10-35) / M35W (10 : 1), (c) Aβ(10-35) / Y10KdM35W (10 : 1), (d) Aβ(10-35) / E22W (10 : 1), (e) Aβ(10-35) / E22WM35Kd (10 : 1), (f) Aβ(10-35) / Y10KdE22W (10 : 1)   and (g) Aβ(10-35) / K16KdM35W (10 : 1).

CD spectra of (h) Aβ(10-35) fibrils, (i) Aβ(10-35) / M35W (10 : 1), (j) Aβ(10-35) / Y10KdM35W (10 : 1) and (k) Aβ(10-35) / E22W (10 : 1), Aβ(10-35) / E22WM35Kd (10 : 1) and Aβ(10-35) / E22WY10Kd (10 : 1).

(l) The fluorescence emission spectra of Aβ(10-35) / M35W (10 : 1) fibrils (black) and Aβ(10-35) / Y10KdM35W (10 : 1) fibrils (red). The fibrils were excited at 295 nm and the emission spectra were collected between 310 nm to 400 nm.

In each case, the fibrils were prepared by incubation of 0.11 mM total peptide in the presence of 5.0 mM pH5.6 MES buffer in 20% acetonitrile/water at room temperature for 2 weeks.

At 0.01 mM under the assembly conditions, Y10KdM35W assembled as particles with a tryptophan emission maximal wavelength at 358 nm (Figure 7-7a, b, e), significantly red-shifted from the emission at 346 nm when co-assembled as homogeneous fibrils with 0.1 mM Aβ(10-35) (Figure 7-7c, d, e). The blue-shift of the
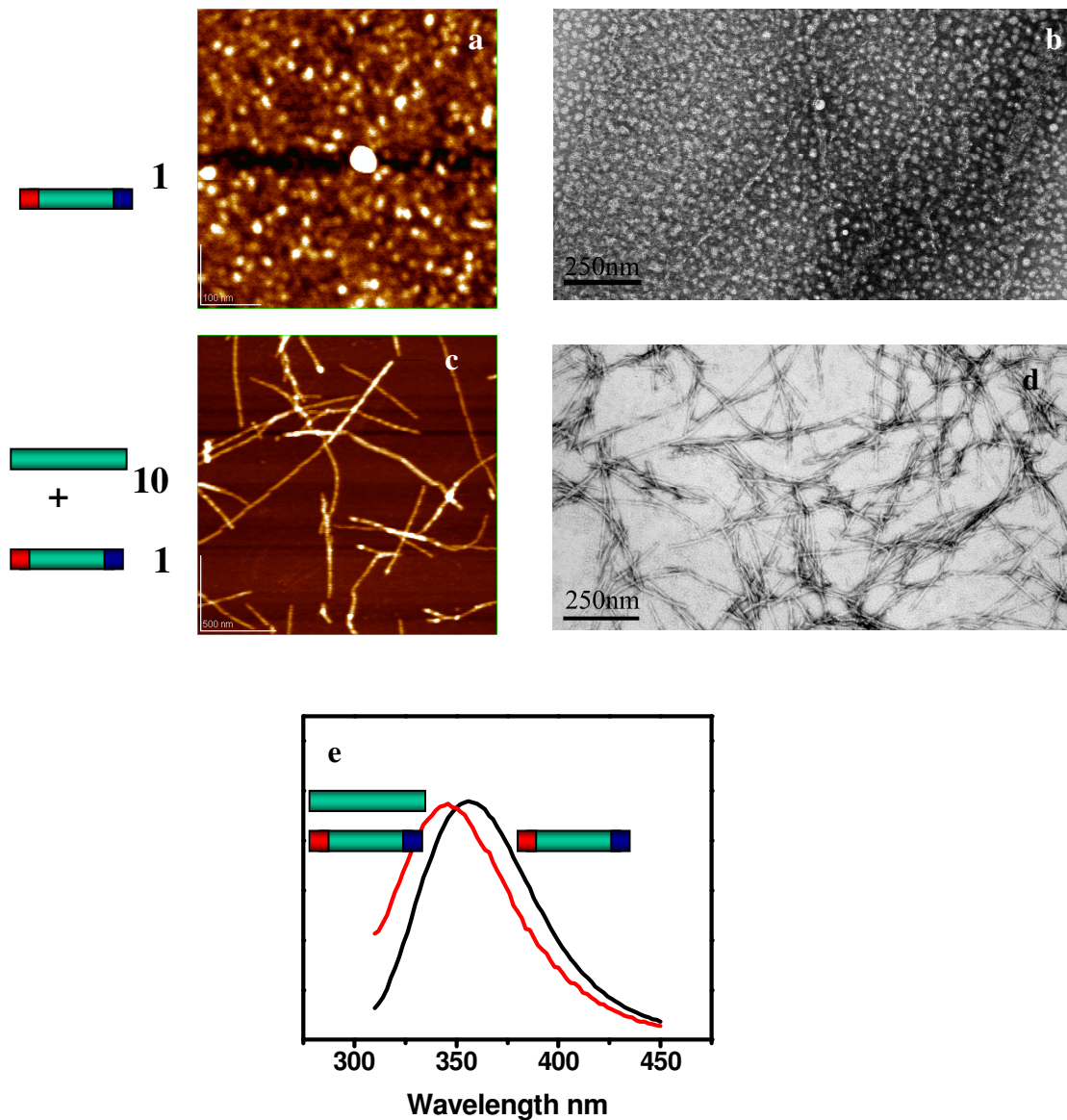
Figure 7-7. AFM/TEM images and fluorescence emission spectroscopy of the indicated assemblies.

AMF images of (a) 0.01 mM Y10KdM35W particles and (c) 0.1 mM Aβ(10-35) + 0.01 mM Y10KdM35W fibrils. TEM images of (b) 0.1 mM Y10KdM35W particles and (d) 0.1 mM Aβ(10-35) + 0.01 mM Y10KdM35W fibrils.

(e) Fluorescence emission of tryptophan in particles (Em = 358 nm, black line) and fibrils (Em = 346 nm, red line) when exited at Ex = 295 nm. To better compare the maximum emission wavelength, the curves are normalized according to the peak intensity.
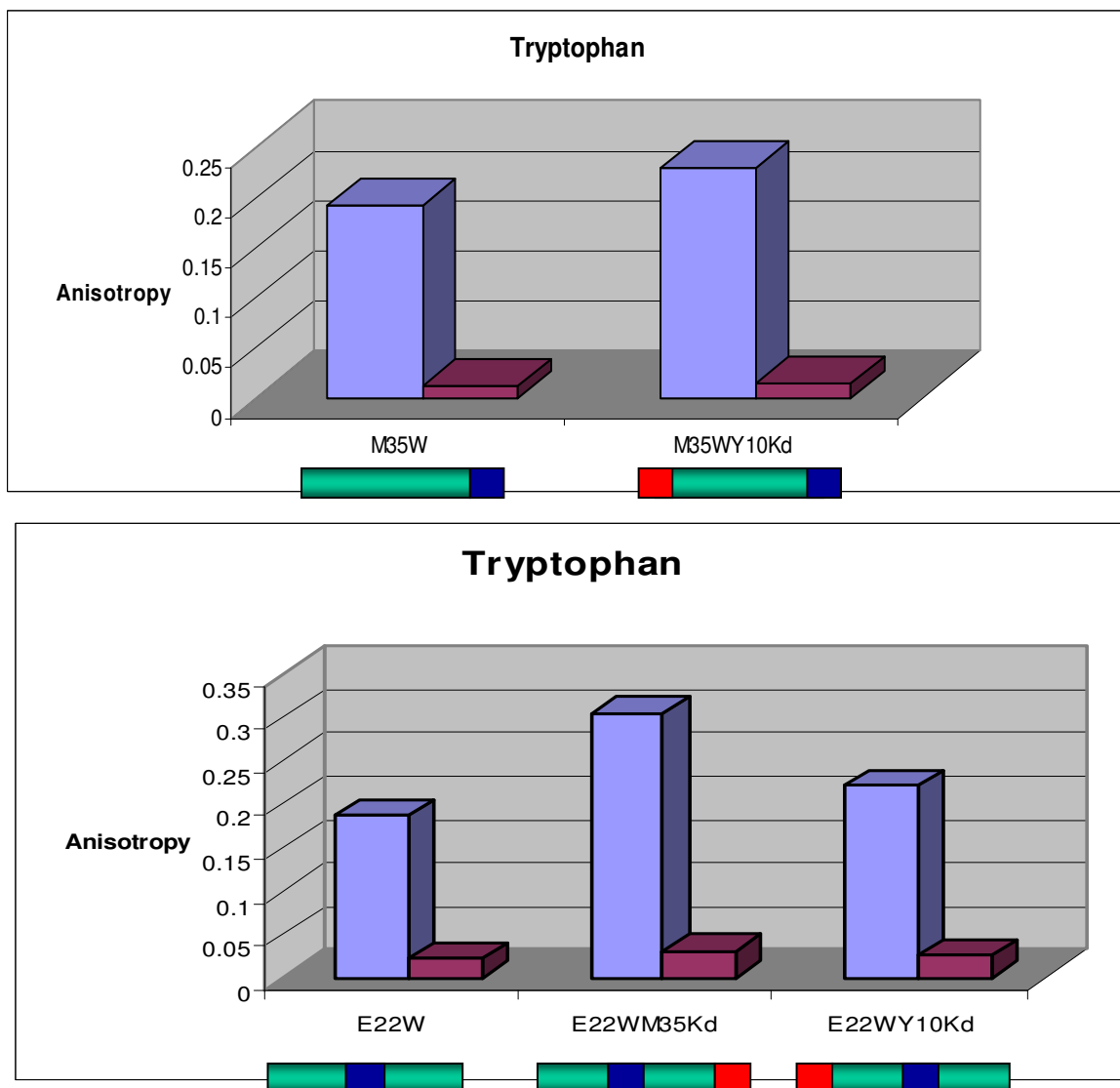
Figure 7-8. Tryptophan fluorescence anisotropy in fibrils and monomers.

The blue bars represent fibrils and purple one is monomers. In each case, the fibrils were prepared by incubation of 0.01 mM fluorophore-substituted peptide with 0.1 mM Aβ(10-35) (1 to 10) at pH5.6 in 5 mM MES and 20% acetonitrile / water for 2 weeks. Due to the fast aggregation of peptide in the assembly condition, the monomer solution was prepared by dissolving 0.01 mM peptide powder in pure DMSO without water dilution. 220 μL of the prepared sample was loaded in fluorescence quartz curvette with 2 mm path length. The sample was excited with Ex = 295 nm, and the fluorescence anisotropy was collected at the maximal emission wavelength (when W is at C-terminus: Em = 346 nm and W at the peptide center: Em = 332 nm). The final anisotropy is the average of four individual data collections.

maximum emission in fibrils is consistent with a more hydrophobic environment in the fibrils (Callis, 2001).

To further confirm co-assembly, the rotational motion of the chromophores was compared via fluorescence anisotropy analysis (Benzinger et al., 1998a; Koo et al., 2008). In each case, the anisotropy increased significantly when the peptides self-assembled to fibrils (Figure 7-8), supporting that fluorophore-peptides incorporated into fibrils.

Fluorescence resonance energy transfer in co-assembled fibrils

In the M35W/Aβ(10-35) and E22W/Aβ(10-35) co-assembled fibrils, the tryptophan emission intensity was at 0.51 and 1.23, respectively (Figure 7-9). When the A (acceptor) was placed at the N-terminus for Y10KdM35W and Y10KdE22W, the tryptophan
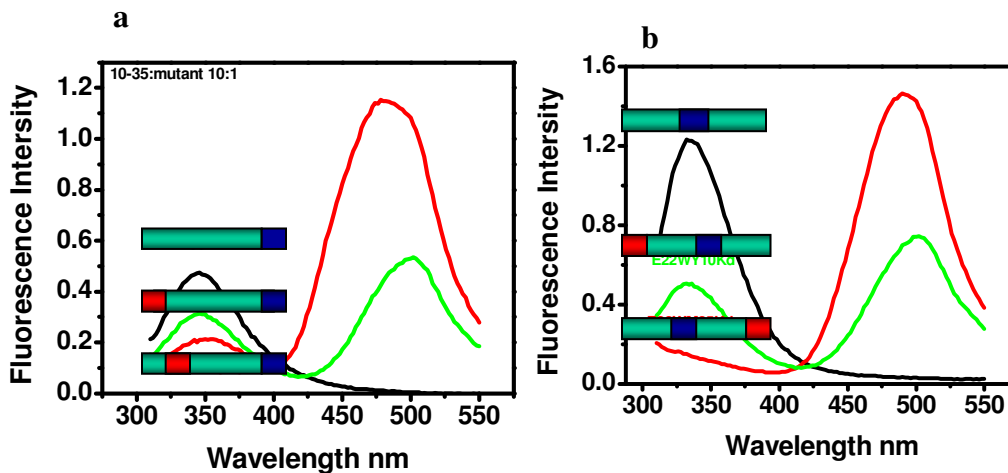
Figure 7-9. Fluorescence emission spectra of co-assembled fibrils.

(a) With the donor at N-terminus: black line (M35W), red line (Y10KdM35W) and green line (K16KdM35W), and (b) with the D at the peptide center: black line (E22W), red line (Y10KdE22W) and green line (M35KdE22W). All samples were excited at 295 nm. The indicated peptides were co-assembled with Aβ(10-35) as fibrils and the cartoon inserts indicate the relative positions of the D / A pairs.

fluorescence emission intensity in the fibrils was reduced to 0.34 and 0.5, respectively. Moving A to the 16th position (K16KdM35W) further decreased the tryptophan fluorescence emission to 0.25, and switching the A position from N- to C-terminus (E22WM35Kd) cut this number in half to 0.14.

To evaluate the contributions of inter- vs intra-molecular energy transfer to the overall FRET signal, the total concentration was raised from 0.11 mM to 0.30 mM, but this change resulted in very little change in efficiency for any of the assemblies. However, increasing the dilution of the probe within the fibril, changing the ratio from 10:1 to 50:1
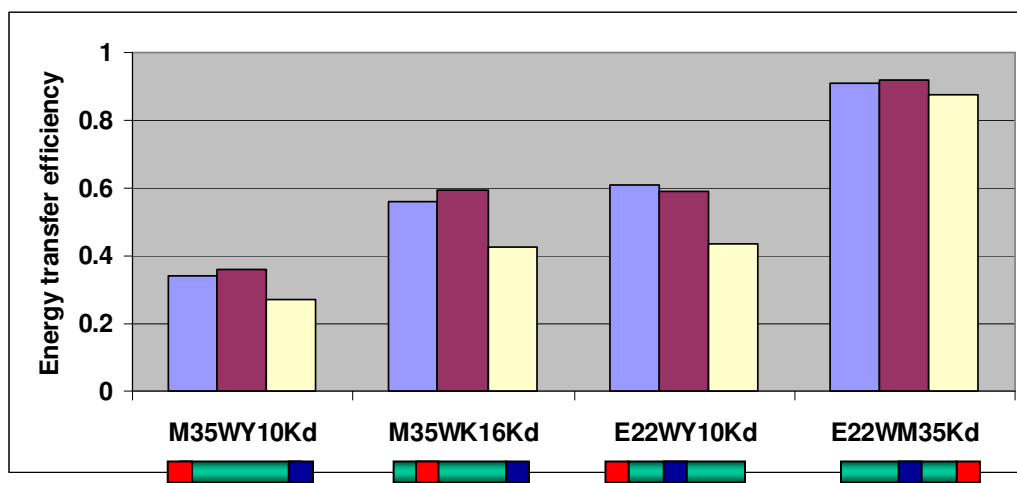
Figure 7-10. Concentration and the peptide mixing ratio-dependence of FRET.

The indicated four double-labeled peptide probes were incubated in 20% acetonitrile/water and 5 mM pH5.6 MES buffer for 2 weeks with Aβ(10-35) at total peptide concentrations of 0.11 mM (blue column) and 0.30 mM (purple column) at a ratio of Aβ(10-35) to probe of 10 : 1. The white column represents 0.30 mM peptide at a ratio of 50 : 1. The excitation wavelength was 295 nm and the energy transfer efficiency was determined according to the equation $E=(F_D-F_{DA})/F_D$. F_D and F_{DA} are the tryptophan maximal emission intensity in the absence and presence of dansyl. When tryptophan is at C-terminus (M35W, M35WY10Kd and M35WK16Kd), the maximal emission wavelength is 346 nm, and when W is at the peptide center (E22W, E22WY10Kd and E22WM35Kd), the maximal emission wavelength is at 332 nm.

the FRET efficiency was reduced by 10 to 25% depending on the peptide (Figure 7-10). Therefore, intermolecular interaction does contribute to overall energy transfer, even though the exact percentage has not been defined.

The contribution of intermolecular energy transfer was further evaluated by isolating the D and A in individual peptides. At pH5.6, the mixtures of wild type Aβ(10-35) with either probe peptide or with two individual probe peptides assembled into fibrils indistinguishable from Aβ(10-35) (Figure 7-11a-c). In the absence of the
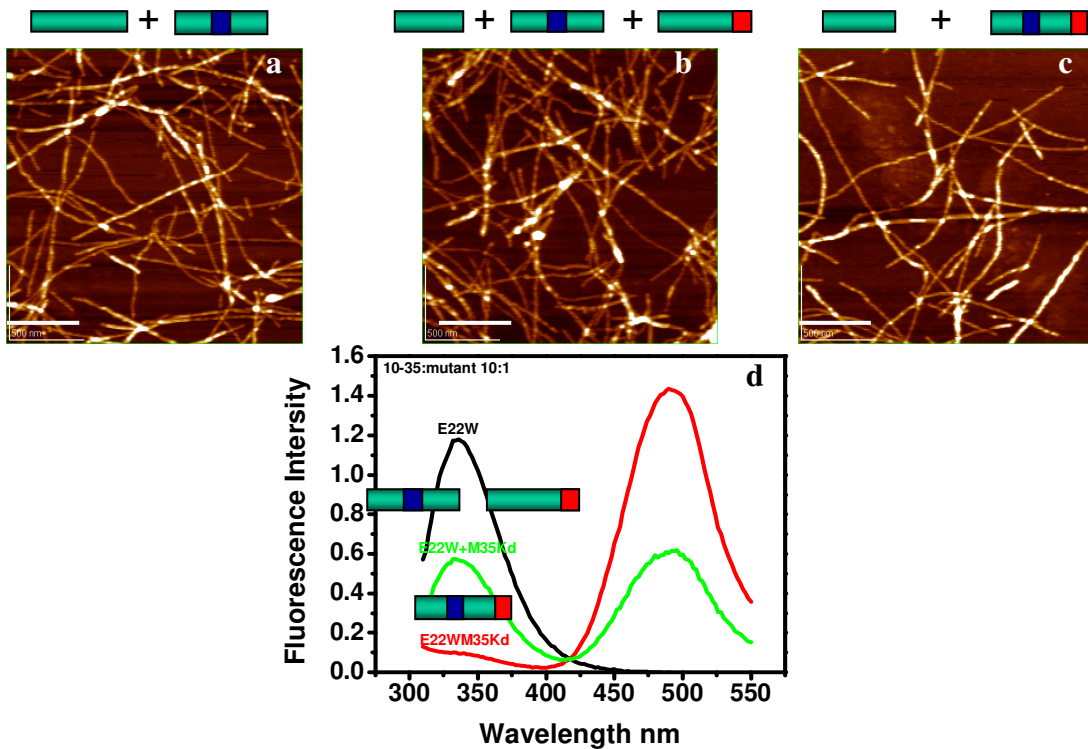
Figure 7-11. AFM images and fluorescence emission spectra of co-assembled fibrils.

AFM images of the fibrils formed from (a) Aβ(10-35) / E22W (10 : 1), (b) Aβ(10-35) / E22W/M35Kd (10 : 1 : 1) and (c) Aβ(10-35) / E22WM35KD (10 : 1).

(d) The fluorescence emission spectra of Aβ(10-35) / E22W (10 : 1) fibrils (black), Aβ(10-35) / E22W/M35Kd (10 : 1 : 1) fibrils (green) and Aβ(10-35) / E22WM35KD (10 : 1) fibrils (red). The scale bar represents 500 nm.

dansyl acceptor A, the tryptophan fluorescence emission intensity was 1.18. The addition of the third peptide containing the acceptor decreased the tryptophan fluorescence emission to 0.57, and when the D and A were in the same peptide, the tryptophan fluorescence emission dropped sharply to almost 0.1 (Figure 7-11d).

To provide the good comparison, the concentration of Aβ(10-35) was kept at 0.1 mM and tryptophan and dansyl at 0.01 mM. Therefore, in the final assemblies, peptides at total concentration of 0.11 mM (for two-component mixture) or 0.12 mM (for three-component mixture) were allowed to co-assemble in 20% acetonitrile / water and 5 mM pH5.6 MES buffer for 2 weeks. Based on Figure 7-10, slight increases of the total peptide concentration while keeping the ratio of wild-type peptide to the probes has little or neglect impact on the final fluorescence energy transfer efficiency.

The signatures above could arise from both intra- and inter-molecular energy transfers. To test these contributions between the peptide termini, the fibrils assembled from only Y10KdM35W and E22WM35Kd are evaluated in Figure 7-12. The dansyl groups in both fibrils show strong emission with equivalent intensity, but the tryptophan fluorescence emission intensity of E22WM35Kd is significantly lower than that of Y10KdM35W. This result is consistent with an intermolecular distance between Y10 and M35 being longer than the distance between E22 and M35.
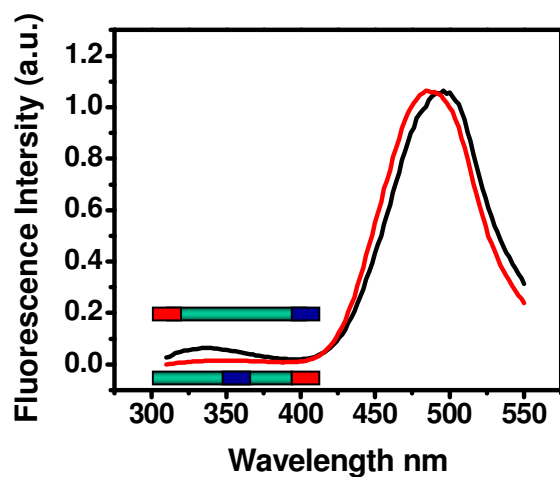
Figure 7-12. The fluorescence emission spectra of Y10KDM35W (black) and E22WM35KD (red) fibrils.

In each case, 0.1 mM peptide was incubated in 20% acetonitrile / water and 5 mM MES buffer for 2 weeks. The resulting fibrils were excited at 295 nm to obtain the fluorescence spectra.

The local environment of peptide N- and C-termini was determined by acrylamide quenching (Dusa et al., 2006; Garzon-Rodriguez et al., 2000). As shown in Figure 7-13, neither Y10W nor M35W fibrils was efficiently quenched even at high acrylamide concentrations under conditions where the unassembled peptides were quenched almost as efficiently as the free amino acid. Therefore the N- and C-termini appear to be significantly shielded from solvent in these assemblies.
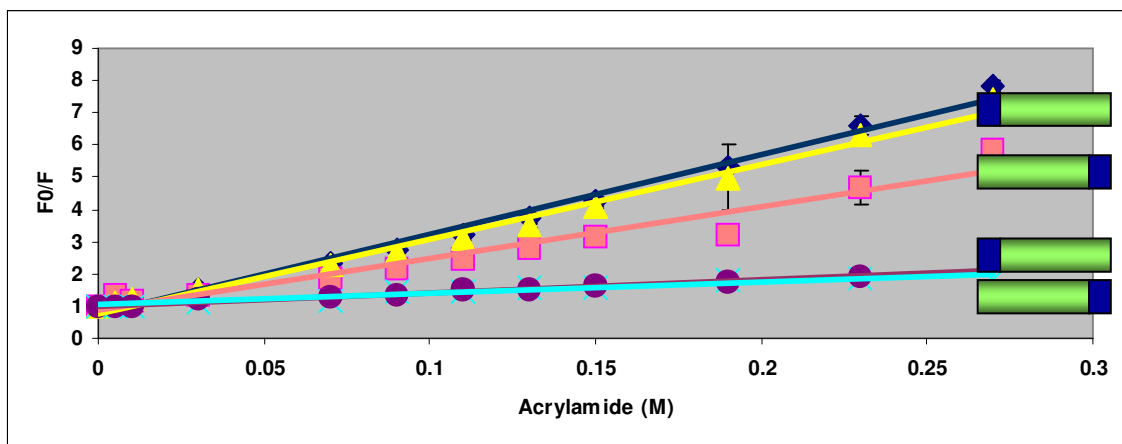
Figure 7-13. Acrylamide quenching of fibril assemblies.

The M35W and Y10W fibrils were prepared by incubation individual peptide (0.1 mM) in 20% acetonitrile / water and 5.0 mM pH5.6 MES buffer for 2 weeks. The monomers were prepared by dissolving the same amount peptides in 6 M GnHCl. All samples were mixed individually with concentrated acrylamide to reach the final indicated concentration and incubated for 30 min before monitoring the tryptophan fluorescence via excitation at 295 nm. F_0/F was determined at their maximal emission wavelength (M35W in fibrils Em = 346 nm, in monomer: Em = 360 nm; Y10W in fibrils: Em = 342 nm, in monomer Em = 358 nm). The color code of each line: M35W fibrils (light blue), Y10W fibrils (purple), M35W monomer (pink), Y10W monomer (yellow), and free tryptophan amino acid (dark blue).

Discussion

The secondary structural arrangement of the Aβ(10-35) peptide within its amyloid fibril has been well described (Benzinger et al., 1998a; Benzinger et al., 2000; Burkoth et al., 2000), but the arrangement of the β-sheets in the fibril remains unclear. Three models for this arrangement have been published (Benzinger et al., 1998a; Benzinger et al., 2000; Benzinger et al., 1998b; Burkoth et al., 2000; Lakdawala, 2003; Petkova et al., 2002b; Petkova et al., 2006), and in this study, I have incorporated fluorescence probes at four

different positions in Aβ(10-35) to test these models. Not only in the resulting evidence inconsistent with the existing models, but is sufficient to allow me to propose a new peptide strand conformation for the Aβ(10-35) fibril (Figure 7-14).

The Aβ(10-35) *extended β-sheet* model is consistent with the ssNMR data, and predicts a similar distance between N-/C- terminus and internal probes ($R_{10-22} \approx R_{22-35}$), which is closer than between the two termini ($R_{10-22} \approx R_{22-35} < R_{10-35}$). In addition, the long distance between two termini in this model should not give observable intramolecular energy transfer. However, 34% transfer efficiency was detected when D/A was at the separate termini. Moreover, it was found that R_{22-35} was much shorter than both of R_{10-22} and $R_{10-35,}$ indicating there is a turn at the peptide C-terminus, inconsistent with *extended β-sheet* model.

The *β-helix* model predicts closer distance between N- and C- termini than between terminus and central probes ($R_{10-35} < R_{10-22} \approx R_{22-35}$). However, the terminal distance (R_{10-35}) was determined to be the longest among the four different relative positions. Moreover, the distance between terminus and the center residue is not same but R_{10-22} is longer than R_{22-35}.

The *turn* model predicts a closer distance between C-terminus and the peptide center than between N-terminus and peptide center ($R_{22-35} < R_{10-22}$), which should also be longer than the distance between peptide two termini ($R_{10-22} > R_{10-35}$). In deed, we obtained the stronger energy transfer efficiency when probes were at C-terminus and peptide center than at N-terminus and the peptide center, consistent with the prediction

217

$R_{22-35} < R_{10-22}$. Surprisingly, the distance between N-terminus and peptide center (R_{10-22}) is shorter than between peptide two termini (R_{10-35}), inconsistent with the extended conformation for the peptide N-terminal part, suggesting a turn at peptide N-terminus.

Table 7-2. The order of relative distance between residues for each model.

Structure model	The order of distance between residues
Extended *β-sheet* model	$R_{10-35} > R_{16-35} > R_{22-35} \approx R_{10-22}$
β-helix model	$R_{10-22} \approx R_{22-35} > R_{16-35} > R_{10-35}$
Turn model	$R_{10-22} > R_{10-35} > R_{22-35} > R_{16-35}$
Experimental observation	$R_{10-35} > R_{16-35} > R_{10-22} > R_{22-35}$

Based on the relative distance between two specific residues ($R_{10-35} > R_{16-35} > R_{10-22} > R_{22-35}$) obtained from the experiment (Table 7-2), *double-turn* monomer conformation was proposed (Figure 7-14). The turn at C-terminus starts from residue G25 to residue G29, consistent with the turn observed in Aβ(1-40) fibrils (Petkova et al., 2002b; Petkova et al., 2006), while the turn at the N-terminus is from residue H14 to K16, which requires further verification via ssNMR. The *turn* in this *double-turn* model is stabilized primarily by the side chain hydrophobic interaction with the intramolecular lamination distance of 10 Å, similar to that proposed in the Aβ(1-40) *turn* model (Petkova et al., 2002b), and the extra N-terminal turn provides additional intramolecular interaction between peptide segments such as residue [10]YEV and [17]LVF (Figure 7-14).
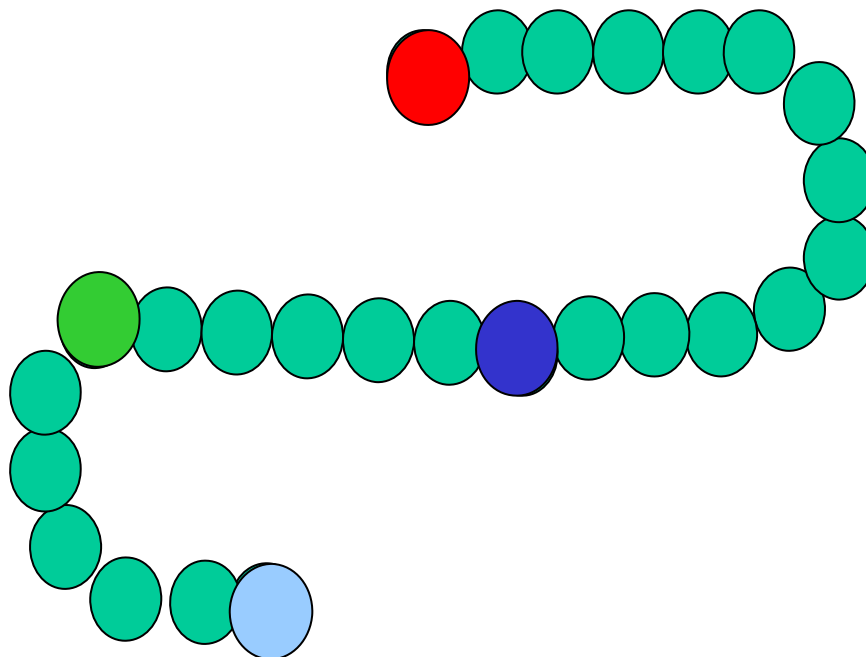
Figure 7-14. Proposed Aβ(10-35) strand conformation within fibrils.

The region from residue K16 to 25 is extended; the N-terminal turn is from H14 to K16 and C-terminal turn is from G25 to G29. Light blue bead is Y10, green one is K16, dark blue is E22, red is M35 and blue is the rest of amino acids.

Therefore, new peptide strand conformation leads to a new structure model for Aβ(10-35) fibrils. The fibril height and width measured from AFM and TEM images (Figure 7-5) imply four peptide monomers as the basic unit within fibrils, consistent with Aβ(1-40) fibril model (Petkova et al., 2002b). Therefore, stacking of four peptides gives six possible models (Models I-VI, Figure 7-15). The group I, including Models I to IV, features a similar local environment of N- and C- termini, while group II, including Models V and VI, has different terminal environment. The same quenching efficiency of Y10W and M35W fibrils by acrylamide indicates that the N- and C-termini are both buried, arguing against Models V and VI. In the remaining four models, Model III has

shorter intermolecular distance between N- and C-terminus than that between E22 and M35, inconsistent with the lower intermolecular energy transfer efficiency between Y10 and M35 than between E22 and M35. While in Model IV, separated N- and C-termini are predicted to have no or very weak intermolecular energy transfer, inconsistent with the strong energy transfer efficiency observed for Y10KdM35W fibrils in the absence of Aβ(10-35). In Model I, peptide C-terminus is kind of buried interior of fibrils, and addition of hydrophilic PEG at its C-terminus would disrupt fibril formation, against the experimental observation of PEG coated fibril (Burkoth et al., 2000). Therefore, Model II is most consistent with these data, maintaining the same environment for the N- and C-termini, allowing for intermolecular N and C-terminal energy transfer, as well as fitting the fibril dimension and allowing for PEG assembly. Moreover, the model predicts the outcome of specific ssNMR experiments including 1) the distance between $[1-^{13}C]$ K16 and $[^{15}N]$ H13 could be measured to evaluate the N-terminal turn; 2) the residue side chain at the N-terminus such as $[\delta-^{13}C]$ Q15 and C-terminus such as $[^{15}N_\delta]$ N27 could be selectively isotope-labeled to measure the inter-sheet distance (highlighted in Figure 7-15 black box); and 3) the N-terminal turns of Aβ(10-35) could be covalently linked between residue E11 and K16. If this N-terminal turn is required for the assembly, the preformed N-turn may accelerate the assembly rate relative to wild-type Aβ(10-35) (Sciarretta et al., 2005).
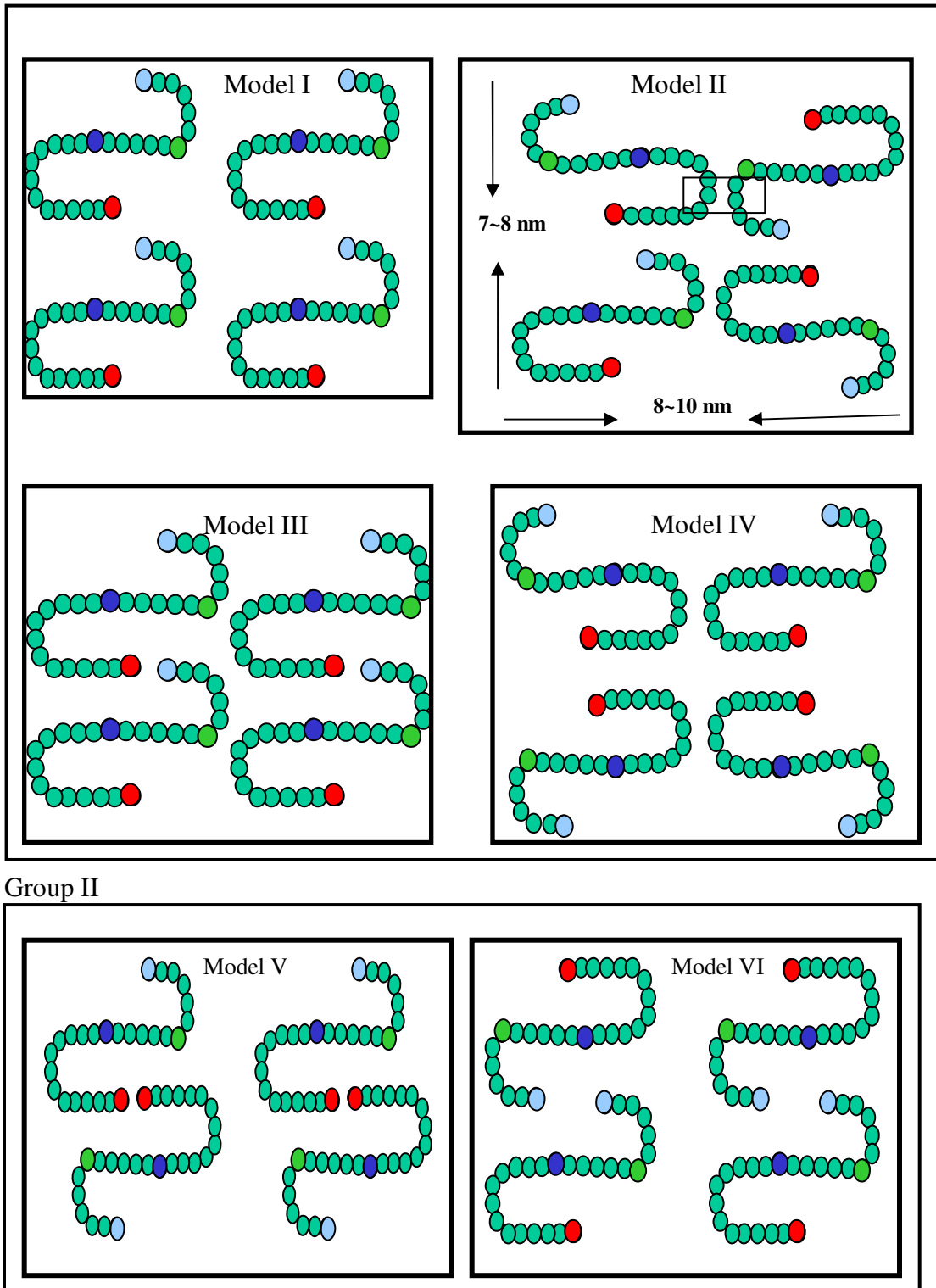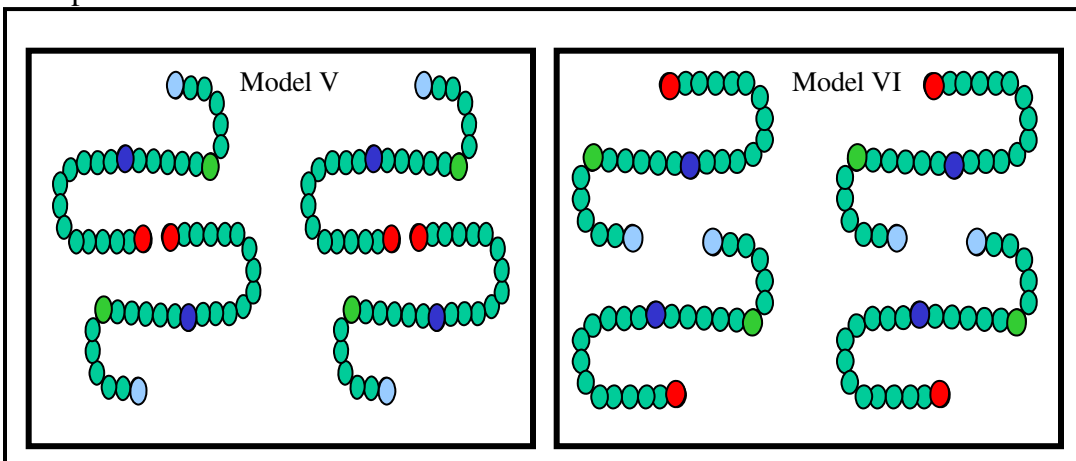
Figure 7-15. Structure models of Aβ(10-35) fibrils.

The color codes are light blue for Y10, green for K16, dark blue for E22 and red for M35.

These experiments have allowed me to develop additional constraints for the Aβ(10-35) fibrils, and allowed for the development of a new *double-turn* model. This model conforms intramolecular interaction at both N- and C-terminus, and opened the way for this FRET strategy to be applied to other self-assembly systems of even more complex structure.

Materials and methods

Synthesis of fluorophore-labeled peptides

All the peptides were synthesized on a Rainin Symphony Quartet peptide synthesizer with FMOC Rink-amide polystyrene resin (Anaspec, Inc.) through standard FMOC chemistry. For dansyl labeled peptide, N-Fmoc-N'-dansyl-L-lysine-OH (Anaspec, Inc.) in DMF was added to the reaction vessel manually and allowed to react overnight. The crude peptide was purified with reverse phase-HPLC and characterized with MALDI-mass.

FRET sample preparation

The fluorophore-labeled peptide was mixed with wild-type peptide Aβ(10-35). To make sure the peptides randomly mixing together, each peptide powder has been treated with hexafluoroisopropanol (HFIP) (10 mg/ml) for 30 min on ice (Srinivasan et al., 2003; Wood et al., 1996), then three aliquots of peptide HFIP solution were taken to distribute into three eppendorf tubes: one for the mixing, one as a control and the third one for the

concentration detection with UV. The mixed peptide HFIP solution was incubated for additional 20 min, followed by evaporation of HFIP to yield peptide film, which was dried further on lyophilizer overnight. For the mixing sample, their HFIP solution was mixed and incubated for the extra 20 min before evaporation of HFIP. The dried peptide film was dissolved in 20% acetonitrile / water and the pH was adjusted with 5.0 mM pH5.6 MES buffer and incubated at room temperature for 2 weeks before imaging and fluorescence study.

FRET measurement

Fibril sample (220 μL) was loaded into a 2 mm-path-length quartz curvette and the fluorescence spectra were collected between 310 nm to 550 nm with the excitation wavelength of 295 nm. The Aβ(10-35) fibrils without any fluorophore was scanned as background and each fluorescence spectrum was obtained by the background subtraction. The fluorescence intensity was normalized according to the peptide concentration. The FRET efficiency E was calculated according to the following equation (1):

$$E = 1 - \frac{F_{DA}}{F_{DA}}$$

where F_{DA} and F_D are the fluorescence intensity of fibril samples in the presence of donor/acceptor and donor only, respectively. The average distance between donor and acceptor could be determined according to the Föster equation (2):

$$E = \frac{R_0{}^6}{R_0{}^6 + r^6}$$

where R_0 is the Föster distance for a specific FRET pair when FRET efficiency is 50%.

Föster distance can be defined by using the equation 3:

$$Ro = [8.8 \times 1023 \kappa^2 n^{-4} QdJ]^{1/6} \text{ (Angstrom)}$$

where Q_0 is the fluorescence quantum yield of the donor in the absence of the acceptor, κ^2 is the dipole orientation factor, n is the refractive index of the medium.
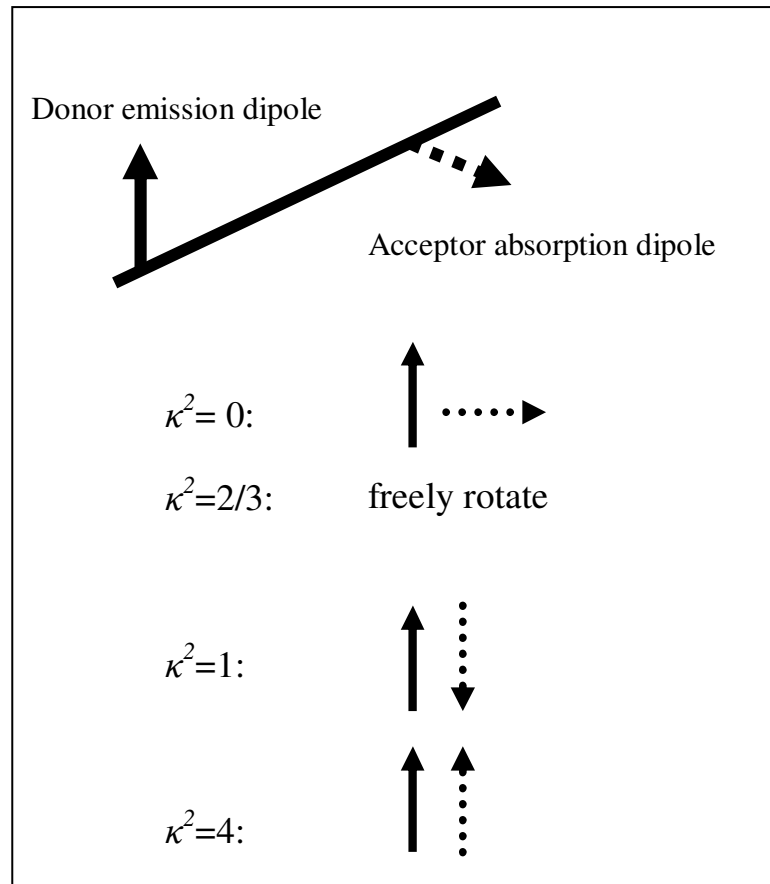
Figure 7-16. Illustration of the relationship between D/A dipole direction and the dipole orientation factor κ.

Black line represents peptide strand; solid arrow points donor dipole and dashed arrow points toward acceptor dipole.

Usually, the Föster distance used is based on the freely rotated fluorophores with κ^2 assumed to be 2/3 (Dale et al., 1979; Wu and Brand, 1992). For our system, when the fluorophore labeled peptides were incorporated into fibrils, the freedom was largely restricted. The fluorescence anisotropy of fibrils was much higher than that of monomers. However, the actuarial κ^2 is difficult to be determined experimentally, so in this study the Förster distance between tryptophan and dansyl was ranging from 21 Å to 31 Å when we took the extreme value for κ^2 from 2/3 to 4.

Fluorescence anisotropy

The mature fibrils were prepared by incubation of 0.01 mM fluorophore-substituted peptide with 0.1 mM Aβ(10-35) in 20% acetonitrile / water for 2 weeks; while the monomer solution was prepared by dissolving 0.01 mM peptide powder in pure Dimethyl sulfoxide (DMSO) without water dilution, due to the fast aggregation of peptide in the assembly condition. 220 μL sample was loaded into a 2 mm-path-length quartz curvette and scanned with Ex = 295 nm and collected at their maximal emission wavelength based on the fluorescence spectra of each sample. Each sample was scanned ten times to give the averaged value. Four sets of the same experiments were done to test the reproducibility.

Fluorescence quenching

The M35W and Y10W fibrils were prepared by incubation individual peptide (0.1

mM) in 20% acetonitrile / water and 5.0 mM pH5.6 MES buffer for 2 weeks. The

monomers were prepared by dissolving the same amount peptides in 6.0 M GnHCl.

Seven aliquots (0.25 mL each) of each sample were mixed individually with acrylamide

stock solution to reach the final indicated acrylamide concentration, and the final peptide

concentration was same by adjusting with fresh buffer. The mixed samples were

incubated for extra 30 min before monitoring tryptophan fluorescence in the range of 310

nm to 400 nm via excitation at 295 nm.

References

Alston, R. W., Lasagna, M., Grimsley, G. R., Scholtz, J. M., Reinhart, G. D., and Pace, C. N. (2008). Peptide sequence and conformation strongly influence tryptophan fluorescence. Biophys J *94*, 2280-2287.

Benzinger, T. L., Gregory, D. M., Burkoth, T. S., Miller-Auer, H., Lynn, D. G., Botto, R. E., and Meredith, S. C. (1998a). Propagating structure of Alzheimer's beta-amyloid(10-35) is parallel beta-sheet with residues in exact register. Proc Natl Acad Sci USA *95*, 13407-13412.

Benzinger, T. L., Gregory, D. M., Burkoth, T. S., Miller-Auer, H., Lynn, D. G., Botto, R. E., and Meredith, S. C. (2000). Two-dimensional structure of beta-amyloid(10-35) fibrils. Biochemistry *39*, 3491-3499.

Benzinger, T. L. S., Gregory, D. M., Burkoth, T. S., Miller-Auer, H., Lynn, D. G., Botto, R. E., and Meredith, S. C. (1998b). Propagating structure of Alzheimer's beta-amyloid (10-35) is parallel beta-sheet with residues in exact register. Proc Natl Acad Sci USA *95*, 13407-13412.

Burkoth, T. S., Benzinger, T. L. S., Urban, V., Morgan, D. M., Gregory, D. M., Thiyagarajan, P., Botto, R. E., Meredith, S. C., and Lynn, D. G. (2000). Structure of the beta-amyloid(10-35) fibril. J Am Chem Soc *122*, 7883-7889.

Callis, J. T. V. a. P. R. (2001). Mechanisms of Tryptophan Fluorescence Shifts in Proteins. Biophys J *80*, 16.

Catherine A. Kraft1, Jose Luis Garrido1, Luis Leiva-Vega1, and Guillermo Romero1 (2009). Quantitative Analysis of Protein-Lipid Interactions Using ryptophan Fluorescence. Science *2*, p14.

Dale, R. E., Eisinger, J., and Blumberg, W. E. (1979). Orientational Freedom of Molecular Probes - Orientation Factor in Intra-Molecular Energy-Transfer. Biophys J *26*, 161-193.

Decatur, S. M. (2000). IR spectroscopy of isotope-labeled helical peptides: Probing the effect of N-acetylation on helix stability. Biopolymers *54*, 180-185.

Decatur, S. M. (2006). Elucidation of residue-level structure and dynamics of polypeptides via isotopp-edited infrared spectroscopy. Acc Chem Res *39*, 169-175.

Deeb, T. S. (2000). Researchers Develop Method for Specific Covalent Labeling of recombinant Protein Molecules Inside Live Cells. In., (NC: Department of Biology, Davidson College, Davidson), pp. :2001.

Domanov, Y. (2006). Fluorescence Resonance Energy Transfer. In., (Helsinki Biophysics and Biomembrane Group, University of Helsinki).

Dusa, A., Kaylor, J., Edridge, S., Bodner, N., Hong, D. P., and Fink, A. L. (2006). Characterization of oligomers during alpha-synuclein aggregation using intrinsic tryptophan fluorescence. Biochemistry *45*, 2752-2760.

Garzon-Rodriguez, W., Vega, A., Sepulveda-Becerra, M., Milton, S., Johnson, D. A., Yatsimirsky, A. K., and Glabe, C. G. (2000). A conformation change in the carboxyl terminus of Alzheimer's A beta(1-40) accompanies the transition from dimer to fibril as revealed by fluorescence quenching analysis. J Biol Chem *275*, 22645-22649.

GarzonRodriguez, W., SepulvedaBecerra, M., Milton, S., and Glabe, C. G. (1997). Soluble amyloid A beta-(1-40) exists as a stable dimer at low concentrations. J Biol Chem *272*, 21037-21044.

Hogue, I. B., Hoppe, A., and Ono, A. (2009). Quantitative Fluorescence Resonance Energy Transfer Microscopy Analysis of the Human Immunodeficiency Virus Type

1 Gag-Gag Interaction: Relative Contributions of the CA and NC Domains and Membrane Binding. J Virol *83*, 7322-7336.

Kinoshita, A., Fukumoto, H., Shah, T., Whelan, C. M., Irizarry, M. C., and Hyman, B. T. (2003). Demonstration by FRET of BACE interaction with the amyloid precursor protein at the cell surface and in early endosomes. J Cell Sci *116*, 3339-3346.

Kinoshita, A., Whelan, C. M., Smith, C. J., Mikhailenko, I., Rebeck, G. W., Strickland, D. K., and Hyman, B. T. (2001). Demonstration by fluorescence resonance energy transfer of two sites of interaction between the low-density lipoprotein receptor-related protein and the amyloid precursor protein: Role of the intracellular adapter protein Fe65. J Neurosci *21*, 8354-8361.

Koo, B. W., Hebda, J. A., and Miranker, A. D. (2008). Amide inequivalence in the fibrillar assembly of islet amyloid polypeptide. Protein Eng Des Sel *21*, 147-154.

Lakdawala, A. S. (2003), Ph.D. Thesis, Emory University, Atlanta, GA, USA.

Liebman, S. W. (2005). Structural clues to prion mysteries. Nat Struct Mol Biol *12*, 567-568.

Munoz, V., Ghirlando, R., Blanco, F. J., Jas, G. S., Hofrichter, J., and Eaton, W. A. (2006). Folding and aggregation kinetics of a beta-hairpin. Biochemistry *45*, 7023-7035.

Nannepaga, S. J., Gawalapu, R., Velasquez, D., and Renthal, R. (2004). Estimation of helix-helix association free energy from partial unfolding of bacterioopsin. Biochemistry *43*, 550-559.

Petkova, A. T., Ishii, Y., Balbach, J. J., Antzutkin, O. N., Leapman, R. D., Delaglio, F., and Tycko, R. (2002a). A structural model for Alzheimer's beta-amyloid fibrils based on experimental constraints from solid state NMR. Proc Natl Acad Sci USA *99*, 16742-16747.

Petkova, A. T., Ishii, Y., Balbach, J. J., Antzutkin, O. N., Leapman, R. D., Delaglio, F., and Tycko, R. (2002b). A structural model for Alzheimer's beta -amyloid fibrils based on experimental constraints from solid state NMR. Proc Natl Acad Sci USA *99*, 16742-16747.

Petkova, A. T., Yau, W. M., and Tycko, R. (2006). Experimental constraints on quaternary structure in Alzheimer's beta-amyloid fibrils. Biochemistry *45*, 498-512.

Sciarretta, K. L., Gordon, D. J., Petkova, A. T., Tycko, R., and Meredith, S. C. (2005). Abeta40-Lactam(D23/K28) models a conformation highly favorable for nucleation of amyloid. Biochemistry *44*, 6003-6014.

Selvin, P. R. (2000). The renaissance of fluorescence resonance energy transfer. Nat Struct Biol *7*, 730-734.

Srinivasan, R., Jones, E. M., Liu, K., Ghiso, J., Marchant, R. E., and Zagorski, M. G. (2003). pH-dependent amyloid and protofibril formation by the ABri peptide of familial British dementia. J Mol Biol *333*, 1003-1023.

Wasmer, C., Lange, A., Van Melckebeke, H., Siemer, A. B., Riek, R., and Meier, B. H. (2008). Amyloid fibrils of the HET-s(218-289) prion form a beta solenoid with a triangular hydrophobic core. Science *319*, 1523-1526.

Wood, S. J., Chan, W., and Wetzel, R. (1996). Seeding of A beta fibril formation is inhibited by all three isotypes of apolipoprotein E. Biochemistry *35*, 12623-12628.

Wu, P., and Brand, L. (1992). Orientation factor in steady-state and time-resolved resonance energy transfer measurements. Biochemistry *31*, 7939-7947.

CHAPTER 8

Conclusion and Outlook

The amyloid aggregates have been implicated in Alzheimer's Disease (AD) as their neurotoxicity inducing cell death through either forming transmembrane channel or disrupting cell-membrane integrity and fluidity. The importance of this lipid bilayer context has been evaluated (Ashley et al., 2006; Bystrom et al., 2008; Kremer et al., 2001; Lemkul and Bevan, 2009; Matsuzaki, 2007; Wong et al., 2009; Yip et al., 2001), where evidence for peptide association with lipid head-groups (Ikeda and Matsuzaki, 2008; Wong et al., 2009) and lipid alkyls (Ashley et al., 2006; Kremer et al., 2001) has been identified and implicated in disease (Van Broeck et al., 2007), but no clear structural models have emerged. Even though amyloid is the misfolded state of peptide occurring in nature, it provides a source to construct novel biomaterials through the self-assembly of small peptides. Therefore, during the past decade it has been a big challenge in pathological and nano-technology fields to define amyloid structures and elucidate the factors that govern the self-assembled morphology and the peptide arrangements. Recently, significant progress including defining peptide organization (parallel or antiparallel) within fibrils by ssNMR characterization, modulating assembled morphologies (fibrils vs nanotubes) through metal chelating (Dong et al., 2006) and

nuclear base H-bonding interaction between the adjacent β-sheets (Liu et al., 2008), has been made. But, the role of peptide termini interaction (one of the amyloid growth plane) remains poorly understood.

Inspired by the studies of peptide-amphiphiles (Bull et al., 2005; Deng et al., 2009; Gordon et al., 2004; Hartgerink et al., 2001; Hartgerink et al., 2002; Meijer et al., 2007), we envisioned that covalent linkage of Aβ-peptides with lipid alkanes of variable length/bulkiness would allow direct interrogation of peptide-lipid hydrophobic interaction, as well as the systematical investigation of peptide terminal interaction in amyloid assembly. Therefore, in this dissertation, a series of alkyl chains with different length and degree of branching have been introduced at Aβ(16-22) termini as the probes, and significant findings have been obtained regarding novel Aβ-peptide-amphiphile architectures, amyloid assembly driving forces (cross-sheet electrostatic interaction and cross-strand glutamine side chain H-bonding interaction), the peptide bilayer interaction, as well as unexpected Aβ(10-35) strand *double-turn* conformation within fibril.

This study presents a discovery of novel Aβ-peptide-amphiphile architectures, which arise from direct interaction between Aβ-peptide and covalently linked alkanes through the bending of terminal alkanes to fit in β-sheet laminates. This is different from conventional peptide-amphiphile cylindrical fibrils that bury the alkane chain in assembly interiors with peptide segments splaying along their outer surface. Aβ-peptide-amphiphiles are able to assemble to a wide range of morphologies including nanotubes, sheets and fibrils, different from the uniform cylindrical fibrils observed with conventional peptide-amphiphile assemblies (Hartgerink et al., 2002). The β-sheet registry within these different morphologies ranges from antiparallel out-of registry,

antiparallel in-registry to parallel in-registry, dramatically distinct from the only parallel in-register β-sheets in conventional peptide-amphiphile cylindrical fibrils (Hartgerink et al., 2001; Hartgerink et al., 2002). Most interestingly, the terminal alkanes in these novel architectures gradually transit from extending to bending between the antiparallel or parallel β-sheet laminates, widening the lamination distances significantly, but do not really compromise the robust cross-β structure; while in conventional peptide-amphiphiles, the alkanes are always extending to point the interior of cylindrical fibrils. These significant differences may derive from the higher assembly propensity and the inherent property of Aβ-peptides. For example, Aβ(16-22) itself could assemble to nanotubes and fibrils at acidic and neutral pH, respectively. The hydrophobic peptide residues are able to create a hydrophobic laminates to accommodate terminal alkane carbon chains. Last but not the least is that the rectangle shape of Aβ peptide is more favorable to form regular β-sheets, different from the cone-shape peptide-amphiphile in cylindrical fibrils.

The systematic studies have established that these wide ranges of assembled morphologies with variable peptide arrangements are derived from different driving forces, instead of the energetically hydrophobic collapse of the alkane occurring in conventional peptide-amphiphile assemblies (Hartgerink et al., 2001; Hartgerink et al., 2002). The antiparallel out-of register β-sheet nanotubes and sheets at acidic pH are driven by the cross-strand pairing interaction between Val18 and Ala21 when the electrostatic attraction is reduced by either protonation of Glu22 at acidic pH, substitution of the Glu22 with leucine or shortening of the lysine side chain (Liang et al., 2008; Mehta et al., 2008). When Glu22 is deprotonated at neutral pH, Val18 / Ala21 cross-strand

pairing interaction is overwhelmed by the electrostatic interaction between Lys16 and Glu22, resulting in the antiparallel in-register β-sheet fibril formation (Mehta et al., 2008). The terminal alkane hydrophobic interaction and cross-sheet Lys16/Glu22 electrostatic interaction work together to direct parallel in-register β-sheet fibril formation in the case that the N-alkanes are elongated from N-acetyl to N-propyl or longer alkanes. The cross-sheet electrostatic interaction is a novel driving force, complementary to the existed library and changing the length of charged residues is able to be applied to modulate the self-assembly structure and morphology. When alkane substitution is at C-terminus, the hydrophobic interaction between C-alkane and N-acetyl overwhelms Vla18/Ala21 cross-strand pairing interaction and cross-sheet electrostatic interaction, directing antiparallel in-registry β-sheet fibril formation independent of C-alkane length at neutral pH. The similar role of terminal hydrophobic interaction in molecular assembly has been reported before (Iqbal et al., 2008), but the underneath mechanism of how short acetyl interacts with long C-alkane to direct amyloid assembly remains unclear.

The C-terminal substitution also presents an effect way to modulate peptide registry and the number of nanotube wall-layers. C-terminal amide protons have the strong H-bonding propensity, while completely eliminating these protons changes the β-sheet registry from out-of registry to in-registry and nanotube wall-layers from bilayer to monolayer, suggesting that H-bonds number between adjacent peptide strands modulates peptide registry and that the cross-leaflets interaction (H-bonding interaction or hydrophobic interaction) regulates nanotube layer, which indirectly supports amyloid bilayer structure.

Amyloid bilayer structure has also been evaluated by changing the bulkiness of N-alkanes, which also presents an efficient way to manipulate self-assembly morphology/architecture. The impact of N-bulky alkanes on assembled morphology/architecture is the β-sheet terminal structure dependent. The cavity created by out-of registry at acidic pH is able to accommodate all three tested bulky alkanes, resulting in the same peptide morphology and peptide arrangement independent of N-alkanes; while the flat surface of in-registry β-sheet at neutral pH is sensitive to N-alkanes, and any substitution of acetyl methyl H with methyl groups significantly changes the assembled morphology and peptide arrangement, resulting in the pH-independence of the bulkiest alkane N-*t*Butyl (Liang et al., 2008) . Therefore, the defined modulating effects of N-bulky alkyl chains identify the role of peptide terminal interaction at the bilayer interface, further supporting amyloid bilayer structure.

Moreover, in this dissertation, the mechanism of glutamine on amyloid assembly has been explored with single, double glutamine-substitutions and glutamine side chain amide proton substitutions as the consideration of the significant role of glutamine/arsparigine in several neurodegenerative diseases (Davis and VanNostrand, 1996); (Kvam et al., 2009; Rousseau et al., 2009). We have in the first time provided experimental evidence, complementary to the theoretical studies (Perutz, 1999a; Perutz, 1999b; Perutz et al., 1994) to support the role of glutamine side-chain cross-strand H-bonding interaction on parallel β-sheet fibril formation, accounting for the specific assembly behavior of glutamine/arsparigine-containing peptides in amyloid-related diseases. This simple strategy, glutamine substitution, also provides extra tool to

modulate parallel β-sheet formation, and may now be used in the rational design of new nanomaterials.

Finally, a new *double-turn* model has been proposed for the longer fragment Aβ(10-35) based on the studies of peptide strand conformation in fibrils with fluorescence resonance energy transfer (FRET). This new model confirms intramolecular interaction at both N- and C-terminus, and opens the way for this FRET strategy for applications in other self-assembly systems of even more complex structure.

In this research work, several significant discoveries clearly uncover some new aspects of amyloid self-assembly mechanism, driving force, assembled architectures, as well as Aβ-lipid interaction, complementary to our current knowledge. These novel Aβ-peptide-amphiphile architectures expand our view for the conventional peptide-amphiphile assemblies, providing extra regulating factors to diversify the molecular self-assemblies. Moreover, these findings clearly establish that the length, bulkiness and H-bonding capability of terminal alkyl chains and glutamine/arsparigine side chain are able to tune the amyloid self-assembled morphology, peptide orientation, tube/fibril surface properties and the distance between specific residues. The tuning capability could be utilized to design distinct materials with properties that range from novel self-assembling surfaces, robust compartments, and other components for building supramolecular self-assemblies. Moreover, the accommodating capability of amyloid β-sheet laminates offers a new application as drug carriers. Most importantly, Aβ-lipid interaction is an inherent phenomenon, independent of final peptide orientation and registry within β-sheets and the lipid alkyl chains at either peptide terminus. This may occur in cells and contribute to the toxicity of amyloid oligomers through insertion into lipid bilayer or extracting lipid from

cell membranes. The clarification of this mechanism may be useful for the rational design of effective therapeutical inhibitors to prevent Aβ-lipid interaction by accelerating amyloid assembly or increasing cell membrane rigidity.

References

Ashley, R. H., Harroun, T. A., Hauss, T., Breen, K. C., and Bradshaw, J. P. (2006). Autoinsertion of soluble oligomers of Alzheimer's A beta(1-42) peptide into cholesterol-containing membranes is accompanied by relocation of the sterol towards the bilayer surface. Biochim Biophys Acta: Struct Biol *6*

Bull, S. R., Guler, M. O., Bras, R. E., Meade, T. J., and Stupp, S. I. (2005). Self-assembled peptide amphiphile nanofibers conjugated to MRI contrast agents. Nano Lett *5*, 1-4.

Bystrom, R., Aisenbrey, C., Borowik, T., Bokvist, M., Lindstrom, F., Sani, M. A., Olofsson, A., and Grobner, G. (2008). Disordered Proteins: Biological Membranes as Two-Dimensional Aggregation Matrices. Cell Biochem Biophys *52*, 175-189.

Davis, J., and VanNostrand, W. E. (1996). Enhanced pathologic properties of Dutch-type mutant amyloid beta-protein. Proc Natl Acad Sci USA *93*, 2996-3000.

Deng, M. L., Yu, D. F., Hou, Y. B., and Wang, Y. L. (2009). Self-assembly of Peptide-Amphiphile C-12-A beta(11-17) into Nanofibrils. J Phys Chem B *113*, 8539-8544.

Dong, J., Shokes, J. E., Scott, R. A., and Lynn, D. G. (2006). Modulating amyloid self-assembly and fibril morphology with Zn(II). J Am Chem Soc *128*, 3540-3542.

Gordon, D. J., Balbach, J. J., Tycko, R., and Meredith, S. C. (2004). Increasing the amphiphilicity of an amyloidogenic peptide changes the beta-sheet structure in the fibrils from antiparallel to parallel. Biophys J *86*, 428-434.

Hartgerink, J. D., Beniash, E., and Stupp, S. I. (2001). Self-assembly and mineralization of peptide-amphiphile nanofibers. Science *294*, 1684-1688.

Hartgerink, J. D., Beniash, E., and Stupp, S. I. (2002). Peptide-amphiphile nanofibers: a versatile scaffold for the preparation of self-assembling materials. Proc Natl Acad Sci USA *99*, 5133-5138.

Ikeda, K., and Matsuzaki, K. (2008). Driving force of binding of amyloid beta-protein to lipid bilayers. Biochem Bioph Res Co *370*, 525-529.

Iqbal, S., Miravet, J. F., and Escuder, B. (2008). Biomimetic self-assembly of tetrapeptides into fibrillar networks and organogels. Eur J Org Chem, 4580-4590.

Kremer, J. J., Sklansky, D. J., and Murphy, R. M. (2001). Profile of changes in lipid bilayer structure caused by beta-amyloid peptide. Biochemistry *40*, 8563-8571.

Kvam, E., Nannenga, B. L., Wang, M. S., Jia, Z., Sierks, M. R., and Messer, A. (2009). Conformational targeting of fibrillar polyglutamine proteins in live cells escalates aggregation and cytotoxicity. PloS one *4*, e5727.

Lemkul, J. A., and Bevan, D. R. (2009). Perturbation of membranes by the amyloid beta-peptide - a molecular dynamics study. Febs J *276*, 3060-3075.

Liang, Y., Pingali, S. V., Jogalekar, A. S., Snyder, J. P., Thiyagarajan, P., and Lynn, D. G. (2008). Cross-strand pairing and amyloid assembly. Biochemistry *47*, 10018-10026.

Liu, P., Ni, R., Mehta, A. K., Childers, W. S., Lakdawala, A., Pingali, S. V., Thiyagarajan, P., and Lynn, D. G. (2008). Nucleobase-directed amyloid nanotube assembly. J Am Chem Soc *130*, 16867-16869.

Matsuzaki, K. (2007). Physicochemical interactions of amyloid beta-peptide with lipid bilayers. Biochim Biophys Acta *1768*, 1935-1942.

Mehta, A. K., Lu, K., Childers, W. S., Liang, Y., Dublin, S. N., Dong, J., Snyder, J. P., Pingali, S. V., Thiyagarajan, P., and Lynn, D. G. (2008). Facial symmetry in protein self-assembly. J Am Chem Soc *130*, 9829-9835.

Meijer, J. T., Roeters, M., Viola, V., Lowik, D. W. P. M., Vriend, G., and van Hest, J. C. M. (2007). Stabilization of peptide fibrils by hydrophobic interaction. Langmuir *23*, 2058-2063.

Perutz, M. F. (1999a). Glutamine repeats and neurodegenerative diseases. Brain Res Bull *50*, 467.

Perutz, M. F. (1999b). Glutamine repeats and neurodegenerative diseases: molecular aspects. Trends Biochem Sci *24*, 58-63.

Perutz, M. F., Johnson, T., Suzuki, M., and Finch, J. T. (1994). Glutamine Repeats as Polar Zippers - Their Possible Role in Inherited Neurodegenerative Diseases. Proc Natl Acad Sci USA *91*, 5355-5358.

Rousseau, E., Kojima, R., Hoffner, G., Djian, P., and Bertolotti, A. (2009). Misfolding of proteins with a polyglutamine expansion is facilitated by proteasomal chaperones. J Biol Chem *284*, 1917-1929.

Van Broeck, B., Van Broeckhoven, C., and Kumar-Singh, S. (2007). Current insights into molecular mechanisms of Alzheimer disease and their implications for therapeutic approaches. Neurodegener Dis *4*, 349-365.

Wong, P. T., Schauerte, J. A., Wisser, K. C., Ding, H., Lee, E. L., Steel, D. G., and Gafni, A. (2009). Amyloid-beta Membrane Binding and Permeabilization are Distinct Processes Influenced Separately by Membrane Charge and Fluidity. J Mol Biol *386*, 81-96.

Yip, C. M., Elton, E. A., Darabie, A. A., Morrison, M. R., and McLaurin, J. (2001). Cholesterol, a modulator of membrane-associated A beta-fibrillogenesis and neurotoxicity. J Mol Biol *311*, 723-734.